Development of Phosphate Based Glass Scaffolds for the Repair of Craniofacial Bone

A thesis submitted to the University College London in fulfilment of the requirements for the degree doctor of philosophy by

Mustafa Al-Qaysi BDS (Iraq), MSc(Iraq)

University College London

2018

UCL Eastman Dental Institute

Biomaterials and Tissue Engineering Research Division

University College London

Declaration

I, Mustafa Al-Qaysi confirm that the work presented in this thesis is my own. Where information has been derived from other sources, I confirm that this has been indicated in the thesis.

Signature: date: 6th December 2017

This thesis is dedicated to

the memory of my father

and my grand mother

Acknowledgements

Firstly, I would like sincerely to thank my primary supervisor, Professor Jonathan Knowles, for his educational advice and guidance and for his immense support and encouragement throughout my PhD study.

I would like to acknowledge my secondary supervisor, Dr Rishma Shah for her support.

I would like to thank the higher Committee of education development in Iraq (HCED) for funding my PhD study as a part of educational scholarship programme.

I would like to acknowledge Dr Graham Palmer, Dr George Georgiou, Dr Nicola Mordan for their training and technical assistance. I would like to thank Dr Farzad Fouroutan for his teaching and supervision regarding glass making procedure. I would like to thank Dr Nick Walters, Dr Tuula Eriksson, Dr Nasser Al-Qhatani for their help and advice concerning cell culture related studies.

I would gratefully thank Dr Piyaphong Panpisut, Dr Alaa Aldaadaa, Mayda Arshad, Nazanin Owji, SongYi Baek for their support.

Finally, I would like to hugely acknowledge my wife and my two daughters Sura and Sadan for their whole support and patience through my PhD journey.

Abstract

Degradable phosphate-based glasses have been known to have many potential properties to work as biomaterials for bone repair clinical applications. Although several studies were performed on different compositions to investigate the most appropriate glass formula, no specific formula was found to be the most favourable for clinical application.

The main aim of this thesis was to fabricate and biologically assess phosphate glass scaffold made from specific elements known for their potential in promoting bone growth.

To achieve this, primary studies were done on four different compositions of both zinc and strontium phosphate-based glass discs. The next study was to further investigate the best two zinc and strontium glass compositions that were obtained from the primary studies using glass beads. As a result of this study, specific composition of both zinc and strontium phosphate glass, having the most favourable cellular response, was recommended to be used for the following experiments. Based on previous compositions, another study was performed to surface functionalise glass discs by coating them with carbon nanotubes (CNTs) and polycaprolactone polymer (PCL) to assess the effect of surface modification on cellular adhesion and metabolic activity. This was subsequently followed by manufacturing, mechanical

testing and structural evaluation of zinc and strontium scaffolds. Another experiment was carried out to identify the most suitable technique for scaffold cells seeding by coating scaffolds with fibronectin and collagen. The final study aimed to assess different types of zinc and strontium phosphate glass scaffolds (non-coated, CNT-coated) in both static and dynamic conditions. For the assessment of these scaffolds under dynamic conditions, a perfusion bioreactor was custom made that worked continuously for 28 days.

The results revealed that the most preferable glass compositions were identified as ZnO5% and SrO17.5%. Also, glass coating with CNTs and PCL has found to encourage cells adhesion and metabolic activity as it enhanced both surface roughness and hydrophilicity. Scaffold production by sintering technique was thermally optimised and scaffold cellular seeding using collagen coating has yielded the most efficient seeding density. The final results displayed that the most suitable cellular response was found in CNT and PCL coated scaffolds under dynamic conditions (perfusion bioreactors cultivated scaffolds).

Impact Statement

Nowadays, many patients are suffering from bone defects. These defects may be due to trauma such as traffic accidents or war injuries, pathology such as tumours or may be due to congenital defects such as cleft palate.

Clinical procedures for managing bone repair defects are mainly dependant on the severity and extent of the defect. While simple defects can be treated by conservative procedures where the body repairs the defect by itself, the huge defects may need to the surgical procedures intervention as the defect is beyond human body repair. These procedures may involve the application of graft material to be placed in the defect site to accelerate the repair procedure. These graft materials could be derived from humans or animals and could be synthetically fabricated.

The main aim of this study is to produce scaffolds from phosphate-based glasses for bone repair applications. This may be of valuable individual and industrial importance.

Regarding its importance to individuals, the treatment of such defects nowadays is usually performed using autografts (grafts taken from the same patient) or allografts (grafts taken from other donors). It is important to mention that these treatments need extensive surgical procedures that are associated with many side effects such as discomfort, chronic postoperative pain, donor site morbidity, unpredictable bone resorption and high risk of infection at the donor site. In addition to all of these complications, other

complications are associated with allografts which are potential immunological rejection and cross infection. Therefore, the developed phosphate-based glasses scaffolds could be a good alternative as it is made of biologically acceptable material and can be applied directly without the need for doing further surgical procedures.

Concerning its impact on industry, the majority of the synthesised materials for bone defect repair are mainly dependant on xenografts such as BioOss. Although these choices have shown impressive clinical results, there are limitations in their application as they have low mechanical properties and they are used particularly for repairing small bone defects in bones that are not under load. For example, BioOss is used in dental applications for alveolar ridge augmentation or for managing periodontal defects. There is another disadvantage which is linked to the material of these xenografts. These materials are basically animal bones (cows or pig’s bones) that are treated by special methods to remove the bone proteins leaving the inorganic core materials of these bones to be used clinically. This procedure may be costly and also there are some obligations to be observeded for some patients who refuse the application of such materials for ethical and religious reasons. The produced phosphate-based glasses scaffolds have been shown to have mechanical properties slightly better than BioOss and also are cost effective because they are made basically of element oxides that are available in the market within a reasonable price. Moreover, their production is not as complicated as that for xenografts.

As a result of the previous aspects, if more research is done on these materials in future, these materials may be valuable in helping many people around the world who are presenting with severe bone injuries and may therfore improve their personal lives.

Table of Contents

Chapter 1 Introduction and review of the literature 34

1.1 Bone 34

1.1.1 Classification of bone 34

1.1.2 Bone microscopic anatomy 35

1.1.3 Bone chemical compositions 37

1.1.4 Bone development 44

1.1.5 Osteogenic differentiation of stem cells 48

1.1.6 In Vitro osteoblast adhesion to biomaterials 51

1.2 Craniofacial biomaterials 53

1.2.1 Autogenous bone graft (autograft): 54

1.2.2 Allograft bone 55

1.2.3 Xenograft bone 56

1.2.4 Alloplastic (synthetic) graft. 57

1.3 Phosphate glasses 64

1.3.1 Introduction to phosphate glasses 64

1.3.2 Glass composition 67

1.3.3 Glass synthesis 71

1.3.4 Phosphate glass structural analysis 75

1.3.5 Phosphate glass degradation and Ion release 76

1.3.6 Phosphate glass biocompatibility..... 81

1.4 Bone scaffolds 89

1.4.1 Scaffold requirements..... 89

1.4.2 Fabrication techniques of scaffolds for bone tissue engineering 94

1.5 Carbon nanotubes (CNTs)..... 99

1.6 Bioreactors: 104

1.6.1 Spinner bioreactors: 106

1.6.2 Rotating-wall vessel bioreactors (RWV) 107

1.6.3 Perfusion bioreactors..... 108

1.7 Statement of the problem: 112

1.8 Aim of and objectives..... 114

1.9 Null hypothesis 116

Chapter 2 Assessment of physical, chemical and biological properties of strontium phosphate based glass 118

2.1 Introduction..... 118

2.2 Materials and methods 121

2.2.1 Materials 121

2.2.2 Glass precursors calculation 121

2.2.3 Glass preparation 123

2.2.4 Materials characterisation 125

2.2.5 Chemical, physical studies of strontium phosphate bioactive glass discs 126

2.2.6 Cell studies 130

2.2.7 Statistical analysis 134

2.3 Results 135

2.3.1 Density measurement 135

2.3.2 X-ray diffraction 135

2.3.3 Thermal analysis 136

2.3.4 Degradation study (mass loss) 137

2.3.5 pH measurement 139

2.3.6 Ion release measurement 140

2.3.7 Cytocompatibility study 143

2.3.8 Alkaline phosphatase activity 144

Chapter 3 Assessment of physical, chemical and biological properties of zinc phosphate-based glass 151

3.1 Introduction 151

3.2 Materials and Methods 154

3.2.1 Materials 154

3.2.2 Glass precursor calculations 154

3.2.3 Glass preparation 156

3.2.4 Materials characterization 156

3.2.5 Chemical and physical studies 157

3.2.6 Cell Studies 158

3.2.7 Statistical analysis 161

3.3 Results 162

3.3.1 Density measurement 162

3.3.2 X -ray diffraction 162

3.3.3 Thermal analysis 163

3.3.4 Degradation study (mass loss) 164

3.3.5 Ion release 166

3.3.6 pH measurements 170

3.3.7 Cell proliferation 171

3.3.8 Measurement of metabolic activity 172

3.3.9 SEM Imaging 174

3.4 Discussion 176

Chapter 4 Development of strontium and zinc phosphate based glass microcarriers for biomedical applications. 183

4.1 Introduction 183

4.2 Materials and methods 185

4.2.1 Materials 185

4.2.2 Glass precursors calculations 185

4.2.3 Glass beads preparation 185

4.2.4 Material characterization 188

4.2.5 Chemical and physical studies 189

4.2.6 Cell Culture Studies 191

4.2.7 Statistical analysis 200

4.3 Results 201

4.3.1 X -ray diffraction 201

4.3.2 Glass beads size distribution 201

4.3.3 Degradation study 203

4.3.4 Ion release 205

4.3.5 pH Measurement 209

4.3.6 Cell assays 210

4.4 Discussion 216

Chapter 5 Surface functionalisation of phosphate based glasses 223

5.1 Introduction 223

5.2 Materials and methods 226

5.2.1 Glass discs preparation 226

5.2.2 CNT solution preparation 227

5.2.3 Glass discs coating 228

5.2.4 Characterisation of CNT coated glass discs 229

5.2.5 Hydrophilicity and hydrophobicity assessment 230

5.2.6 Surface roughness measurement 231

5.2.7 Cell culture studies 232

5.2.8 Statistical analysis 235

5.3 Results 236

5.3.1 CNT carboxylation validation. 236

5.3.2 Characterisation of CNT coated glass discs 237

5.3.3 Hydrophilicity and hydrophobicity assessment 239

5.3.4 Surface roughness estimation 240

5.3.5 Measurement of metabolic activity of cells 241

5.3.6 DNA assessment 242

5.3.7 Cells imaging by scanning electron microscopy (SEM) 243

5.3.8 Confocal microscopy cell imaging 244

5.4 Discussion 246

Chapter 6 Development of Zinc and Strontium Phosphate Based Glass Scaffolds 251

6.1 Introduction 251

6.2 Material and methods 255

6.2.1 Phosphate glass scaffold preparation 255

6.2.2 Glass scaffolds production optimisation 257

6.2.3 Cellular studies 260

6.2.4 Statistical Analysis 265

6.3 Results 266

6.3.1 Porosity 266

6.3.2 Diametral compressive strength 268

6.3.3 Cell Detachment 269

6.3.4 Cell metabolic activity 271

6.3.5 Metabolic assay (CCK Assay) 273

6.3.6 Confocal imaging 274

6.4 Discussion 275

Chapter 7 Determination of the Effect of Cultivating Stem Cells on Scaffolds Under Dynamic and Static Conditions on Osteodifferentiation ... 284

7.1 Introduction ... 284

7.2 Materials and Methods ... 288

7.2.1 Sample preparation ... 288

7.2.2 Samples characterisation ... 290

7.2.3 Perfusion Bioreactor System ... 291

7.2.4 Cell culture studies ... 294

7.2.5 Statistical Analysis ... 297

7.3 Results ... 298

7.3.1 Scaffold porosity estimation ... 298

7.3.2 Diametral compressive strength ... 300

7.3.3 Degradation study (mass loss) ... 301

7.3.4 DNA assessment ... 303

7.3.5 Mineralisation assay (Ca assay) ... 304

7.3.6 SEM imaging ... 305

7.4 Discussion ... 308

Chapter 8 Conclusions and Future Work Suggestions ... 317

8.1 Conclusion ... 317

8.2 Future work 326

Chapter 9 References 327

List of Tables

Table 2-1 Glass compositions 121

Table 2-2 Density measurement of all strontium containing phosphate glass compositions 135

Table 2-3 DTA for strontium containing phosphate-based glasses measured in °C 136

Table 2-4 Mass loss in (mg.cm-^{2}) for all glass compositions at four different time points 138

Table 3-1 Glass compositions 154

Table 3-2 Density measurement of all zinc containing phosphate glass compositions 162

Table 3-3 DTA for zinc containing phosphate-based glasses measured in °C 163

Table 3-4 Mass loss in (mg.cm^{-2}) for all glass compositions in four different time points 165

Table 4-1 phosphate glass beads composition 186

Table 5-1 Glass composition weight (gram) 226

Table 6-1 phosphate glass scaffold composition 256

List of Figures

Figure 1-1 Cortical and cancellous bone. Reprinted from Regenerative Medicine and Tissue Engineering, chapter 24, (Chao Le Meng Bao and K.Y., 2013), Advances in Bone Tissue Engineering, Regenerative Medicine and Tissue Engineering, copyright (2013), with permission from In Tech..... 36

Figure 1-2 Development of endochondral bone. Schematic diagram showing the events leading to replacement of an embryonic cartilage model by bone. (A) Cartilage model. (B) Initiation of formation of the primary centre of ossification in the centre of the cartilage model (C) Well established primary centre of ossification cartilage. (D) The formation of secondary centres of ossification and formation of growth plate (E) In the adult bone, the metaphyseal and epiphyseal bone have fused to each other. Reprinted from International Journal of Biochemistry and Cell Biology, volume 40, (Mackie et al., 2008) Endochondral ossification: how cartilage is converted into bone in the developing skeleton, page 46-62, with permission from Elsevier. 46

Figure 1-3 Postulated steps in the osteoblast lineage implying recognizable stages of proliferation and differentiation as detectable from in vitro and in vivo experiments. Reprinted from Principles of bone biology, volume 1, chapter 4, (Aubin and Triffitt, 2002). Mesenchymal stem cells and osteoblasts..... 51

Figure 1-4 Illustration of the basic phosphate tetrahydrate. Reprinted from the journal of materials Chemistry, Volume 13, issue 10, (Knowles, 2003). Phosphate-based glasses for biomedical applications. page 2395-2401. with the permission of Elsevier. 68

Figure 1-5 Effect of monovalent ion addition to P_2O_5 network. Reprinted from the journal of materials Chemistry, volume 13, issue10, (Knowles, 2003). Phosphate-based glasses for biomedical applications, page 2395-2401 with the permission of Elsevier. 70

Figure 1-6 The effect of temperature on the enthalpy (or volume) of a glass forming melt. Reprinted from Introduction to Glass Science and Technology (Shelby, 1997). 72

Figure 1-7 Example of an anion chromatogram for phosphate species collected using a Dionex ICS2500 system, showing the presence of PO_4^{3-}, $P_2O_7^{4-}$, $P_3O_9^{3-}$ and $P_3O_{10}^{5-}$ and higher phosphates. Reprinted from the journal of Advanced Drug Delivery Reviews, volume 65, issue 4 (Lakhkar et al., 2013). Bone formation controlled by biologically relevant inorganic ions: Role and controlled delivery from phosphate-based glasses. page 405-420. With the permission of Elsevier. 79

Figure 1-8 Foam replica technique. Reprinted from the journal of Biomaterial, volume 27, (Chen et al 2006) 45S5 Bioglass-derived glass–ceramic scaffolds for bone tissue engineering, page 2414-2425 95

Figure 1-9 Schematic diagram of a (a) single-walled carbon nanotube, (b) double-walled carbon nanotube, and (c) multi-walled carbon nanotube. Reprinted from Carbon Nanotube Reinforced Composite (Loos, 2015). Chapter 3, Allotropes of Carbon and Carbon Nanotubes, page 76..... 99

Figure 1-10 Schematic view of a spinner flask bioreactor. The cell/scaffold constructs are attached to a needle, and shear stress is applied by convection of medium. Reprinted from Tissue Engineering Part B Rev, volume 17, issue4, (Rauh et al., 2011). Bioreactor systems for bone tissue engineering, page 263-280, with the permission from Elsevier. 107

Figure 1-11 Schematic drawings of rotation-based bioreactor systems. Reprinted from Tissue Engineering Part B Rev, volume 17, issue4, (Rauh et al., 2011). Bioreactor systems for bone tissue engineering, page 263-280, with the permission from Elsevier. 108

Figure 1-12 (A, B) Schematic drawings of perfusion flow principles. (A) shows indirect perfusion where medium flows around and only partly through the scaffold. (B) In direct perfusion, medium flow is forced through the scaffold and shear stress is directly transferred to the cells within the scaffold. Arrows illustrate the magnitude and direction of fluid flow. Reprinted from Tissue Engineering Part B Rev, volume 17, issue4, (Rauh et al., 2011). Bioreactor systems for bone tissue engineering, page 263-280, with the permission from Elsevier. 109

Figure 2-1(A, B) Pictures explained the prepared glass (A) glass rods (B) glass discs 124

Figure 2-2 Calibration curve of ALP assay. Done by preparing different concentrations of ALP and correlate the corresponding fluorescence reading with each of the concentration. 134

Figure 2-3 X-ray diffraction showing the amorphous nature of the prepared glasses..... 135

Figure 2-4 Differential thermal analysis showing the glass transition temperature (T_g) which is the midpoint of the first slope in each composition , crystallisation temperature (T_c) which is the upward peak in each line and melting temperature (T_m) which is the last downward peak in each line . Showing that these parameters declined as SrO content increased 137

Figure 2-5 Mass loss in ($mg.cm^{-2}$) for all glass compositions over 14 weeks 138

Figure 2-6 pH measurement 139

Figure 2-7 Anion release showing higher release of phosphates ions (PO_4^{3-}, $P_2O_7^{4-}$, $P_3O_9^{3-}$, $P_3O_{10}^{5-}$) in the free strontium oxide based glass in comparison to strontium oxide containing glass 141

Figure 2-8 Cations release for all glass compositions a Sr^{2+}, b. Ca^{2+} and c. Na^{+}..... 142

Figure 2-9 Cell metabolic activity results determined by using alamar blue assay 143

Figure 2-10 Alkaline phosphatase (ALP) activity of MG63 on different glass composition..... 144

Figure 3-1 Transparent paper circular template 160

Figure 3-2 X-ray diffraction showing the amorphous nature of the prepared glasses..... 162

Figure 3-3 Differential thermal analysis of glasses showing the glass transition temperature (T_g) which is the midpoint of the first slope in each composition , crystallisation temperature (T_c) which is the upward peak in each line and melting temperature (T_m) which is the last downward peak in each line . Showing that these parameters declined as SrO content increased 164

Figure 3-4 Mass loss in ($mg.cm^{-2}$) for all glass compositions over 14 days 165

Figure 3-5 Anion release showing higher release of phosphates ions (PO_4^{3-}, $P_2O_7^{4-}$, $P_3O_9^{3-}$, $P_3O_{10}^{5-}$) in the high concentration zinc based glass (ZnO15) in comparison to other prepared glass compositions..... 167

Figure 3-6 Cations release for all glass compositions Na^+ and Ca^{2+}..... 168

Figure 3-7 Transition metal Zn^{2+} ions release showing the highest release for glasses with the highest zinc concentration. 169

Figure 3-8 pH measurement 170

Figure 3-9 Live cells counting 171

Figure 3-10 Dead cells counting 172

Figure 3-11 Metabolic activity estimation showing the percentage of alamar blue reduction as an indication for cellular metabolic activity.. 173

Figure 3-12 Scanning electron microscope images showing that the lowest number of attached cells was found with ZnO15 at all time points 175

Figure 4-1 Glass beads production. a. image showing the whole complex apparatus including flame torch, glass beads dispenser and glass beads collector. b. image displaying glass powder burning through the flame 187

Figure 4-2 Glass beads under light microscope..... 187

Figure 4-3 CCK calibration correlating cell numbers with their fluorescent readings..... 194

Figure 4-4 Calibration line of ALP assay. Done by preparing different concentrations of ALP and correlate the corresponding fluorescence reading with each of the concentration. 196

Figure 4-5 Ca calibration curve..... 198

Figure 4-6 X- ray diffraction pattern for all the produced glasses..... 201

Figure 4-7 A-SEM picture of glass beads B- frequency distribution of glass beads..... 202

Figure 4-8 SEM pictures for glass beads after incubation in deionised water showing the least degradation was with ZnO10 in day 14. 204

Figure 4-9 Anion release showing higher release of phosphates ions (PO_4^{3-}, $P_2O_7^{4-}$, $P_3O_9^{3-}$, $P_3O_{10}^{5-}$) by zinc based glasses in comparison to strontium glass 206

Figure 4-10 Cation release showing higher release of phosphates ions (Na^{+}, Ca^{2+}, Sr^{2+}) release 208

Figure 4-11 Zn^{2+} ions release revealing more zinc ions yielded from ZnO10 209

Figure 4-12 pH level showing that ZnO10 was with the least pH level in comparison to the control which remained steady. 210

Figure 4-13 CCK assay for MG63 cells showing that both ZnO5 and SrO17.5 supported cell proliferation in comparison with the control 211

Figure 4-14 Alkaline phosphatase for hMSCs measured by µg/ trans-well, displaying an acceptable enzyme concentration in ZnO5 and SrO17.5 in relation to the control. 212

Figure 4-15 Ca concentration for hMSCs measured by µg/ trans-well for day 14 and 21, revealing that ZnO5 and SrO17.5 have the highest calcium concentration. 213

Figure 4-16 SEM pictures of MG63 on SrO17.5 strontium glass beads. a- day1, b- day7 214

Figure 4-17 Confocal images of hMSCs showing the cellular attachment on beads. Red resemble propidium iodide (nucleus). Green staining is Phalloidin (cells actin) 215

Figure 5-1 ZnO15 glass discs. a- uncoated, b-PCL coated and C- CNT-PCL coated 229

Figure 5-2 Contact angle measurement. Reprinted from Advances in Colloid and Interface Science journal, vol81, issue 3, D.Y.Kwok and A.W.Neumann. Contact angle measurement and contact angle interpretation, page 167, copyright (1999) with permission from Elsevier. 231

Figure 5-3 Calibration line of DNA assay. Done by preparing different concentrations of DNA and correlate the corresponding fluorescence reading with each of the concentration. 235

Figure 5-4 Carbon nanotube sedimentation after 2 hours A: unfunctionalised 236

Figure 5-5 SEM images of CNT- PCL coated ZnO5 discs (a) ultrasonic non-treated discs and (b) ultrasonic treated discs, showing the stability of coating layer after the mechanical ultrasonic stimulus. 237

Figure 5-6 SEM images of coated SrO17.5 glass discs after three-time points: (a) day7, (b)day 14 and (c)day28. CNT layer was present along all the whole study, but polymer layer exhibited more cracks within time. 238

Figure 5-7 Contact angle measurement explaining the difference in hydrophilicity and hydrophobicity of glass surfaces 239

Figure 5-8 Roughness average (RA) for the different glass discs groups showing that CNT-PCL coated glass discs are more rough than other groups 240

Figure 5-9 Laser scan images for a. uncoated glass discs, b- PCL coated discs and c. CNT-PCL coated discs 240

Figure 5-10 Alamar fluorescence reduction percentage for free coated, PCL coated and CNT-PCL coated ZnO5 and SrO17.5 glass discs for three-time points (day 1, 4,7) 241

Figure 5-11 DNA concentration measured by pg/ml for the control and all glass disc groups displaying the acceptable detected concentration that was found in all groups after one week and two-week periods 242

Figure 5-12 SEM images of MG63 cells seeded on CNT-PCL coated glass discs. a-ZnO5 (day4), b- SrO17.5(day4), c-ZnO5 (day7) and d-SrO17.5 (day7) 243

Figure 5-13 Confocal images of hMSCs cells seeded on SrO17.5 glass discs. a-uncoated discs (day7), b- PCL coated discs (day7), c-CNT-PCL coated (day7), d-uncoated discs (day14), e- PCL coated discs (day14) and f-CNT-PCL coated (day14) 245

Figure 6-1 Glass scaffold manufacturing steps. a. quenched glass, b. glass powder, c. glass powder loaded into the graphite mold, d. sintered glass road and e. cylindrical glass scaffold 257

Figure 6-2 3-D image of phosphate -based porous scaffold 258

Figure 6-3 Diagram showing the orientation of phosphate glass scaffolds during diametral compressive strength (Drawn by Sketch Up Software) 259

Figure 6-4 Diagram explaining the six different seeding techniques. The upper pink row denotes the low attachment well plates (a. uncoated scaffold, b. fibronectin coated scaffold and c collagen 1 coated scaffold). Whereas the lower row is normal well plates (d. free coated scaffold, e. fibronectin coated scaffold and f collagen 1 coated scaffold)...... 262

Figure 6-5 Porosity percentage of SrO17.5 scaffolds sintered in different temperatures showing that porosity is indirectly related with the sintering temperature 266

Figure 6-6 CT-cross sections of strontium scaffolds made at different temperatures. a 480°C, b. 485°C and c.490°C displaying the decrease in porosity as sintering temperature rose..... 266

Figure 6-7 Porosity percentage of ZnO5 scaffolds sintered in different temperatures showing that porosity is indirectly related with the sintering temperature 267

Figure 6-8 CT-cross sections of zinc scaffolds made at different temperatures. a 470°C, b. 475°C and c.480°C displaying the decrease in porosity as sintering temperature rose..... 267

Figure 6-9 Diametral compressive strength for different manufactured strontium glasses..... 268

Figure 6-10 Diametral compressive strength for different manufactured zinc glasses..... 269

Figure 6-11 The percentage of detached cells from Zn O5 scaffolds(1 and 2 hours post seeding) displaying that the most percentage of cells detachment was found in the non-coated scaffold groups..... 270

Figure 6-12 Microscope images of the seeding well plates one-hour post seeding. A. normal plate/ uncoated scaffold, b. normal plate/ fibronectin coated scaffold, c. normal plate/ collagen coated, d. low attachment plate/ uncoated scaffold, e. low attachment plate/ fibronectin coated scaffold and f. low attachment plate/ collagen coated..... 271

Figure 6-13 Alamar blue fluorescence reduction of the six seeding groups at three-time points (day 1,4,7) displaying that free coating scaffolds groups had the lowest metabolic activity..... 272

Figure 6-14 Cells number proliferation on different seeding groups at three-time points (day 1,4,7) displaying that free coating scaffolds groups had the lowest proliferative ability..... 273

Figure 6-15 Confocal images of hMSCs seeded on strontium glass scaffolds by different seeding conditions. a. normal plate/ uncoated scaffold, b. normal plate/ fibronectin coated scaffold, c. normal plate/ collagen coated scaffold, d. low attachment plate/uncoated scaffold, e. low attachment plate/ fibronectin coated scaffold and f. low attachment plate/ collagen coated scaffold 274

Figure 7-1 Scaffolds samples: a. Bio Oss, b. ZnO, c. ZnO-CNT, d. SrO and e. SrO-CNT 290

Figure 7-2 Schematic diagram explaining the different parts of the perfusion bioreactor (common reservoir, peristallic pump and the bioreactor chambers) and the culture media flow direction that is notated by the arrows. This diagram was drawn by using Sketchup software 293

Figure 7-3 perfusion bioreactor 294

Figure 7-4 porosity percentage of different scaffolds displaying that BioOss is the highest porous material. 298

Figure 7-5 CT-cross sections of different scaffolds a. ZnO, b. ZnO-CNT, c. SrO, d. SrO-CNT and e. BioOss 299

Figure 7-6 Diametral compressive strength for all the tested scaffolds, showing that strontium coated scaffolds had the highest strength among the other prepared scaffolds. 300

Figure 7-7 Percentage of mass loss under dynamic condition showing that ZnO uncoated scaffolds had the highest degradation percentage in relating to the other groups 301

Figure 7-8 Percentage of mass loss under static condition showing that ZnO non-coated scaffolds had the highest degradation percentage in relating to the other groups 302

Figure 7-9 DNA concentration measured by pg/ml for the tested scaffolds (CNT-coated glass scaffolds, uncoated glass scaffolds and Bio Oss) after one week and two-week periods. 303

Figure 7-10 Ca concentration under static and dynamic conditions revealing that more calcium was released under dynamic conditions 304

Figure 7-11 SEM showing cells cultured under static and dynamic conditions. (Ai) BioOss scaffolds under static conditions, (Aii) BioOss scaffolds under dynamic conditions, (Bi) uncoated strontium glass scaffolds under static conditions, (Bii) uncoated strontium glass scaffolds under dynamic conditions, (Ci) PCL-CNT coated strontium glass scaffolds under static conditions, (Cii) PCL-CNT strontium coated glass scaffolds under dynamic condition 307

Publications

Mustafa Al Qaysi, Nick J Walters, Farzad Foroutan, Gareth J Owens, Hae-Won Kim, Rishma Shah, Jonathan C Knowles (2015) Strontium-and calcium-containing, titanium-stabilised phosphate-based glasses with prolonged degradation for orthopaedic tissue engineering. Journal of biomaterials applications ,30 (3), 300-310.

M Al Qaysi, A Petrie, R Shah, JC Knowles (2016).Degradation of zinc containing phosphate-based glass as a material for orthopedic tissue engineering. Journal of Materials Science: Materials in Medicine, 27 (10), 157.

Gareth J Owens, Rajendra K Singh, Farzad Foroutan, Mustafa Alqaysi, Cheol-Min Han, Chinmaya Mahapatra, Hae-Won Kim, Jonathan C Knowles (2016). Sol–gel based materials for biomedical applications. Progress in Materials Science 77, 1-79.

M Al Qaysi, A Aldaadaa, N Mordan, R Shah, JC Knowles (2017).Zinc and strontium based phosphate glass beads: a novel material for bone tissue engineering. Biomedical Materials 12 (6), 065011.

Presentation

Mustafa Al Qaysi, Rishma Shah, Jonathan C Knowles. Strontium and Zinc Based Phosphate Glass Beads Potential as a Biomaterial in Tissue Engineering. TERMIS- EU 2016, 28June-1July 2016, Upsala, Sweden.

Mustafa Al Qaysi, Rishma Shah, Jonathan C Knowles. Development of Phosphate Based Glass Scaffold for Bone Tissue Engineering. TERMIS - EU 2017, 26-30 June 2017, Davos, Switzerland.

Chapter 1 Introduction and review of the literature

1.1 Bone

Bone is an important and dynamic living human tissue that has the ability to continuously repair and remodel during human life (Widmaier et al., 2006).There are also various functions that bone does such as storage of minerals and production of blood cells within its marrow spaces (Seeley, 2000). Its primary function is to maintain a physiological support and mechanical protection to the human body which play an essential role in providing a body framework (Taichman, 2005).

1.1.1 Classification of bone

Bone can be classified according to their morphology into three types; long bones, short bones or flat bones. Long bone usually has length that is greater than its width and it is formed by cartilaginous precursors via endochondral ossification. An example of such bone is limbs' bones such as tibia, femur and radius. Short bone, in turn, is bone that is formed with the same precursor as long bone though its width is as similar as its length. An example of it are the carpals and the tarsals of the hands and feet. Flat bones, furthermore, do not have cartilaginous precursors and they are made usually via intramembranous ossification. They have usually flat and/or a curved appearance and commonly form the skull bone, the ribs, the sternum and the scapulae (Lieberman, 2009).

1.1.1.1 Long Bones

These are made of three distinctive segments which are epiphysis, metaphysis and diaphysis (Clarke, 2008). The epiphysis is the polar most outer layer of the bone that covers the area of the joints. It is mainly formed by compact bone providing it with mechanical properties (Einhorn et al., 2007). The metaphysis is the area of transformation between epiphysis and diaphysis. It is formed from thin compact bone and thick trabecular bone beneath it. This part has significant role in skeletal growth because it involves the epiphyseal plate (growth plates) and its nourishing blood vessels (Lewis, 1956). Conversely, the diaphysis is mainly composed from thick compact bone and thin trabecular bone surrounding the central intramedullary canal that is also called the marrow cavity (Clarke, 2008).

1.1.1.2 Short, flat and irregular bones

They share similar structural patterns involving thin bony plates of both compact bone; covered by periosteum on the outside, and cancellous bone; covered by endosteum in the middle. These bones lack the cylindrical shape, and they are usually flat (Currey, 2002a).

1.1.2 Bone microscopic anatomy

At a microscopic view, two types of bone can be identified according to bone architecture; cortical (compact) and cancellous bone (spongy bone) (Hing, 2004). Cortical bone forms the external part of a bone. It is characterised by its solid and dense structure so as to withstand the external forces. It is

composed of well organised structural units called osteons or the Haversian system (Currey, 2002b). This system has a cylindrical shape and is made of appropriately arranged bone matrix (bone lamella). The bone matrix arranges itself in multiple circles around the central Haversian canals. These canals serve as the main channel for supplying the bone with blood vessels and nerves (Widmaier et al., 2006). Moreover, there are other various small channels, perpendicularly intersecting the parallel arranged bone lamella, called Volkmann's canals. Volkmann's canals main role is to connect the blood vessels and nerves all the way in the whole compact bone (Figure 1.1) (Guyton and Hall, 2006). There are multiple well-arranged spaces distributed in the bone lamella called lacunae that are occupied by osteocytes. Osteocytes are spider shaped cells that are mature bone cells (Figure 1.1)(Currey, 2002b).

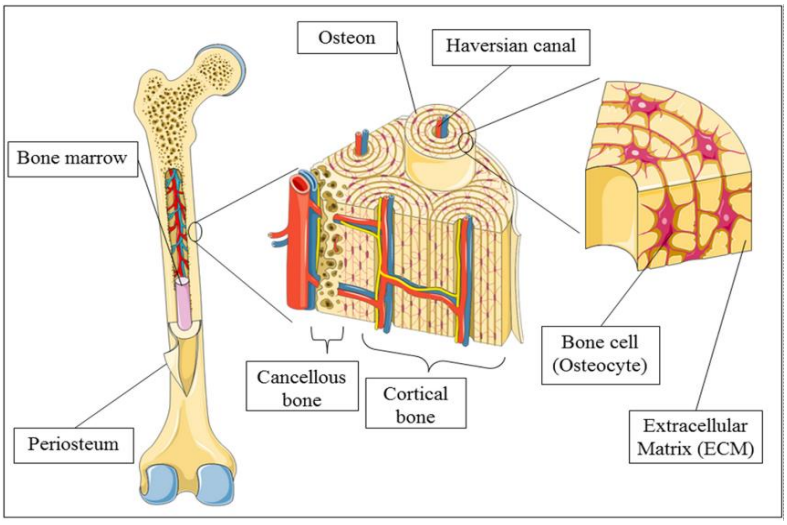

Figure 1-1 Cortical and cancellous bone. Reprinted from Regenerative Medicine and Tissue Engineering, chapter 24, (Chao Le Meng Bao and K.Y., 2013), Advances in Bone Tissue Engineering, Regenerative Medicine and Tissue Engineering, copyright (2013), with permission from In Tech

Spongy bone is not as organised as compact bone. It locates at the inner part of bone and is formed from poorly arranged bone. It consists of irregular interconnected bone rods and plates called trabeculae (Figure 1.1). These trabeculae embrace osteocytes that are interconnected with each other by canaliculi. The nutrient distribution through spongy bone occurs through the sporadically scattered canaliculi (Currey, 2002b).

1.1.3 Bone chemical compositions

Bone is composed of inorganic and organic components. The organic part constitutes around 30-35% of bone mass whereas the inorganic part occupies around 65-70% of it (Widmaier et al., 2006). The organic element constitutes both the cellular component and the osteoid which is part of the bony matrix that includes ground substance (proteoglycan and glycoproteins) and collagen fibres. There are three types of bones cells: osteoblasts, osteocytes and osteoclast (Guyton and Hall, 2006, Philippart et al., 2015).

Osteoblasts are originally multi-potential mesenchymal stem cells derivatives (Maher et al., 2015). Stem cells have the potential to differentiate into different cell types. If these cells were stimulated *in vitro* via specific markers such as dexamethasone, they may give rise to mono-potential progenitor cells called osteoprogenitors, which have an extensive proliferation capability (Pittenger et al., 1999). This differentiation can lead to pre-osteoblast development, as a preliminary step preceding osteoblast formation, and may yield in confined intercellular substance production (Aubin and Triffitt, 2002). The final differentiated osteoblasts are responsible for the deposition of

extracellular matrix (osteoid). Osteoid has many roles such as providing the bone with the needed mechanical requirement ,promotion of intercellular adhesion and also cellular signalling (Florencio-Silva et al., 2015).

Once engulfed by the mineralised bony matrix, fully differentiated osteoblasts become osteocytes that are interconnected among themselves by fluid filled small canals (Currey, 2002b). Osteocytes have two main functions; the first one is mechanotransduction as they transform the stress induced signals of bone bending or stretching through the canalicular fluid flow. The second function is the secretion of some matrix proteins such as osteocalcin and hyalouranate that play an important role in cellular adhesion (Bonewald, 1999).

Osteoclasts are multinucleated huge cells containing 4 to 40 nuclei. They have the capability of bone removal and resorption. Osteoclasts are generally derived from marrow monocyte-macrophage lineage (Boyle et al., 2003). During bone resorption processes, osteoclasts tend to secrete both hydrogen ions and cathepsin K enzyme. H^+ ions will decrease the pH and enhance the required acidic environment for the resorption processes of inorganic compound , whereas cathepsin K enzymes play a significant role in the destruction of the highly saturated type I collagen intercellular matrix (Parfitt, 1994, Boyle et al., 2003).

1.1.3.1 Organic matrix components

The extracellular matrix of bone is defined as a substance that surrounds the cellular component of bone and is composed from mineral and an organic

component which is produced by osteoblasts (Currey, 2002b). The organic compound constitutes about 35% of bone mass. Bone matrix is composed of many proteins; collagenous and non-collagenous. The collagenous proteins represent about 85 to 90% in which type I collagen is the most predominant. The rest (10-15%) is non-collagenous proteins such as osteocalcin, osteonectin, bone sialoproteins, proteoglycans and osteopontin (Brodsky and Persikov, 2005).

1.1.3.1.1 Collagen

Collagen is the major organic protein of the bony extracellular matrix. It constitutes about 70-90% of the bony organic component. While 97% of this is type I collagen, the remnant is of type II, III, V and X collagen (Marks and Popoff, 1988). Collagen has a major role in bone health and function. Keene *et al* (1991) supposed that the different types of collagen present in bone may improve the attachment of different muscloskeletal related tissues such as tendons, ligaments and periosteum to the cortical bone (Keene et al., 1991). Moreover, collagen especially type 1 may enhance the maturation of osteoblasts and encourage matrix mineralisation (Lynch et al., 1995). Salaszynk *et al* (2004) examined the effect of collagen on stem cells and hypothesised that collagen may have a promoting effect for osteogenic differentiation of stem cells (Salasznyk et al., 2004). A later study showed the important action of collagen in preserving bone strength and mineral content maintenance. This study linked the age-related collagen modifications and collagen diseases with the decreased bone quality and fragility of bone

(Viguet-Carrin et al., 2006). McNerny *et al* (2015) suggested that collagen crosslinking may play a highly important role in bone health and that cross linking disorders may impact negatively on bone quality and bone strength resulting in bone with a high susceptibility to fractures (McNerny et al., 2015).

1.1.3.1.2 Glycoproteins

Glycoproteins are protein matrix compounds produced by the attachment of carbohydrates to a protein core. They may have various active sites on their structure, which may react with cell wall and membrane receptors (Hughes, 2014). There are various types of glycoproteins such as fibronectin, vitronectin, bone sialoprotein, osteonectin, osteocalcin and osteopontin (Boskey and Robey, 2013).

Fibronectin is a bone matrix protein synthesised by connective tissue cells. Although it has many functions, its' essential role is to work as an adhesive glycoprotein and helping in the fibrous network assembly of the extracellular matrix. This property enhances binding and interaction among different extracellular matrix components and cell surface receptors (Romberger, 1997). Fibronectin was reported to be formed during the first step of bone formation and has a central role in osteoblast regulation (Grzesik and Robey, 1994).

Vitronectin is serum protein, initially known as S-protein. Due to its cell-spreading activity and attachment hyperactivity to cells, it is not found at high levels in bone mineralised matrix (Grzesik and Robey, 1994). Beside its cell attachment activity, it shows good ability to bind to plasminogen activator

inhibitor and affect the regulation of coagulation and complement factors (Schvartz et al., 1999).

Bone sialoprotein is also a glycoprotein that is defined as sialic acid contained glycoprotein. Apart from bone, it can be found also in other human mineralised tissues such as dentine, cementum and mineralized cartilage (Foster et al., 2015). Generally, there is an idea that its expression is related to the mineralisation process. It is thought to be a late marker for osteoblastic differentiation and at the same time an early marker for matrix mineralisation (Bianco et al., 1991). Recent studies revealed that the lack of this protein may be related to impaired osteochondral bone development (Holm et al., 2015).

1.1.3.1.3 Osteonectin

Osteonectin is the highly abundant non-collagenous organic protein; it is formed by both osteoblasts and fibroblasts (Rosset and Bradshaw, 2016). One of the chemically significant characteristics of osteonectin is that it holds several di-glutamate bonds that have the ability to conjugate with other ions and molecules that play a positive role in bone such as calcium, collagen and hydroxyapatite. Therefore, its suggested to be involved in cell- matrix interaction rather than the mineralisation process (Hing, 2004).

1.1.3.1.4 Osteocalcin

Osteocalcin is an abundant non-collagenous protein like osteonectin. It is a Matrix Gla protein (MGP) whose synthesis is fully dependent on vitamin K (Hauschka et al., 1989). Osteocalcin, clearly has a high affinity to calcium

ions as its structure contains a special alignment of Gla proteins which assists in the absorption of hydroxyapatite. Moreover, its structure terminated with -COOH may help as a site for cellular interaction (Neve et al., 2013). Although the role of osteocalcin is not fully understood, some studies suggested that it plays a role in bone resorption and osteoclast cell differentiation. One study was performed to determine the function of osteocalcin. This study was done by genetically engineering free osteocalcin mice to examine the effect of lacking osteocalcin. The results showed that free osteocalcin mice were able to form more bone than the normal mice with lower remodelling activity because of the reduced action of osteoclasts (Ducy et al., 1996). Rammelt *et al* (2005) concluded in another study of multiple grafting of synthesised hydroxyapatite/collagen implants in the tibia head of rat. Osteocalcin was investigated also by adding it to one of the implanted samples while leaving the other site as control. The results of this *in vivo* experiment suggested that osteocalcin may enhance bone modelling as osteocalcin treated sites displayed bone remodelling activity through the acceleration of transformation from woven bone to lamellar bone (Rammelt et al., 2005). Recently it was found that osteocalcin has a positive role in osteogenesis and bone metabolism (Neve et al., 2013).

1.1.3.1.5 Osteopontin

Osteopontin is identified as a phosphorylated glycoprotein that is present in many tissues and has a high affinity for hydroxyapatite (Butler, 1989). Studies have revealed that it is expressed and secreted in the bone matrix

osteoid as a part of the bone formation process via preosteoblasts, osteoblasts and osteocytes (Marks and Popoff, 1988). Many researchers have reported that osteopontin may enhance cellular attachment of osteoblasts and fibroblasts(Oldberg et al., 1986, Somerman et al., 1987). Some findings claimed that its expression may have a contribution in bone development and showed that its expression is significantly enhanced during the late mature phase of osteoblasts (Butler et al., 1996).

1.1.3.1.6 Proteoglycans

Proteoglycans are extracellular proteins that are made of main protein molecules attached to long sequences of polysaccharides and glycosaminoglycans GAGs. GAGs are simply a sequence of replicating sulphated carbohydrate units (Meisenberg and Simmons, 2016). GAGs can present as keratan sulphate, chondroitin sulphate or heparin sulphate (Iozzo and Schaefer, 2015). According to their size, proteoglycans can be divided into different types; two of these types are popular which are decorin and biglycan. Decorin and biglycan are known to inhibit bone cell attachment to the extracellular matrix by binding to fibronectin and preventing binding with cells. The presence of these proteoglycans in the osteoid makes them potential candidates as nucleators for hydroxyapatite precipitation (Robey, 2002).

1.1.3.1.7 Alkaline phosphatase

Alkaline phosphatase (ALP) is a dimeric enzyme with two active Mg^{2+} and Zn^{2+} sites. This enzyme possess the ability to attack inorganic

pyrophosphate (ppi) groups and release free phosphate (pi) resulting in increasing the local inorganic concentration for mineralisation processes (Harmey et al., 2004). Its action during mineralisation is mostly related to its ability to promote hydroxyapatite crystal formation and the collagen fibril deposition process (Orimo, 2010). ALP is expressed in the process of stem cell development, so it is considered one of the stem cell development indicators (Stefkova et al., 2015). It is also highly expressed during stem cell differentiation to osteoblasts, but this high expression is only recorded in the early stage of differentiation. As the differentiation progresses, other markers are upregulated whereas alkaline phosphatase declines(Golub and Boesze-Battaglia, 2007).

1.1.3.2 Inorganic matrix component

Inorganic bone matrix constitutes about 65-70% of bone mass. It is made of minerals which are mainly calcium and phosphate ions that bind to each other to form hydroxyapatite [$Ca_{10}(PO_4)_6(OH)_2$] that are usually combined with many other elements in the human body such as fluoride, carbonate, and chloride with missing hydroxyl groups that are normally present (Currey, 2002b, Ferraz et al., 2004).

1.1.4 Bone development

1.1.4.1 Intramembranous ossification

This is the ossification process by which flat bones of the skull and mandible are formed. It starts by the proliferation of mesenchymal stem cells. These

cells have the capability to differentiate into osteoblasts. Osteoblasts secrete the proteoglycan proteins which are responsible for trapping calcium ions. This will lead eventually to osteoid formation. Within time, these cells will be surrounded by bone completely. At this stage, they are called as osteocytes instead of osteoblasts (Mitchell and Peel, 2009).

As the bone matrix forms, a lot of trabeculae will be formed and connect to each other to make cancellous bone. These trabeculae will be penetrated by blood vessels in which red bone marrow is present. Finally, the cancellous bone will be substituted by cortical bone. At the outer superficial layer of bone, mesenchymal cells pack and condense to form periosteum (Mitchell and Peel, 2009).

1.1.4.2 Endochondral ossification

This type of ossification involves initially the formation of the cartilage model. The cartilage model is formed as consequence of mesenchymal stem cells accumulation and proliferation in the shape of the future bone. These stem cells will differentiate into chondroblasts then chondrocytes. The latter is responsible for cartilage matrix secretion (Mitchell and Peel, 2009).

Once the cartilage model is formed, it will be invaded by cells at various sites; at the centre and the periphery forming the primary and secondary centres of ossification. By the time, these centres of ossification slowly expand in all directions to end up by replacing the cartilage completely with bone. (except at the articular surfaces) (Figure 1.2) (Mackie et al., 2008).

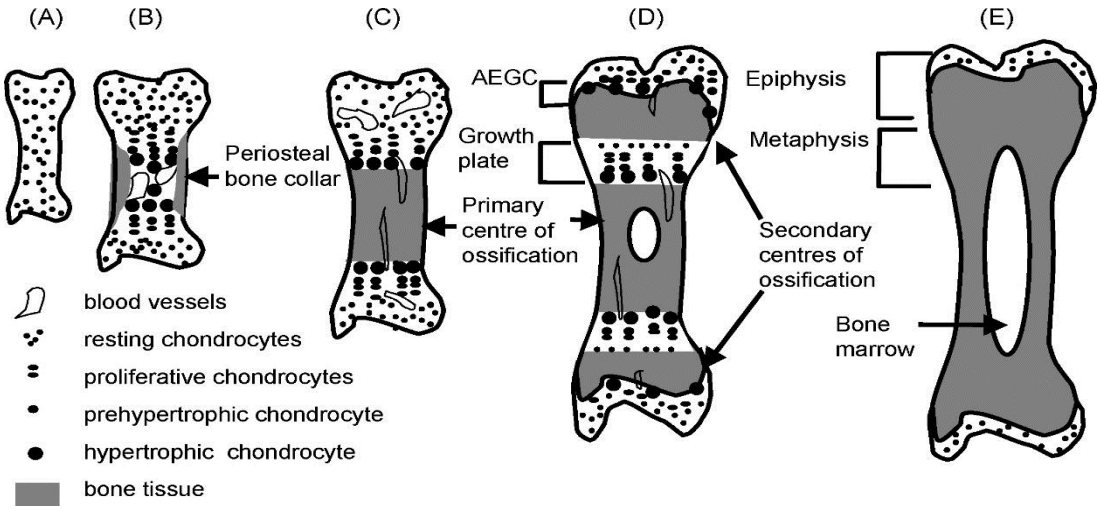

Figure 1-2 Development of endochondral bone. Schematic diagram showing the events leading to replacement of an embryonic cartilage model by bone. (A) Cartilage model. (B) Initiation of formation of the primary centre of ossification in the centre of the cartilage model (C) Well established primary centre of ossification cartilage. (D) The formation of secondary centres of ossification and formation of growth plate (E) In the adult bone, the metaphyseal and epiphyseal bone have fused to each other. Reprinted from International Journal of Biochemistry and Cell Biology, volume 40, (Mackie et al., 2008) Endochondral ossification: how cartilage is converted into bone in the developing skeleton, page 46-62, with permission from Elsevier.

The endochondral ossification takes place at two different locations in the long bones – the primary (diaphyseal) and the secondary (epiphyseal) sites of ossification. Bone formation starts at the primary site, while the secondary (epiphyseal) sites still under autonomous control and are ossified later. As a result of this development, there will be a formation of layer of distinction between these two centers of ossification which is called a growth plate (epiphyseal plate) and is located between the diaphysis and the epiphysis. During bone growth, there will be some fusion between diaphysis and the epiphyseal plate forming an area called metaphysis (Morishima et al., 1995). At the primary central area, chondrocytes segregate into hypertrophic chondrocytes allowing for local calcification. This will consequently result in chondrocyte death because of slow diffusion and low nutrient supply

throughout the hardened bone (Ortega et al., 2004). There are two theories behind the death of hypertrophic chondrocyte. Whereas the earliest theory related that to apoptosis (Wilsman et al., 1981), the recent studies explain that this happens because of another phenomena which is morphologically distinct from apoptosis (Adams and Shapiro, 2002). Because of cell death, thin walled lacunae will be formed which will eventually be broken leaving small holes for microvascularisation. As a result of a highly distributed vascularisation, some of the cells differentiate to osteoblasts. New bone matrix formation happens in the central area because of deposition of both calcium and phosphate as hydroxyapatite with the aid of other proteins and alkaline phosphatase that are expressed from osteoblasts resulting in replacement of most of the central cartilage (Anderson et al., 2004, Kirsch, 2006) .

The osteoblast plays the main role in the new bone formation. This starts at the beginning by producing cancellous bone on the remnant of the cartilage. As bone formation continues to extend to the two peripheral ends, osteoclasts start to remove some bone in the central area to create a hole. This hole will be filled with red bone marrow and called medullary trabeculae (Ortega et al., 2004).

The secondary ossification develops in the same way as the primary centres with help from the epiphyseal artery vascularisation. Although both centres have the same endochondral ossification process, they slightly differ in some aspects. The first difference is that there is no resorption in the secondary

(peripheral) centres and bone remain the same in the epiphysis with no future resorption. The other difference is that hyaline cartilage is completely replaced into bone in diaphysis whereas it is not fully substituted in the epiphysis and there will be trace of cartilage near the end of epiphysis which is called epiphyseal plate that will be ossified in the early adulthood (Mackie et al., 2008).

1.1.5 Osteogenic differentiation of mesenchymal stem cells

Stem cells differentiation into osteoblast is a multi-stage procedure that involves many cellular changes. The first stage includes the differentiation into osteoprogenitors that will further differentiate into preosteoblasts which will lastly differentiate into osteoblasts. The identification of these stages is usually made by detection of specific markers which are secreted by the cells in specific time during the differentiation process (Figure 1.3). There are different types of tissue markers associated with this type of cellular transformation such as type I collagen, alkaline phosphatase and osteocalcin (Aubin et al., 1995). According to Stein *et al* (1990) the osteoblast differentiation process can be divided into three different phases. Each phase is regulated by specific genes which are responsible for expressing the phase related proteins. These phases are 1: proliferation, 2: matrix maturation and 3: mineralisation (Stein et al., 1990). The first phase extends from day 1 to day 4 after seeding, the second phase extends from day 5 to day 14 and the third phase from day 14 to day 28 (Aubin, 2001, Huang et al., 2007).

Regarding the proliferation phase, it was found that there is a high increase in cell replication with significant secretion of collagen type 1. Collagen type 1 reached the peak of secretion on day 3 but it does not appear pronounced in the extracellular matrix until day 7 when collagen biosynthesis diminished (Quarles et al., 1992). The early secretion of collagen may play a stimulating role for other bone marker expression such as alkaline phosphatase and osteopontin which are secreted later (Celic et al., 1998). BSP was found to be upregulated in this phase and preceding alkaline phosphatase expression (Malaval et al., 1999). The second phase is the matrix maturation in which there is preparation of minerals deposition with substantial secretion of alkaline phosphatase (ALP) (Aubin, 2001). The mineralisation phase is characterised by higher expression of osteopontin, osteonectin and osteocalcin. Osteocalcin is not secreted until day 14 (Birmingham et al., 2012).There is a controversy about the actual phase of osteopontin expression. While previous studies believed that this expression commonly happens during the matrix maturation stage (Stein et al., 1990), the following studies placed it as marker for the mineralisation phase as it is expressed together with osteocalcin (Stein et al., 1996). Some studies allocate its expression as an indicator for both phases (Owen et al., 1990).

When looking at tissue markers, it was found that the differentiation is made of seven stages rather than 3 stages in which both collagen and BSP are secreted in the early while alkaline phosphatase is usually secreted in the

intermediate stages and osteocalcin is expressed in the later mineralisation stage (Figure 1.3) (Aubin and Triffitt, 2002).

There is an indirect relationship between proliferation and differentiation. In other words, as osteoblasts reached the final stage of differentiation, their rate of proliferation will decline. This opinion was judged after measuring the levels of both histone (a protein associated with DNA to form chromatin) and mRNA which is known also as a biological indicator of proliferation. The level of expression of the previous two seemed to decline during the maturation phase (Stein et al., 1989a, Stein et al., 1989b).

The original location of osteoblasts is also a factor that has an influence on the way osteoblasts differentiate and the levels of the expressed proteins. This influence was accounted by a study which involved studying bone taken from two different sites (iliac crest and mandible) of the same person to exclude the age factor. This study revealed that the expression of alkaline phosphatase and osteocalcin expression was higher for the cells from the iliac crest, but proliferation was higher for the mandible extracted osteoblasts (Kasperk et al., 1995). Another study was conducted using femoral head and skull bones of different patients. Although this study revealed results similar to the previous study in regard to alkaline phosphatase concentration, the proliferation results were different in that proliferation of femoral head extracted osteoblasts was higher than that of skull cells (McDougall, 2001).

The *in vitro* osteogenic differentiation of human mesenchymal stem cells (hMSCs) can be controlled by the culture media condition and its

components. Adding dexamethasone, ascorbic acid and B-glycerol phosphate to the culture media can stimulate hMSCs to take the osteogenic lineage pathway rather than other differentiation pathways (Vater et al., 2011, Akahane et al., 2016).

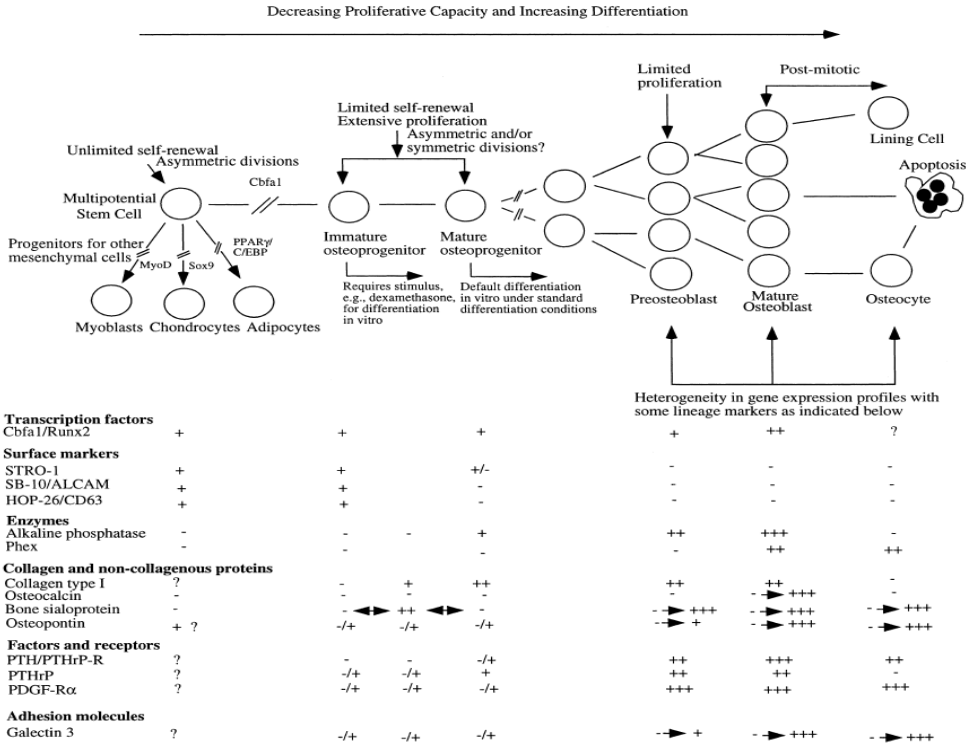

Figure 1-3 Postulated steps in the osteoblast lineage implying recognizable stages of proliferation and differentiation as detectable from in vitro and in vivo experiments. Reprinted from Principles of bone biology, volume 1, chapter 4, (Aubin and Triffitt, 2002). Mesenchymal stem cells and osteoblasts.

1.1.6 *In Vitro* osteoblast adhesion to biomaterials

According to biomaterial definitions, adhesion is a term that involves two aspects: firstly the attachment aspect which happens instantly for a short term such as physicochemical linkages between cells and materials, and secondly is the adhesion aspect that happens over a longer period of time

and includes the intervention of extracellular proteins, cell membrane proteins and cytoskeleton proteins (Anselme, 2000).

There are various organic extracellular matrix formation proteins such as collagen, proteoglycan, osteopontin and osteocalcin. These proteins are produced by osteoblasts and mostly are involved in cell adhesion. However, there are other molecular proteins *in vitro* that can aid the adhesion of osteoblasts such as fibronectin and vitronectin (El-Amin et al., 2003). Studies have shown that cells do not have high adherence ability to normal unconditioned materials. These materials may need to be soaked in a conditioning biological liquid to enhance their attachment ability (Boyan et al., 1996) .

To investigate cells adhesion related proteins, primary human osteoblasts have been seeded and cultured on different protein coated dishes. In one study, osteoblasts showed good adherence to fibronectin as well as to type I, type IV collagen and vitronectin coating, but they possessed a weak adherence ability to laminin and type V collagen coated dishes (Gronthos et al., 1997). This may be due to adhesion related proteins e.g. fibronectin, vitronectin and type I collagen revealing that they have a specific structure of Arg-Gly-Asp (RGD) peptide sequence that plays a positive role in cell membrane receptor fixation processes such as integrins. Other study confirmed the previous one in which it displayed that Arg-Gly-Asp (RGD) peptide coated surfaces showed better adhesion property than RGE (Arg-Gly-glu) peptide coated surface (Rezania et al., 1997).

1.2 Craniofacial biomaterials

Bone loss defects in human bodies are mainly caused by trauma, neoplasms and congenital abnormalities (Miloro et al., 2004). Although bone has the internal capacity to regenerate by itself, clinical intervention by bone construction (repair) procedures may be needed in some situations when there is a severe defect that exceeds the host tissue's regenerative capacity (Smith et al., 2015a). Generally, there is a misunderstanding or confusion regarding using the terms "bone repair" and "bone regeneration". Whereas the term "bone repair" defines the continuous physiological remodelling process that aims to restore the optimum physiological bone structure, the term "bone regeneration" explains the complicated process of forming new bony tissue (Donati et al., 2007). Bone regeneration procedures are mainly varied according to the graft materials used. These materials should have specific properties, (Damien and Parsons, 1991, Goldberg, 2001) such as:

1: Mechanical requirement enabling them to support the load and maintain the structure.

2: Osteoactivity requirement for enhancing the new bone formation. Osteoactivity involves both osteoinduction and osteoconduction. Osteoinduction refers to the ability to enhance the recruitment and osteogenic differentiation of mesenchymal cells situated near the graft (implant) or from revascularization. Whereas osteoconduction means that these materials should have spatial properties that permit the ingrowth of

vessels and osteoprogenitor cells from the host subject to support bone formation.

3: It should not cause any pain, fracture, excessive bleeding, foreign body response or transmission of diseases.

Bone engineering is a term involving both mechanical and biological (bone regeneration) aspects for the restoration of lost or affected tissue in order to provide functional bone tissue by inducing the new cells to produce bone (Bose et al., 2012).

1.2.1 Autogenous bone graft (autograft):

Autograft is still considered to be the benchmark grafting material (Farre-Guasch et al., 2015). It can be divided into both cortical and cancellous grafts, or into non-vascularised and vascularised grafts (Fillingham and Jacobs, 2016). It is free from immunological rejection as it is a harvested graft originating from the same individual (Sharif et al., 2016b). They offer good structural support with low viral transmission possibilities. For maxillofacial bone repairs, it can be gained either from intraoral or extraoral sites. While Intraoral are the symphysis, the ramus, and the angle of the mandible, extraoral sites are the iliac crest, ribs, tibia, fibula, calvaria, and sternum (Zimmermann and Moghaddam, 2011). However, grafts that are harvested from iliac crest are more optimal than other graft types and the mandible is the most common transplant site in dental surgery (Cypher and Grossman, 1996).

Autogenous grafts are osteoactive materials that have both the osteoinductive and osteoconductive properties capable of enhancing mesenchymal stem cell differentiation into osteoblasts and hence bone formation (Garcia-Gareta et al., 2015). Cortical autogenous grafts offer good support and mechanical properties, whereas cancellous grafts are rich with osteoprogenitor stem cells making them of benefit to the repair site. Following transplantation, the non-vascularised graft goes via a process of resorption and revascularisation, whereas the vascularised graft heals rapidly going through different remodelling stages similar to that of normal bone (Zimmermann and Moghaddam, 2011). The main disadvantages linked to this type of graft are discomfort, chronic postoperative pain, donor site morbidity, unpredictable bone resorption and high risk of infection (Sharif et al., 2016b).

1.2.2 Allograft bone

Allograft bone is one of the main types of bone graft material. They are usually obtained from human donors to eliminate the drawbacks of a second surgical site and the increased surgical time that are associated with autogenous graft options (Jovanovic et al., 1992). Similar to the autogenous graft, they are considered osteoconductive materials, though their osteogenic ability is lower than that of autogenous graft (Oklund et al., 1986). Allograft can be prepared in different sizes and be used in different augmentation procedures. They are applied in surgical procedures as sterilised fresh frozen or freeze dried materials both approved by the Food and Drug Administration

(FDA) (Roberts and Rosenbaum, 2012). Although many advanced procedures are used in their sterilisation, cross infection remains their most significant drawback as some incidental cases of bovine spongiform encephalopathy infection have been reported after allograft implantation (Control and Prevention, 2002).

1.2.3 Xenograft bone

Xenografts are bovine or pig derived skeletal tissues that have been deproteinated to produce inorganic bone scaffolds (Thuaksuban et al., 2010) . The deproteination process is performed usually by using ethylene diamine to extract all the organic components of bone (King et al., 2006). Commercial xenografts such as Bio – Oss or Pepgen-P15 are organic-free composition grafts that are constituted mainly from calcium phosphate, making their chemical and morphological properties similar to the mineral component of normal bone. For example; they are porous materials, and their porosity and spatial microstructure mimics that of human cancellous bone. This structural arrangement may play a positive role in angiogenesis and osteoblast migration (Sartori et al., 2003). Nowadays, they are used in diverse cases extending from small bony defect repair in clinical periodontology to complicated surgical cases such as maxillary sinus augmentation (Mardas et al., 2010, Piattelli et al., 1999). Many studies investigated the clinical use of xenograft alone or mixed with other bone substitutes. These clinical trials were performed by using different surgical procedures, and showed very promising clinical outcomes in regard to bone growth (Wallace et al., 2005).

Although xenograft materials showed good potential in the bone repair field, there are some ethical, personal and religious reasons that may prevent their medical application (Sharif et al., 2016a).

1.2.4 Alloplastic (synthetic) graft.

Alloplastic is a type of synthesised material used for bone tissue repair applications. It is mainly produced to overcome the drawbacks associated with the natural bone substitutes; autograft, allograft and xenograft (Hench, 1998, Bucholz, 2002). Alloplast can be produced in different forms and with different physicochemical properties. They can be degradable or nondegradable and can be also customised in terms of their network structural properties such as pore size and the level of porosity (Sheikh et al., 2015). According to their materials, they can be classified into three main different groups: bioceramics, polymers and biocomposites (Sharif et al., 2016a). These synthetic bone alternatives should fulfil the ideal requirements of being biocompatible, showing no fibrotic reaction and supporting the newly formed bone (Giannoudis et al., 2005). Moreover, they should essentially be biodegradable and produced as a three-dimensional framework that can enhance the cellular growth (Smith et al., 2015b).

1.2.4.1 Bioceramics:

<u>Tricalcium phosphate (TCP)</u>

TCP is porous form of calcium phosphate complex that has the formula $Ca_3(PO_4)_2$ where the calcium to phosphate ratio is 3:2 (Damien and Parsons,

1991). It occurs in two main crystalline forms known as αTCP or βTCP (Tamimi et al., 2012). αTCP showed promising mechanical and chemical results as an injected material when it was mixed with calcium carbonate and other calcium phosphate precursors as a fracture site filler (Sanchez-Sotelo et al., 2000). Similarly, βTCP is also popularly used as a filler, and showed acceptable results in many clinical studies (Hashimoto-Uoshima et al., 1995). Nyan *et al* (2016) clarified that both αTCP and βTCP are degradable, and that αTCP has higher degradation rate than that βTCP (Nyan, 2016). Moreover, many studies and reports presented many drawbacks associated with TCP application such as higher resorption rate (within 6 weeks), formation of fibrous tissue rather than bone during healing process (Parikh, 2002).

Hydroxy Apatite:

The natural mineral phase of bone is nano-sized hydroxyapatite crystals having a generalised composition of $Ca_{10}(PO_4)_6(OH)_2$. In human bone, it presents always in combination with other ions such as F^-, CO_3^{2-} Na^+ or Mg^{2+and} other ions. Synthetically, it can be manufactured in many techniques such as wet chemical deposition, biomimetic deposition, sol-gel and electrodeposition (Ferraz et al., 2004). Sheikh *et al* (2015) mentioned that the synthetic type can be produced in different forms: porous non-resorbable, solid non-resorbable, and resorbable porous. Heat is considered to play a major factor in synthesising the HA form and shape; using high temperature during manufacturing can lead to forming a non- resorbable sintered dense

form. Conversely, a low manufacturing temperature is responsible for the formation of resorbable porous HA (Sheikh et al., 2015). Many studies were performed to test the biological effect of both the dense and the porous types as an implant material in bone defect repair and revealed promising clinical results. One study, performed by Foster *et al* (2016) showed the successful results of using HA as cement for correcting cranial bone defects (Foster et al., 2016) . The main drawbacks of using hydroxyapatite is its poor mechanical properties as it is known for its brittleness that limits its use to powders, coatings, and low-loaded porous implants only (Suchanek and Yoshimura, 1998). As a result, many procedures were introduced to incorporate these materials with others, such as polymers, to enforce their mechanical features.

Silicate Bioglass

Bioglass®, invented by Larry Hench, is composed mainly of silicate with other metal oxide additives such as phosphorous, calcium and sodium oxides (Vogel and Höland, 1987). It has been studied extensively due to its potential in bone tissue engineering as it displayed excellent bioactive properties (Kaur et al., 2014a). It has been suggested that these silicate glasses have the ability to produce a layer of calcium phosphate crystals after immersion in SBF (Hayakawa et al., 1999, Takadama et al., 2001, Sriranganathan et al., 2017). Many experiments were performed on silicate based glasses alone or silicate glass composites and all revealed the potential of this material to be clinically applied in bone defect repairs as it is biodegradable, has the ability

to support differentiation of hMSCs and the proliferation of osteoblasts (Rezwan et al., 2006, Lin et al., 2009, Demirkiran et al., 2010, Thakur et al., 2017). Despite all the advantages of the bioglass, its low degradation rate in comparison to phosphate glass and its brittleness are considered its weak points (Knowles, 2003, Lizzi et al., 2017).

Borate Bioglass

Nowadays, borate based glasses are being investigated more, because of its chemical durability (Li et al., 2007). One study incorporated boron into silicate glass to encourage calcium phosphate layer deposition as it has a higher conversion rate than that of silicate; the outcomes were acceptable (Yao et al., 2007). Other studies aimed to partially or completely substitute silicates with borates to produce bioglass scaffolds with different structural compositions and different biodegradation properties. Although results were promising in regards to biodegradation and hydroxyapatite deposition and were in agreement with the previous study, the results were less satisfactory in regards to mechanical strength as boron may decrease the mechanical properties of glass (Fu et al., 2010b). Although *in vitro* studies revealed the ability of boron glass to promote cell proliferation at specific boron ion concentrations, the main identified drawback was its low mechanical properties that decrease with time when immersed in solutions (Fu et al., 2009).

1.2.4.2 Polymers

Polymers can also be used in bone tissue engineering since many of these materials are biocompatible and biodegradable. Moreover, they are highly versatile because of their controlled copolymerisation that may help them to be produced with different biodegradation rates (Sharif et al., 2016a).

The most commonly used polymer in cranioplasty is polymethylmethacrylate (PMMA). PMMA provides a protective, defect filling replacement with minimal postoperative inflammation (Unterhofer et al., 2017). Lara *et al* (1997) explained that the size of the bony defect may determine the type of PMMA used; PMMA without mesh is highly suitable for small defects (5-15cm^2) while mesh reinforced PMMA is used for larger sized defects (16-49 cm^2) (Lara et al., 1997). Nevertheless, the highly exothermic polymerisation process when it occurs in place can severely damage brain tissue. Moreover, being prone to infection, pulmonary embolism and lack of osseointegration have limited the use of such materials (Jaberi et al., 2013, Milojkovic and Homsi, 2014, Pikis et al., 2015).

The poly hydroxy group polymers such as poly-lactic acid (PLA), poly-glycolic acid (PGA) and poly-caprolactone (PCL) have been investigated also for bone tissue engineering. PLA-PGA were used mainly as binders or conjugators to bio ceramics or allografts. The conditions associated with their manufacture affect the biodegradation and the mechanical properties negatively (Coombes and Meikle, 1994). Many studies tested its use in conjunction with other bioceramics (TCP or HA) to form scaffolds and

showed that it has good properties in terms of increasing bone growth (Chuenjitkuntaworn et al., 2010, Terranova et al., 2017, Bai et al., 2016). Another comprehensive study was conducted to examine PCL samples that were coated in three different bioceramics (CaP, bioglass and strontium added bioglass). Although all the samples exhibited good results *in vitro* regarding the cell adhesion and gene expression, the *in vivo* study on rats did not show any bone formation in any of the samples in 8 and 16 weeks period after implantation (Poh et al., 2016). However recent attempts have developed a form of memory material that is composed from PCL and polydopamine for cleft palate application repairs and showed acceptable properties (Grunlan et al., 2016).

1.2.4.3 Biocomposites

Biocomposites is a term used to describe any material that is produced from the combination of more than one material such as ceramic–ceramic, ceramic–polymer or polymer–polymer for clinical use. This combination can result in the improvement of biological and mechanical properties of the scaffold to work as an acceptable substitute for the autograft or allograft (Basha and Doble, 2015). There are different examples of biocomposites such as collagen 1 with TCP, collagen 2 with HA bioceramics, and self-reinforced Polymers such as (PLLA, PLGA) with calcium phosphate. One study tested prepared collagen coated PCL/ βTCP biocomposite scaffold and found that this combination of biomaterials played a positive role in enhancing MG63 cell attachment and viability (Yeo and Kim, 2011). Other *in*

vivo studies looked at the effect of carbon nanotubes (CNTs) filled polymer biocomposite as an implant in rabbit femoral condyles and showed that this biocomposite had enhanced the osteogenecity (Sitharaman et al., 2008). These biocomposites were designed to overcome the drawbacks of using bioceramics and polymer individually as they aim to combine the flexibility found in a polymer with the hardness of HA resulting in new material that has better properties than the two separate materials (Qidwai et al., 2014). Moreover, porosity can be introduced in these materials so that they can fulfil the bone tissue engineering requirements. Porosity can be produced by implanting many techniques such as thermally induced phase separation, salt leaching/freeze-drying, wet spinning, and electrospinning.

1.3 Phosphate glasses

1.3.1 Introduction to phosphate glasses

Phosphate-based glass has been investigated for more than a century. Although it is one of the popular oxides forming glass (along with SiO_2, GeO_2 and B_2O_3), it lacked the popularity in research due to its reactive and hygroscopic nature (Knowles, 2003). Phosphate glasses have been examined for the last few decades as a potential biomaterial for various biomedical applications such as dental, maxillofacial and orthopaedic implants; scaffolds for bone tissue engineering, and also as a carrier for antimicrobial agent delivery (Knowles, 2003, Abou Neel et al., 2009b)

Phosphate-based glasses have been studied to examine their potential for biomaterial applications in bone tissue engineering because they have two important properties. First, they have a predictable controlled degradation rate in aqueous media. Different glasses with different degradation rate ranging from 2–3 hours to 1 year or longer can simply be developed in the laboratory; for instance, the ternary P_2O_5–Na_2O–CaO glasses can be modified by adding appropriate oxides to form quaternary or higher order systems with low degradation rates. Second, their main inorganic elemental components (e.g. Na, Ca and P) are essential elements that are naturally present in bone. The latter point is important especially when assessing the relation between phosphate glass materials and bone cells within both *in vitro* and *in vivo* conditions. It is even more important for bioactive implant

production since there should be an essential chemical bond between the bioactive implant interface and the surrounding tissue (Anselme, 2000).

The basic unit of phosphate-based glass is the highly reactive and hygroscopic pure P_2O_5 molecule (Hudgens et al., 1998). The foremost studies on phosphate glass biomaterials concentrated on the incorporation of metal oxides such as Na_2O and CaO to form the ternary P_2O_5–Na_2O–CaO phosphate glass systems (Burnie et al., 1981, Burnie et al., 1983). It was found that the change in the ternary P_2O_5–Na_2O–CaO glass composition may have an effect on degradation (dissolution) rate; in which increasing Na_2O at the expense of CaO in the composition can lead to higher degradation rate and vice versa. Despite all the attempts that were carried out to find the appropriate dissolution rate of the ternary phosphate glass, it persisted with a relatively high degradation rate that leads to poor biocompatibility. This was the motivation behind performing other later studies to produce phosphate glass with more appropriate degradation rate for the application. These studies were done by adding different metal oxides to the glass system such as Fe_2O_3 (Reis et al., 2002, Kokubo et al., 2003), CuO (Mulligan et al., 2003, Abou Neel et al., 2005), Al_2O_3 (Shah et al., 2005),TiO_2 (Abou Neel E et al., 2007), ZnO (Abou Neel et al., 2008c, Salih et al., 2007), and SrO (Lakhkar et al., 2009). The purpose of additional metal oxide addition to the glass structure is two-fold: First, metal oxides serve as the most effective means to control the degradation rate by increasing the covalent nature of the bonds within the glass structure. Second, the metal

ions released from such glasses can have a biological function such as an antimicrobial effect and/or positively impact on cell proliferation and bone tissue regeneration (Knowles, 2003).

According to Le Geros (2008), the use of phosphate glasses in the biomedical field necessitates these glasses to have specific properties to act as bone replacement materials (LeGeros, 2008). These properties are:

1-Glass chemical composition that should mimic natural bone composition.

2-Physical and chemical properties giving the glass the appropriate strength to withstand stress.

3-Biological factors interaction between implanted glass and living cells that includes (adhesion, degradation, osteoconductivity, bioactivity).

4- The ability to produce these glasses in different forms that may facilitate bone growth.

Therefore, glass should be made or modified to cover all the required properties. For an example, P_2O_5–Na_2O–CaO ternary glass may dissolve quickly which may affect the cellular mechanical attachments and may yield in significant changes in pH levels that may have an affect on cellular responses. To overcome this degradation, titanium oxide was added to it at a specific 5 mol% percentage to form the quaternary P_2O_5–Na_2O–CaO–TiO_2 making it more resistant to degradation and with good mechanical properties (Lakhkar et al., 2012).

Phosphate- polymer based biocomposites have been produced to be used for bone repair. An experiment was carried out by preparation of PLA (polylactic acid) and phosphate glass powder at different contents

(0%,5%,10%,20%). The results revealed that adding the glass enhanced the mechanical strength of the polymer and also enhanced the degradation rate. The biocompatibility results were satisfactory (Georgiou et al., 2007). The combination of phosphate glass with PCL (polycaprolactone) polymer bone composite was tested also, and suggested that adding the glass component to the polymer may lead to improvement of the composite properties (Liu et al., 2015).

1.3.2 Glass composition

Oxides are the basic component of any glass type, these oxides usually classified under three categories (Zachariasen, 1932) :

1-Network forming oxides: they are the basic oxides that can form glass by themselves alone without the addition of other components, they are one of the four Zacharasian glass forming oxides (SiO_2, P_2O_5, B_2O_3, and GeO_2).

2- Network modifying oxides: they are the oxides that can modify glass network geometry when they bond to it, therefore the glass characteristics will be altered by the different percentages of these oxides, basically they are oxides of alkali and alkali-earth metals such as sodium oxide and calcium oxide.

3- Intermediate oxides: elements such as (Al, Ga, Ti, C, V, Bi, Mo, W, S, Se and Te) that can replace network formers in some cases, but they lack the ability to form glass by themselves alone.

Pure phosphate glass are based on the tetrahedral phosphate anion PO_4^{3-} unit that forms a three-dimensional network (Hoppe, 1996). This network has resulted due to the formation of 5 free electrons in the outer orbit (3s2 3p3). Three of these electrons tend to form a single covalent bond with the oxygen atom (BO bridging oxygen), leaving the other two electrons to make double bond with oxygen (Figure 1.4) (Knowles, 2003). According to this molecular framework, the bridging oxygens are the bonding site for modifying oxides such as (Na_2O, CaO) (Kirkpatrick and Brow, 1995).

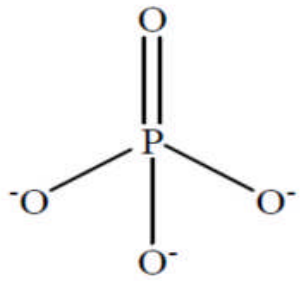

Figure 1-4 Illustration of the basic phosphate tetrahydrate. Reprinted from the journal of materials Chemistry, Volume 13, issue 10, (Knowles, 2003). Phosphate-based glasses for biomedical applications. page 2395-2401. with the permission of Elsevier.

Furthermore, the connection between different phosphate units occurs through covalent bonds with their bonded oxygen atoms that are called bridging oxygens (BO's).

This bridging oxygen (BO) is a popular method to classify the type of the glass via the implementation of Q^i terminology in which *Q* represents the P atom that is linked to several oxygen atoms to form the phosphate tetrahedron. Whereas 'i' refers to the number of BO's per tetrahedron, as a result of adding different metal oxides (MO) to this structure that will terminate the P-O-P bond in the polymer network, replace the P to form P-O-

M non-bridging bond (NBO), decrease the number of present BO and whenever we add more we will end with a state of saturation where all the bridging oxygens are linked with metals and that will lead to PO_4^{-3} structures, following the sequence of Q^3 Q^2 Q^1 Q^0 (Figure 1-5)(Brow, 2000, Knowles, 2003).

Depending on the glass composition that is based on the formula $(M_{2/V}O)_x(P_2O_5)_{1-x}$ where M is modifying cation oxide, v is the cation valency and x is the number of cation oxides molecules attached to the phosphate molecule, the glass can be classified into five types: ultraphosphate, metaphosphate, polyphosphate and pyrophosphate and orthophosphate glasses (Brow, 2000).

Ultraphosphate glasses have $0 \leq x < 0.5$ and their O/P (oxide/ phosphate) ratio is $2.5 \leq O/P < 3$. They usually have Q^3 and Q^2 units in the glass structure. Glass structure starts to resemble the vitreous P_2O_5 when $x < 0.25$ with Q^3 being the predominant structure, and for this reason they are known as highly reactive glasses. Metaphosphate glasses are formed when the cation content (x) is little higher which is equal to 0.5. As a result of that, less bridging oxygens are present and the oxygen to phosphate ratio (O/P) = 3. Metaphosphate glass structure is usually Q^2 because there are less bridging oxygens linked to the long phosphate chain. The addition of more modifying oxides modifies glass structure from type Q^2 to Q^1 where there are more element oxides preventing the phosphate bridging resulting in the polyphosphate glass. Polyphosphate glasses have $x > 0.5$ and $O/P > 3$.

Further increasing of x content of cation oxide to the level of 0.67 yields in pyrophosphate glasses formation with O/P = 3.5, predominantly having Q^1 structure. Orthophosphate is characterized by higher x content (x = 0.75) and (O/P > 3.5) with mainly Q^0 network structure (Figure 1.5) (Brow, 2000, Knowles, 2003).

P_2O_5+ <1M_2O ⟶ Ultraphosphate (Q^3)

P_2O_5+1 M_2O ⟶ Metaphosphate /polyphosphate (Q^2)

P_2O_5+1-2 M_2O ⟶ Pyrophosphate (Q^1)

P_2O_5+ 3 M_2O ⟶ Orthophosphate (Q^0)

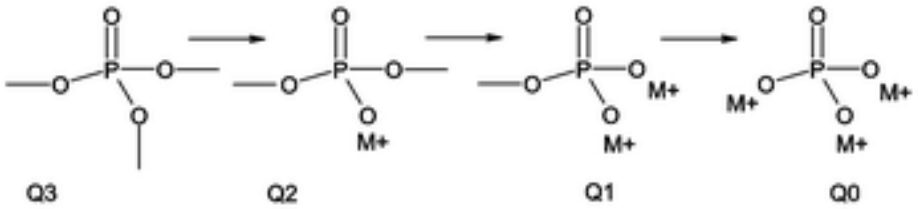

Figure 1-5 Effect of monovalent ion addition to P_2O_5 network. Reprinted from the journal of materials Chemistry, volume 13, issue10, (Knowles, 2003). Phosphate-based glasses for biomedical applications, page 2395-2401 with the permission of Elsevier.

With this variation in network structure, negative solubility property and hygroscopicity of the ultraphosphate glasses can be modified to obtain appropriate solubility rate by adding other metal oxides to increase the durability and control the degradation rate which can make the end product applicable in tissue engineering applications (Wazer, 1950, Brow et al., 1990).

1.3.3 Glass synthesis

1.3.3.1 Melt quenching

Preparation of phosphate glass by this technique firstly requires melting the elements oxides to the temperature exceeding the melting point temperature of phosphate (P_2O_5), the melted phosphates will eventually flux the other glass components and aid in their melting. This step should be followed by either pouring (quenching) the molten glass onto a cold surface or in graphite moulds. Apart from quenching glass onto a cooled surface or moulds, there is another method in which the glass will be quenched in water; this is called fritting. The fritting technique is used when the precursors are not hygroscopic in nature (such as phosphate glass) and when the glass may be needed to be produced as beads or small fragments (Kaur et al., 2016) .

Amorphous glass production is performed by rapid cooling of the molten glass to a temperature below the glass transition temperature. This is done to pass the glass crystallisation point and ensure that the glass is crystal free. The glass transition temperature is the temperature of which the glass solid starts to behave like a viscoelastic solid. The gradual cooling of a molten glass to any temperature below the melting temperature (Tm) would normally result in crystals formation with a decrease in enthalpy. As the temperature declines further, more crystals will be formed and there will be a highly viscous mixture. While if there is a rapid decrease in glass temperature at or around the eutectic point temperature, temperature less than Tg (glass transition), the liquid will generally be highly cooled and transformed directly

from a liquid state to a solid state without passing through the crystallisation phase (Figure 1.6) (Shelby, 1997).

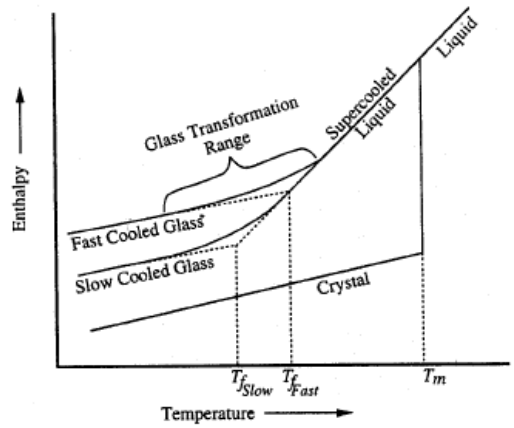

Figure 1-6 The effect of temperature on the enthalpy (or volume) of a glass forming melt. Reprinted from Introduction to Glass Science and Technology (Shelby, 1997).

1.3.3.2 Sol-Gel

The sol-gel technique is a method used to produce glass without using high temperatures that are used in the conventional melt quenching technique. Glass can be produced in this procedure in nanometre or micrometre sized particles that can be used as drug carrier for drug delivery application. Another property that encourages its use in drug delivery applications is that its relatively low processing temperatures may allow some therapeutic molecules to be included during processing (Owens et al., 2016).

Sol-gel is a multistep procedure that starts initially with the mixing of metallic precursors with alkoxide precursors. The next step includes the hydrolysis of the whole precursors using deionised water. As a result, the hydrolysis of (for example) silicon alkoxide, silanol groups will be formed (equation 1). This will be followed by silanol groups bonding with each other to form silica network

Si-O-Si via a process called polycondensation where the water is removed as a by-product resulting in sol formation (equation 2)(Kaur et al., 2016).

$$Si(OR)_4 + 4\,H_2O \longrightarrow Si(OH)_4 + 4\,R(OH) \quad \text{.....1}$$

$$Si(OH)_4 + Si(OH)_4 \longrightarrow Si(O)_3 + H_2O \quad \text{.....2}$$

Gelation is the next step after sol formation where there will be extra condensation and further networking and cross- linking between silica and colloid molecules. In the gelation process, there is an increase in viscosity and the material starts to act as an elastic solid (Brinker et al., 1985). The next step is aging of the gel or synergesis, and this involves a decrease of porosity and strengthening of gel because of continuous polycondensation. Hydrothermal treatment can accelerate this process. The ageing phase has a prominent effect on the physical properties such as porosity and mechanical properties of sol gel (Hench and West, 1990).

1.3.3.3 Phosphate glass microspheres

The use of the glass in biomedical applications necessitates production with specific features that can fulfil the application requirements. Many studies were conducted on glass microspheres to assess its potential for use in various biomedical applications such as drug and protein delivery, tumour therapy, and as bone repair materials (Kawashita et al., 2003, Kawashita, 2005).

The procedure by which glass microspheres are produced is called spheriodisation which is the production of glass particles in spherical shape

via the application of surface tension forces to the molten glass (Huang, 1992, White and Day, 1994).

Although many studies were performed to design the spheriodisation apparatus, the main idea behind it is the presence of a high temperature flame source that can be used for particle heating. Also, this procedure required the presence of a collector for collecting all the spheroidal shaped particles along their path through the flame. Various types of flame source can be utilised such as: gas/oxygen with acetylene, radio frequency based plasma flame (Gu et al., 2004, Cacaina et al., 2006, Cacaina et al., 2008, Sene et al., 2008). Others used other sources of heat (Methylacetylene-propadiene propane (MAPP) cylinder) for production of titanium based phosphate glasses because of its high flame temperature of 2925°C in air (Lakhkar et al., 2012). A vertical tubular electric furnace may be used also for the microspheres manufacturing process, where the powder particles released at the top end of the furnace are altered into microspheres as they fall through the furnace under the effect of gravity (Martinelli et al., 2010). The selection of the temperature source and the type depends mainly on the precursor's particle size; high temperatures may be needed to spheroidise larger particles size.

The particles are usually introduced to the flame bath either manually or by automated feeding assembly. After having been spheriodised, the microspheres are collected in containers. However there are also other procedures to produce microspheres by sol gel (Park et al., 2013a), and this

procedure is more suitable for silicate glasses more than phosphate glasses because of both the tetraethyl orthosilicate (TEOS) or the aminopropyel triethoxy silicate (APTES) that is used as silicate precursor to produce porous and hollow microspheres in the sol gel polycondensation (Wu et al., 2010, Poorbaygi et al., 2011, Wu et al., 2011). The flame spheriodisation process however tends to produce mainly non-porous solid microspheres.

1.3.4 Phosphate glass structural analysis

1.3.4.1 X-ray Diffraction

X-ray diffraction is a useful technique that affords valuable information about the atomic and molecular structure of solids. This technique works by investigating the interaction between X-rays and a solid substance. When a focused x-ray beam hits any sample at a specific wavelength, electrons surrounding solid atoms will start to oscillate at a wave length equal to the beam wavelength causing further secondary waves. These secondary waves usually cancel each other out especially if they were not arranged in a specific manner. However, if these atoms are arranged in phase or in a repeated manner, secondary waves will be added to each other producing scattered X-ray waves that may be emitted from the sample again to be detected by the device in the shape of well-defined peaks. The beams that are detected are called a ‘diffraction pattern’ and serve as a fingerprint of the solid sample. This usually happens in case of a crystalline substance because each crystalline substance has a unique diffraction pattern (Warren, 1969).

Glasses are amorphous substances which means that their compositional atoms are arranged in randomly. As a result, glass X-ray diffraction patterns do not usually show sharp peaks. They usually exhibit a broad peak pattern and this may be a good method to investigate the success of amorphous glass production (Dias et al., 2005).

1.3.5 Phosphate glass degradation and Ion release

Glass degradation is an important property of phosphate glasses enabling this type of glass to act as a good choice for biomaterial applications including bone tissue engineering. This property may permit glass to work primarily as a temporary device or scaffold for bone cells attachment with controlled release of therapeutic ions. Although many of these ions are proven to play a positive role in bone stasis, their release is mainly related to the chemistry of the glass composition. For this reason many attempts were made to find the appropriate composition with the most preferred ion release rate (Knowles, 2003).

Generally, mass degradation and ion release start as soon as phosphate glass is immersed in liquid, but this degradation is varied according to glass composition. Commonly, both mass degradation (weight loss) and ions release follow a linear trend and they have direct relation between them (Franks et al., 2000, Navarro et al., 2003, Brauer et al., 2006, Khor et al., 2011). This relatively linear pattern of degradation and ion release suggests the benefit of phosphates glass over their silicate peers because of the sustainability of the release over time.

Gao *et al* (2004) suggested that degradation is a two-phase procedure; the first stage is an initial slow degradation while the second is called as subsequent uniform degradation stage. The first stage involves the initial diffusion of H_2O molecules into the glass surface while the second phase involves the release of molecules from the hydrated surface which will then seep into the surrounding medium. The change between these two phases are governed by internal and external factors (Gao et al., 2004).

Bunker *et al* (1984) hypothesised that the internal factors involve glass composition and the external ones involve solution related factors such as: pH, solution temperature, saturation of solution and surface area to volume ratio. These external factors play an important role in glass degradation, for example, while a higher degradation rate is more related to acidic solutions and higher temperatures and vice versa, lower degradation rates occur in highly saturated solutions or when there is a low ratio of glass surface exposed to the solubilising medium. Generally. There are three chemical reactions that are related to glass degradation: (1) acid-base reactions, controlled by pH at the outer surface of glass, which help in the disruption of the glass ionic chains; (2) hydrolysis reactions that includes the breakage of the P-O-P bonds, damaging and changing the glass network by breaking the high phosphate glass to the smaller one of $PO4^{3-}$ ions and (3) hydration reactions that involve the incorporation of hydroxyl groups to phosphate molecules in a stage opposite to that of hydrolysis reactions (Bunker et al., 1984).

Ions released from phosphate glasses includes the release of all its compositional ions including the anions and cations. Anions include the phosphate groups that constitute the network of the glass whereas the cations include all the other metal oxides that may modify the glass compositions. When phosphate ions cleaved from glass because of hydrolysis, they may occur in various compositions and morphology ranging from the commonly present simple phosphate molecules as (PO_4^{3-}) ions to the linear phosphates such as pyrophosphate ($P_2O_7^{4-}$) and tripolyphosphate ($P_3O_{10}^{4-}$) to the cyclic species such as cyclic trimetaphosphate ($P_3O_9^{4-}$) and ending with the highly phosphate species (have more than four molecules of phosphate) (Ahmed et al., 2005b). Although ion chromotgraphy techniques are used commonly to assess the concentration release of different phosphates ions in glass, higher phosphates ions (higher than $P_3O_{10}^{4-}$) were not assessed by this method because standard compounds were not available to allow calibration (Figure 1.7) (Baluyot and Hartford, 1996, Lakhkar et al., 2013).

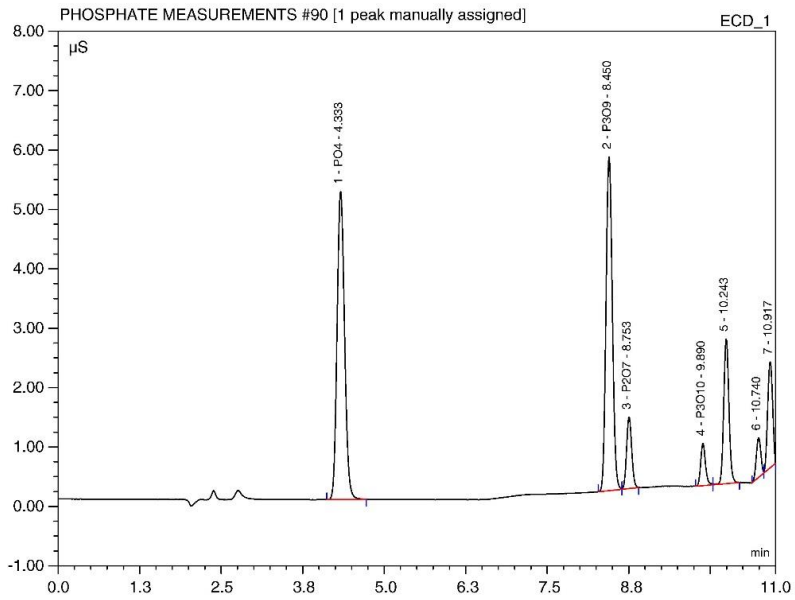

Figure 1-7 Example of an anion chromatogram for phosphate species collected using a Dionex ICS2500 system, showing the presence of PO_4^{3-}, $P_2O_7^{4-}$, $P_3O_9^{3-}$ and $P_3O_{10}^{5-}$ and higher phosphates. Reprinted from the journal of Advanced Drug Delivery Reviews, volume 65, issue 4 (Lakhkar et al., 2013). Bone formation controlled by biologically relevant inorganic ions: Role and controlled delivery from phosphate-based glasses. page 405-420. With the permission of Elsevier.

Network modifier and intermediate oxide content in ternary phosphate glasses also play an important role in controlling phosphate release, this role may be variant according to the element oxides themselves. It was found that increasing CaO content in glass can enhance the cross linkage among phosphate molecules in glass and resulting in reducing the mass loss and ions released too (Ahmed et al., 2005a).

Also, adding other oxides such as gallium and titanium which have valency of +3 and +4 had the same effect of reducing the degradation rate and ions release (Abou Neel et al., 2008d, Valappil et al., 2008). Conversely, adding some divalents oxides to the ternary glass system may not show the same

pattern or trend as that for more higher +3 valency atoms. For example, adding ZnO in different ratios to the tertiary P_2O_5–CaO–Na_2O glass did not show significant effects on phosphates ions release or degradation rates and the same was seen for SrO to the same tertiary glass (Salih et al., 2007, Abou Neel et al., 2008b). This is due to the ZnO or SrO being added at the expense of CaO and so there is little change in the overall charge of the structure.

Concerning other ions released from phosphate glasses such as Na^+ and Ca^{2+}, it was found that Na^+ release is inversely related to CaO content especially in ternary P_2O_5–CaO–Na_2O glasses systems having P_2O_5 at a ratio between 50-55 Mol%. This can be explained as any addition of Na_2O content at the expense of CaO to the glass may lead to decreased glass connectivity and increased glass degradation(Ahmed et al., 2004a, Ahmed et al., 2004b, Ahmed et al., 2005a).

Previous studies showed that there is a direct relationship between CaO and Ca^{2+} ion release in ternary P_2O_5–CaO–Na_2O glasses containing 55 mol% of P_2O_5 (Ahmed et al., 2005a). The inclusion of 2+ charge oxides, e.g. MgO, SrO or ZnO with quaternary phosphate glasses as substitution to CaO or Na_2O may affect glass ions release. As a result of this substitution, other factors will control the degradation which are related to the atom, such as ionic radius, electronegativity, bond lengths. For example, the addition of 2+ charge oxides such as SrO or ZnO to the titanium containing quaternary P_2O_5–CaO–Na_2O-TiO_2 glass may change titanium release causing an

enhancement in titanium ion release with the SrO or ZnO as these atoms can disrupt quaternary glass network making it closer to that of ternary P_2O_5–CaO–Na_2O (Abou Neel et al., 2009a, Lakhkar et al., 2011).

1.3.6 Phosphate glass biocompatibility

Some phosphate-based glasses have been studied previously to assess their biocompatibility.

Generally, there are three methods of examining phosphate-based glass biocompatibility: (a) *in vitro* including immersing the produced phosphate glass in artificial environment liquids, for example : citric acid or simulated biological fluid (SBF); (b) *in vitro* involving cell culture assessment by examining viability, proliferation, adhesion, differentiation and cytotoxicity; (c) *in vivo* including implantation of the produced glass in animal models and subsequent histological studies after sacrificing the animal.

Regarding the first method, the most popular method is by immersing the phosphate glass in SBF. SBF is basically a mixture of Na^+, K^+, Mg^{2+}, Ca^{2+}, Cl^-, HCO^{3-}, HPO_4^{2-}, and SO_4^{2-} ions in distilled water at specific concentrations nearly equivalent to those in human plasma. The bioactivity assessment is usually done via qualitative and quantitative estimation of hydroxyapatite crystal formation on the glass surface exposed to the fluid.

Many previous studies investigated the immersion of four different compositions of titanium contained phosphate glass in SBF. These studies reported the absence of apatite layer in all the samples after incubation for

14 days at 37°C (Abou Neel E et al., 2007, ElBatal et al., 2009, Lucacel et al., 2010). Even though phosphate-based glass does not form apatite which would be considered as a measure of lacking bioactivity, these materials may attach directly to bone tissues even without hydroxyl apatite formation. Therefore, this attaching ability can give them the biocompatibility which is needed to be studied further by doing cell culture studies (Kokubo and Takadama, 2006, Lee et al., 2006).

The second approach which is *in vitro* cell culture studies is a common methodology in material biocompatibility assessment. This approach involves seeding cells on the surface of the material, or to extracts form the biomaterial under test, followed by different biological tests, hence, it can give a significant amount of quantitative and qualitative information regarding the potential of the material to affect short term and long term cellular events. Two types of cells may be used *in vitro* testing according to their origin; (a) primary cells which are cells isolated directly from human or animal tissue having a limited useful life span of 10-100 days after the initial formation of cells, and (b) cell lines which are the cells that are tumorigenic in nature and have the stability to live for a long period of time for cell culture uses. Cell lines are the most commonly used because of their stability, long term, in comparison to the primary cells (Ratner, 2004).

Many studies were done to assess the cellular effects of different phosphate glass compositions. Uo *et al* (1998) investigated the cytotoxicity of different compositions of ternary P_2O_5–Na_2O–CaO glasses on human pulp cells, and

the results revealed that cytotoxicity is clearly-correlated to decreasing CaO content (Uo et al., 1998). Salih *et al* (2000) also assessed tertiary calcium/sodium phosphate glass. This study assessed the biological reaction of seeded osteosarcoma MG63 cells on phosphate glass by firstly performing MTT metabolic assay and secondly an ELISA to assess the expression of BSP, ON and fibronectin (FN). The results were similar to that of Uo et al in which lower calcium content enhanced glass degradation and caused inhibition in both cellular growth and bone antigens expression (Salih et al., 2000). However, these studies were done for short periods of times that did not exceed 1 week. Conversely, the work performed later by Gough *et al (*2003) assessed the long-term effects of calcium/sodium phosphate glasses on seeded colony forming cells CFCs. This study extended out to 28 days to fully understand all the stages of the osteoblast differentiation cycle on phosphate glass by detection of specific markers secreted during different stages of differentiation (Gough et al., 2003) .

Other studies were done to test quaternary glass systems, especially zinc, strontium and titanium glass compositions to assess their effect on bone cells. Zinc phosphates glass studies showed many variations in terms of its effect on bone cells. In one study, human osteoblasts cells (HOB) were seeded on different zinc containing phosphate glass discs. This was followed by cell attachment and cell proliferation assessment showing that zinc incorporation in glass may have a positive role in both cellular attachment and proliferation (Salih et al., 2007). These results were confirmed later on in

other studies that examined the addition of different zinc oxide contents to silicate based glass that showed adding zinc oxide at 3.9 mol% can improve cellular attachment, whereas adding it at more than 7.8 mol% proportion may affect negatively on cellular attachment (Lusvardi et al., 2008). Other studies explained that adding zinc oxide to phosphate glass in higher proportions (more than 10 mol%) may lead to negative cytotoxic effects on MG63 cells (Abou Neel et al., 2008c). Later attempts aimed to evaluate the outcome of zinc oxide addition to bioactive silicate glass scaffolds containing Na_2O, K_2O, MgO, CaO, B_2O_3, TiO_2, P_2O_5 and SiO_2 on the proliferation and osteogenesis of human adipose stem cells (hASCs). The results revealed that zinc oxide addition had no significant effect on DNA content, alkaline phosphatase and osteopontin concentration (Haimi et al., 2009). Addition of zinc oxide to sol gel silicate prepared glass was evaluated also and showed that zinc addition can enhance alkaline phosphatase activity of rat calvarium-derived osteoblasts (Badr-Mohammadi et al., 2014).

Regarding strontium phosphate-based glasses, one trial investigated the cellular effects of strontium oxide doping into phosphate glass on Human osteosarcoma cells (HOS). It was found that adding strontium oxide can enhance cell attachment and also change cell morphology from round to flat (Abou Neel et al., 2008b). Other studies done by Lakhkar and his colleagues, found that increasing strontium oxide content in phosphate glass may lead to better biological effect on MG63 in terms of cellular growth (Lakhkar et al., 2009). Another experiment performed by Massera *et al* aimed to evaluate the

effect of adding strontium to both phosphate and silicate glass separately on human gingival fibroblast. This study revealed that adding strontium to any of these glass systems may have the potential effect of increasing cell growth and that cells seeded on the free strontium phosphate glass were dead at day 7 (Massera et al., 2015).

Concerning titanium oxides, Navarro *et al* (2003) evaluated the effect of changing titanium oxides content on toxicity, adhesion and proliferation activity of human skin fibroblasts that were seeded on 44.5 P_2O_5–44.5CaO–(11 – *x*)Na_2O–TiO_2 (*x* = 0 and 5 mol%) (Navarro et al., 2003). The toxicity data showed that adding titanium oxides at 5 mol% will decrease glass solubility resulting in enhancing cell viability. Whereas titanium dioxide free samples had greater solubility. Conversely, the highly soluble titanium dioxide free glass showed better cell adhesion ability. The explanation of these contrary results was unclear and may be related to glass composition and solubility.

Other comprehensive results concluded that adding TiO_2 to phosphate glass may improve the physical network of glass, hence, decreasing glass solubility resulting in more favourable cellular effects (Brauer et al., 2006).

Later studies were carried out to investigate the biocompatibility of adding TiO_2 to the phosphate glass by using different *in vitro* cell biology methodologies. One of these studies was interested in studying glass discs that had the composition of 50 P_2O_5–(20 – *x*)Na_2O–30CaO–*x*TiO_2 (x = 0, 1, 3 and 5 mol%), and using MG63 human osteosarcoma cells for seeding (Abou

Neel and Knowles, 2008). These cells were cultured on the glass discs for a 7 days period which were investigated later with confocal microscopy and scanning electron microscopy (SEM) to evaluate cell viability and cell attachment. It was found that the best results in terms of both vitality and attachment were detected in glasses containing 3 and 5 mol% TiO_2. The explanation was similar to that of (Brauer et al., 2006) where increasing biocompatibility may be due to decreased degradation rate of titanium dioxide containing phosphate glasses which was further confirmed by DTA analysis. Another study aimed to increase TiO_2 content in phosphate glass to enhance biocompatibility. This study revealed the same results in which glass with TiO_2 showed the most favourable results compared to TiO_2-free glass. This study revealed that further additions of TiO_2 at 10 mol% to 15 mol% does not show any significant further changes in biological results (Abou Neel et al., 2008d). Another study aimed to investigate the biocompatibility of titanium phosphate glass beads on MG63 cells. Glass beads were produced in three compositions as 50 P_2O_5–40CaO–(10-x) – Na_2O–xTiO_2, where x = 3, 5 and 7mol % to investigate the optimum concentration of titanium dioxide by using Alamar blue assay. The results demonstrated that incorporation of 5 mol% TiO_2 may lead to the most favourable outcomes while glass containing 7 mol% TiO_2 did not exhibit any significant improvement compared to the glass containing 5 mol%TiO_2 (Lakhkar et al., 2012).

The *in vivo* implantation approach of glass has not been studied extensively because these studies face a lot of challenges and difficulties with the regulations and ethical approvals. These studies generally involved examination of implanted glass granules in bony defects of either rat or rabbit subjects. This step was usually followed by histological examinations after specified time points by using either light microscopy or polarized microscopy.

Ito *et al* (2002) assessed the effect of adding zinc calcium phosphate glass ceramics into the femora of rabbit where zinc content was different. Four weeks after grafting, femora were histologically studied showing that zinc addition can encourage bone formation area by 51% in comparison to the free zinc composites (Ito et al., 2002). Later on, Dias *et al* assessed the implantation of two different glass compositions granules (45CaO–45 P_2O_5–5MgO–5K_2O and 45CaO–37P_2O_5–5MgO–13TiO_2) into rabbit tibiae. This study showed that that glass solubility and degradation may influence the outcomes within *in vivo* study; the former titanium dioxide free glass composition degraded much faster compared to the phosphate glass containing titanium dioxide. Therefore, the first glass composition granules caused empty spaces in the newly formed bone, whereas the second composition was surrounded completely by bone (Dias et al., 2006). Other studies included the implantation of various compositional quaternary P_2O_5–Na_2O–CaO–TiO_2 glasses in rabbit models. This study revealed that the incorporation of 0.5 mol% TiO_2 in the glass might result in the best bone cell

growth, whereas adding a higher content of titanium dioxide may be associated with reduced bioactivity (Monem et al., 2008). These results were quite similar to Abu Neel *et al* (2007) study that examined the implantation of different compositions of titanium phosphate particles in the calvaria of rats. It was found that when the TiO_2 content was 5 mol%, bone formation was more significant (Abou Neel E et al., 2007).

1.4 Bone scaffolds

1.4.1 Scaffolds requirements

Scaffolds are materials that are designed and engineered in a specific way so as they can fulfil the biological and physical requirements of the repaired organ. The use of biomaterials to produce a bone scaffold is not a simple stage. It can be considered that there are three various generations or stages. The difference among these generations of scaffolds is explained as technical, where many modifications and adjustments were made to improve the scaffold properties (Navarro et al., 2008). The first generation was mainly concerned about using inert materials having physical properties matching that of the replaced bone. Metals such as titanium and stainless steel, ceramics and polymers such as silicone rubber, polypropylene, and polymethylmethacrylate were examples of the first generation of materials. One of the drawbacks in this generation was the formation of fibrous tissue in the interface area between the implant and body tissue. This fibrous tissue is formed as an immune response of the body to the implants which occurs as an inflammation process of body ending in shielding the implant from the surrounding tissue by fibrous wall (Morais et al., 2010).

The second generation was introduced to overcome the undesirable immune reaction in the previous generation. In this generation, bone graft substitutes were modified by for example making them with either bioactive or biodegradable materials. The structure was by using materials designed to encourage mineralisation such as HA or TCP or by bioglass. The other type

of implant was by making the scaffolds from biodegradable materials that have degradation rate similar to that of the normal healing process. For example, making the implants from polymers such as polylactide, poly(*ε*-caprolactone), and polyglycolide can offer a controlled material degradation (Polo-Corrales et al., 2014).

According to Hench and Polak, the third-generation scaffold was aimed at enhancing the physiological cellular response at the molecular level. This was proposed by creating a scaffold that has mechanical and spatial features that facilitates the recruitment of progenitor cells and at the same time enhancing these cells to proliferate and differentiate to other types of cells by incorporation of some molecules that are known to be growth activators (Hench and Polak, 2002). Hence theses scaffolds should acquire some of the following properties (Amini et al., 2012):-

1-Mechanical integrity, structure and mechanotransduction: one of the most important scaffold features is to offer a transient mechanical strength in the replaced bone site that permits for bone repair and regeneration and fulfil the physical needs of the surrounding bone during the healing process (Bauer and Muschler, 2000). The normal mechanical properties of bone differs between cortical and cancellous bone; it was found that the compressive strength of cortical bone is between 90 and 230 MPa (tensile strength is between 90 to 190 MPa), while the cancellous bone compressive strength ranges between 2 and 45 MPa (An and Draughn, 1999). These scaffolds should possess mechanical properties similar or close to that of repaired

bone. Apart from mechanical integrity, scaffold should be produced in a way that permits for mechanical transduction. Mechanical transduction can be considered as an osteoinductive factor controlling cell response and enhancing cell differentiation through the mechanical flow of the fluid through the whole scaffold. It was determined that the optimum scaffold permeability that can lead to successful implant in regard to vascularisation and mineralisation is about 3×10^{-11} m^2 (Jones et al., 2009). These mechanical properties should be varied according to the replacement site to prevent any complication such as stress shielding and subsequent refracture. These mechanical properties are generally controlled by scaffold composition and structure. For example, HA and TCP have elastic modulus and compressive strength similar to that of the compact bone, but they are brittle. On the other hand, polymers mechanical properties resemble those of human cancellous bone. for this reason, producing composite scaffolds that have both bioceramics and polymers can give the required properties of these two materials in one scaffold (Rezwan et al., 2006). Other methods can be used to enhance polymer mechanical properties, for example by adding carbon nanotubes (CNT), bioglass particles or alloy particles (Mikael and Nukavarapu, 2011, Wong et al., 2010).

2-Scaffold porosity: porosity is considered as an important factor in successful scaffold production. Its role is mainly linked to the scaffold osteoconductivity or permeability as it will offer the scaffold internal spaces that permits for cell growth, nutrient flow, vascularisation and spatial cellular

organization (Zeltinger et al., 2001). Hing (2005) stated that scaffold permeability is mainly dependent on pore interconnection size which is basically the net result of both pore size and the degree of scaffold porosity (porosity percentage) (Hing, 2005).

However, there is no clear consensus concerning the ultimate porosity requirements such as (porosity percentage, pore size), and many studies were performed to ascertain the appropriate dimensions. One study was performed on porous hydroxyapatite and revealed that a scaffold with pore size between 300-400 µm had better results on enhancing the rate of bone formation (Tsuruga et al., 1997). Other later studies were done on glass scaffolds in which they tested different scaffolds with different pore sizes and with different percentage of porosities. These studies showed that it is recommended for the scaffold to have a pore size of about 100-500 µm and suggested that a porosity that is more than 40% may be applied in bone tissue engineering (Yuan et al., 2001, Sepulveda et al., 2002, El-Ghannam, 2004). It is believed that bone graft substitutes should have two important types of pores sizes: microporous (<5 µm pores) and macroporous (>100 µm pores). Although both of them are important for the biodegradation (bioresorbility) of the material, the latter type is more required for appropriate osteoconductivity (Hannink and Arts, 2011). Concerning porosity percentage, it was found that increasing scaffold porosity may have a potential effect for bone growth. A previous study was done by implanting silicate bioceramics with different porosities (22%, 36% and 47%) in an ovine

model and assessing their ability to enhance bone growth, the outcome showed that better bone growth was related with the highest porosity (Chan et al., 2012).

Generally, controlling pore size and porosity for scaffolds is an imperative factor. Concerning pore size, it is more preferable to have larger than 100 µm pores sizes as this will enhance bone formation while the unmineralised or fibrous tissues may interpose into the small size pores (10-100 µm), these results are because large size pores may permit better vascularisation and nutrient delivery while for porosity percentage it was also believed that there is an indirect relationship between porosity and mechanical properties; increasing porosity by 10-20% can decrease the mechanical features by 4 times, for this reason it is not advisable to prepare high degradation rate ceramics with 90% porosity because this may compromise the mechanical integrity for the scaffold (Karageorgiou and Kaplan, 2005).

3. Nano-Featured Scaffolds: Scaffolds are a model of extracellular matrix (ECM) that is intended to support the defective bone. It is known that normal bone cells interact usually with osteoinduction related factors such as proteins like collagen type 1 and mineral nanoparticles such as HA which are components of the ECM. As a result of that, it is highly favourable to include nanoparticles within the scaffold. These may add nanotopographical features to an implant material and enhance osteoinduction and osteointegration properties (Laurencin et al., 2009, Harvey et al., 2010). Studies have showed that scaffold surface modification by nanoparticles boosts an osteoblasts

ability to adhere, differentiate and secrete many osteogenic markers such as alkaline phosphatase and osteocalcin (Smith et al., 2010).

1.4.2 Fabrication techniques of scaffolds for bone tissue engineering

1.4.2.1 Bioactive glass scaffold techniques

1.4.2.1.1 Sol –gel process

It is the process entitling the production of inorganic bioglass scaffold by using the sol -gel process. In this process, glass precursors are mixed with alkoxides such as Tetraethylortho-silicate (TEOS) or triethylphosphate (TEP) with the addition of surfactant and catalyst as a gelling agent. As the gelling point of this mixture is approached, the whole mixture is cast into moulds, then aged at (60°C), dried (130°C) and thermally stabilised (600°C)(Sepulveda et al., 2002). As a result of this technique, porous scaffolds can be produced with different pore sizes as mesopores (2-50nm) and macropores (10-500 µm) (Chen et al., 2008a).

Many studies were performed on these types of scaffolds, and the results were promising as they were found to promote cell proliferation, metabolism and mineralisation activities (Gough et al., 2004, Solgi et al., 2017).

1.4.2.1.2 Foam replica technique

This technique involves the use of custom made polymer as a template (green body) for the bioglass. The polymer template is custom made from polyurethane with desired foamy internal macrostructure. The template is immersed in slurry made by bioglass powder. After the immersion process,

the slurry dries and infiltrates between the polymer forming an homogenous layer of bioglass coating the polymer framework. This will be followed by burning the polymer using high temperature (>450°C) leaving empty sites of the burned polymer that represent the scaffold pores. After the polymer removal the glass is sintered to the desired density (Figure 1-8)(Chen et al., 2006).

Chen *et al* (2008) stated that this technique has many advantages over other methods of scaffold manufacturing such as the ability to form highly porous scaffolds (>90%) in different irregular shapes by using non-toxic chemicals (Chen et al., 2008a). The main drawback of scaffolds synthesised by this techniques is the lack of mechanical properties that limits their application to be used only in the repair of low-load bone defects (Fu et al., 2011).

In vitro studies displayed that these scaffold macrostructure may enhance cellular penetration inside the scaffold construct and promote cellular metabolic responses (Chen et al., 2008b).

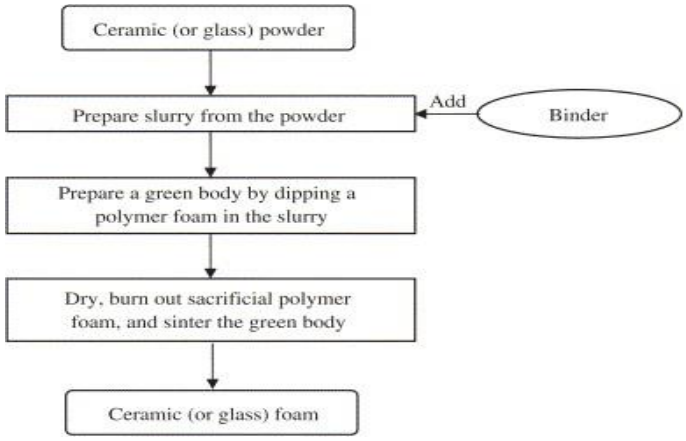

Figure 1-8 Foam replica technique. Reprinted from the journal of Biomaterial, volume 27, (Chen et al 2006) 45S5 Bioglass-derived glass–ceramic scaffolds for bone tissue engineering, page 2414-2425

1.4.2.1.3 Polymer coated bioceramics

This technique involves coating of bioceramics (HA, Bioactive glasses) by dipping these ceramics in biodegradable polymer solution for specific time to improve the mechanical properties of the porous bioceramics (Kim et al., 2005a). Apart from enhancing the strength of material, the coating material may enhance the surface bioactivity (Mohamad Yunos et al., 2008). A recent study has suggested that coating bioactive glasses (BAG) scaffolds designed for bone repair applications with polymer may enhance the expression of vascular endothelial growth factor (VEGF) (Björkenheim et al., 2017). Xiao *et al* (2017) examined material strength of polymethylacrylate (PMMA) polymer -coated silicate bioglass and found that the strength of the coated bioceramic was significantly improved in comparison with the non-coated samples (Xiao et al., 2017).

1.4.2.2 Polymer scaffolds techniques

1.4.2.2.1 Solvent casting and particle leaching

This technique entitles dissolving polymer alone or with ceramic granules in organic solvent, water soluble salts are added also to the polymer solution. Then the whole polymer solution is casted in fabricated 3D moulds and left for a time to allow for solvent evaporation. After the solvent is evaporated, salt particles are leached out forming pores in their position (Liu and Ma, 2004). Rezwan *et al* (2006) stated that there are main drawbacks related to this technique which are related to the limitation of producing scaffolds in different shapes, the possibility of retention of some toxic particles of solvent

within the polymer that may cause denaturation of proteins (Rezwan et al., 2006). Parsad *et al* (2017) stated that porosity of scaffolds manufactured in this procedure are mainly dependent on the shape and sizes of the leached particles and there is possibility of retention of some particles within the scaffold that may affect the pores interconnectivity. Therefore, most of scaffolds produced in this technique are limited up to 3-4mm in thickness (Prasad et al., 2017).

1.4.2.2.2 Thermally induced phase separation (TIPS)/ freeze casting

This technique has been used first to produce porous polymer scaffolds. In this technique, the polymer is dissolved by solvent at specific temperature, inorganic ceramic can be added also to the solution. After that, the whole mixture is sonicated in a flask and then exposed to low temperature using liquid nitrogen for a specific time. As a result of that, the solution is crystallised (solidified). This will be followed by transferring the whole frozen construct into a cooling bath that is connected to a vacuum pump to aid in solvent sublimation. The space that was taken by solvent crystals become pores (Rezwan et al., 2006).Generally the pores formed in these scaffolds are tubular in shape with variant diameter (>100 μM) with small interconnecting networks between them (≃ 10 μM). The diameter size of pores is mainly dependent on the type of polymer, solvent and the concentration of polymers(Chen et al., 2008a).

Although the main advantage of this technique is the ability to produce a scaffold with high porosity, the disadvantages relate to the produced pores

having small sizes and the produced scaffold morphology not being controlled (Prasad et al., 2017).

1.4.2.2.3 Solid freeform fabrication (SFF) (rapid prototyping)

This technique involves the use of various techniques in manufacturing the scaffolds in a layer-by-layer fashion using computer aided design (CAD) without using the conventional methods such as moulds. The produced scaffolds have predesigned structure and morphology that are modelled previously in a computer (Fu et al., 2011). The main positive aspect of this technique is that the synthesised scaffolds have complex structure and satisfactory mechanical properties. However, the drawbacks are limitation of the used polymers and the high expenses of the equipment (Prasad et al., 2017).

1.5 Carbon nanotubes (CNTs)

Since the discovery of these macromolecules in 1991 by Lijima by using the arc-discharge evaporation method (Iijima and Ichihashi, 1993), these nanotubes have attracted attention around the world. Generally they are cylindrical in shape with a few nanometres diameter and length extending from a few micrometres up to 20 cm (Ajayan et al., 2009). Their walls are formed from carbon atoms that are organized in a hexagonal shape and usually occur as two types either single walled (SWCNT) which they are formed from one cylinder or multiple walls (MWCNT) that formed from multiple cylinders that are organized inside each other. In the latter form their diameter can be up to 100 nm (Figure 1.9)(Balasubramanian and Burghard, 2005, Loos, 2015),

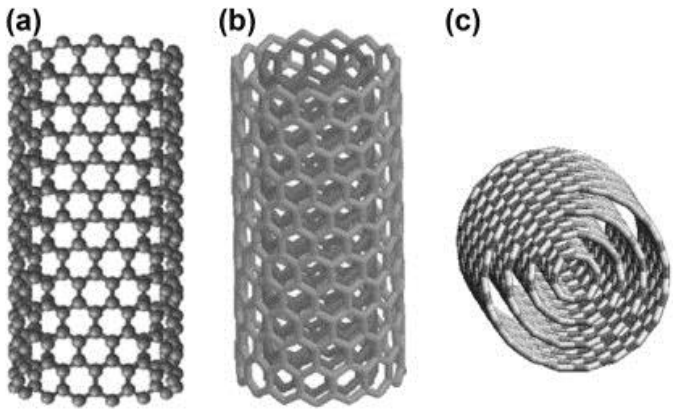

Figure 1-9 Schematic diagram of a (a) single-walled carbon nanotube, (b) double-walled carbon nanotube, and (c) multi-walled carbon nanotube. Reprinted from Carbon Nanotube Reinforced Composite (Loos, 2015). Chapter 3, Allotropes of Carbon and Carbon Nanotubes, page 76.

Carbon nanotubes can be produced by three different procedures the (i) Electric arc discharge (ii) Laser ablation and (iii) the catalytic chemical vapour

deposition (CCVD) which has a high production rate and control of the type produced (Scott, 2004, Dupuis, 2005, Farhat and Scott, 2006).

Carbon nanotubes have excellent mechanical, electrical and chemical properties because of their structural composition (Zhang and Zhang, 2017). This has encouraged many studies to test their application in biomedical fields such as the drug delivery or imaging fields (Son et al., 2016, Puett et al., 2017). Moreover, it has been identified that carbon nanotubes could form hydroxyapatite crystals on their surface when they are immersed in stimulated body fluid (SBF) and this has encouraged many studies to investigate them as a potential biomaterial in bone tissue engineering (Akasaka et al., 2006, Harrison and Atala, 2007).

A lot of work was done to produce and biologically examine carbon nanotubes and polymer composites. Luo *et al* (2017) produced and examined biodegradable composite from CNTs and polycaprolactone (PCL) polymer both *in vitro* and *in vivo* environment. The findings of this study stated that addition of CNT to PCL enhanced the mechanical properties of the polymer and led to apatite layer formation. Furthermore, the 0.5 wt/volume % CNT to polymer ratio resulted in the most acceptable results (Luo et al., 2017). Another study was also performed but with a different polymer, polyvinyl alcohol (PVA) polymer suggested that adding these nanoparticles to this polymer may enhance MG63 cell viability (Zhang et al., 2012a).

Adding CNTs to ceramics has been studied also. In one study, multiwall carbon nanotube (MWCNT) were added to a collagen and hydroxyapatite composite. Mesenchymal stem cells were seeded on this modified bone biocomposite material. The results showed that carbon nanotubes significantly enhanced the mechanical properties of the scaffold and also improved the proliferation and differentiation of the seeded stem cells (Jing et al., 2017). Other experiments intended to test a CNT scaffold both *in vitro* and *in vivo* revealed promising results for using carbon nanotube 3 D scaffold for bone repair applications (Katz and Willner, 2004, Hu et al., 2004, Tanaka et al., 2017). It has been assumed that these positive results for using CNT in bone tissue engineering field is not only because of the good mechanical properties of this material but also because CNT's tend to increase surface roughness that may enhance osteoblast adhesion and proliferation (Sinha and Yeow, 2005).

The cytotoxic effect of CNT needs to be addressed. Carbon nanotube physical and chemical features can affect their biocompatibility and result in cytotoxicity; it was found that SWCNT showed lower *in vivo*- related undesirable effects compared to MWCNT. The reason behind that is that the simple shape of SWCNT made them easily to be phagocytosed and transferred to the lymphatic while the MWCNT can form large aggregates that prevents human immune cells from processing them (Aillon et al., 2009). Other studies correlated CNT shape with cell death. CNT sharp end may act as a lance traumatising the cellular plasma membrane causing cellular death

(Hirano et al., 2008). Moreover, it was stated that the longer CNTs about (≥ 20 μm) may be more destructive and inflammatory than the short CNT (Poland et al., 2008). Other researchers correlated the chemical functionalisation of CNT with their toxicity. Non-functionalised CNT (Pristine CNT) are hydrophobic and are more susceptible to form aggregates and accumulate in different organs causing inflammatory responses. Also, it is difficult to be eliminated from human organs because of their aggregation status (Sayes et al., 2006, Aillon et al., 2009).

It has been known that the exposure to these nanoparticles may trigger cells to produce a reactive form of oxygen as a way of self-defending. Oxygen may be produced in the form of superoxide anion radicals ($O_2 \cdot^-$), hydrogen peroxide (H_2O_2) and hydroxyl radicals ($\cdot HO$), these have high redox reaction potential. This process is called oxidative stress which is considered the most likely mechanism of CNT toxicity (Pacurari et al., 2016). Veetil and Ye (2009) mentioned that cellular death caused by CNTs occurs only in the cases of exposure to high concentration of CNTs (Veetil and Ye, 2009). Many studies were performed to investigate CNT toxicity and it showed contradictory results. While some studies revealed they are highly cytotoxic and can cause reduction in cellular viability (Cui et al., 2005), other studies mentioned that CNT are biocompatible if they were used in low concentration (25 μg/ml) and for short period (not exceeding 2 hours) (Kam and Dai, 2005). However, later an *in vivo* experiment which involved long duration (more than 3 months) CNT implantation in mice showed a low toxicity effect with no apoptosis

(Yang et al., 2008a). The recent comparative study on SWCNT aimed to investigate the cytotoxic effect and biocompatibility of these nanoparticles on osteoblasts revealed that functionalised CNTs can easily be dispersed in the osteoblast cytoplasm resulting in promoting cellular activity such as the expression of collagen type 1 while the pristine type remained on the cellular periphery wall. This study showed that using CNT in concentration less than 100ug/ml does not show unwanted or harmful cellular effects (Tong et al., 2014).

1.6 Bioreactors:

These can be defined as the mechanical apparatus made to mimic the physiological and functional properties of the human body in order to enhance cell culture growth and stimulate extracellular matrix production (Obregón et al., 2017). Bioreactors should require the ability to provide cells with nutrients such as glucose and growth factors and remove all the cellular product in a continuous way at the same time. Moreover, bioreactors should be designed to work for long periods of time (3-4 months) in an aseptic and disinfected environment (Korossis et al., 2005). All the cell culture parameters such as temperature, pH, biochemical gradients and mechanical properties should be controlled over the whole period of cell culture within the bioreactor because of their important role in cell culture growth (Chen and Hu, 2006). Temperature is considered the most important factor. If it decreases below the optimum range, cellular growth will be affected negatively. Whereas if it was higher than the normal value, cellular death might occur (Taya and Kino-oka, 2011). pH is also important since any decrease in its level may cause more acidity. pH level is mainly maintained by buffering through the presence of sodium bicarbonate $NaHCO_3$ or sodium hydroxide NaOH in the culture media through the addition of CO_2 to the culture media. Hence controlling the level of CO_2 throughout the whole period of bioreactor working time will ensure suitable environmental conditions for cell growth (Birla, 2014). Mechanical stimulus is another

significant factor in bioreactors. This stimulus is presented by the shear stress that is formed due to media flow within the system. Studies have mentioned that shear stress can help in the differentiation of mesenchymal stem cells to an osteogenic lineage and also aid in bone health and maintenance through upregulation of prostaglandin and nitric oxide levels (Ng et al., 2017, Chen et al., 2017). However, there is some controversy about it, and some studies has showed the positive role of mechanical or shear stress on the cell growth while others explained that higher shear stress levels can be harmful for cell growth especially for stress sensitive cell species (Taya and Kino-oka, 2011, Korossis et al., 2005). It has been calculated previously that shear stress of 5×10^{-5} Pa can encourage bone cell proliferation whereas any shear stress above that may lead to an increase in bone markers gene expression (Porter et al., 2005). Other attempts have found that the magnitude of shear stress is affected by scaffold pore size while porosity percentage affects only the stress distribution within the scaffold (Boschetti et al., 2006). Generally, Birla (2014) mentioned that each bioreactor design should fulfil four main aspects: 1- presence of stimuli that are planned to be applied to cells to enhance their proliferation and differentiation. 2- control of environmental variables which are important for cellular growth such as pH, temperature and gaseous environment. 3- presence of sensors to screen and monitor the environmental variables. And 4- the ability to apply the stimulus protocol, for example the ability to control frequency, amplitude of stimulus and time (Birla, 2014).

Bioreactors used for bone cell culture applications can be classified according to the method of their action into four types: 1- Spinner-flask bioreactor, 2- Rotating wall vessel, 3- Wave bioreactor, 4- Perfusion bioreactor which can be subdivided into parallel plates, hollow fibers and fixed and fluidized beds (Rauh et al., 2011) .

1.6.1 Spinner bioreactors:

The design of this type of bioreactor involves the presence of multiple scaffolds which are either seeded into microcarrier or suspended by needle-supplied metal holders. These holders are suspended from the top of the flask preventing the cell culture scaffold from falling. The culture media flow is maintained by magnetic stirrer in the bottom of the flask which is stirred at the appropriate speed. Whereas oxygen and culture medium exchange take place from the top angled side arms (Figure 1.10) (Sikavitsas et al., 2002, Stich et al., 2014). Shear stress is governed by the stirring velocity. One study showed that the use of 30 rpm speed in 120ml spinner flask bioreactor has led to favourable outcomes with regard to the osteogenic differentiation (Sikavitsas et al., 2002). Other later studies tested the use of 50 rpm velocity in spinner flask and revealed the enhanced osteogenic and chondrogenic differentiation of bone marrow stem cells (Meinel et al., 2004). The formation of turbulent waves associated with fluid stirring motion may have harmful effects on cell culture and is considered as the main drawback associated with this type of bioreactors (Gooch et al., 2001). It has been suggested that

these waves may cause shear stress that is very difficult to adapt to by the cells (Taya and Kino-oka, 2011).

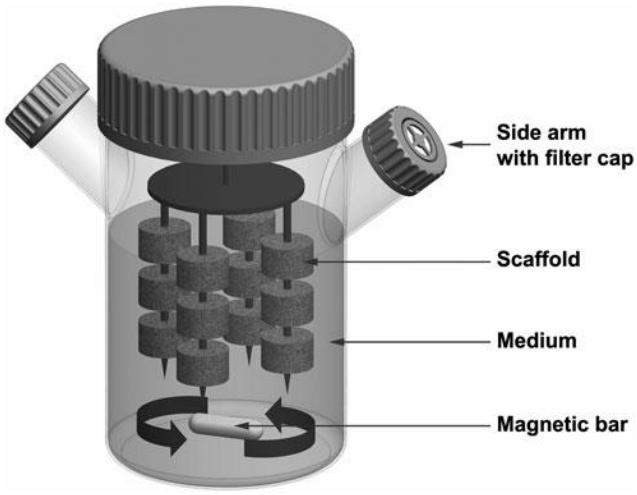

Figure 1-10 Schematic view of a spinner flask bioreactor. The cell/scaffold constructs are attached to a needle, and shear stress is applied by convection of medium. Reprinted from Tissue Engineering Part B Rev, volume 17, issue4, (Rauh et al., 2011). Bioreactor systems for bone tissue engineering, page 263-280, with the permission from Elsevier.

1.6.2 Rotating-wall vessel bioreactors (RWV)

These types of bioreactor have vessels that rotate continuously around horizontal axis in a way that prevent the scaffold from contacting the bioreactor wall. whereas the oxygen is supplied through filtered membrane (Figure 1.11) (Obregón et al., 2017). The shear stress associated with this type of bioreactor is much lower than that of other types because they cause less turbulence than that of a spinner flask bioreactor (Zhao et al., 2016). Many cellular studies were achieved by using (RWV) and showed controversial results; one study revealed that using spinner flask bioreactor for biodegradable scaffold may encourage rat marrow stromal cells to produce calcium at about 6.6 times higher than the RWV bioreactors (Sikavitsas et al., 2002). Other studies showed different results using RWV

bioreactors ended in better results than that of spinner bioreactor in regard to cellular morphology, viability and ability to form bone (Song et al., 2007).

The disadvantages related to this type of bioreactor are that they are more compatible with small size scaffolds and the possibility of scaffold collision with the vessel wall which may harm cell culture (Rauh et al., 2011).

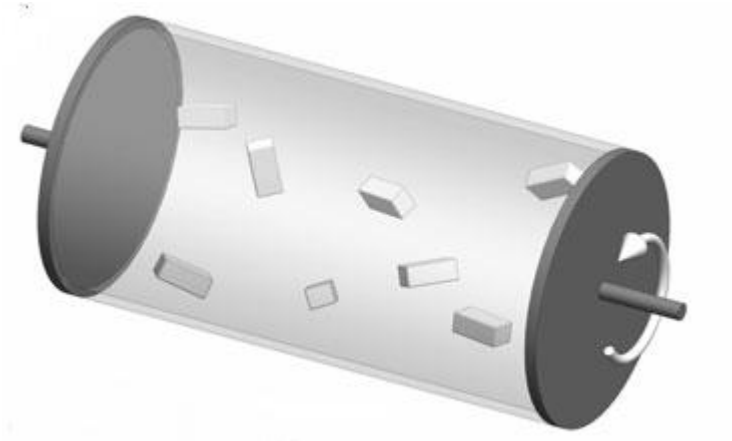

Figure 1-11 Schematic drawings of rotation-based bioreactor systems. Reprinted from Tissue Engineering Part B Rev, volume 17, issue4, (Rauh et al., 2011). Bioreactor systems for bone tissue engineering, page 263-280, with the permission from Elsevier.

1.6.3 Perfusion bioreactors

Although there are many different systems that have been produced, they share the same basic design. Most of these systems consist of media reservoir, a pump, a tubing circuit, and a perfusion cartridge where the scaffolds are packed (Yeatts and Fisher, 2011). They can be divided into direct and indirect medium perfusion. In the indirect system, scaffolds are not tightly attached to the perfusion cartilage which permits fluid to flow with less resistance and low shear stress. Whereas the direct system permits fluid to be forced through the scaffold and increasing the shear stress levels

resulting in improved cell viability and better cell enzymes expression (Figure 1.12) (Rauh et al., 2011, Volkmer et al., 2008).

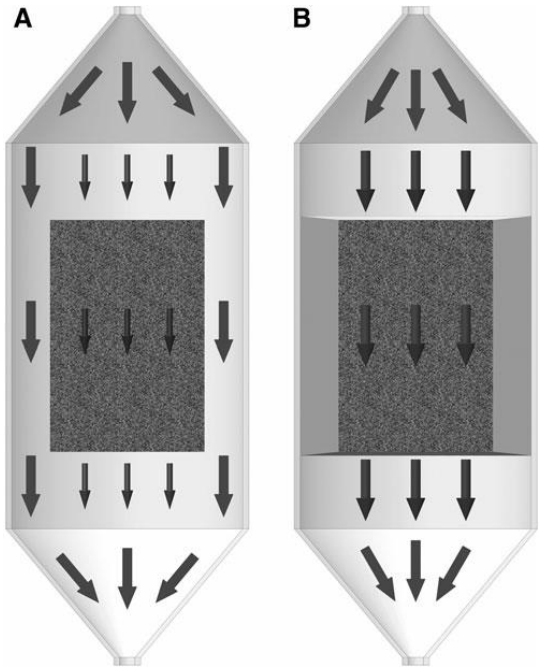

Figure 1-12 (A, B) Schematic drawings of perfusion flow principles. (A) shows indirect perfusion where medium flows around and only partly through the scaffold. (B) In direct perfusion, medium flow is forced through the scaffold and shear stress is directly transferred to the cells within the scaffold. Arrows illustrate the magnitude and direction of fluid flow. Reprinted from Tissue Engineering Part B Rev, volume 17, issue4, (Rauh et al., 2011). Bioreactor systems for bone tissue engineering, page 263-280, with the permission from Elsevier.

Many studies used this type of bioreactor by using different scaffold materials such as titanium, calcium phosphate ceramics and polymer composites. One of these studies utilised the perfusion bioreactor to assess the proliferation of marrow stromal cells that were seeded onto a titanium scaffold and a continuous flow rate of 0.3–3.0 mL/min was used. Results revealed that both calcium matrix deposition and the rate of late osteoblastic differentiation were enhanced through analysing both ALP and osteopontin as bone tissue

markers (Bancroft et al., 2002). Another study was performed by using bovine demineralised bone scaffolds which were seeded by preosteoblasts cell line MC3T3-E1. These scaffolds were placed in the perfusion bioreactor and compared with other scaffold samples but with a static environment. The results showed the perfusion bioreactor can enhance the oxygenation of cells within the scaffold especially for the cells which are centrally located (Volkmer et al., 2008). Polymer based scaffolds were assessed after seeding with stem cells and incubating in a perfusion bioreactor. The data showed that the perfusion bioreactor played an important role in enhancing cell viability and mineralisation (Kleinhans et al., 2015). Other attempts used perfusion bioreactors for engineering generated grafts that were implanted later in the mouse head. The study aimed to prepare composite scaffolds of hydroxyapatite, TCP and poly lactic acid polymer. Then these scaffolds were seeded with bone marrow stromal cells and incubated for 10, 20 days before *in vivo* implantation. The results showed that perfusion engineered scaffolds displayed more acceptable results than the free cell scaffolds. However the effect of the engineering time period was insignificant (Ding et al., 2016b). A similar study was done by preparing HA and TCP scaffolds which were implanted in a sheep's femur (Ding et al., 2016a). This study displayed that bioreactor engineered results were slightly less than those of the allograft control samples. Another study used mouse pre-osteoblastic MC3T3-E1 cell lines as a model. These cells were seeded into a composite scaffold that is composed of Thai silk fibroin (SF)/gelatine (G)/hydroxyapatite (HA). The whole cell culture with the scaffold was incubated in a custom made

perfusion bioreactor under different flow rates of 1, 3 and 5 ml/min. the results showed that a flow rate of 5 ml/min can cause cell detachment while a flow rate of 3 ml/min resulted in promising results (Sinlapabodin et al., 2016). Other studies suggested that the optimum flow rate that can enhance osteogenic differentiation of mesenchymal stem cells is about 1.5 ml/min (Egger et al., 2017).

1.7 Statement of the problem:

Bone injury in the head and facial area is multifactorial and can affect functional and cosmetic aspects negatively. However, the repair of the severe defects could be undertaken by following various radical surgical procedures that may necessitate the aid of implant applications to repair and substitute the missing bony part. These implants could be natural or synthetic.

Until now, bone autografts are considered the most popular and common implant,althoughh it has certain drawbacks especially surgery- related complications such as pain, bleeding, discomfort and mortality.

Other options for implant materials are the allografts which have a negative side regarding cross infection and immune rejection. Xenografts are considered a good choice for bone repair applications, athough there are some ethical, personal and religious concerns related to their application.

As a result of the limitation of the previous natural implant materials, many attempts were madwe to produce synthetic bone implants that should possess accepted biological and mechanical characteristics. The first synthetic materials that was used for this purpose were the calcium phosphate bioceramics materials such as tri calcium phosphate (TCP) and hydroxyapatite (HA). Although these ceramics have good osteoconductive properties, their mechanical properties were unsatisfactory as they are very brittle. Polymers are considered as an alternative flexible synthetic material

for bone tissue engineering applications. But their downside can be linked to their poor mechanical properties.

Glasses are considered as another type of bioceramics used for bone tissue engineering. There are three main types of glasses; silicate glass, borate glass and phosphate glass. Silicate glasses were the first produced type and have showed acceptable results with regard to its application in tissue engineering. Its slow biodegradation rate is the main concern limiting its use. Borate glass exhibited better degradation rate and HA layer formation ability than silicate bioglass but with poor mechanical properties. Phosphate glass has been shown to have better properties than silicate and borate glass because its biodegradation rate is higher than silicate glass and can be controlled to be lower than borate glass. It has been shown to have a good potential to function as an implant material for bone tissue engineering, even though brittleness remains as an obstacle in the way of producing the proper material with the optimum composition and optimum mechanical, chemical and biological properties.

Based on what has been explained previously about the limitation of all synthetic bony implant choices, it is essential to produce other biocomposite materials that combine all the positive characteristics and overcome the individual downsides. For this reason, some of these biocomposites were made of polymer and phosphate glass where polymers were the main component and glass powder has been added in low percentage as fillers to

enhance the mechanical properties of composite. However, there are no known implant biomaterials that are made mainly of phosphate glass.

1.8 Aim of and objectives

The aims of this study are:

1- Determine the optimum composition of both zinc and strontium phosphate glasses that can be applied as an implant material for bone tissue engineering.

2- Surface modification of glass surface by coating the glass surfaces with CNT-PCL layer.

3-Development of phosphate-based 3D scaffolds that exhibit the appropriate mechanical, chemical, morphological and biological properties.

4- Designing and installing perfusion bioreactors to mimic the physiological environment. Hence, assessment of the effect of mechanical stimulation that results from the culture flow on the cells seeded on the developed 3D scaffolds.

The objectives are:

1-Production of two main groups of phosphates-based glass discs based on composition (zinc group and strontium group). Each group is subdivided into four subgroups according to the variation in concentration.

2-Production of two main groups of phosphate-based glass beads based on the composition (zinc group and strontium group). Each group is subdivided

into two groups according to the most acceptable results found using glass discs.

3- Producing scaffolds and assessing cell seeding efficiency by using different reagents and different procedures.

1.9 Null hypothesis

The general Null hypothesis of this thesis stated the following:

1-There are no significant biological and cellular differences between the different compositions of developed zinc and strontium phosphate-based glass discs and control groups (tissue culture plastic or silicate glass beads).

2-There is no clear difference of cellular response to the CNT-PCL coated glass discs in comparison to the control tissue culture plastic.

3-There is no mechanical and morphological variation between different scaffolds produced by different sintering temperatures.

4- There is no cellular response difference in term of cellular attachment between cells seeded on different scaffolds (CNT-PCL coated glass scaffolds, uncoated glass scaffolds, BioOss scaffolds).

5- There is no cellular response difference in term of mineralisation between cells seeded on different scaffolds (CNT-PCL coated glass scaffolds, free coated glass scaffolds, BioOss scaffolds) under both static and dynamic environment.

Chapter 2 Assessment of physical, chemical and biological properties of strontium phosphate-based glass

2.1 Introduction

Phosphate-based glasses are a type of bioceramic material that has specific properties for use in bone tissue engineering applications. The preference for using phosphate glasses have increased because phosphate glasses are more controllable in regard to their degradation rate (Knowles, 2003). The degradation rate of phosphate glass can be varied from 2 h to >1 year and this is mainly dependent on the variation of their compositions. The addition of specific oxide modifiers such as TiO_2 may improve the glass network stability and may help in reducing the degradation rate (Lakhkar et al., 2011). Hence, it is possible to obtain a precise tuning of the degradation rate and also to control the release of ions that are known for their role in promotion of bone formation such as calcium, phosphate and strontium (Lakhkar et al., 2013). The inclusion of Ca^{2+} and Sr^{2+} ions in biomaterials has gained more interest over the last decades because they are generally identified to stimulate osteoinduction and osteogenesis (Bose et al., 2013). Strontium has been shown to aid in bone health due to its apparent dual anabolic and anticatabolic mechanisms of action. Through these synergistic processes, Strontium simultaneously upregulates mineral deposition by osteoblasts and inhibits bone resorption by osteoclasts. This will result in a net gain in mineralised tissue. Hence many studies have investigated the

addition of strontium to different types of glass that are intended to be used for bone defect repair applications (Mentaverri et al., 2012).

One study investigated the addition of strontium oxide to silicate glass in the formula of $(SiO_2)46.5–(P_2O_5)1–(Na_2O)26.4–(CaO)(23.1-x)–(SrO)x$ (x = 0, 2.3, 11.5 or 23.1) (mol%). This addition of strontium oxide resulted in upregulation of both cell proliferation and normalized alkaline phosphatase (ALP) activity in human osteosarcoma cell line Saos-2 (Gentleman et al., 2010). Sriranganathan *et al* (2016) investigated different composition of silicate-based glasses containing different calcium and strontium contents (Ca35Sr0, Ca17Sr17, Ca0Sr35). The main aim of the study was to assess the effect of substituting strontium with calcium on the formation of hydroxyapatite layer. The results showed that the addition of strontium in favour of calcium might result in less apatite formation (Sriranganathan et al., 2016). Other *in vivo* studies on strontium containing silicate glasses was carried out to establish the efficiency of the Sr-containing bioglass in encouraging bone formation in rabbits. The results suggested that implants containing strontium presented more promising results than those free of strontium (Newman et al., 2014).

Other series of studies inspected the incorporation of strontium into tertiary, quaternary and quinternary phosphate glasses where Sr concentration varied as 0, 1, 3 and 5 mol% and Ti concentration was 0, 3 and 5% (Abou Neel et al., 2008a, Lakhkar et al., 2009, Lakhkar et al., 2011). Generally, the results of these studies showed that direct increase in glass stability and cytocompatibility occurred when TiO_2 content was increased. Whereas

regarding SrO, the inclusion of 1 mol% of SrO to the glass seemed to disrupt the glass network and cause more rapid degradation than was observed in SrO-free compositions. This will subsequently cause a decline in cell proliferation on the surface of the materials. Conversely, increasing of SrO content to 3 or 5 mol% led to a decline in glass degradation rate, therefore, enhancing cytocompatibility.

Although many studies have been carried out to investigate adding strontium oxide to phosphate-based glass, little information is available on adding high levels of strontium oxide to phosphate glass. The purpose of this chapter is to discuss the production of high strontium oxide content quinternary phosphate-based glasses and examine their properties. Glass was produced in the formula of $(P_2O_5)50–(Na_2O)10–(TiO_2)5–(CaO)(35-x)–(SrO)(x)$ when x = 0, 3.5, 17.5 or 35 (mol%). Titanium dioxide content was fixed at 5 mol% to control glass degradation. While calcium oxide content was substituted with strontium oxide (up to 35 mol%, compared with SrO content in the previous studies at 5 mol%).

The results of this chapter could be useful in recognising the effect of incorporation of high strontium oxide concentration in phosphate glass and identify the potential of the produced material in biomaterial applications.

2.2 Materials and methods

2.2.1 Materials

Different composition of strontium-containing phosphate-based glass discs were prepared by using the following chemical precursors: diphosphorus pentoxide (P_2O_5, 98%, VWR, Lutterworth, UK), sodium dihydrogen phosphate (NaH_2PO_4, 99%, VWR, Lutterworth, UK), titanium oxide (TiO_2, 99%, VWR, Lutterworth, UK), calcium carbonate ($CaCO_3$, 98.5%, VWR, Lutterworth, UK) and strontium carbonate ($SrCO_3$, 98.5%, BDH Laboratory Supplies, Poole, UK).

2.2.2 Glass precursors calculation

Four different quinternary strontium-containing phosphate-based glass (P_2O_5–$CaCO_3$–NaH_2PO_4– $SrCO_3$–TiO_2) were made. The details of glass composition codes and weight are listed in (Table 2.1).

Table 2-1 Glass compositions

Glass code	***and composition***	***Concentration (grams)***				
		P_2O_5	***NaH_2PO_4***	***TiO_2***	***$CaCO_3$***	***$SrCO_3$***
SrO_0	***$P_{50}Na_{10}Ti_5Ca_{35}$***	***56.8***	***24***	***4***	***35***	***0***
$SrO_{3.5}$	***$P_{50}Na_{10}Ti_5Ca_{31.5}Sr_{3.5}$***	***56.8***	***24***	***4***	***31.5***	***5.16***
$SrO_{17.5}$	***$P_{50}Na_{10}Ti_5Ca_{17.5}Sr_{17.5}$***	***56.8***	***24***	***4***	***17.5***	***25.8***
SrO_{35}	***$P_{50}Na_{10}Ti_5Sr_{35}$***	***56.8***	***24***	***4***	***0***	***51.66***

Mole concentration of the precursors were calculated as follows: using the SrO17.5 glasses as an example ((P_2O_5 = 50 mol%; Na_2O = 10 mol%; TiO_2 = 5 mol%; CaO = 17.5 mol%; SrO= 17.5 mol%).

A. Sodium dihydrogen orthophosphate (NaH_2PO_4)

$$2NaH_2PO_4 \longrightarrow Na_2O + P_2O_5 + 2H_2O$$

Mol. wt. ($g.mol^{-1}$)	240	62	142	36
Relative mol. wt. ($g.mol^{-1}$)			0.258	0.59

0.15

To get 10 mol% Na_2O, the needed amount of NaH_2PO_4 is:

= [(mol. fraction of Na_2O) × (mol. wt. of Na_2O)]/ (relative mol. wt. of Na_2O)

= (0.10 × 62)/ (0.258) = **24 g**

B. Phosphorus pentoxide (P_2O_5)

Amount of P_2O_5 produced in the above reaction

= (amount of NaH_2PO_4 required) × (relative mol. wt. of P_2O_5)

= 24× 0.59 = 14.16 g

Amount of P_2O_5 required to produce 50 mol% P_2O_5

= 0.50 × 142 = 71.00 g

Therefore, actual amount of P_2O_5 to be added

= 71.00 – 14.14= **56.8 g**

C. Calcium carbonate ($CaCO_3$)

	$CaCO_3$ ⟶	CaO +	CO_2
Mol. wt. ($g.mol^{-1}$)	100	56	44
Relative mol. wt. ($g.mol^{-1}$)		0.56	0.44

To get 17.5 mol% CaO, the required amount of $CaCO_3$ is:

= (0.175 × 56)/0.56 = 17.5g

D. Titanium(IV) dioxide (TiO_2)

Mol. wt. of TiO_2 = 47.90 + (2 × 16) = 79.9

To get 5 mol% TiO_2, the needed amount of TiO_2 is:

= 0.05 × 79.9 = **4g**

E. Strontium carbonate ($SrCO_3$)

	$SrCO_3$ ⟶	SrO +	CO_2
Mol. wt. ($g.mol^{-1}$)	147.63	103.62	44
Relative mol. wt. ($g.mol^{-1}$)		0.7	0.29

To get 17.5 mol% SrO, the needed amount of $SrCO_3$ is:

= (0.175 × 103.62)/0.7= **25.8g**

2.2.3 Glass preparation

The required amounts of precursors powders were weighed according to proportions by two decimal electronic balance (Sartorius). Then all the

powder mixture was mixed by using a blender (Stomacher 400 circulator/Seward) for one minute. Once the mixing step had been finished, the precursor mixture was introduced into 200 ml volume Pt/10%Rh crucible type 71040 (Johnson Matthey, Royston, UK) which was placed in a furnace (Carbolite) at 1350^{o}C for four hours. Afterwards, the melted glass was taken out from the furnace and casted into (15mm diameter) rods graphite moulds. The mould was preheated at 420^{o}C. Then, the graphite mould was introduced again into a furnace for one hour at 420^{o}C which then left in the furnace to cool down gradually to room temperature overnight to remove the residual stress. The glass rods were removed from the mould the following day and were cut into 2mm thick glass discs using a diamond saw (Accutom 50 electric diamond saw, Struers, Catcliffe, UK) (Figure 2.1) which were prepared for different experiments. Other samples of glass powders were prepared by grinding each glass composition with (MM 301 Mixer Mill, Retsch GmbH, Hope, UK) grinder. These glass powder samples were used as samples for XRD.

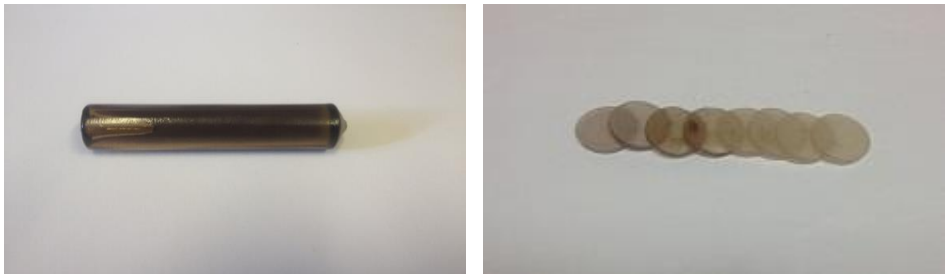

A B

Figure 2-1(A, B) Pictures explained the prepared glass (A) glass rods (B) glass discs

2.2.4 Materials characterisation

2.2.4.1 Density determination

For Measuring density, an analytical balance and density determination apparatus (AG 204 & MS-DNY-43, Mettler Toledo, Beaumont Leys, UK) were used according to Archimedes' principle. The immersion liquid was ethanol (99.8%, Sigma- Aldrich, Dorset, UK) to avoid phosphate glass dissolution in water. Each glass disc was initially weighted in air then weighed again in the ethanol.

The density of each composition was determined and calculated using the equation 1.

$$Pglass = \frac{M\ air}{M\ air - M\ ethanol} X\ P\ ethanol \ldots\ldots\ldots\ldots\ldots\ldots\ldots\ldots 1$$

Where ρ_{glass} is the density of the specimen ($g.cm^{-3}$), $\rho_{ethanol}$ is the density of ethanol at the environment temperature in ($g.cm^{-3}$) at which the measurement was performed, m_{air} is the mass (g) of the specimen in air and $m_{ethanol}$ is the mass of the specimen under ethanol.

2.2.4.2 X-ray diffraction

X-ray diffraction of each glass composition was performed by using XRD device (D8 Advance diffractometer, Bruker, Coventry, UK) to ensure the amorphocity of the produced glasses. All the glass powder specimens were placed in flat plate geometry which was loaded in the x-ray machine. X-ray was filtered by Ni to give Cu Kα radiation. After loading the samples in the machine, diffraction was measured over an angular range of $2\theta=10^{o}$-100^{o}

and a count time of 12 seconds. Afterwards, x-rays were detected using a Lynx eye detector that was used to collect the data.

2.2.4.3 Thermal analysis

Differential thermal analysis was performed for the four compositions by using powder of each glass disc composition that was prepared by using (MM 301 Mixer Mill, Retsch GmbH, Hope, UK) grinder. About 45 mg of powder of each glass composition was loaded into 10 µl platinum crucible that was afterward placed in the DTA Analyser (Setaram differential thermal analyser, France). These samples were heated from the room temperature to about 1000°C at a rate of 20°C. min^{-1}. An empty platinum crucible was used as a reference and air was used as the purge gas.

Three thermal parameters were measured: (1) T_g the glass transition thermal temperature, (2) T_c the glass crystallization temperature and (3) T_m the melting temperature.

2.2.5 Chemical, physical studies of strontium phosphate bioactive glass discs

2.2.5.1 Degradation study (Mass loss)

Triplicates of each composition were initially weighed then stored in plastic vials (Sterilin tube) and immersed with 25ml high-purity deionized water (resistivity = 18.2 $M\Omega.cm^{-1}$) gained from a PURELAB UHQ-PS (Elga Labwater, Marlow, UK). The pH of the deionized water was preadjusted to pH 7 by (HCl or NH_4OH) over the whole experiment. All the samples were

incubated at 37^{o}C. After 1, 4, 7 and 14 days, the solution was removed and kept for ion release and pH measurement. Glass discs were dried for 1 hour and weighed at each time point to determine the mass loss. The mass loss was done in cumulative with the previous mass loss reading. Following weighing, the discs were stored again in new fresh deionized water for the next time point. Mass loss was calculated at every time point by dividing the mass difference by the surface area of discs. Disc surface areas were measured individually by the equation 2.

$A= 2\pi r^2 + 2\ \pi rh$ ……2

When A: surface area of disc, r= radius of the disc (mm) and h= height of disc (mm).

2.2.5.2 Ion release

Ion release measurement was performed for each stored sample from the degradation study, this was done for the anions (PO_4^{3-}, $P_2O_7^{4-}$, $P_3O_9^{3-}$, $P_3O_{10}^{4-}$) and the cations (Na^+, Ca^{2+}, Sr^{2+}) by using the ion chromatography systems ICS 2500, ICS1000 (Dionex, Thermo scientific, Hemel Hampstead, UK) respectively.

2.2.5.2.1 Anion release

Ion chromatography (ICS 2500) system was used for measuring the anion release. Samples were prepared by pipetting 550 µl from each sample and load it into labelled plastic vials. The labelled vials were arranged in specified metal vials tray that was inserted into the machine for ion release detection.

Calibration for anion chromatography was done prior each time point measurement. The calibration (standards) solutions were prepared in five dilutions (0 ppm, 1ppm, 5ppm, 25ppm, 50ppm). A calibration curve was determined from these five samples reading. this curve was used by the Chromeleon® software as a reference for other sample calculations. These calibration samples were formed by using the following reagents: sodium phosphate monobasic, trisodium trimetaphosphate, sodium tripolyphosphate (Sigma–Aldrich, Dorset, UK) for PO_4^{3-}, $P_3O_9^{3-}$and $P_3O_{10}^{5-}$ respectively, and tetrasodium pyrophosphate (BDH, Poole, UK) for $P_2O_7^{4-}$. Ultrapure water was the solution for preparing the basic stock solution of 100 ppm concentration. This was followed by subsequent dilutions to prepare the five standard solutions.

Anions detection was carried out using a 4 × 250 mm Ion Pac® AS16 anion exchange column which is packed with an anion exchange resin. The background was decreased by a Dionex regenerative suppressor Dionex (Anion Self- Regenerating Suppressor (ASRS®)) which was used at a current of 223 mA. A potassium hydroxide cartridge was equipped with Dionex EG40 eluent generator which its main functions are: transport of the samples through the system, and to contribute in the selection of ion separation and provoke time reproducibility. The sample was injected using a 25µl injection loop.

The running program setting were fixed at 30 minutes run time for each sample in which KOH concentration was variables as follows: initial

concentration at 30 mM KOH for 6.5 minutes, followed by rising concentration to 55mM KOH for 15.5minutes, then maintaining concentration at 55mM KOH for 6 minutes and finally concentration decrease 30 mM for 2 minutes.

2.2.5.2.2 Cation release

A Dionex Ion chromatography (ICS 1000) system was used for measuring the cation release. Sample preparation was similar to the anion chromatography except that there are extra filtration steps which was done to all the samples prior measurement to remove the anions (OnGuard II, Dionex) which bind to the cation detection column.

Calibration standards were prepared as well by using ultrapure water using the following reagents: Sodium chloride (Sigma–Aldrich, Dorset, UK), calcium chloride and strontium chloride (BDH, Poole, UK). The basic standard stock was prepared were used as reagents to prepare a 50ppm stock solution that was further diluted to prepare five standards solutions (0 ppm, 0.1ppm, 1ppm, 5ppm, 25ppm). The resultant calibration curve was used by the Chromeleon® software for the other sample concentration calculations. The eluent was prepared by using 30 mM methanesulphonic acid (Fluka, Dorset, UK) and cation detection process was carried out through a 4 × 250 mm Ion Pac® CS12A separator column. The sample injection volume was done by 25 µl injection loop.

2.2.5.3 pH measurement

At all the time points, pH was measured for each stored solution from the degradation study using a pH meter (Orion star A111Thermo Scientific, UK). the pH electrode of the pH meter was calibrated by using the standard solutions of pH 4 and 7 before usage.

2.2.6 Cell studies

2.2.6.1 Cells preparation

MG63 osteoblast-type cells were gained from in-house stocks at Eastman Dental Institute of University College London. These cells were kept at -80°C in liquid nitrogen. Cells were taken out from the liquid nitrogen tank, then were revived by thawing in a water bath at 37°C. The thawed cells were dispersed in a 15-ml falcon tube containing 5 ml of 37°C culture media and then centrifuged later for 5 minutes at 1000rpm speed at 20°C. After the centrifugation process, the supernatant culture media was removed from the falcon tube and the MG63 pellet in the bottom of the centrifugation were dispersed in 1 ml of Dulbecco Modified Eagles' Medium (DMEM) (Sigma Aldrich, D5546). Later, the cells were introduced into a 150 cm^2 flask containing low-glucose Dulbecco Modified Eagles' Medium (DMEM) which was supplemented previously with 10% foetal bovine serum (FBS) (Gibco) and 1% penicillin-streptomycin (PAA Laboratories, GE Healthcare, Chalfont St. Giles, UK).

Cell proliferation measurement in the flask was carried out in a 37°C/ 5%CO_2 incubator till the cells were 80–90% confluent. Cells confluency was checked daily under a light microscope (Olympus CK 2). When cells reached confluency of 80%-90%, they were washed with phosphate buffer solution (PBS) and then trypsinised by adding 6 ml of 0.025% trypsin-EDTA to the flask and incubated at 37°C/ 5%CO_2 for 3–4 minutes to ensure cell detachment from the flask surface. Cell detachment was checked under light microscope by identifying the floating cells. Then trypsinisation process was prohibited by adding 6 ml of fresh media to the trypsinised live cells. The whole 12 ml cell suspension was then pipetted from the flask and added to 15 ml falcon tube which was centrifuged subsequently at a speed of 1000 rpm for 5 minutes. After this centrifugation process, gentle removal of the 12ml supernatant was done to avoid disturbing the cell pellet. Finally, cells were suspended in 1 ml of media prior to the cell counting procedure, this procedure was done by using the Trypan blue dye following the recommended protocol (Strober, 2001).

2.2.6.2 Metabolic activity study

Metabolic activity was measured by using the alamar blue assay. For this study, cells were seeded on triplicate of glass discs of each composition at a density of 10000 cells per disc in 24 well plates. This was followed by adding 1 ml of DMEM culture media to each well plate then incubation at 37^{o}C in an atmosphere of 5%CO_2 for 7 days. Cell culture medium was replaced every 3 days. Tissue culture plastic (TCP) was used as control group.

Cytocompatibility assay was done at three times points (days 1, 4 and 7) in which a 10% solution of water soluble tetrazolium salt-8 (alamar blue, ABD Serotec) was added to the aspirated culture then stored in the incubator for four hours at 5 % CO_2. Alamar blue is a cell viability assay reagent which contains the cell permeable, non-toxic and weakly fluorescent blue indicator dye called Resazurin which is used as an oxidation-reduction (REDOX) indicator that undergoes colorimetric change in response to cellular metabolic reduction. The reduced form Resorufin is pink and highly fluorescent, and the fluorescence produced is proportional to the metabolic activity of cells and was detected at 570 nm by a fluorimeter (Infinite M200, Tecan, Männedorf, Switzerland).

Metabolic activity was measured by calculating the percentage of alamar blue stain reduction in comparison to the fully reduced alamar blue. To perform this step, the first step was the full reduction of alamar with culture media which was done by autoclaving the mixture (culture media with alamar blue) at 121°C for 15 minutes. To correlate the fluorescence reading with that of the full reduction the following equation was used.

$$\%\ of\ reduced\ alamar\ blue = \frac{fl\ sample - fl\ control}{Fl\ of\ 100\%\ reduced\ alamarblue - fl\ \ control} x\ 100$$

Where fl sample is fluorescence reading for sample, fl control is fluorescence reading of the untreated culture media and fl of 100% is the fluorescence of the fully reduced alamar blue.

2.2.6.3 Alkaline phosphatase activity

The alkaline phosphatase (ALP) activity analysis was carried out by using a p-Nitrophenyl phosphate-based assay (SensoLyte pNPP Alkaline Phosphatase Assay Kit, AnaSpec, Seraing, Belgium). Initially, MG63 cells were seeded on triplicates of all the discs samples and controls tissue culture plastics (TCP) at a density of 30000 cells/disc and alkaline phosphatase activity were measured at three different time points (day 4, 7,14).

At each time point, culture media was aspirated first. This was followed by rinsing disc and cell complexes with assay buffer (prepared by dilution of the assay buffer with ultrapure water ten folds) and repeated twice. Then, a prepared solution of 0.002 Triton x-100 (20 µl of Triton x -100 in 10 ml of assay buffer) was added to lyse the cells membrane which was followed by using cell scrapers to scrap cells from the discs. The scraped cells were aspirated and collected in small plastic tubes which were agitated at 4°C for 10 minutes. After that, cells were separated from their culture media suspension by centrifuging them at (2500 X g, 10 min, 4 °C). Then triplicate of 50 µl of supernatant solution from each vial was aspirated in 96 well plate. Another 50 µl of pNPP solution was added to each sample.

Calibration was done by preparing a sequence of ALP standard (10 µg/ml) dilutions. Seven dilutions (100, 50, 25, 12.5, 6.25, 3.1, 0 ng /ml) were prepared by diluting the alkaline phosphatase standard reagent with the buffer solution (Figure 2.2). Triplicate of 50µL of each standard was added to 50µL pNPP substrate in a 96 well plate.

After adding the pNPP solution to both sample and standard substrate, incubation of 96 well plates were carried on at 37°C for 30 minutes. Finally, a stopping reagent was added into each well before taking triplicate absorbance measurements of each glass disc by (Infinite® M200, Tecan) at 405 nm wavelength.

The calibration curve was obtained from the standards readings. The equation of this curve was used to relate the absorbance reading with the ALP concentration in the samples (Figure 2.2).

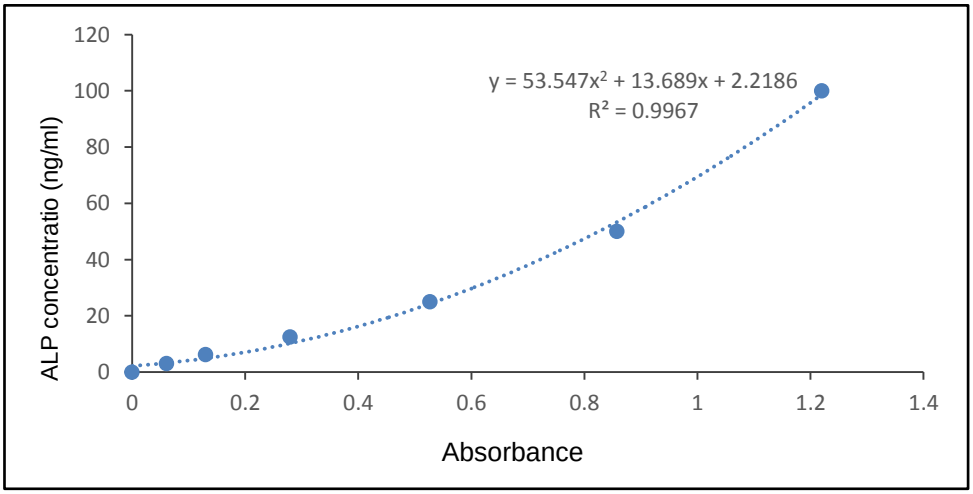

Figure 2-2 Calibration curve of ALP assay. Done by preparing different concentrations of ALP and correlate the corresponding fluorescence reading with each of the concentration.

2.2.7 Statistical analysis

Cell work data for both cells counting and alkaline activity assay studies were statistically assessed by Kruskal-Wallis to examine the null hypothesis stating that there is no clear biological and metabolic difference between the produced strontium oxide containing glass discs and the control TCP group where $p<0.05$ has been used as a significance degree estimation.

2.3 Results

2.3.1 Density measurement

As is shown in (Table 2.2), glass density increased as the content of incorporated strontium oxide had increased. The density was ranging from 2.6 ± 0.017 $g.cm^{-3}$ in the quaternary glass (strontium free glass) to stand at 3.0 ± 0.011 $g.cm^{-3}$ for SrO 35.

Table 2-2 Density measurement of all strontium containing phosphate glass compositions

Glass code	SrO0	SrO3.5	SrO17.5	SrO35
Density (g/cm^3)	2.63	2.68	2.82	3.03

2.3.2 X-ray diffraction

The XRD patterns for all the prepared glass samples are shown in (Figure 2.3). All the XRD patterns were free from any detectable peaks due to crystalline phases and displayed a broad peak was observed as expected in each spectrum at 2θ values of around 20–40°.

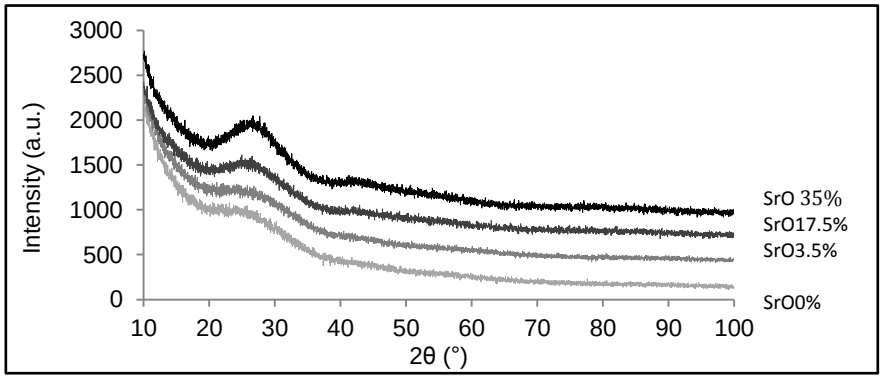

Figure 2-3 X-ray diffraction showing the amorphous nature of the prepared glasses

2.3.3 Thermal analysis

Table 2.3 explains the T_g values of the observed glasses. It showed that the incorporation of strontium oxide had led to decrease T_g value from 483 °C for the SrO 0 to 468°C for the SrO35.

Table 2-3 DTA for strontium containing phosphate-based glasses measured in °C

Glass code	SrO0	SrO3.5	SrO17.5	SrO35
Tg (°C)	483	480	475	468
Tc (°C)	775	715	706	701,647
Tm (°C)	850	840	833	752

DTA spectra of the glasses are presented in (Figure 2.4). The T_c trend exhibited a clear variation between SrO35 and the other three compositions; SrO35 seemed to have two crystallisation peaks at of 647°C and 701°C, whereas the other three compositions has one peak which was higher than that of SrO35. A similar trend was observed for the T_c and T_m values which both showed that temperature values decreased in a trend from free strontium glasses to the higher strontium compositions.

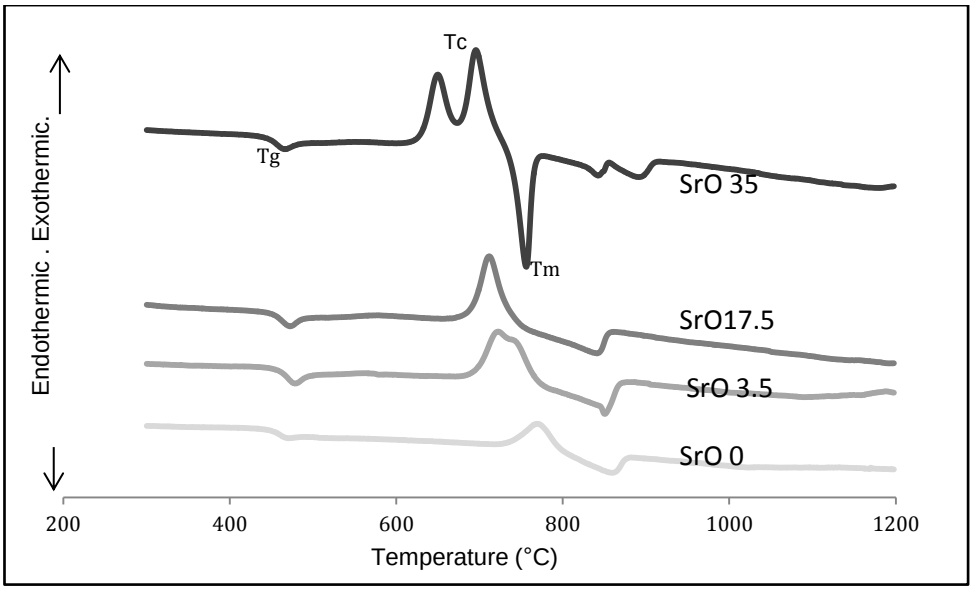

Figure 2-4 Differential thermal analysis showing the glass transition temperature (T_g) which is the midpoint of the first slope in each composition , crystallisation temperature (T_c) which is the upward peak in each line and melting temperature (T_m) which is the last downward peak in each line . Showing that these parameters declined as SrO content increased

2.3.4 Degradation study (mass loss)

Both (Table 2.4) and (Figure 2.5) show the mass loss per unit area measured in (mg.cm^{-2}) for a two weeks period. However, there was continuous mass loss over the time frame, but the highest increase was in the compositions with higher metal oxide substitutions. In other words, the higher mass loss was in SrO35 for the whole-time points. In day 1, mass loss of SrO 0 and SrO3.5 was about 0.052±0.01 (mg.cm^{-2}) which was about half of that of SrO35 at 0.103±0.013 (mg.cm^{-2}) while SrO 17.5 was slightly less than SrO 35 at about 0.074±0.013 (mg.cm^{-2}). This pattern remained the same for the other time points. In day 14, the maximum mass loss was 0.266±0.03 (mg.cm^{-2}) for SrO35 whereas the minimum loss was about 0.164±0.025 (mg.cm^{-2}) for SrO0.

Table 2-4 Mass loss in (mg.cm-^{2}) for all glass compositions in four different time point

Glass composition	Mass loss (mg.cm^{-2})				
	Day 0	Day 1	Day 4	Day 7	Day 14
SrO 0%	0	0.052	0.096	0.134	0.164
SrO 3.5%	0	0.051	0.104	0.141	0.185
SrO 17.5%	0	0.074	0.134	0.164	0.209
SrO 35%	0	0.103	0.185	0.229	0.266

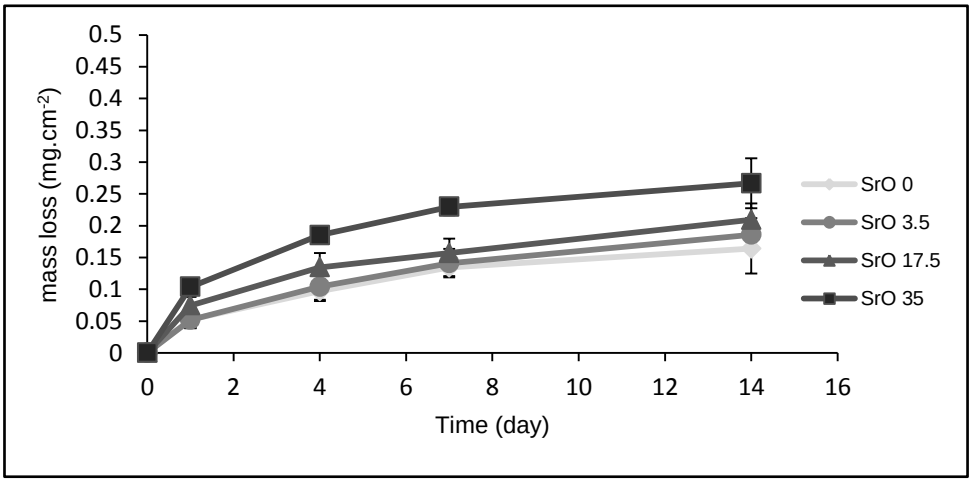

Figure 2-5 Mass loss in (mg.cm^{-2}) for all glass compositions over 14 weeks

2.3.5 pH measurement

pH measurements are displayed in (Figure 2.6). Generally, pH trend was similar for all the glass compositions in that it dropped sharply for the first day from 7 at day 0 to 5.5-5.9 at day 1. This was followed by continuous gradual decrease for the next time points, however it increased slightly for the last week to finish at 5.5-6. The general view indicated that the free strontium composition was the more acidic (lowest pH) 5.75 at the end of the time frame just slightly less than the other strontium compositions.

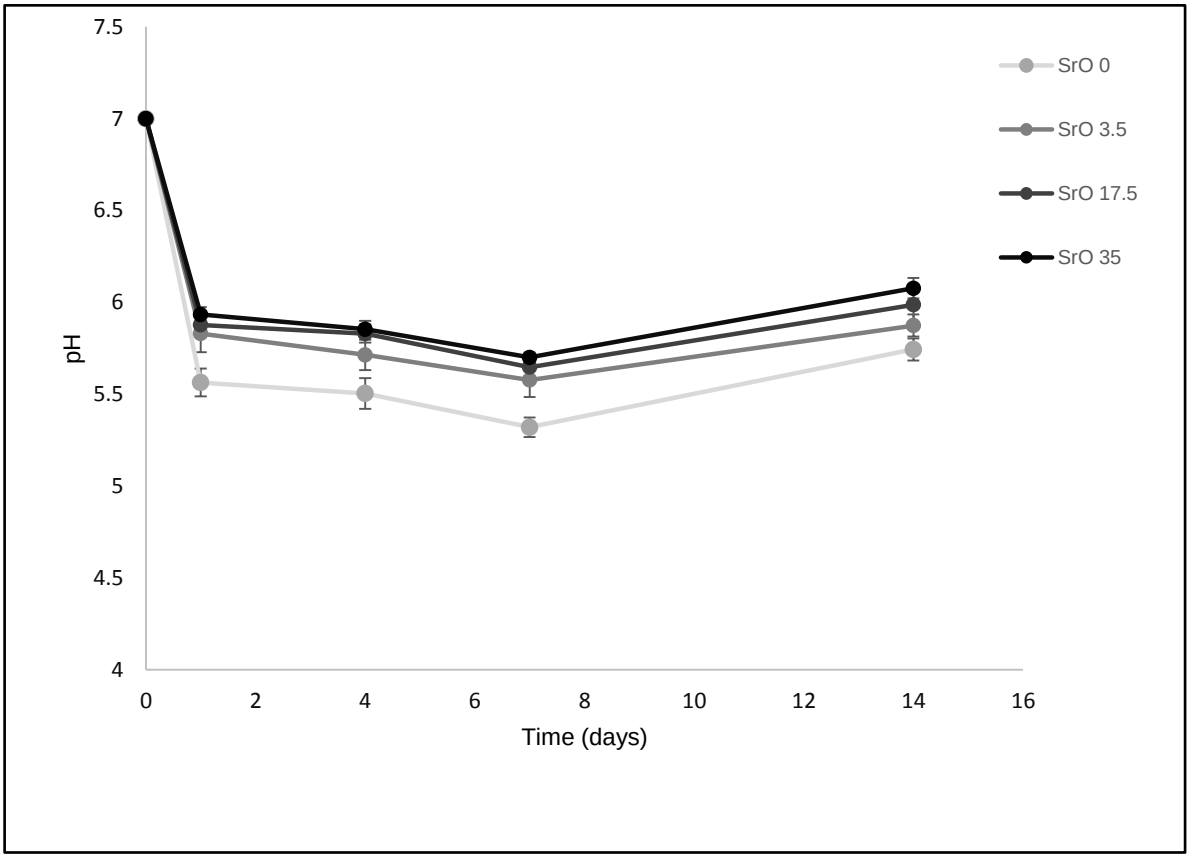

Figure 2-6 pH measurement

2.3.6 Ion release measurement

2.3.6.1 Anion release

Strontium glass anion release is shown in (Figure 2.7). Anion release was measured for four different anions (PO_4^{3-}, $P_2O_7^{4-}$, $P_3O_9^{3-}$, $P_3O_{10}^{5-}$). All the ions released for all the compositions showed a cumulative increase with time. Concerning PO_4^{3-} ions release, SrO0 glass compositions were found to have the highest release in comparison with the other compositions over the whole study. It was nearly two times that of high strontium oxide content glasses (SrO17.5 and SrO35) over the whole time, whereas SrO3.5 glasses showed slightly less release from that of the strontium free glass. For $P_3O_9^{3-}$, the ion release was similar to that of PO_4^{3-} ions. At day 1, the release was about 0.67±0.08 for SrO0 samples clearly higher than the other three composition release which was around 0.04-0.06 ppm. This relation remained the same for the whole experiment and ended at day 14 at about 2.8 ±0.3 ppm for SrO 0 that was more than the high strontium (SrO35) at 2.1 ±0.1 ppm. The highest release was with strontium free glasses and the release starts to be down regulated gradually as strontium content has risen. Regarding both $P_2O_7^{4-}$, $P_3O_{10}^{5-}$ ions, these ions witnessed the highest rise for SrO0 in which there was a clearly significant variation between it and the other strontium oxide containing glasses. Generally, it was found that phosphate ions release was inversely proportional to strontium oxide content in glass.

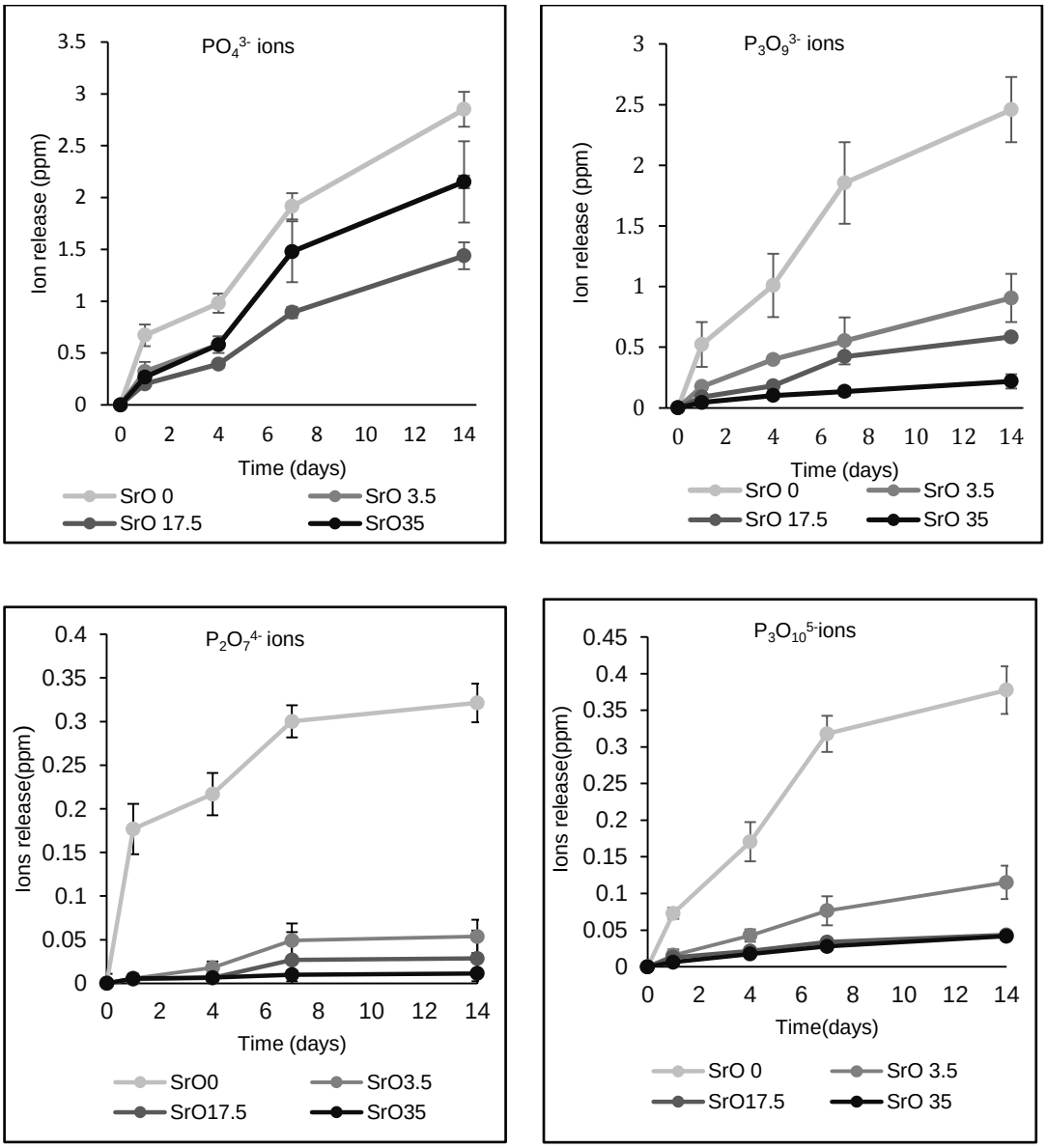

Figure 2-7 Anion release showing higher release of phosphates ions (PO_4^{3-}, $P_2O_7^{4-}$, $P_3O_9^{3-}$, $P_3O_{10}^{5-}$) in the free strontium oxide based glass in comparison to strontium oxide containing glass

2.3.6.2 Cation release

Figure 2.8 displays the cation release for all glass compositions. Regarding calcium and strontium ions, the trend for both of them was opposite to each other because it was varied in relation to the glass composition and was directly correlated to the percentage of these ions within the glass. In other words, high strontium content glass displayed the maximum strontium ion

release and the lowest calcium ions. Concerning sodium ions, it was found that sodium concentration declined as a function of increasing SrO content in the glass. This relationship, however, was inversely correlated with weight loss (Figure 2.4).

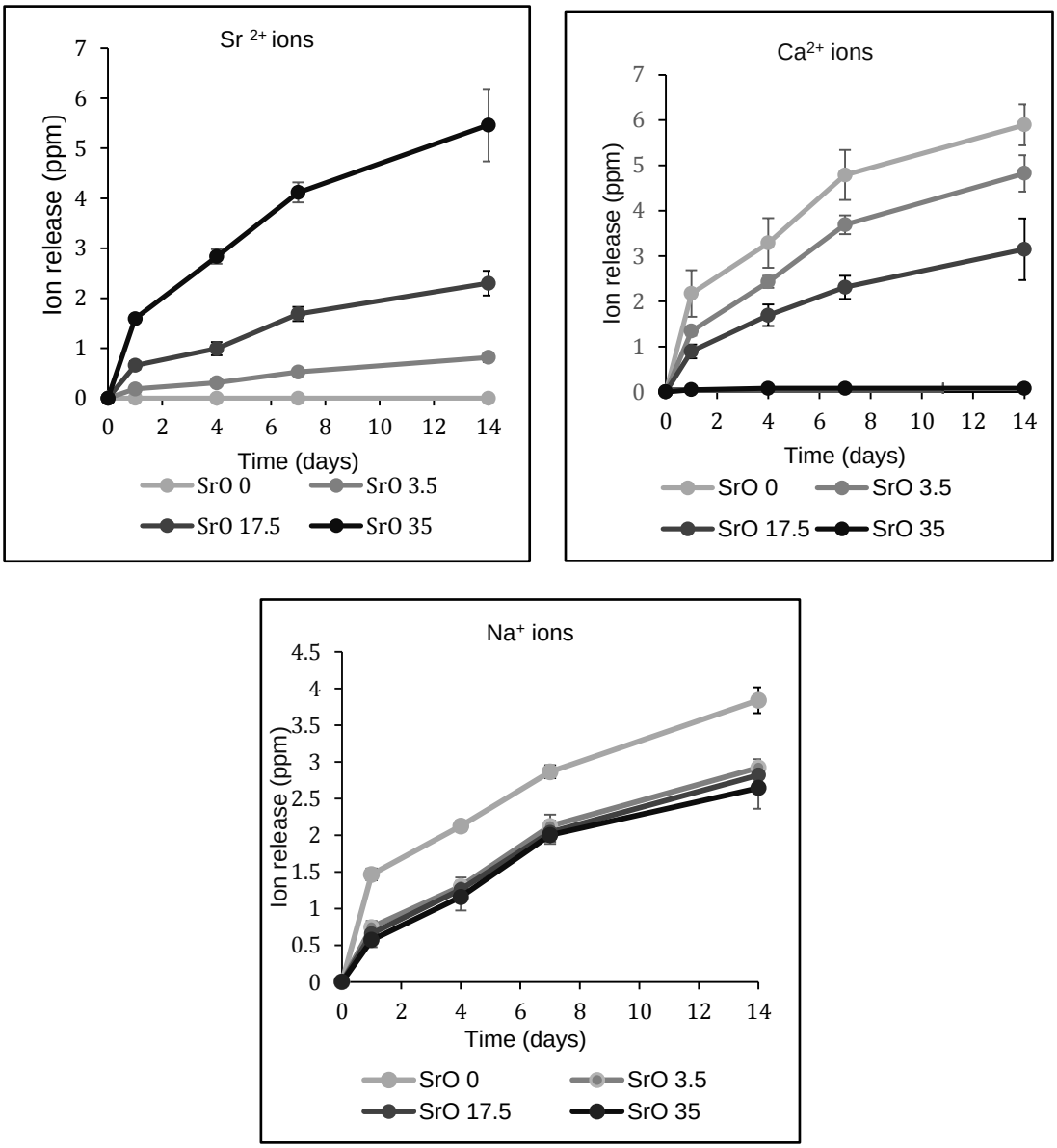

Figure 2-8 Cations release for all glass compositions a Sr^{2+}, b. Ca^{2+} and c. Na^{+}

2.3.7 Biocompatibility study

The measurement of the cellular metabolic activity is presented in (Figure 2.9). The results were measured at three different time points (day 1,4,7). They were represented by the percentage of the samples alamar blue fluorescence reduction in relation to the fully reduced alamar blue when the higher reduction percentage is related to the higher metabolic activity and vice versa. At day 1, TCP displayed around 11.8 ± 0.9% of fluorescence reduction which was about similar to that of SrO 0, SrO 3.5 and SrO17.5 and about double the reduction of SrO 35. At day 4, TCP reduction rate rose by three times to stand at about 30% which was significantly different from SrO 3.5 and SrO 35 ($P < 0.05$).

After one week, the pattern of reduction remained similar to the previous two times points where the TCP (54 ± 1.5 %) showed the ultimate amount of reduction followed by SrO0 (46 ± 2.7 %), SrO 3.5 (40.6± 0.9 %) and SrO17.5 (43.1 ± 4 %) and SrO 35 (39.4 ±1.5 %) respectively.

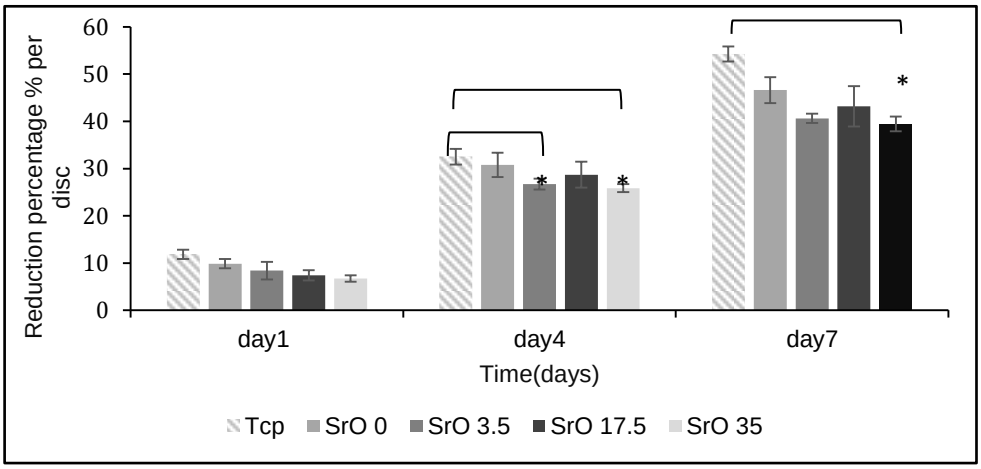

Figure 2-9 Cell metabolic activity results determined by using alamar blue assay

2.3.8 Alkaline phosphatase activity

Figure 2.10 illustrates the ALP activity of MG63 on different glass compositions. At day 4, there was insignificant difference between glass and the control (TCP) results. However, clear variation was noticed in day 7,14. Interestingly, Sr17.5 showed an unexpected rise in the 14 days which was highly significant from the other glass compositions. Cells cultured on TCP displayed the lowest ALP activity at day 14 at about 0.27±0.04 ng in comparison to 1.27±0.21 ng to SrO17.5 glass discs and around 0.65 ng for the other disc samples.

The general pattern of ALP showed that all the glass samples had good ALP activity which was significantly higher than that of TCP (p value < 0.05) at days 4 and 7.

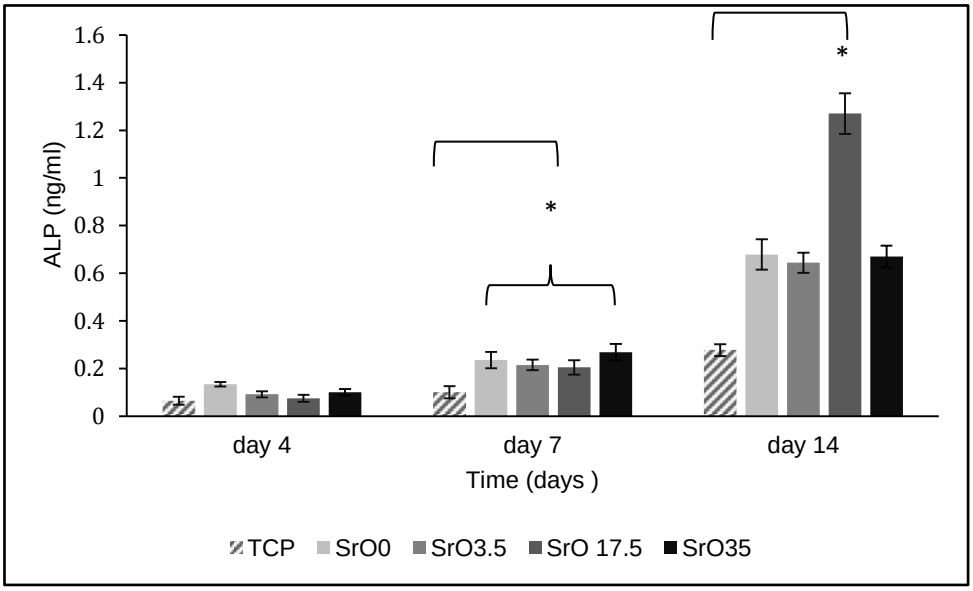

Figure 2-10 Alkaline phosphatase (ALP) activity of MG63 on different glass composition

2.4 Discussion

This chapter focused on the doping of strontium oxides for the development of phosphate-based glasses for tissue engineering applications. Many studies leading up to the present work have been carried out. One of the earliest studies hypothesised that there is poor cytocompatibility when seeding human osteosarcoma cells (HOS) on ternary (Sr free glasses) and quaternary phosphate glasses that have low strontium contents in their compositions (1, 3 or 5) (mol%). The explanation was because of the rapid degradation rate of these strontium glasses (Abou Neel et al., 2008a). In a follow-up study, inclusion of 3 mol% Ti in quaternary and quinternary $(P_2O_5)50–(Na_2O)17–(TiO_2)3–$ (CaO)(30-x)–(SrO)(x) (x = 0, 1, 3 or 5) (mol%) glasses were revealed to reduce the degradation rate and enhance cytocompatibility compared to Ti-free compositions (Lakhkar et al., 2009). The substitution of CaO with SrO, has yielded an increase in the degradation rate, but with an inverse trend as follows: Sr0 < Sr5 < Sr3 < Sr1. These degradation results were directly correlated with a decrease in cytocompatibility where Sr0 supported best cell growth: Sr0 > Sr5 > Sr3 > Sr1. A subsequent study of $(P_2O_5)50–(Na_2O)15–(TiO_2)5–$(CaO)(30-x)–(SrO)(x) (x = 0, 1, 3 or 5) (mol%) composition suggested that increasing TiO_2 into 5mol% was shown to decline degradation rates by more than two times than the previous prepared compositions containing 3mol% TiO_2. This slower dissolution rate also enhanced cell attachment. Again, degradation

was highest in the composition with low Sr content, reaffirming the prominent Sr0 < Sr5 < Sr3 < Sr1 trend observed previously (Lakhkar et al., 2011). Other research investigated the addition of high strontium oxide contents to silicate glass and it was found that addition of strontium oxide at 17.5 mol % or 35 mol% might yield in enhancing HOS cells proliferation as these amounts of strontium are similar to the concentration of strontium ranelate drugs that is used for osteoporosis and may work as an optimum concentration for bone repair therapy applications (Gentleman et al., 2010).

According to the previous studies, the production of the strontium phosphate glass in this study was planned; by adding TiO_2 in 5 mol% to control degradation and enhance cellular proliferation and metabolism, adding SrO in higher contents since the low content SrO showed higher degradation and poor cytocompatibility in previous studies.

Many comprehensive studies were carried out in the present study to investigate the chemical and biological characterization of the produced glass.

Based on the density results, CaO replacement with SrO yielded an increase of glass density. These results can be explained by considering the fact that density of strontium is (2.64 g/cm^{-3}) which is higher than that of calcium at (1.54 g/ cm^{-3}), and this was clearly compatible with the results. XRD data confirmed the amorphous nature of the produced glass. Depending on these two results, it seemed that the production phosphate-based glasses containing up to 35mol% was successful.

On the other hand, DTA data showed that the thermal properties reduced as incorporation of strontium oxide increased. The thermal properties presented in terms of glass transition, glass crystallisation and melting temperatures were reduced. This reduction is likely due to the weaker strontium bonds with other glass compositions. Usually the main factors that control both thermal properties and degradation of material is the atom size and the bond length and when these features increase the degradation will be enhanced and make the material easily to be affected by thermal effects. The strontium atom (200pm) is larger than that of calcium (114 pm). This may decrease the attraction force between the nucleus and the outer shell (valent level) and make their ionic bonds more susceptible to be affected by the change in thermal changes comparing to the calcium ions. Similarly, these weakly formed bonds affect the dissolution rate in the same pattern as the thermal changes resulting in high degradation rate for the high strontium oxide composition both of them (Sr0 < Sr 3.5< Sr17.5 < Sr35). Hence, the inclusion of a larger ionic radius cation may make the glass network more susceptible to hydrolysis.

Another obtained finding was that the anion release trend was opposite to the degradation rate pattern and that could be explained as degradation is more governed by the heavy strontium ion Ions release data for the strontium oxide containing glass was compatible with the mass dissolution. These findings were similar to previous data that hypothesised that fully strontium substitution may not yield the highest phosphate ions release (Maçon et al.,

2017). Regarding Ca^{2+} and Sr^{2+} cations, strontium and calcium release were compatible with percentage of these atoms in the glass composition. For the sodium data, the values of Na^{+} release were all nominally very similar. interestingly some Ca^{2+} ion was detected in the totally replaced Calcium phosphate glass, it's source is likely from the fresh strontium carbonate which can contain as much as 0.7 weight %. pH results were compatible with anion release data, it can be hypothesised that the higher release of phosphates ions may lead to the formation of phosphoric acid that can cause pH decline which could be the most suitable explanation for pH data.

All glass formulations were shown to have good metabolic activity. The metabolic activity after one day was similar in all formulations and the TCP control. Although there was clear statistical difference between TCP and SrO 35 (p value < 0.05) at day 4 and 7, this did not neglect the biocompatibility of SrO 35. The results of ALP activity of cells seeded on glass discs of all formulations were promising, approximately double that of the control at each time point. The one exception to this was Sr17.5, which induced similar ALP activity per cell to other glass formulations at all time points except day 14, by which time it had doubled. The higher ALP activity of cells cultured on Sr17.5 fits with previous data concerning the optimal concentration of Sr for induction of osteogenic differentiation of bone marrow stromal cells (Lopa et al., 2013) . A concentration of 5 µg/ml SrCl2 was shown to induce higher levels of COL1A1 expression and calcified matrix deposition than 1 or 10 µg/ml. In the present study, the concentration of Sr^{2+} in extracts of Sr0, Sr3.5,

Sr17.5 and Sr35 after 14 days was 0.0, 1.1, 4.5 and 8.1 µg/ml, respectively. The concentration of Sr^{2+} released from Sr35 is therefore higher than optimal and explains the lower ALP activity induced by Sr35 than Sr17.5. These results explained that null hypothesis was not rejected for the glass discs formulations studied here.

In summary, strontium oxide and calcium oxide containing titanium dioxide stabilised glasses were successfully produced via melt quenching technique All formulations displayed controlled rate of degradation due to the incorporation of TiO_2 that may play a significant role in crosslinking the glass network. Moreover, glasses displayed acceptable cytocompatibility and ALP activity due to the incorporation of both strontium oxide and calcium oxide. SrO 17.5 glass formulation was considered the best composition that induced ALP activity which was about 3.5 times that of the control because of its degradation rate of strontium might be similar to the optimum Sr rate of 5 mg/ml as has been identified by previous studies (Lopa et al., 2013).

Further work is needed to be carried on some of the strontium compositions and on other compositions of phosphate glass that may be with good potential for bone growth such as zinc oxide containing phosphate glass.

Chapter 3 Assessment of physical, chemical and biological properties of zinc phosphate-based glass

3.1 Introduction

Zinc is considered as an essential element for bone health and growth (Yamaguchi, 2010). It plays an influential role on bone mineralisation through different mechanisms. One of these mechanisms is by enhancing the synthesis of aminoacyl-tRNA synthetase enzyme in osteoblasts. This enzyme is important for proteins production and genes expression The other mechanism is by the suppression of osteoclast proliferation and activity through its inhibitory action to special genetic and inflammatory molecules such as RANKL, PTH and PGE2 that are known to play the important role in osteoclastogenesis (Kishi and Yamaguchi, 1994, Park et al., 2013b). Moreover, zinc has a favourable effect in stimulating ALP activity and collagen production (Seo et al., 2010a).

As a result of all the identified advantages of zinc to human bone, many studies were done to incorporate zinc in glasses for bone biomedical applications. One research examined zinc-containing phosphate-based glass of different compositions, it was shown that zinc containing glasses has enhanced osteoblast like cells (HOB) cellular proliferation and attachment especially when it was added to a ternary phosphate glass at less than 5mol% of glass composition (Salih et al., 2007). Other researchers hypothesised that adding zinc to bioactive glasses may be necessary for hydroxyapatite formation on the glass surface after soaking in simulating

body fluid (SBF) (Lusvardi et al., 2008). A comprehensive study, carried out on a quaternary phosphate glass, suggested that adding zinc in more than 10% of glass composition may yield poor biocompatibility and cell death because of its high dissolution rate (Abou Neel et al., 2008c). Other correlated work concerned with the production of zinc containing silicate-based glasses which assessed different concentrations of zinc that did not exceed 5 mol%. The results were promising in regards to glass durability and cellular activity (Haimi et al., 2009). These results were confirmed later by other researchers who found that adding zinc containing silicate glass to biphasic calcium phosphates (BCP) which is composed of hydroxyapatite and β-tricalcium phosphate showed a positive impact on rat calvarium-derived osteoblast cell proliferation and behaviour (Badr-Mohammadi et al., 2014).

Despite all the studies that were performed on zinc incorporation in glass, there is very little work has been done on zinc containing quinternary phosphate glasses that have a controllable and fixed degradation rate.

The main aim of this chapter is to discusses the production of different zinc phosphate-based glasses that have a stabilised dissolution rate and examine their physical and cytocompatibility properties. Glass was produced in the formula of $(P_2O_5)50–(Na_2O)10–(TiO_2)5–(CaO)(35\text{-}x)–(ZnO)(x)$ when x = 0, 5, 10 or 15 (mol%). Titanium dioxide content was fixed at 5 mol% to control glass degradation. While zinc oxide content was added in a sequential way up to 15 mol%.

This study may lead to better understanding of zinc action in phosphate glass and its effect on the cellular activity that might be helpful in identifying their potential as a new biomaterial.

3.2 Materials and Methods

3.2.1 Materials

Four different glass compositions of phosphate glass were made by using phosphorus pentoxide (P_2O_5 98%, VWR, Lutterworth, UK), sodium dihydrogen phosphate (NaH_2PO_4, 99%, VWR, Lutterworth, UK), titanium dioxide (TiO_2, 99%, VWR, Lutterworth, UK), calcium carbonate ($CaCO_3$, 98.5%, VWR, Lutterworth, UK) and zinc oxide (ZnO, 99.95%, Sigma-Aldrich, Dorset, UK) as precursors.

3.2.2 Glass precursors calculations

Four different quinternary zinc oxide containing phosphate–based glasses (P_2O_5–$CaCO_3$–NaH_2PO_4–ZnO−TiO_2) were made. The details of glass composition codes and weight are listed in (Table 3.1).

Table 3-1 Glass compositions

Glass code	***and composition***	***Concentration (grams)***				
		P_2O_5	***NaH_2PO_4***	***TiO_2***	***$CaCO_3$***	***ZnO***
ZnO_0	***$P_{50}Na_{10}Ti_5Ca_{35}$***	***56.8***	***24***	***4***	***35***	***0***
ZnO_5	***$P_{50}Na_{10}Ti_5Ca_{30}Zn_5$***	***56.8***	***24***	***4***	***30***	***4***
ZnO_{10}	***$P_{50}Na_{10}Ti_5Ca_{25}Zn_{10}$***	***56.8***	***24***	***4***	***25***	***8.14***
ZnO_{15}	***$P_{50}Na_{10}Ti_5Ca_{20}Zn_{15}$***	***56.8***	***24***	***4***	***20***	***12.21***

Molar concentration of the precursors was calculated as follows: using the ZnO_{15} glasses as examples (P_2O_5 = 50 mol%; Na_2O = 10 mol%; TiO_2 = 5 mol%; CaO = 20 mol%; ZnO= 15 mol%).

A. Sodium dihydrogen orthophosphate (NaH_2PO_4)

$$2NaH_2PO_4 \longrightarrow Na_2O + P_2O_5 + 2H_2O$$

Mol. wt. ($g.mol^{-1}$)	240	62	142	36
Relative mol. wt. ($g.mol^{-1}$)		0.258	0.59	0.15

To get 10 mol% Na_2O, the required amount of NaH_2PO_4 is:

= [(mol. fraction of Na_2O) × (mol. wt. of Na_2O)]/ (relative mol. wt. of Na_2O)

= (0.10 × 62)/ (0.258) = **24 g**

B. Phosphorus pentoxide (P_2O_5)

Amount of P_2O_5 produced in the above reaction

= (amount of NaH_2PO_4 required) × (relative mol. wt. of P_2O_5)

= 24× 0.59 = 14.16 g

Amount of P_2O_5 required to produce 50 mol% P_2O_5

= 0.50 × 142 = 71.00 g

Therefore, actual amount of extra P_2O_5 to be added

= 71.00 – 14.14= **56.8 g**

C. Calcium carbonate (CaCO3)

	$CaCO_3$ ⟶	$CaO + CO_2$	
Mol. wt. ($g.mol^{-1}$)	100	56	44
Relative mol. wt. ($g.mol^{-1}$)		0.56	0.44

To get 20 mol% CaO, the needed amount of $CaCO_3$ is:

= (0.20 × 56)/0.56 = **20 g**

D. Titanium(IV) dioxide (TiO_2)

Mol. wt. of TiO_2 = 47.90 + (2 × 16) = 79.9

To get 5 mol% TiO_2, the needed amount of TiO_2 is:

= 0.05 × 79.9 = **4 g**

E. Zinc Oxide (ZnO)

Mol. wt. of TiO_2 = 65.4 + 16 = 81.4

To get 15 mol% ZnO, the needed amount of ZnO is:

= 0.15 × 81.4 = **12.21 g**

3.2.3 Glass preparation

This is explained previously in 2.2.3.

3.2.4 Materials characterization

3.2.4.1 Density Measurements

This is explained previously in 2.2.4.1.

3.2.4.2 X -ray diffraction

This is explained previously in 2.2.4.2.

3.2.4.3 Thermal analysis

This is explained previously in 2.2.4.3.

3.2.5 Chemical and physical studies

3.2.5.1 Degradation study (mass loss)

This is explained previously in 2.2.5.1.

3.2.5.2 Ion release

Ion release measurement was performed for each stored sample from the degradation study, this was done for the anions (PO_4^{3-}, $P_2O_7^{4-}$, $P_3O_9^{3-}$, $P_3O_{10}^{4-}$) and the cations too (Na^+, Ca^{2+}, Zn^{2+}) by using the ion chromatography systems (ICS1000, ICS 2500, Dionex, Thermo scientific, Hemel Hempstead, UK).

3.2.5.2.1 Anion release

This is explained previously in 2.2.5.2.1.

3.2.5.2.2 Cation release

This is explained previously in 2.2.5.2.2. except there is no strontium release.

3.2.5.2.3 Transition metal ion release

Ion chromatography (ICS 2500) system was used for measuring the transition ion (Zn^{2+}) release. This system was supplied by a 25 µl sample loop for sample injection and Ion Pac® CS5A cation ion exchange column in

combination with a CG5A guard column for transition and lanthanide metals ions detection. The program was set to run for 10 minutes.

The used eluent was Met Pac® PDCA (Dionex, UK), in which pyridine-2,6-dicarboxylic acid (PDCA) functions as a complexing agent for metal complex separation via anion exchange. This eluent was passed through reaction coil as a diluent for 4-(2-pyridylazo) resorcinol (PAR). This diluent has a controlled pH and low metal contamination and reacts with a wide range of metals, allowing detection limits in the parts per billion (ppb) range.

The calibration was done by preparing 100 ppm zinc stock solution. this was further diluted by deionized water into five different concentrations of 0, 1, 5, 25, 50 ppm.

3.2.5.3 pH measurements

This is explained previously in 2.2.5.3.

3.2.6 Cell Studies

3.2.6.1 Cells preparation

This is explained previously in 2.2.6.1.

3.2.6.2 Cell proliferation

Initially, sterilisation of three discs of each glass group was performed by immersion in ethanol then exposure to ultra-violet light for 10 minutes on each side. The sterilised glass discs samples were moved to 24 well plates on which MG63 cells were seeded evenly over the glass surface at a density

of 10000 cells per disc. To ensure the even distribution of cells on glass discs, 50µl of culture media with cells was used for seeding to ensure that the culture media would cover the glass discs with a meniscus only and not flow away from them. Then, the seeded cells were left for about 30 minutes in the incubator to permit for the proper attachment of cells to the glass discs. Afterwards, culture media was added to end up with 1 ml of culture media for each glass discs. After that all the samples were incubated at $37^{o}C$ in an atmosphere of 5%CO_2 for 7 days, Standard plastic glass cover slides were used as controls. Cell culture medium was replaced every 3 days.

At each time point, Live and dead assay was done for all the compositions by using calcein AM (4mM) as an indicator for live cells and Ethidium homodimer-1 (2mM) for dead cells. The working concentration of the both reagents was assigned by doing an initial calibration for both of them to get the most appropriate molarity that result in the optimal fluorescent colour. This calibration was carried out by seeding MG63 cells on 10 glass slide discs (five for calcien and five for ethidium). Various concentrations of reagents were prepared as recommended by the protocol. To determine the proper concentration of ethidium, triton x-100 was added to five calibration discs to aid in pre-treating and killing the cells. The best results were found with 1 µM calcien and 2 µM ethidium. Which were considered as the working concentration.

At each time point, the media was aspirated, and the cells were then washed gently with Dulbecco's phosphate buffered saline (D-PBS). After the

washing procedure, 3 mL of calcien and ethidium mixed working solution was added to each well plate and incubated for about 45 minutes. Following that, the solution was removed, and the samples were ready for the cell counting BioRad Radiance 2100 Confocal Laser Scanning Microscope (Bio-Rad Laboratories Ltd, Hemel Hempstead, Hertfordshire, UK) with the help of BioRad LaserSharp2000 v.6 software (Bio-Rad Laboratories Ltd, Hemel Hempstead, Hertfordshire, UK).

The direct cell counting was performed on 13 different pre-identified 1 mm squares on each glass discs. These squares were positioned on 15mm circle template which was made by transparent paper as is shown on (Figure 3.1). Live and dead cell counting was performed at three-time points (day 1, day 4 and day 7) using the Image J software program.

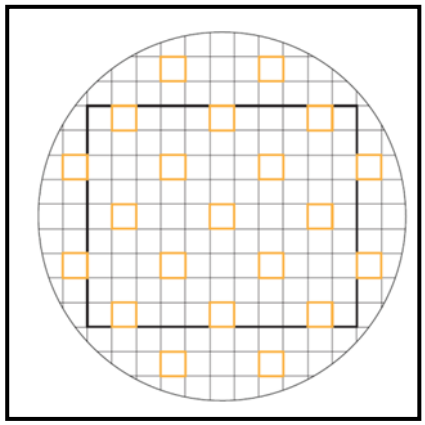

Figure 3-1 Transparent paper circular template

3.2.6.3 Measurement of metabolic activity of cells

This was explained previously in 2.2.6.2.

3.2.6.4 Cell imaging by scanning electron microscopy (SEM)

Scanning electron microscopy (SEM) images were done for MG63 cells over all glass discs composition. Cells were seeded according to the protocol discussed in 2.6.2.1. This was done for each sample at three-time points. (days 1,4 and 7). The procedure involved removing the culture media initially. Then, the cells with the glass discs were transferred to new 24 wells plate where they were fixed by adding 1 ml of 3% glutaraldehyde (Sigma Aldrich,UK) and leftover night for fixation. A dehydration step was the following step in which the glutaraldehyde was removed first, then cells were passed through a sequential process of washing. This washing step was carried out by using graded ethanol (50, 70, 90 and 100%) then drying by hexamethyldisilazane (Aldrich, UK).

3.2.7 Statistical analysis

Cell work data for both cells counting and metabolic activity studies were statistically assessed by hierarchal ANOVA to examine the null hypothesis stating that there is no clear biological and metabolic difference between the produced zinc glass discs and the control TCP group where $p<0.05$ has been used as a significance degree estimation.

3.3 Results

3.3.1 Density measurement

As is shown in (Table 3.2), glass density increased as the content of incorporated zinc oxide had increased. The density was ranging from 2.61 ± 0.004 $g.cm^{-3}$ in the quaternary glass (zinc free glass) to stand at 3.16 ± 0.039 $g.cm^{-3}$ for ZnO 15.

Table 3-2 Density measurement of all zinc containing phosphate glass compositions

Glass code	ZnO 0	ZnO 5	ZnO 10	ZnO 15
Density (g/cm^3)	2.61	2.7	2.95	3.16

3.3.2 X -ray diffraction

The XRD patterns for all the prepared glass samples are shown in (Figure 3.2). All the XRD patterns were free from any detectable crystalline phases and displayed a broad peak was observed in each spectrum at 2θ values of around 20–40°.

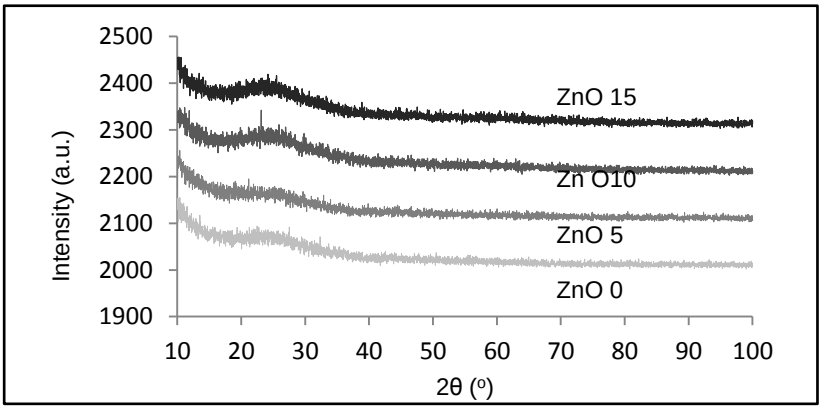

Figure 3-2 X-ray diffraction showing the amorphous nature of the prepared glasses

3.3.3 Thermal analysis

Table 3.3 explains the T_g values of the observed glasses. It showed that the incorporation of zinc oxide had led to decrease T_g value from 483 °C for the ZnO 0 to 429°C for the ZnO 15.

Table 3-3 DTA for zinc containing phosphate-based glasses measured in °C

Glass code	ZnO 0	ZnO 5	ZnO 10	ZnO 15
Tg (°C)	483	461	443	429
Tc (°C)	764	739	715	703
Tm (°C)	850	835	819	793

DTA spectra of the glasses are presented in (Figure 3.3). Similarly to T_g, *Tc* and *Tm* were also indirectly correlated with zinc oxide content in the glass. Regarding T_c, it was about 764 °C for ZnO 0% and declined as ZnO content increased to 703°C for 15mol% ZnO. The same trend was displayed for the melting point in which it declined with the extra incorporation of zinc oxide, it extended between the wide endothermic peak at 850°C for the zinc oxide free glass to about 793°C for ZnO15 %.

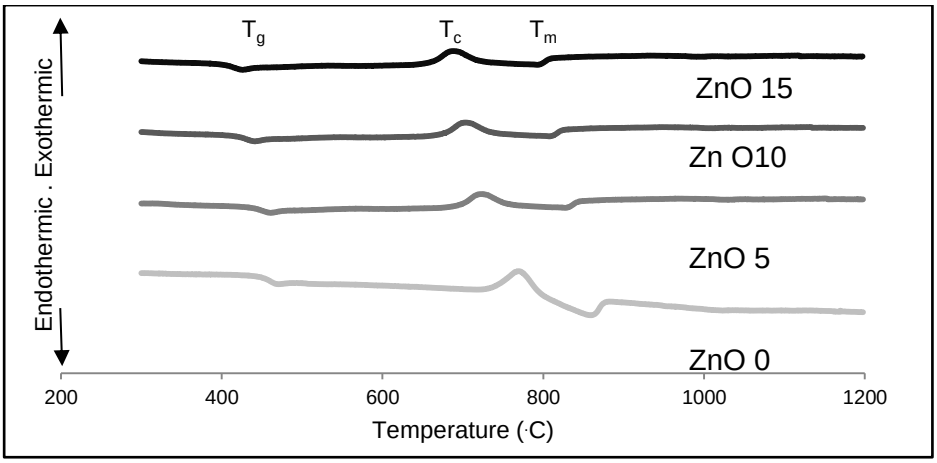

Figure 3-3 Differential thermal analysis of glasses showing the glass transition temperature (T_g) which is the midpoint of the first slope in each composition , crystallisation temperature (T_c) which is the upward peak in each line and melting temperature (T_m) which is the last downward peak in each line . Showing that these parameters declined as SrO content increased

3.3.4 Degradation study (mass loss)

Both (Table 3.4) and (Figure 3.4) show the mass loss per surface area measured in ($mg.cm^{-2}$) for two weeks period. There was a general cumulative mass loss per unit area measured ($mg.cm^{-2}$) over the whole-time frame for the all formulations. Though, the highest mass loss rate was in the compositions with higher zinc oxide contents. In other words, there was clear direct relation between zinc content in glass and mass loss rate.

For the whole-time frame, ZnO 15 formulation displayed the high mass loss rate. At day one, its degradation rate seemed to be seven times higher than that of ZnO0. This degradation pattern continued for the other time points to end up in day 14 at about 0.65 ± 0.013 $mg.cm^{-2}$ for ZnO 15 comparing to ZnO0 which was about 0.22± 0.021 $mg.cm^{-2}$ at the same time point. Both

ZnO 5 and ZnO 10 revealed similar degradation rates at all the time points which was between that of ZnO0 and ZnO15.

Table 3-4 Mass loss in (mg.cm^{-2}) for all glass compositions in four different time points

Glass composition	Mass loss (mg.cm^{-2})				
	Day 0	Day 1	Day 4	Day 7	Day 14
ZnO 0	0	0.037	0.119	0.164	0.223
ZnO 5	0	0.156	0.274	0.312	0.378
ZnO 10	0	0.171	0.283	0.321	0.410
ZnO 15	0	0.214	0.370	0.466	0.659

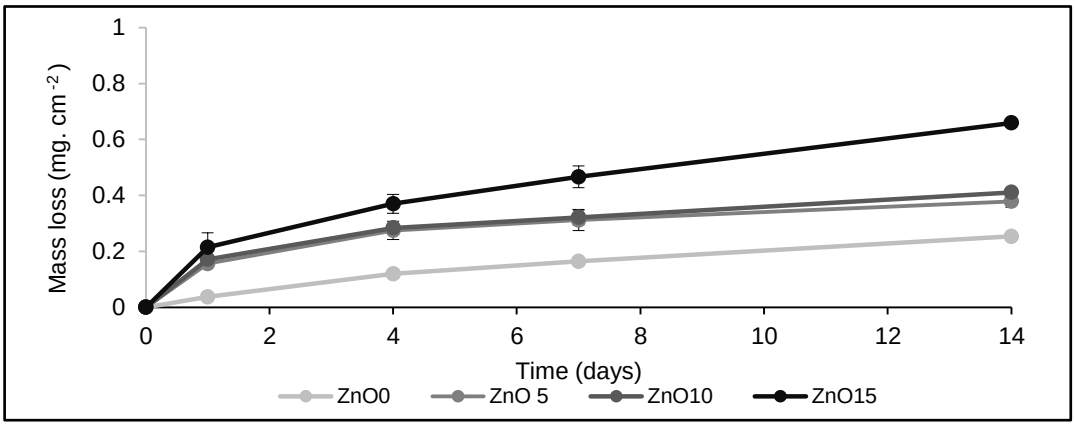

Figure 3-4 Mass loss in (mg.cm^{-2}) for all glass compositions over 14 days

3.3.5 Ion release

3.3.5.1 Anions release measurement

Zinc glasses anions release is displayed in (Figure 3.5). Anion release was measured for four different anions (PO_4^{3-}, $P_2O_7^{4-}$, $P_3O_9^{3-}$, $P_3O_{10}^{5-}$). All the glass compositions exhibited continuous cumulative increase for all the anions release with time. Regarding PO_4^{3-}release, ZnO15 glass compositions was found to have the highest release in comparison with the other compositions. It started at about 4.9 ±0.5 ppm in day 1 and ended at about 24 ±1.2 ppm after two weeks. The other compositions exhibited the same trend but with lower levels of anions release that did not exceed that of ZnO15. $P_3O_9^{3-}$ ions release displayed the same trend where the highest release was found in ZnO15 which was nearly three times more than other glass compositions over the whole study.

Regarding both $P_2O_7^{4-}$, $P_3O_{10}^{5-}$ ions, the maximum release was found in ZnO15 similar to the previous ions in which there was a very highly significant variation between it and the other types of glasses.

Generally, it was found that phosphate ions release was directly related with zinc content in glass and the sequence of the anions release was as follow (ZnO15>ZnO10>ZnO5>ZnO0).

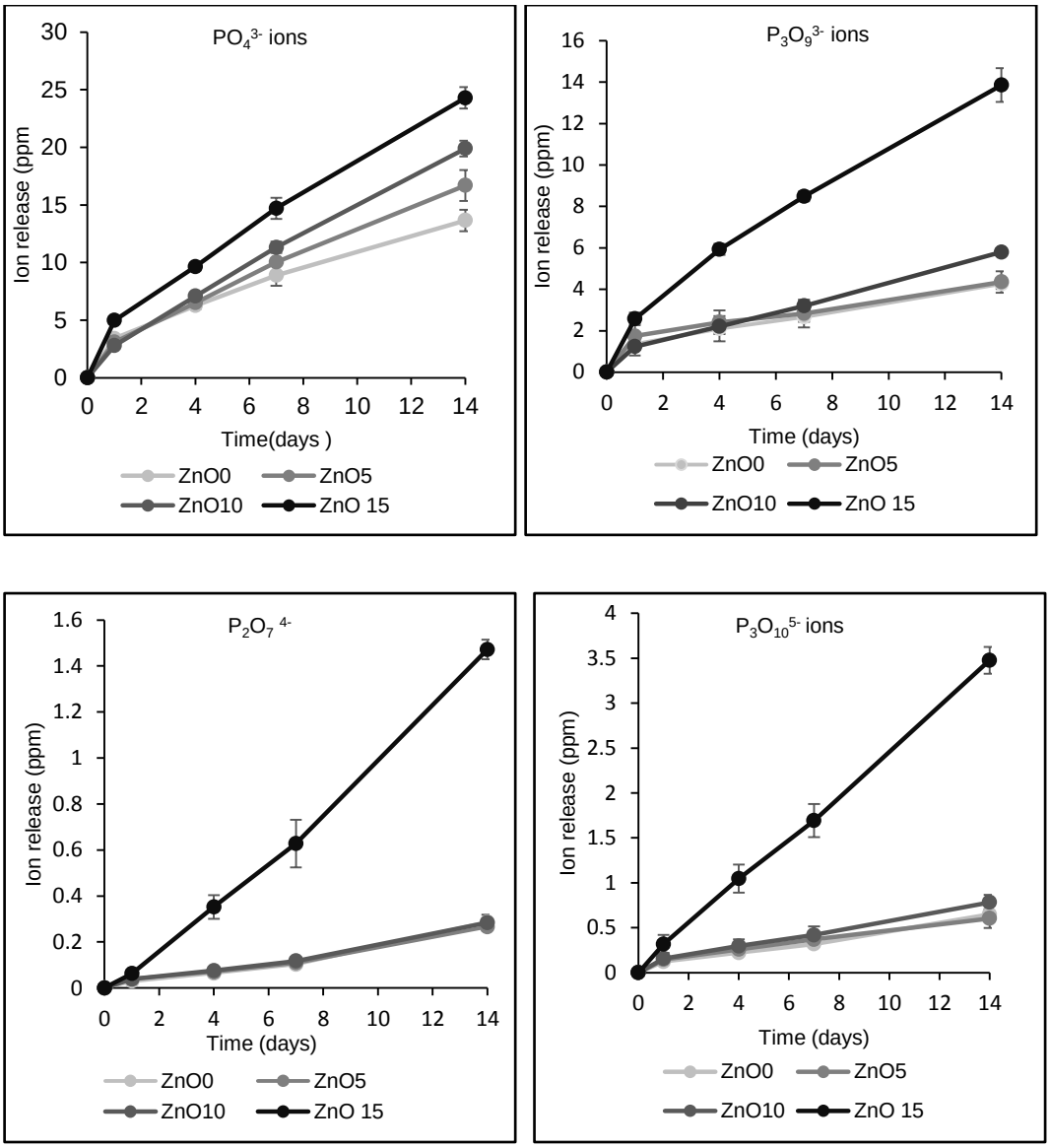

Figure 3-5 Anion release showing higher release of phosphates ions (PO_4^{3-}, $P_2O_7^{4-}$, $P_3O_9^{3-}$, $P_3O_{10}^{5-}$) in the high concentration zinc based glass (ZnO15) in comparison to other prepared glass compositions

3.3.5.2 Cations release measurement

Figure 3.6 displays the cations release of all glass compositions. Concerning sodium release, it was compatible with that of mass degradation and anions release in which the highest released Na^+ ions were found with the highest zinc content (ZnO15). This release rate dropped as zinc content declined in the glasses to be the lowest for the free zinc glasses (ZnO0). For Calcium ion release, its pattern was directly linked with calcium concentration in glasses; in other words, the highest free Ca^{2+} ions in water was detected in glasses that had the highest calcium content and the lowest zinc contents.

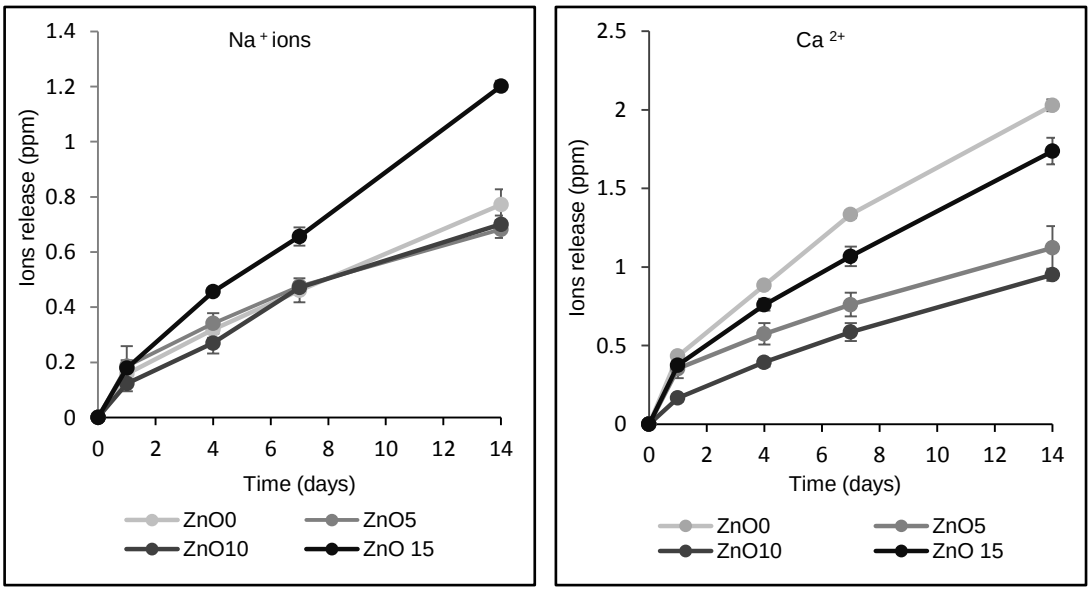

Figure 3-6 Cations release for all glass compositions Na^+ and Ca^{2+}

3.3.5.3 Transition metals ions release measurement

Zinc ion release is presented in (Figure 3.7). Its pattern generally followed that of degradation rate and anion release where it was directly related with the zinc percentage in glasses. The ultimate release was identified in ZnO15. It initiated at 0.3±0.13 ppm in day 1 and ended at about 1.3 ±0.22 ppm after two weeks. The second composition in the list was ZnO10 that commenced at 0.08 ±0.008 ppm and finished at about 0.59±0.03 ppm. This was followed by ZnO5 and ended with the free zinc formulations.

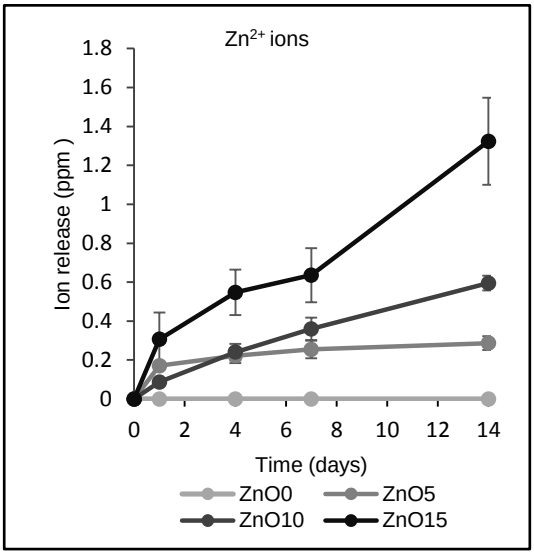

Figure 3-7 Transition metal Zn $^{2+}$ ions release showing the highest release for glasses with the highest zinc concentration.

3.3.6 pH measurements

pH measurements are displayed in (Figure 3.8). Generally, pH trend was similar for all the glass compositions in that it dropped sharply for the first day from 7 at day 0 to about 5- 5.5 at day 1. Although there was some slight fluctuation in pH values, it remained within the same range for the whole set of experimental time points.

Generally, as the amount of zinc oxide increased, the pH dropped, so the more acidic media was with the glass containing 15mol% zinc oxide followed by ZnO10, ZnO5 and ZnO 0.

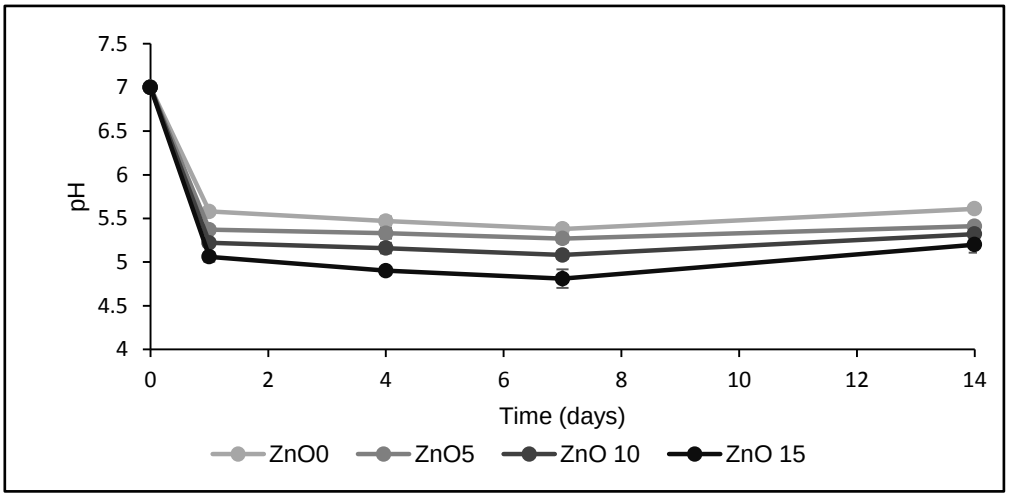

Figure 3-8 pH measurement

3.3.7 Cell proliferation

Figure 3.9 describes the cells proliferation data. Regarding the live cells results, cells were initially seeded at about 10000 cells per disc. Although this number has increased over the three -time points for all the compositions, there was a statistically significant difference between the produced glass discs and the control samples (TCP). The highest cells number was seen with TCP which was around 25972± 971 cells in day 1 and 125680± 23127 cells in day 7. These results were highly significant ($p < 0.05$) from all the samples especially ZnO15 glass discs samples which showed the lowest proliferative activity at around 13292±573 cells and 51894 ±15261 cells for day 1 and day 7 respectively. ZnO5 and ZnO0 glass formulation showed acceptable cellular proliferation activity but was less than that of control.

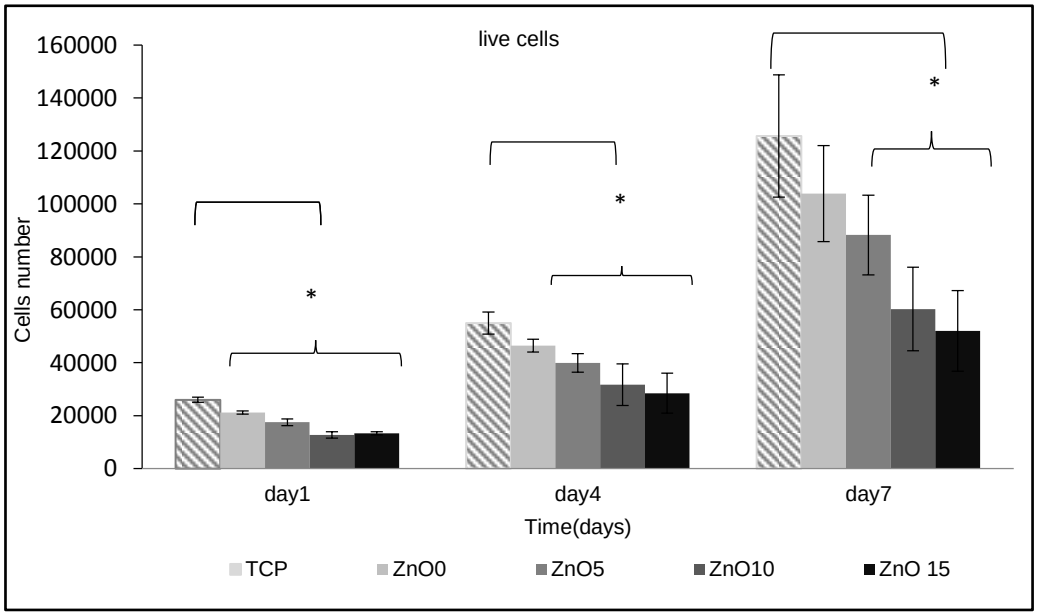

Figure 3-9 Live cells counting

The dead cell counting is displayed in (Figure 3.10). The data was clearly opposite to that of live cells counting where high content zinc composition (ZnO15) exhibited the highest number of dead cells over the time frame that was ranging from 873 ± 136 cells in day 1 to about 6057±1339 cells in day 7. TCP, ZNO0 and ZnO5 showed lower numbers of dead cells which were around half of that of ZnO15 in day 7. Dead cell number on ZnO10 glass disc was slightly closer to that of ZnO15 in day 7. ZnO15 was significantly higher than the all other composition over the whole study (p value<0.05).

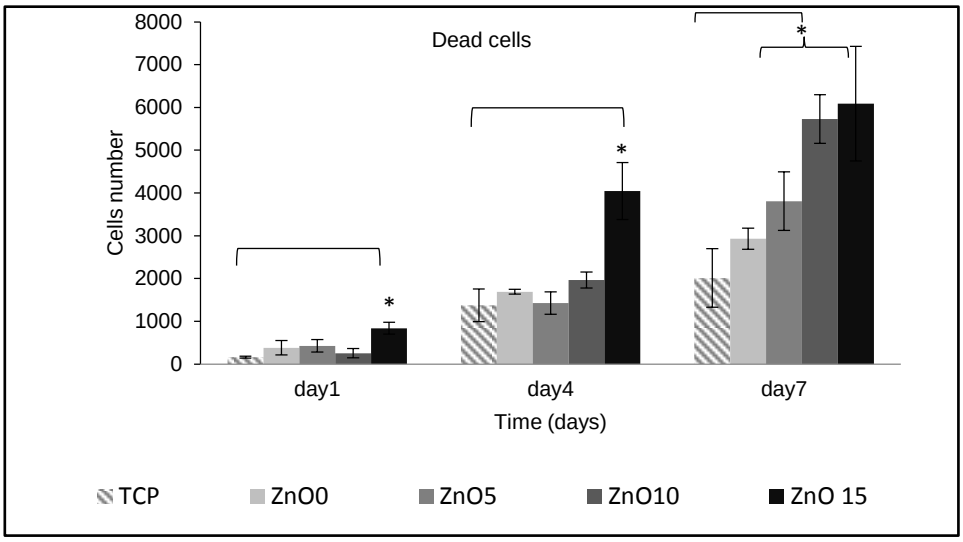

Figure 3-10 Dead cells counting

3.3.8 Measurement of metabolic activity

The measurement of the cellular metabolic activity is presented in (Figure 3.11). The results were measured at three different time points (day 1,4,7). They were represented by the percentage of the samples alamar blue fluorescence reduction in relation to the fully reduced alamar blue when the higher reduction percentage is related to the higher metabolic activity and

vice versa. Apart from ZnO15, all the compositions including the control displayed acceptable metabolic activity.

At day 1, TCP displayed around 6 ±1.2% of fluorescence reduction which was about double the percentage of all of ZnO0, ZnO5 and ZnO10 and about four times more than that of ZnO15 which had the lowest reduction value. At day 4, TCP reduction rate rose by three times to stand at about 16% which was significantly different from ZnO0, ZnO5 and ZnO10. This statistical difference cannot neglect the existence of enhanced metabolic activity that happened in these glass formulations whereas ZnO15 show sign of significance compared to the other remaining groups ($P < 0.05$).

After one week, the pattern of reduction remained similar to the previous two times points where the TCP (42 ± 3.3 %) showed the ultimate amount of reduction followed by ZnO0 (40 ±1.1 %), ZnO5 (35±2.2 %) and ZnO10 (33 ±1.12 %) respectively. ZnO15 continued to give the lowest values at about 2.5 ± 0.9 % fluorescence reduction.

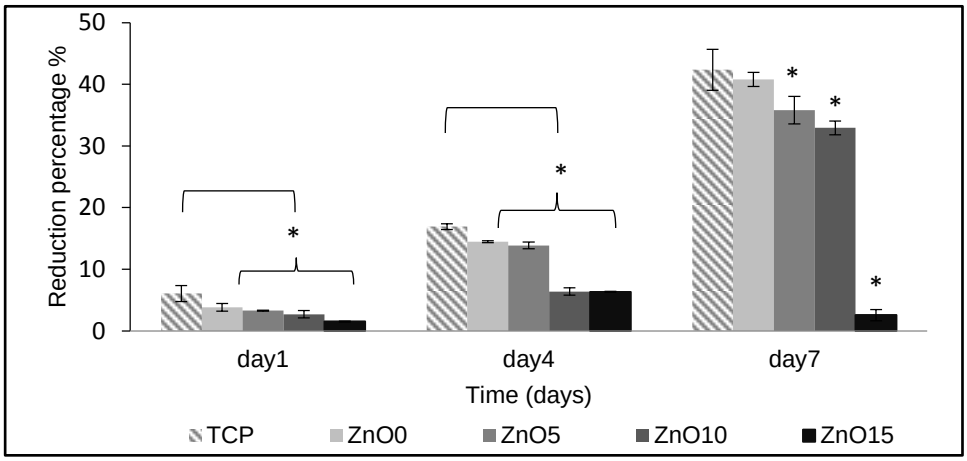

Figure 3-11 Metabolic activity estimation showing the percentage of alamar blue reduction as an indication for cellular metabolic activity

3.3.9 SEM Imaging

SEM images of MG63 cells attachment on glass discs are displayed in Figure 3.12. On day 1, MG63 cells did not have uniform shape and were generally evenly distributed over the glass disc surface. Though, cells on ZnO15 were slightly smaller in size. On day 4, more intercellular connections can be identified, and nucleus are more pronounced in their shape. Apart from ZnO15 discs, the images of all glass discs in day 7 displayed that cells were consistently spread over the surface. Moreover, there was a clear growth in cell numbers which were mostly interconnected with each other forming a semi-complete cellular layer. The only exception was in ZnO15 in which there was a low number of cells which were small in size and separated from each other.

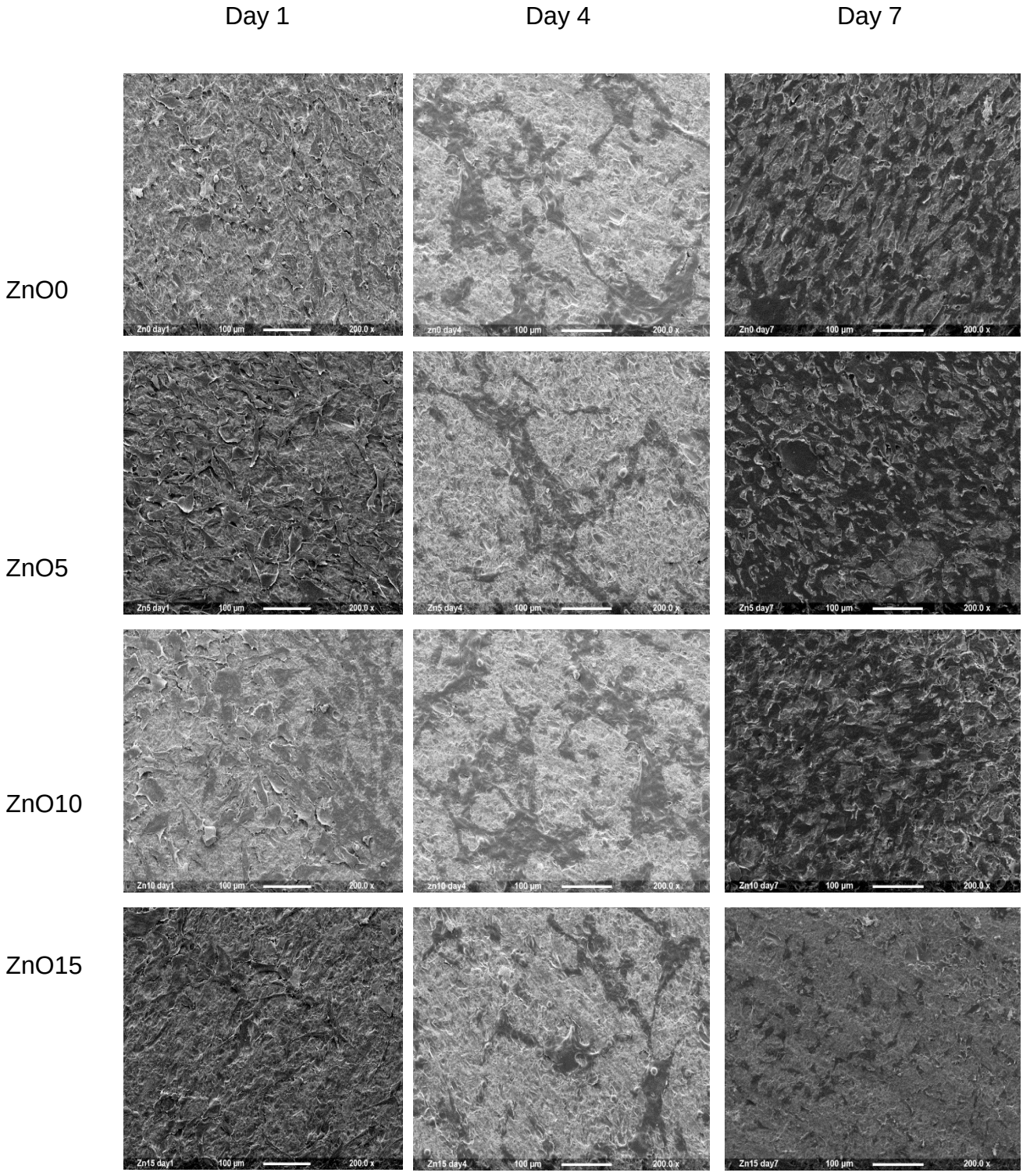

Figure 3-12 Scanning electron microscope images showing that the lowest number of attached cells was found with ZnO15 at all time points

3.4 Discussion

This chapter is mainly concerned with the development of different zinc containing phosphate-based glasses for hard tissue (bone) engineering applications since zinc is well known for its role in bone metabolism and structure (Seo et al., 2010b). This was performed by adding ZnO ions in different amounts to the quaternary glasses in place of CaO ions.

Previous studies have been carried out to analyse various zinc phosphate glass formulations of (P_2O_5-Na_2O-CaO-ZnO). The results of these studies suggested that zinc contained phosphate glass might have poor cytocompatibility because of its fast dissolution rate. This rate was enhanced as ZnO content increased within the glass network (Salih et al., 2007, Abou Neel et al., 2008c).

The results of this study were designed initially to confirm the successful production of glass discs. This was determined through density and XRD results. Density data displayed the positive relation between the increase in glass density and the incorporation of zinc content within glass which is mainly related to the difference between zinc density (7.14 $g.cm^{-3}$) and calcium density (1.54 $g.cm^{-3}$). Whereas XRD findings showed the amorphous nature of the prepared glass discs.

The differential thermal analyses data revealed that all the thermal variables had declined with the increasing incorporation of zinc oxide. This could be linked to the difference in bond enthalpies. When zinc oxide bond enthalpy is

about 284 Kj/ mol is less than that of calcium oxide bond 464 Kj/mol. Hence, less thermal energy is needed to break Zn-O bonds.

Degradation findings were similar to the DTA where adding ZnO to the glass composition has yielded a faster dissolution rate. This could be explained by two points. The first one is the difference of bond enthalpy and the second one may be due to the difference of bond electronegativity. Both of Zn-O and Ca-O bonds have pure ionic bonds (Ghadah S. Alghamdi, 2013). There is clear variation in electronegativity between both of Zn-O and Ca-O; Ca-O seems to be more electronegative (3.44-1=2.44) than that of Zn-O (3.44-1.65= 1.79) when 3.44, 1.65 and 1 are the electronegativity of O, Zn and Ca respectively. As a consequence, Ca-O bond polarity and bond strength are greater than that of Zn-O which may explain the glass susceptibility to dissolution when more zinc oxides percentage were added. This could affect the whole glass compositional structure and resulted in this pattern of weight loss seen (ZnO0< ZnO5< ZnO10< ZnO15).

Regarding ion release, it was found that adding zinc oxide content in the glass composition might be correlated with the high release of different phosphate anions and this may be due to the weak bond formation in a zinc phosphate glass as explained previously. Concerning cations, Na^{+} and Zn^{2+} ion release was comparable with the anion and mass degradation (ZnO0< ZnO5< ZnO10< ZnO15). The only exception was for Ca^{2+} ions which was released at higher levels in the glass with ZnO 0mol% glass and this result was the opposite to the previous findings, but that can be interpreted as this

composition has no CaO substitution, and its CaO content is higher than the others. Hence, it may release more calcium ions. pH results were clearly related with the anion results and that could be explained as phosphate ions are released at high levels and more phosphoric acid may be produced that can decrease the pH. All of these findings were consistent with that of Salih *et al* (Salih et al., 2007).

In regard to cell studies, the proliferation study was carried out through the direct counting of live and dead cells using confocal microscopy. This was done with the aid of a template. Many previous studies used live and dead fluorescent stain as a subjective tool for cell proliferation estimation. Though, this technique can have visual bias and poor sample presentation. The main aim in this study was to objectively establish the accurate live and dead cells number, and this was achieved by using the template. Only 13 identified squares per each sample were chosen for the cells counting measurements. Although the total area of these 13 squares composed only 7% of the whole disc area, their positions were selected in a way that ensure the full distribution over the whole central area of the disc to prevent repeated readings and give a valid picture of cell distribution over the disc since each of the selected squares was surrounded by non-interpreted squares. Cells number counting was performed only in the empty areas inside the square and avoiding the square borders that were fluorescent.

Seeding technique for cells was performed gently to attain a uniform cell distribution over the whole discs samples. This was performed through the

preparation of the intended seeding cell density in 50 µl of culture media which was found to be the optimum media volume to cover the whole disc surface area. The main outcomes of this experiment revealed that live cell number was mostly significantly different between the zinc glasses and control sample for all time points, this does not cancel the positive impact of these two compositions on cell proliferation. Conversely, cells number was apparently low for ZnO15 and ZnO10 formulations and were significant when they were compared with the control group having about half the cell number of the control samples. This was further confirmed by the dead cell counting data which was linked to zinc oxide content (ZnO15>ZnO10>ZnO5>ZnO0>control) which suggested that the glass with higher dissolution rate gave poorer cellular related data. Findings from ZnO15 dead cells numbers showed that they composed about 10% of live cell numbers on the same day for the all times points which signified cytotoxicity (Figures 3.9, 3.10).

Alamar blue assay is a useful tool for cell metabolic activity through its ability to be fluorescently influenced by the main by-products of reduction–oxidation (Redox) reaction because the live metabolic cells tend to produce H^+ ions that have the capability to reduce the weakly purple fluorescent Resazurin salt to strongly red fluorescent Resorufin (Lancaster, 1996). The alamar blue findings were concurrent with cell proliferation (live and dead cells counting) as it showed that ZnO15 had very low impact on MG63 metabolic activity and they were again clearly significantly different in comparison to the other glass

formulations at all time points. For ZnO10 data showed little variation from control samples (TCP) and were slightly different with ZnO10 live and dead cells findings. Though it showed an acceptable metabolic activity with time. The other two formulations (ZnO0 and ZnO5) appeared to have slightly lower levels of effect on metabolic activity compared to the control samples which matched that of live and dead cells data. The general trend of alamar blue metabolic activity was (Control>ZNO0>ZNO5>ZnO10>ZnO15). Although there was clear statistical difference ($P<0.05$) between the control and ZnO0 and ZnO5, these two compositions had a sign of metabolic activity enhancement that might indicate their benign effect on cellular activity.

SEM images emphasized the previous cellular related results; ZnO15 SEM images revealed that there was a decline in cell number with poor cellular interconnection.

All of these findings may be explained as a result of the fast rate of glass dissolution of ZnO15. This fast degradation rate has yielded high zinc ion release that could have a negative impact on cell proliferation by suppression of the expression of mRNa as was found in previous studies (Aina et al., 2007, Kwang Hwan Park et al., 2013). Interestingly, this study's results were very comparable with the previous study which reported that incorporation of zinc content >1.2 % wt. can lead to cytotoxic effects on osteoblastic MC3T3-E1 cells (Ito et al., 2000). In the present study, Zn composed about 1% wt. of the total glass weight in ZnO15 samples which may explain the undesirable cellular effects seen with this composition. These results described that null

hypothesis was rejected in regard to ZnO15 glass compositions as they showed signs of poor cytocompatibility. Whereas as it was not rejected in regard to the other zinc glass formulations (ZnO10, ZnO5) and the free zinc glass formulation (ZnO0) that possessed acceptable biological and cellular properties in comparison to the control groups.

In conclusion, although the development of zinc containing phosphate-based glass was successful, adding zinc oxide at 15mol% of the whole glass may have cytotoxic effects. However, adding zinc oxide in the percentage of 5-10 mol% may show better outcomes when compared to the ZnO15 samples.

Further work is needed to be carried on some of the ZnO5 and ZnO10 formulations to fully understand their cellular response. Moreover, development of glass in other features that may be more clinically relevant may be needed to carry out as well.

Chapter 4 Development of strontium and zinc phosphate-based glass microcarriers for biomedical applications.

4.1 Introduction

The use of bone graft substitute (BGSs) as biomaterials for orthopaedics and craniofacial bone tissue engineering applications is attracting a lot of interest. However, these biomaterials should acquire specific chemical and structural requirements that may provide these biomaterials with osteoinductivity which is needed to stimulate stem cells and growth factors (Hing, 2004). Beads were found to be one of these substitutes that might act as a good cell microcarrier (Sautier et al., 1992) and glass can be readily produced as beads for this type of application. One study assessed the *in vivo* application of bioactive glass (BAG S53P4) beads as a biomaterial for bone defect repair that resulted from osteomyelitis. This type of bioglass beads had shown good characteristics as both a filler material and as an antibiotic drug reservoir (Lindfors et al., 2010). BAG S53 P4 Bioglass beads were also used for many craniofacial defects repair such as orbital floor repair, nasal septal perforation repair, frontal sinusitis treatment and maxillary sinus augmentation. Most of these studies were clinically followed for an acceptable period of time by clinical and radiological investigations and it was found that they may be beneficial in some bone repair applications (van Gestel et al., 2015). Other research observed the development of 200-300 µm diameter silicate based micro beads by the sol gel technique. This research assessed many aspects

including: incorporation of biological proteins, cell adhesion and reaction to the microbeads and *in vivo* evaluation of the effect of these beads. The results hypothesised that these beads were potentially useful regarding their drug delivery and their ability to support mesenchymal stem cell attachment and proliferation (Perez et al., 2014).

Phosphate-based glasses beads were produced in the formula of ($50P_2O_5$, 40 CaO, (10-x) Na_2O, x TiO_2 mol 5) where x was 3, 5 ,7 mol. This study has found that producing glass beads with 5mol% TiO_2 was successful and may offer advantages for bone repair applications (Lakhkar et al., 2012). This study may be the only study that has been done on phosphate glass beads. Hence, further information is needed to understand the nature of cells biological reaction to phosphate-based glass.

The present chapter discusses the manufacturing of quinternary titanium phosphate-based glasses that contain zinc and strontium ions depending on the previous chapter results. The glass bead formulations were as follows (P_2O_5-Na_2O-TiO_2-CaO – ZnO or SrO). Where TiO_2 was fixed to 5mol% to control glass degradation, CaO was substituted by ZnO or SrO in proportions determined in the previous study.

This study may aid in recognising the useful aspects of phosphate beads as a potential material for dental or craniofacial applications.

4.2 Materials and methods

4.2.1 Materials

Four different glass compositions of phosphate glass were made by using phosphorus pentoxide (P_2O_5 98%, VWR, Lutterworth, UK), sodium dihydrogen phosphate (NaH_2PO_4, 99%, VWR, Lutterworth, UK), titanium dioxide (TiO2, 99%, VWR, Lutterworth, UK), calcium carbonate ($CaCO_3$, 98.5%, VWR, Lutterworth, UK), zinc oxide (ZnO, 99.95%, Sigma-Aldrich, Dorset, UK) and strontium carbonate ($SrCO_3$, 98.5%, BDH Laboratory Supplies, Poole, UK) as precursors.

4.2.2 Glass precursors calculations

This was explained previously in 2.2.2 and 3.2.2.

4.2.3 Glass beads preparation

Development of four different formulations of phosphate glass beads was carried out to examine their physical, chemical properties and the cellular ability to proliferate, adhere and penetrate through them. Initially, glass formulations were divided into zinc and strontium groups. Both zinc and strontium groups were designed to have two compositions. Zinc formulations were as follows: 50 P_2O_5-10Na_2O-5TiO_2-(35-x) CaO – x ZnO (mol %) where x (zinc oxide) was 5 mol% and 10 mol%. Strontium formulations were as follow: 50 P_2O_5 - 10Na_2O - 5TiO_2 – (35-x) CaO – x SrO where x (strontium oxide) was 17.5 mol% and 35 mol%. Precursor powders were weighed by

electronic balance (Sartorius) (Table 4.1). This was followed by powder mixing by using a Stomacher 400 blender (Seward). Following that, the mixture was then placed into a 200-ml volume Pt/10%Rh crucible type 71040 (Johnson Matthey, Royston, UK) which was placed in a furnace (Carbolite) at 1350^{o}C for four hours afterward. Then the melted glass was quenched on a metal plate to cool down. The cooled glass was then ground into small pieces and then further milled by (MM 301 Mixer Mill, Retsch GmbH and Hope, UK).

Table 4-1 phosphate glass beads composition

Glass code	***and composition***	***Concentration (grams)***					
		P_2O_5	***NaH_2PO_4***	***TiO_2***	***$CaCO_3$***	***$SrCO_3$***	***ZnO***
ZnO_5	***$P_{50}Na_{10}Ti_5Ca_{30}Zn_5$***	***56.8***	***24***	***4***	***30***	***0***	***4***
ZnO_{10}	***$P_{50}Na_{10}Ti_5Ca_{25}Zn_{10}$***	***56.8***	***24***	***4***	***25***	***0***	***8.14***
$SrO_{17.5}$	***$P_{50}Na_{10}Ti_5Ca_{17.5}Sr_{17.5}$***	***56.8***	***24***	***4***	***17.5***	***25.8***	***0***
SrO_{35}	***$P_{50}Na_{10}Ti_5Sr_{35}$***	***56.8***	***24***	***4***	***0***	***51.66***	***0***

Glass bead production was done by following Lakhkar protocol (Lakhkar et al., 2012). This was done by passing the powder through high flame source (methylacetylene-propadiene propane (MAPP) gas cylinder that was attached to torch) that can reach the 2925°C (Figure 4.1).

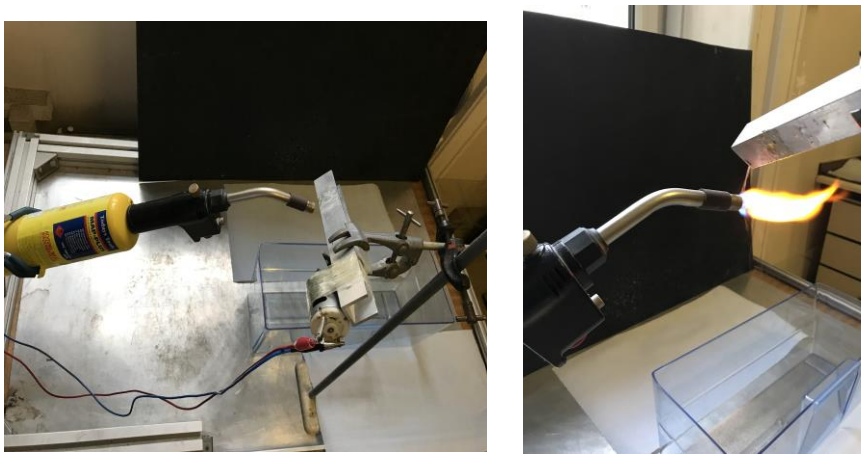

a b

Figure 4-1 Glass beads production. a. image showing the whole complex apparatus including flame torch, glass beads dispenser and glass beads collector. b. image displaying glass powder burning through the flame

The flame melted the glass and surface tension causes the beads to become spherical in shape. The glass beads were collected in a glass container. They were visualised under light microscope to confirm their production (Figure 4.2). Other samples of glass powder were prepared by grinding each glass bead formulation with (MM 301 Mixer Mill, Retsch GmbH, Hope, UK) grinder. The produced powder samples were used for XRD and FTIR analyses.

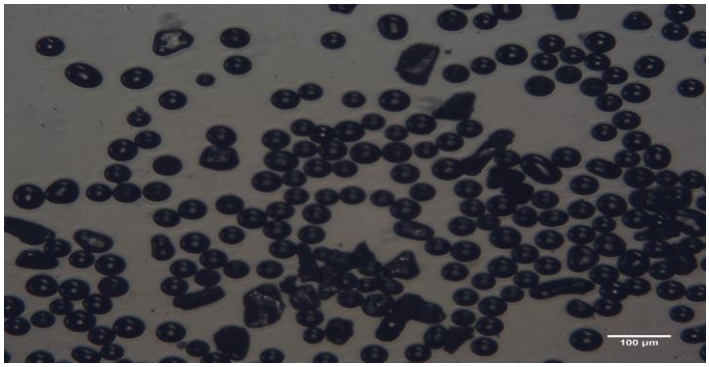

Figure 4-2 Glass beads under light microscope

4.2.4 Material characterization

4.2.4.1 Glass beads size distribution

Around 50 mg was taken from each composition of the produced glass beads; this amount was distributed on sticky dark tabs which were placed on an SEM stub for particle size measurement. The powder was slightly blown by compressed air to ensure its retention and dispersion on the dark tabs. Following this, coating with gold was done and visualisation under scanning electron microscope (SEM) (Philips XL30 FEGSEM) was performed. Five SEM images were chosen from various sites from stub (centre, left, right, up and down), the diameter size in micrometres for each bead in the SEM images were measured by using the Saturn software. The diameter measurement was done by using the software ruler function. Each bead reading was counted and used to measure the frequency distribution of the produced glass beads. For the frequency measurements, ten-diameter periods were designed starting between 25 µm-115 µm. Each period was extending for 10 µm, for example, (25-34 um), (35-44 µm). Each glass bead was added and included according to its diameter.

4.2.4.2 X-ray diffraction

This was described previously in 2.2.4.2.

4.2.5 Chemical and physical studies

4.2.5.1 Glass degradation

Glass degradation study was performed by incubating 300 mg of each composition of glass beads in 3 ml of ultrapure 18M $\Omega.cm^{-2}$ water at 37^{o}C for (day 1, 4, 7, 14). About 50 mg was taken out at each time, these were left for one day to dry in the desiccator. This was followed by spreading the dried glass beads on black stub stickers which were stuck on the stub to subsequently be visualised under SEM to assess the degradation and the surface changes. The ratio between glass bead weights to their immersion fluid volume was fixed in the whole study time which was 100mg.ml^{-1} or its equivalent by taking out 0.5 ml of water at each time point.

4.2.5.2 Ion release

Ion release was carried out for each glass beads formulation. This was done by using triplicate of 100 mg of each glass bead composition. These triplicates were immersed in 1ml of ultrapure 18M Ω/cm^{2}water and incubated at 37^{o}C for four times points (1, 4, 7 and 14 days). At each time point, the deionised water was taken out and stored for ion release study and replaced with fresh deionised water for the next time point. Then anion release was measured for the anions (PO_4^{3-}, $P_2O_7^{4-}$, $P_3O_9^{3-}$, $P_3O_{10}^{5-}$), cations (Na^{+}, Ca^{2+}) and the transition metals ions (Zn^{2+}) by using the ion chromatography systems (ICS1000, ICS 2500, Dionex, Thermo scientific, Hamel Hampstead,

UK). The ion concentration was calculated at each time point and accumulated with the previous time point.

4.2.5.2.1 Anions release

This is explained previously in 2.2.5.2.1.

4.2.5.2.2 Cations release

This is explained previously in 2.2.5.2.2.

4.2.5.2.3 Transition metal ions release

This is explained previously in *3.3.5.3.*

4.2.5.3 pH study

pH measurement was determined by using triplicates of 200 mg glass beads in 2ml DMEM culture media (Gibco, Life Technologies, UK, code 11960-085) in 24 well plates for (day 1, 4, 7, 14). The glass beads were incubated at 37^{o}C for the whole times period and changed every three days to mimic the cell culture study environment. At each point, the culture media was aspirated out and its pH was measured with an Orion star A111 PH meter (Thermo scientific, Hemel Hempstead, UK) and then replaced by fresh culture media for the next study time point. Culture media alone (pure culture media without glass beads) was used as a control for the whole-time course and was changed at each time as well. The pH electrode of the pH meter was calibrated by using the standard solutions of pH 4 and 7 before usage.

4.2.6 Cell Culture Studies

4.2.6.1 Cells preparation

Two types of cells were used for cell culture studies. The first type was human osteoblast-like osteosarcoma cell line (MG63, European Collection of Cell Cultures, Porton Down, UK) which were selected to undertake the preliminary routine screening of the cytocompatibility properties for the phosphate glass beads. The second type was human mesenchymal stem cells (hMSCs) (passage 3) which were chosen for performing the studies related to the ability of osteogenic lineage differentiation since these types of cells are considered the golden standard for such studies. Both of the cells were prepared by the same procedure. Initially, the cells were taken out from the liquid nitrogen tanks in which they were stored. Following thawing they were transferred to 15ml falcon tubes where they were suspended in 5 ml Dulbecco's modified Eagle medium (DMEM, Gibco, Life Technologies, Paisley, UK). This was followed by centrifuging the suspended cells at 1000 rpm at 20°C for 5 minutes to separate cells from media. Following the centrifugation process, the supernatant culture media was removed from the falcon tube and the MG63/hMSCs pellet in the bottom of the centrifugation were suspended in 1 ml of Dulbecco Modified Eagles' Medium (DMEM). Later, the cells were introduced into a 150 cm^2 flask containing Dulbecco Modified Eagles' Medium (DMEM).

Cell proliferation process in the flask was carried out in a 37°C/ 5%CO_2 incubator till the cells were 80–90% confluent. Cells confluency was checked

daily under light microscope (Olympus CK 2). When cells reached a confluency of 80%-90%, they were washed with phosphate buffer solution (PBS) and then trypsinised by adding 6 ml of 0.025% trypsin-EDTA to the flask and incubated at 37°C/ 5%CO_2 for 3–4 minutes to ensure cell detachment from the flask surface. Cell detachment was checked under light microscope by identifying the floating cells. Then, the trypsinisation process was inhibited by adding 6 ml of fresh media to the trypsinised live cells. The whole 12 ml cell suspension was then pipetted out from the flask and introduced into 15 ml falcon tube which was centrifuged subsequently at speed of 1000 rpm for 5 minutes. After this centrifugation process, gentle removal of the 12ml supernatant was done to avoid disturbing the cell pellet. Finally, 1 ml of media was added to the cell pellet prior to the cell counting procedure, this procedure was done by using the Trypan blue dye following the recommended protocol (Strober, 2001).

For cell culture studies, two types of media were used. For the MG63 cell cytocompatibility studies, Dulbecco's modified Eagle medium (Gibco, Life Technologies, UK, code 11960-085) supplemented with 10% foetal bovine serum (Gibco) and 1% penicillin/streptomycin (PAA Laboratories, GE Healthcare, Chalfont St. Giles, UK) was used. Whereas for hMSCs osteogenic differentiation studies, osteogenic medium (OM) was prepared as used in previous work (de Girolamo et al., 2007) by using low glucose Dulbecco's modified eagle medium (DMEM) , supplemented with foetal bovine serum , 1% penicillin/streptomycin, dexamethasone (0.1 μM),

ascorbic acid 2-phosphate (0.2 mM), and glycerol 2-phosphate (10 mM; last three chemicals procured from Sigma–Aldrich, Dorset, UK).

Seeding procedure was preceded by glass bead sterilisation. Sterilisation was done firstly by bead immersion in 99.9 % ethanol (Sigma- Aldrich, Dorset, UK) and then exposing beads to dry heat at 180°C for 1 hour. The seeding procedure was similar for both cell types. A quantity of 100 mg of each glass bead composition was used as a sample. This amount was firstly coated by bovine fibronectin in PBS (10 µg. ml^{-1}) for one hour to aid in initial cell attachment. The coated beads were then transferred into an ultra-low attachment 24-well plate (Corning, USA) in which the plate bottom surface was covered with beads completely. Later on, these glass beads were incubated in culture media overnight at 37°C. The next day, the culture media was taken out from the glass beads and the cell seeding step was carried out on the glass beads according to the preferred seeding density in which cells were left for 30 minutes in an incubator to allow cell attachment. After that the glass beads were transferred into 6.5 mm inserts in 24 well plates. Nondegradable commercial silica based glass microspheres (Polyscience Inc., USA) were used as a control for all the cell culture studies.

4.2.6.2 Metabolic assay (CCK assay)

A CCK study was carried out through using MG63 cells. Seeding density was 3000 cells per 100mg of glass beads. The glass beads were placed in trans-well insert in 24 well plates. Triplicates of each composition were used for this study. The 24 well tissue culture test plate was left in a 37°C/ 5% CO_2

incubator for three times points (1, 4 and 7 days). The control group (silicate beads) were seeded according to the same procedure. In parallel, cells were seeded in a second test plate at different densities (0, 5000, 10000 and 25000 cells) for calibration. The calibration was done by correlating the cell number with the yielded absorbance reading prior to exposing them to the CCK agent. The equation that resulted from the calibration procedure was used to establish the approximate cell number of the study samples groups (Figure 4.3). At each time point, CCK8 (Cell Counting Kit 8, Sigma-Aldrich, Dorset, UK) was added to each well in a 10% proportion of the culture media then incubated for 3 hours. Afterwards, absorbance measurement was performed for each well plate in triplicate by using a plate reader (Infinite® M200, Tecan) at 450 nm wavelengths. The resultant absorbance data were applied in the calibration equation to obtain the quantified cell number.

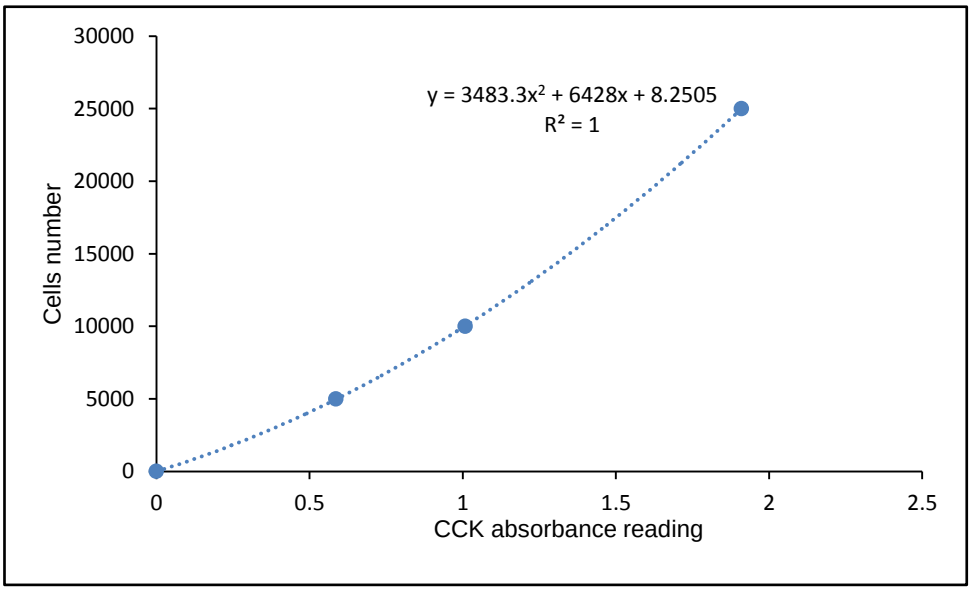

Figure 4-3 CCK calibration correlating cell numbers with their fluorescent readings

4.2.6.3 Alkaline phosphatase Assay

An alkaline phosphatase assay was carried out by using human mesenchymal stem cells (hMSCs). Seeding density was 25000 cells per 100mg of glass beads. The glass beads were placed in a trans-well insert in 24 well plates. Triplicates of each composition were used for this study, and, as before, silicate beads were used as control group. The 24 well tissue culture test plate was left in a 37°C/ 5% CO_2 incubator for two-time points (7 and 14 days). At all the time points, the culture media was aspirated initially following the protocol of (Alkaline Phosphatase Assay, SensoLyte® pNPP). This was followed by rinsing the glass beads and cell mixture with assay buffer (prepared by dilution of the assay buffer with deionized water for ten time) for two times. Then, a prepared solution of 0.002 Triton x-100 (20 µl of Triton x -100 in 10 ml of assay buffer) was added to lyse the cell membranes. Afterwards, the glass beads were pipetted vigorously for 1 minute to aid in cell permeability, cells were lysed further by two cycles of freeze-thawing cycle (- 80^{o}C for 20 min, followed by 37^{o}C for 12 min). Then the glass beads with the permeabilised cell complex were aspirated and collected in small plastic tubes which were agitated at 4°C for 10 minutes. After that, cell separation from their suspension was performed by centrifuging at (2500 G, 10 min, 4 °C). Then triplicates of 50 µl of supernatant solution from each vial was aspirated in a 96 well plate. Another 50 µl of pNPP solution was added to each sample.

Calibration was done by preparing a sequence of ALP standard (10 µg/ml) dilutions. Seven dilutions (100, 50, 25, 12.5, 6.25, 3.1, 0 ng /ml) were prepared by diluting the alkaline phosphatase standard reagent with the buffer solution. Triplicate of 50µL of each standard was added to 50µL pNPP substrate in a 96 well plate (Figure 4.4). After adding the pNPP solution to both sample and standard substrate, incubation of 96 well plates were carried on at 37°C for 30 minutes. Finally, a stopping reagent was added into each well before taking triplicate absorbance measurements of each trans-well by (Infinite® M200, Tecan) at 405 nm wavelength.

A calibration curve was obtained from the standards reading. The equation of this curve was used to relate the absorbance reading with the ALP concentration in the samples (Figure 4.4).

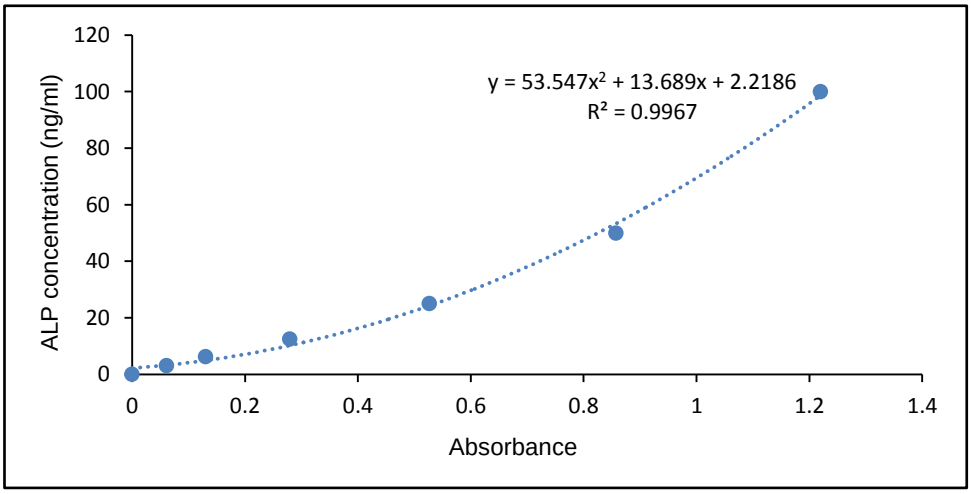

Figure 4-4 Calibration line of ALP assay. Done by preparing different concentrations of ALP and correlate the corresponding fluorescence reading with each of the concentration.

4.2.6.4 Ca assay (mineralisation assay)

Mesenchymal stem cells (hMSCs) were used for the Ca assay. The cells were seeded at density of 25000 cells per 100mg of glass beads. The glass beads were placed in trans-well insert in 24 well plates. Triplicates of each composition were used for this study, and silicate beads were used as control group as well. The 24 well tissue culture test plate was left in a 37°C/ 5% CO_2 incubator for two times points (14 and 21 days). At each time point, the culture media was firstly taken out and the glass beads were washed with phosphate buffered saline (PBS) three times following the protocol (Quantichrom^{TM,} Calcium Assay Kit (DICA-500), Bioassay System). This was followed by transferring the beads to 24 well plate where 1ml of 1M HCl addition was carried out. The plate then was agitated for 40 minutes by shaker. The agitation with HCl step aimed to help in cell lysis. After the lysis step, triplicates of 5µl of each trans-well aliquot was transferred to 96 well plate and about 200µl of prepared Ca working agent was added to each triplicate.

Fresh Ca working agent was prepared at each time point. The preparation was made by mixing 5ml of each of the provided reagent A and B. The mixing of these reagents was done in 15 ml falcon tube covered with aluminium foil to prevent the light affecting the working reagent.

Calibration was done by preparing six gradual dilutions of Ca standard (100µL, 80µL, 60µL, 40µL, 20µL, 0µL) which were made for calibration following the protocol (Quantichrom$^{TM, Calcium}$ Assay Kit (DICA-500), Bioassay

System). Triplicate of each standard was introduced into a 96 well plate with the prepared 200µl of the working solution (Figure 4.5). The slope of the calibration equation was used in determining the calcium concentration of glass beads sample according to the equation 1.

$$Ca\ conc = \frac{\text{OD sample} - \text{OB blank}}{\text{slope}} \quad \ldots\ldots\ldots\ldots\ldots\ldots\ldots\ldots\ldots\ldots\ldots\ldots\ldots\ldots 1$$

Other triplicates of 100 mg of each composition were incubated alone without seeding cells to deduce the effect of glass composition on the final results.

After adding the Ca working solution to both sample and standard substrate, the mixtures were left for two minutws and then absorbance was measured at a wavelength of 612 nm (Infinite® M200, Tecan).

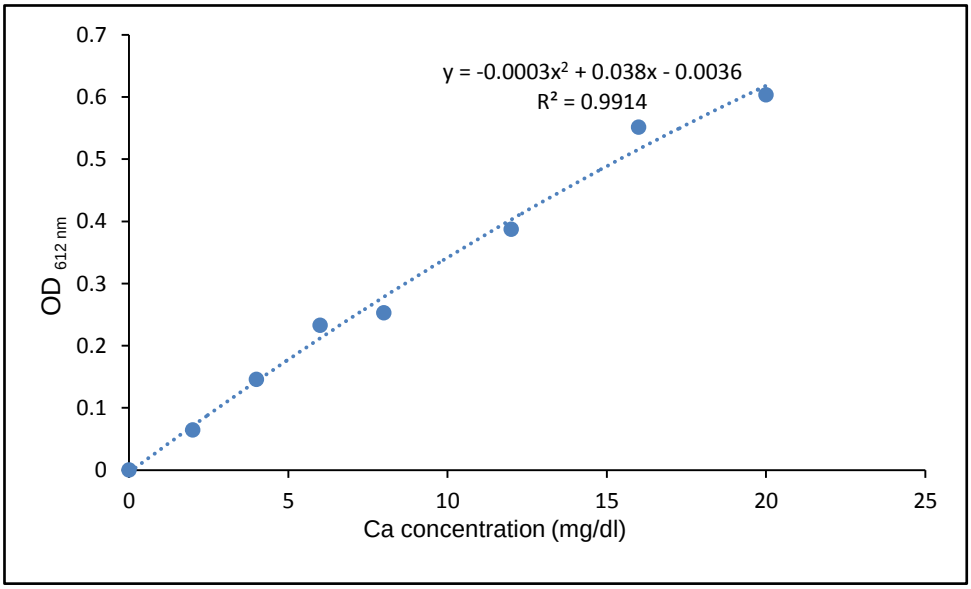

Figure 4-5 Ca calibration curve

4.2.6.5 SEM cells imaging

This was performed for the MG63 cells and done for three times points (day 1, 4,7) following the same procedure that is described previously in 3.2.6.5.

4.2.6.6 Confocal microscope cells imaging

hMSCs imaging was done by confocal microscopy using phalloidin (Alexa Fluor® 488 Phalloidin, Sigma-Aldrich, Dorset, UK) for cytoskeletal staining and propidium iodide (Sigma-Aldrich, Dorset, UK) for nucleus staining. The first step of this procedure was cell fixation in 3.7% formaldehyde followed by cell permalisation by using 0.5% triton X-100. This was succeeded by staining cells with the fluorescence stains. Staining with phalloidin was done by preparing it firstly through dilution 5 µl of stock solution in 200 µl PBS for each sample. Then cells were immersed with the prepared reagent for 20 minutes in dark room to reduce evaporation and photo bleaching. After staining with phalloidin, samples were washed with PBS for two times (1x 1 minute then 1 for 5 minutes) in the dark. Then staining with propidium iodide was done by immersing each sample with it in the concentration of (4 µg/ ml) for 10 minutes at dark. Finally, visualisation of samples was done using a BioRad Radiance 2100 Confocal Laser Scanning Microscope (Bio-Rad Laboratories Ltd, Hemel Hempstead, Hertfordshire, UK) with the help of BioRad LaserSharp2000 v.6 software (Bio-Rad Laboratories Ltd, Hemel Hempstead, Hertfordshire, UK).

4.2.7 Statistical analysis

Cell studies results were statistically assessed by Kruskal–Wallis to examine the null hypothesis that stated that there is no apparent or significance variation between the prepared phosphate glass beads and the control silicate beads in regards to the cellular proliferative ability and cellular osteogenic differentiation where $p<0.05$ has been used as a significance degree estimation.

4.3 Results

4.3.1 X -ray diffraction

The XRD patterns for the whole prepared glass samples are shown in (Figure 4.6). All the XRD patterns were free from any detectable crystalline phases and displayed a broad peak which was observed in each spectrum at 2θ values of around 20–40°.

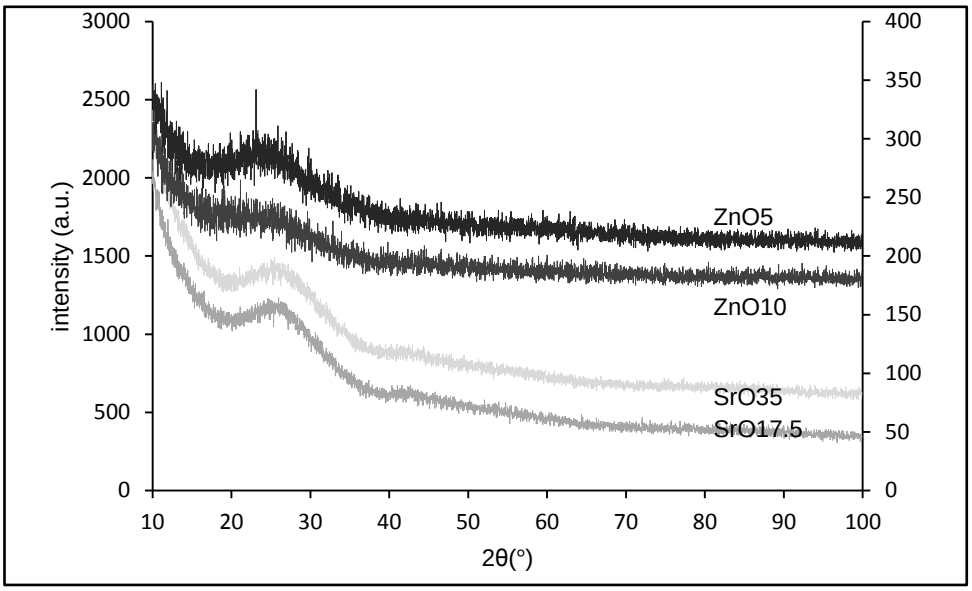

Figure 4-6 X- ray diffraction pattern for all the produced glasses

4.3.2 Glass beads size distribution

Figure 4.7 illustrates the SEM image of beads and their distribution according to their sizes. The analysis of different SEM images of the different glass beads groups revealed that the highest glass beads frequency was found in diameters between 65-84 µm. According to the results, glass beads frequency number did not exceed 10% for the diameters which are

less than 45µm. Though, this number was clearly higher for the diameter periods that are ranging between 65-84 µm where the frequency number reached 25 in some specific groups. Concerning glass beads with diameter more than 85 µm, their frequency number was less than 65-84 µm groups which was around 15. According to all of these findings the majority of glass beads produced were between 65 µm-104 µm.

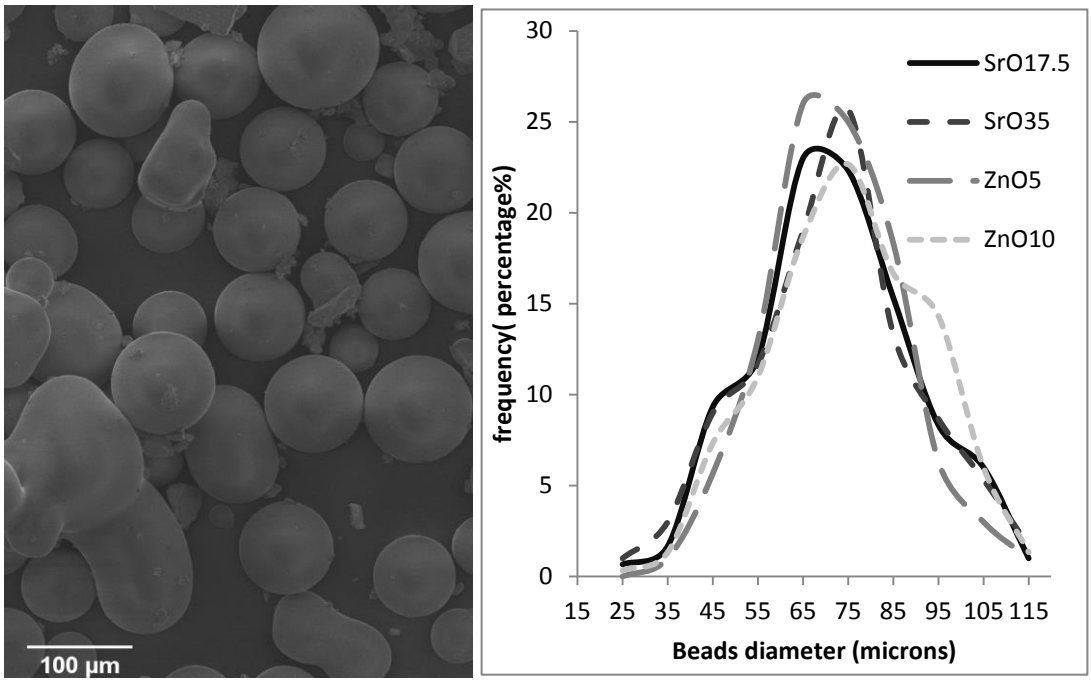

A *B*

Figure 4-7 A-SEM picture of glass beads B- frequency distribution of glass beads

4.3.3 Degradation study

As shown in (Figure 4.8), SEM images were taken to investigate the impact of immersion of glass beads in deionised water on their surface structure. The data revealed that there was a continuous surface wear that increased within time. At day 1, there were no apparent surface changes in comparison with day 0. Though, there was a pronounced surface wear on the glass beads on day 7, this wear was very prominent and clear in the zinc oxide containing glasses and appeared as groups of multiple pits. While strontium oxide containing glasses displayed lower levels of changes especially with SrO17.5 groups which did not appear to be affected. On day 14, glass surface degradation was more prominent in zinc glasses as well as strontium glasses; there were more pits and small cracks appearing in the zinc oxide containing glasses, whereas for the SrO containing glasses, there was more surface wear in SrO35 and small pits occurred in SrO17.5. These results showed that the ZnO10 glass had the highest susceptibility to surface changes followed by ZnO5 then SrO35 and finally SrO17.5, which displayed the minimum level of surface changes.

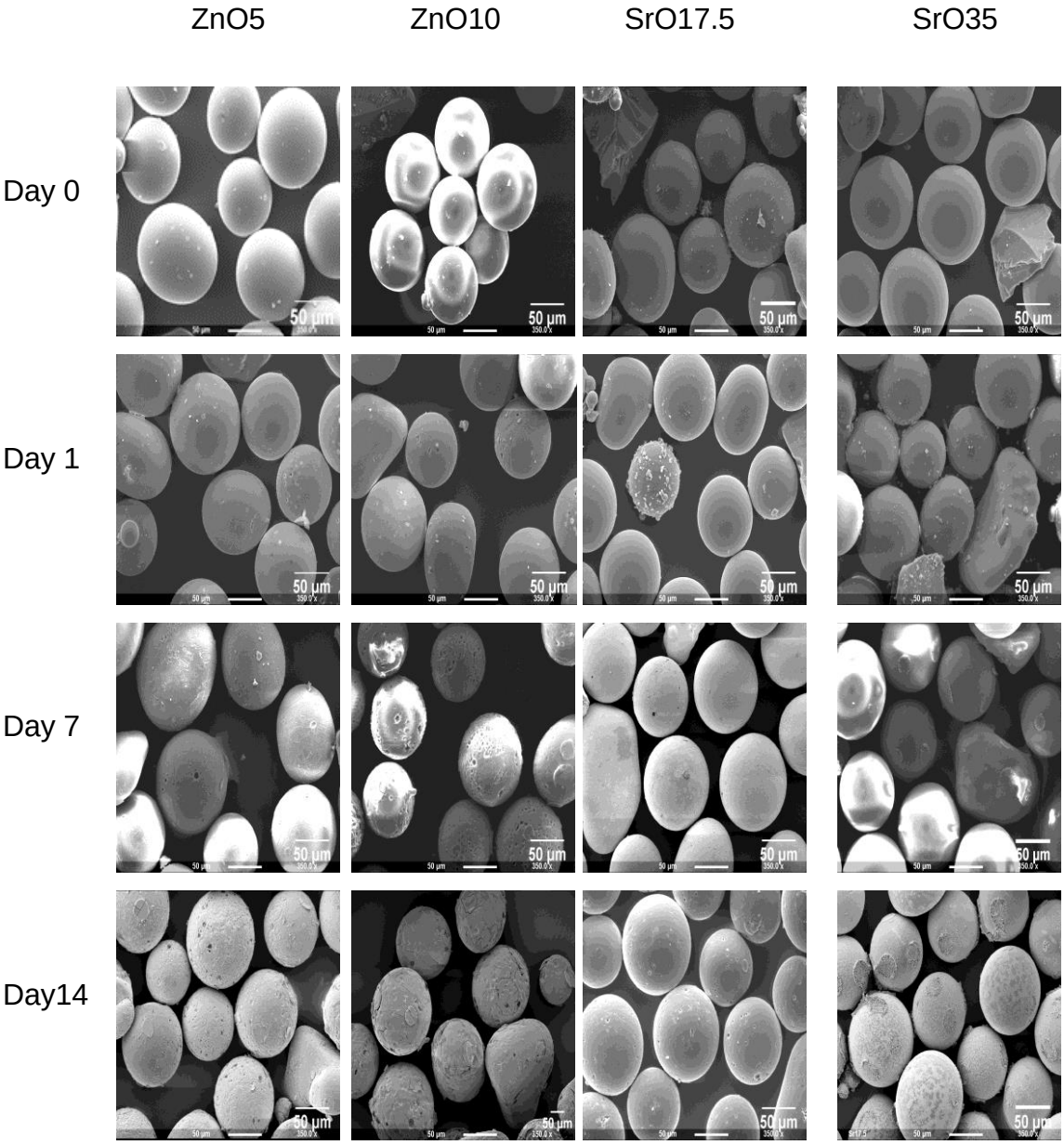

Figure 4-8 SEM pictures for glass beads after incubation in deionised water showing the least degradation was with ZnO10 in day 14.

4.3.4 Ion release

4.3.4.1 Anion release

Glass bead anion release is shown in (Figure 4.9). Anion release was measured for four different anions (PO_4^{3-}, $P_2O_7^{4-}$, $P_3O_9^{3-}$, $P_3O_{10}^{5-}$). All the ions released for all the compositions showed an increase within time. Generally, SrO35 glass beads release of anions was apparently less compared to the other glass bead formulations. Whereas the anions release concentration of both zinc containing glass beads were approximately similar to each other over the whole study.

Concerning PO_4^{3-} release, ZnO5 displayed the highest rate of release of free phosphate over the time frame. At day 14, phosphate ions were released to about 4970 ±197 ppm just slightly higher than ZnO10 release which stood at 4425±229 ppm and was about double that of SrO 17.5 and five times that of SrO35 which were 2456±271 ppm and 716±29 ppm respectively. Both $P_2O_7^{4-}$ and $P_3O_9^{3-}$ anions release followed the same pattern, the release of these two ions were highly pronounced in the ZnO10 formulation which was followed by ZnO5 and SrO17.5 that had about the same ion concentration release leaving the SrO 35 with lowest anion release which was about half that of ZnO10 at day 14. In regard to $P_3O_{10}^{5-}$ ions release, its figure release was analogous to PO_4^{3-} release which was again higher in the zinc oxide containing compositions.

Generally, it was found that phosphate ion release was linked clearly with the incorporation of zinc oxide into the glass compositions.

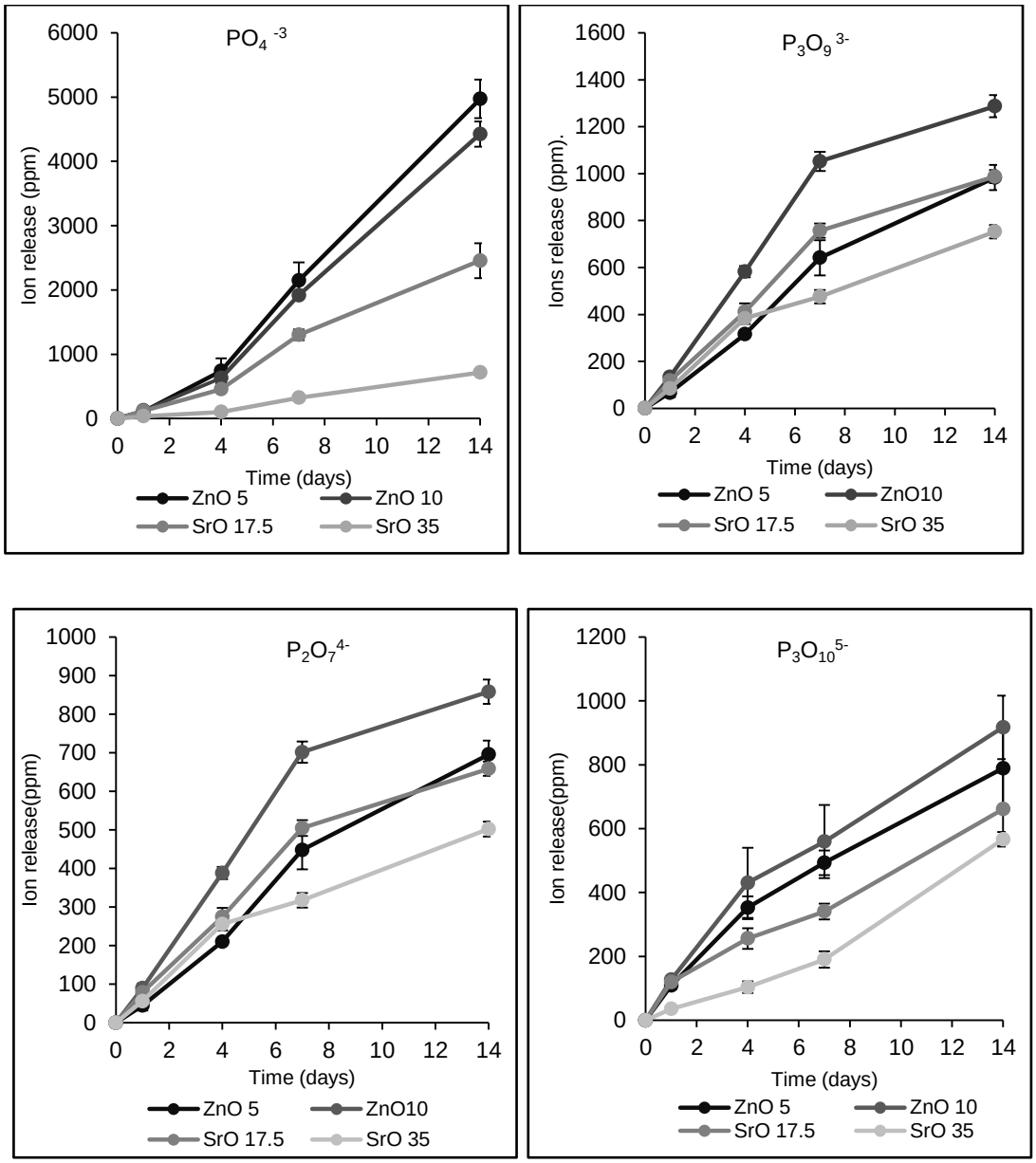

Figure 4-9 Anion release showing higher release of phosphates ions (PO_4^{3-}, $P_2O_7^{4-}$, $P_3O_9^{3-}$, $P_3O_{10}^{5-}$) by zinc based glasses in comparison to strontium glass

4.3.4.2 Cation release

Glass beads cations release is shown in (Figure 4.10). Generally, cations release (Na^+, Ca^{2+}) acted in the same way as anions release where the maximum release was established with zinc glass formulations and the pattern of cations release was as follows ZnO5>ZnO10>SrO17.5>SrO35. Both Na^+ and Ca^{2+} release was increased with time. Though, there was a clear difference in the rate of ions increase among the different compositions. While the release was in its maximum rate with ZnO5 glass beads, it was significantly low in other compositions such as SrO35. At day 1, Na^+ and Ca^{2+} releases for ZnO5 was about 8.5 ± 0.08 and 16 ± 0.3 ppm respectively in comparison to day 14 which was 106 ± 5.5 and 92 ± 6.2 respectively. Whereas for SrO35, it rose up in day 1 from 0.7 ± 0.15 and 0.85± 0.03 for Na^+ and Ca^{2+} respectively to about 8.6 ± 0.4 and 1.8 ± 0.03 in day 14.

Sr^{2+} ion release was around 3 ppm for both SrO17.5 and SrO35 on day 1. As the study continued for the next time points, SrO35 tended to release more Sr^{2+} ion than that of SrO17.5 to end around 33 ± 0.3 ppm on day 14 which was significantly higher than that of SrO17.5 at around 25± 0.6 ppm.

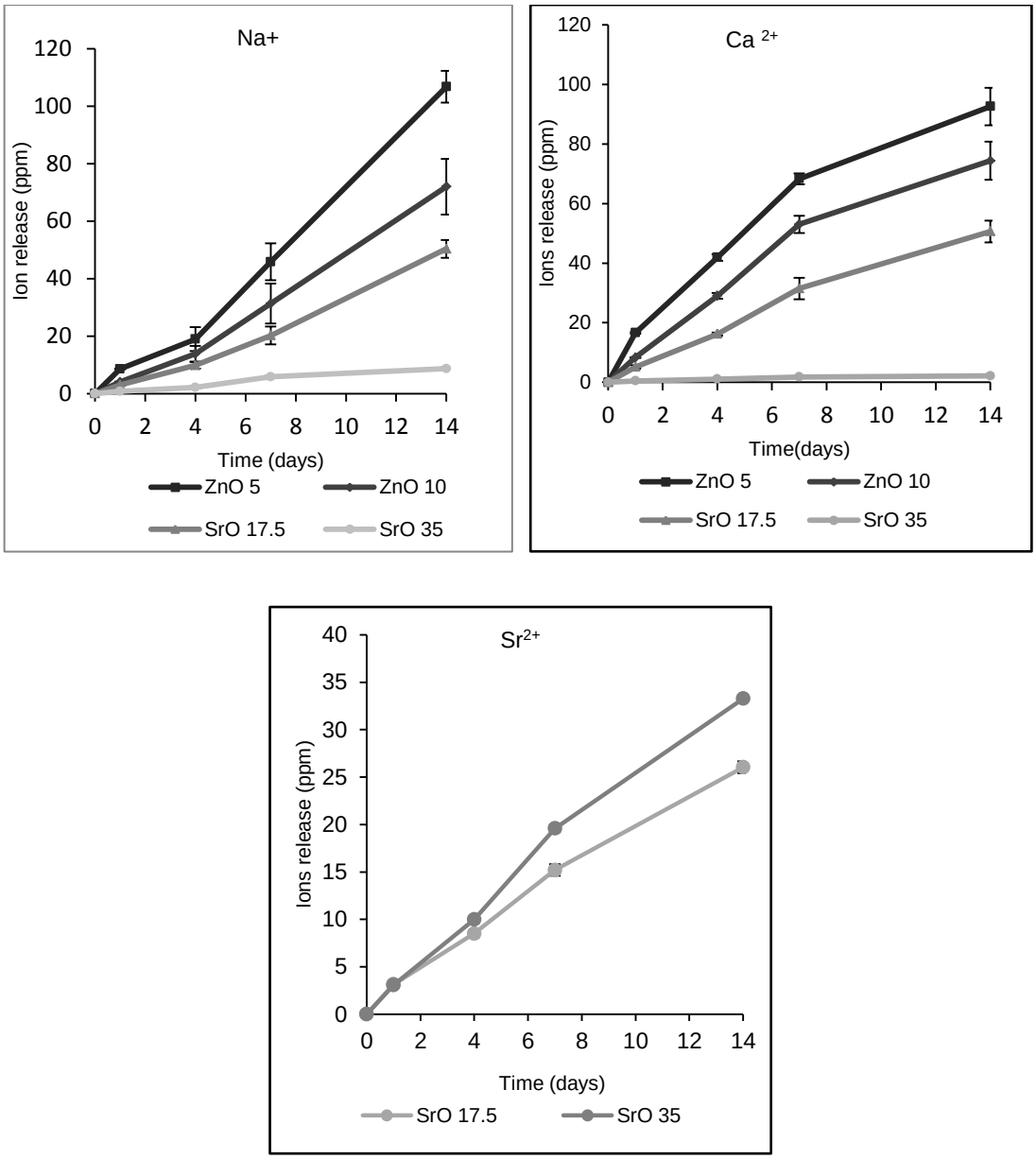

Figure 4-10 Cation release showing higher release of phosphates ions ($Na^{+,}$ $Ca^{2+,}$ Sr^{2+}) release

4.3.4.3 Transition metals ions release

As it can be seen in (Figure 4.11). Zinc ions exhibited variation in regard to their release that was controlled by their composition. Despite Zn^{2+} ions release was quite similar on day 1 at about 35 ppm, ZnO10 glass clearly released more Zn^{2+} ions over the time points after day 1 to stand at around

385±23 ppm after two weeks that was about 100 ppm more than that of ZnO5 which ended at 280±10ppm on the same day point concluding that Zn^{2+} release is directly related with zinc content in glass composition.

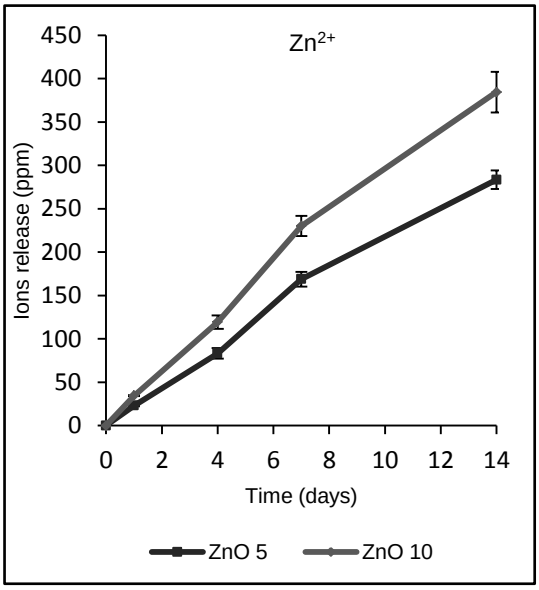

Figure 4-11 Zn^{2+} ions release revealing more zinc ions yielded from ZnO10

4.3.5 pH Measurement

pH measurements are displayed in (Figure 4.12). Generally, pH results revealed an apparent difference in their level over the time course of the study. Initially pH readings were about 8.7 before the study was commenced. Alhough, it moved up in day 1 to reach around 9.2-9.3 for all groups, this increase remained at that level until the second-time point (day 4) when a slight gradual decline was seen for all the formulations apart from the control that remained constant for the whole experiment.

Surprisingly, ZnO10 decreased significantly after day 4 and exhibited the lowest pH level for the whole period until the end of the study finishing just slightly higher than 8.2.

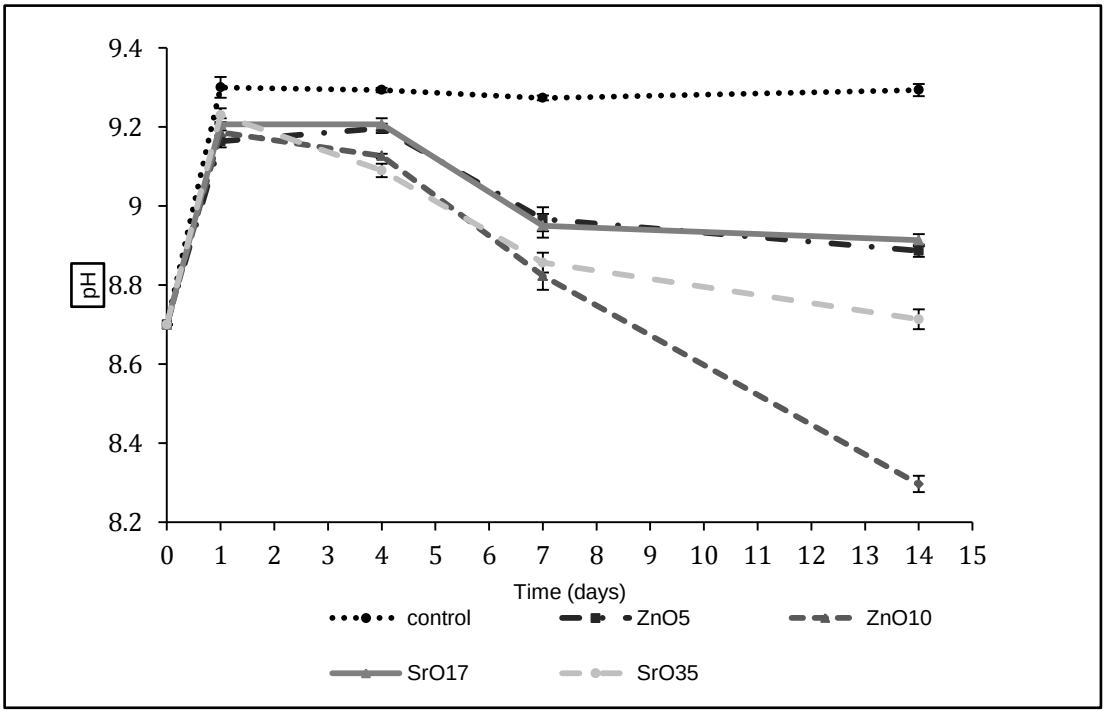

Figure 4-12 pH level showing that ZnO10 was with the least pH level in comparison to the control which remained steady.

4.3.6 Cell assays

4.3.6.1 Metabolic assay (CCK assay)

CCK data are illustrated in (Figure 4.13). the general outcomes of the CCK assay showed that the number of cells increased within the study time. Initial cell seeding density was 3000 cells per trans-well. This number increased sharply to stand at 13000 cells / trans -well at day 1 for both ZnO5 and SrO17.5. The former was higher than the control and more than both of ZnO10 and SrO35 at around 7000 cells. On day 4, cell number in both ZnO5

and SrO17.5 were around 34000 cells which was significantly lower in comparison to the control that was about 38000 cells. At the last time point, cellular growth continued to increase and ended at around 40000 cells for ZnO5 and SrO17.5, which was about 5000 less than that of the control. Whereas ZnO10 and SrO35 displayed again the lowest level of cytocompatibility as indicated by the cell number.

In general, SrO35 and ZnO10 showed the lowest cell numbers for all three times points. Whereas SrO17.5 and ZnO5 displayed more promising results over the same time frame.

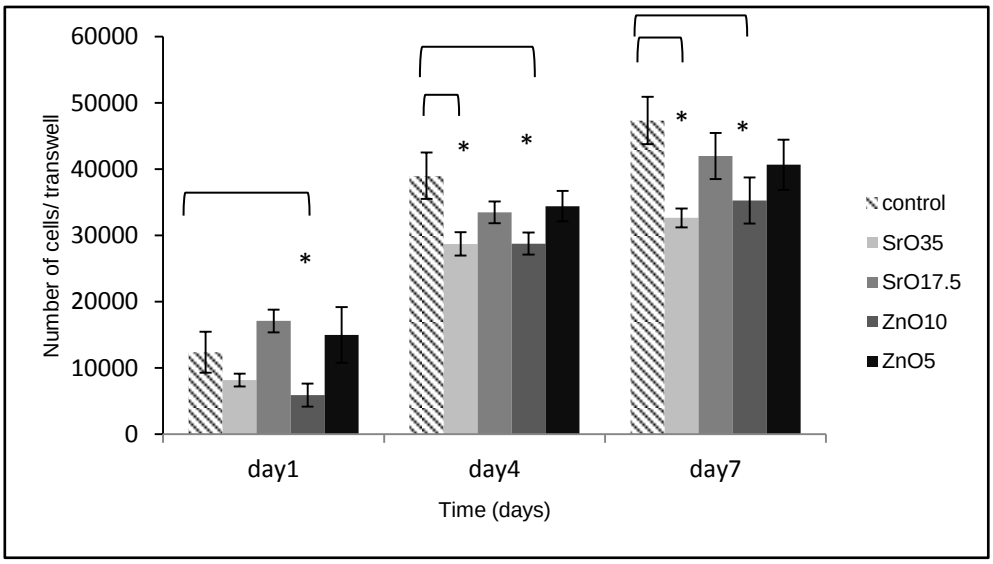

Figure 4-13 CCK assay for MG63 cells showing that both ZnO5 and SrO17.5 supported cell proliferation in comparison with the control

4.3.6.2 Alkaline phosphatase assay

Figure 4.14 summarises the alkaline phosphatase assay results after 7 and 14 days. At day 7, all compositions showed an enzyme production activity approximately identical to the control which was around (6.5 ng/ml) except

ZnO5 and SrO35 glass beads group which were statistically slightly higher than control. On day 14, there was a generally a clear rise in enzyme levels for all the produced glass beads. Though, the maximum level of ALP was shown in ZnO5 and SrO17.5 glass beads about (17.5 ng/ml) which was slightly less than the control (20 ng/ml). Both SrO35 and ZnO10 were significantly different from the control in the whole study time ($p<0.05$).

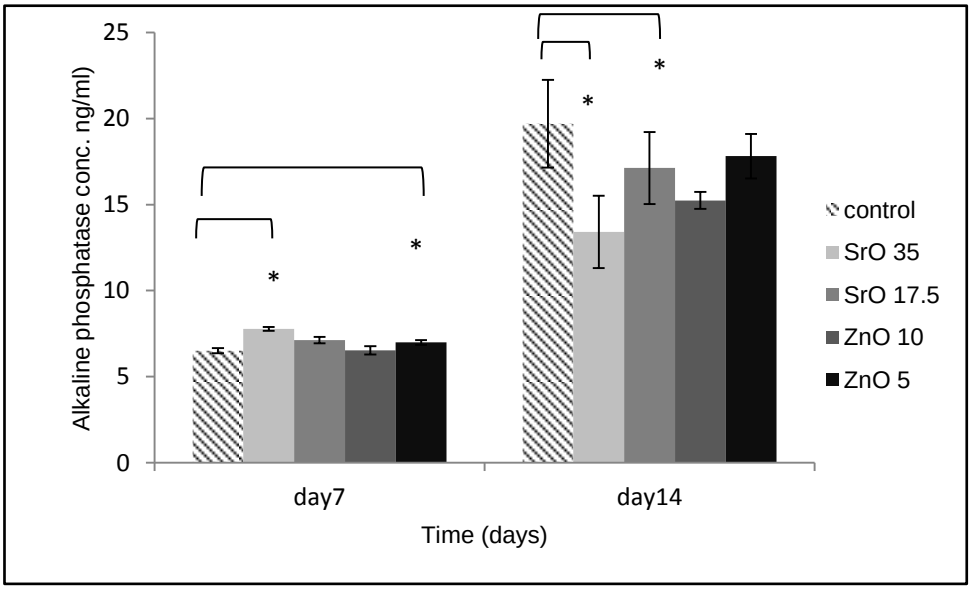

Figure 4-14 Alkaline phosphatase for hMSCs measured by µg/ trans-well, displaying an acceptable enzyme concentration in ZnO5 and SrO17.5 in relation to the control.

4.3.6.3 Mineralisation assay (Ca assay)

Figure 4.15 displays the Ca assay for day 14 and 21. The general summary of this assay revealed that all the strontium and zinc containing glass beads provoked calcium release. At day 14, it seemed that ZnO5 and SrO17.5 beads have stimulated hMSCs cells to produce calcium at levels of (13-14

mg/dl trans-well) which was clearly higher than that of the control that exhibited the lowest concentration of calcium (2 mg/dl trans-well). ZnO10 and SrO35 revealed promising results also (9-11mg/dl trans-well) but not as that of ZnO5 and SrO17.5. Although the control data showed a 4-fold increase on day 21 in comparison to day 14, it showed again the minimum concentration compared to the zinc and strontium-based glasses. ZnO5 and Sr17.5 results were highly significant (28 mg/dl trans-well) compared to the other compositions and the control.

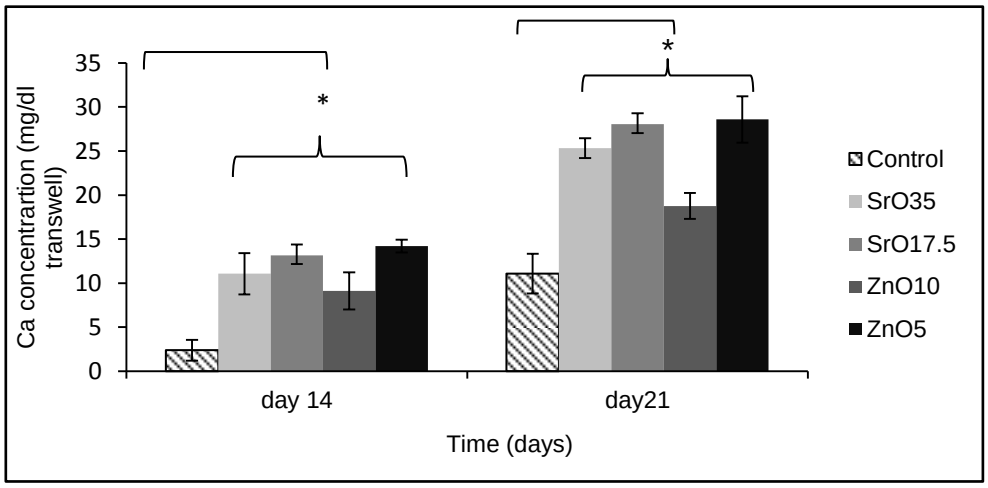

Figure 4-15 Ca concentration for hMSCs measured by µg/ trans-well for day 14 and 21, revealing that ZnO5 and SrO17.5 have the highest calcium concentration.

4.3.6.4 SEM cell imaging

SEM pictures are displayed in (Figure 4.16). The Figures displayed the ability of MG63 cells to attach to SrO17.5 glass beads. At day 1, cells have the stability and the potential to interact with glass beads and adhere to them individually (Figure 4.16a). However, SEM images of cells on day 7 displayed the potential of MG63 to proliferate between glass beads and extend their

appendages to make a continuous layer of cells among the beads on day 7 (Figure 4.16b).

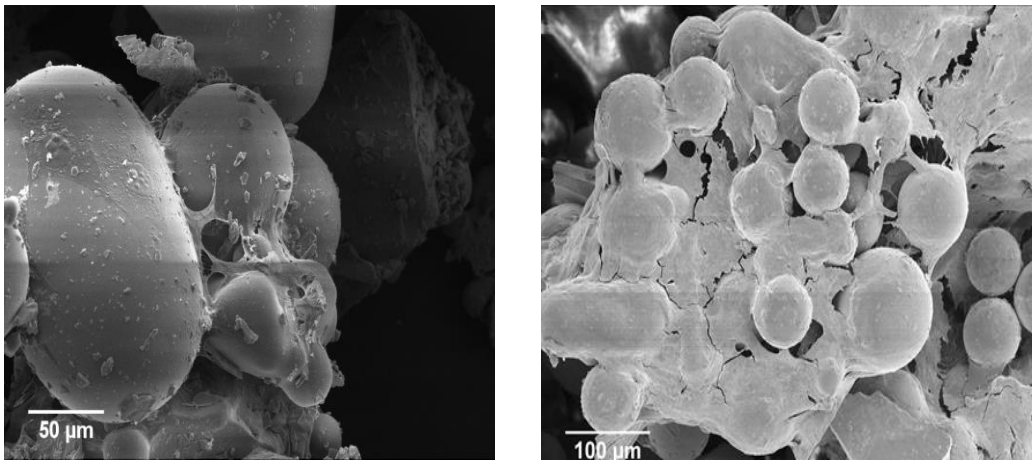

Figure 4-16 SEM pictures of MG63 on SrO17.5 strontium glass beads. a- day1, b- day7

Similarly, confocal images for hMSCs showed that these cells could attach to the beads and even encapsulate these beads and take on their spherical morphology as shown in Figure 4.17.

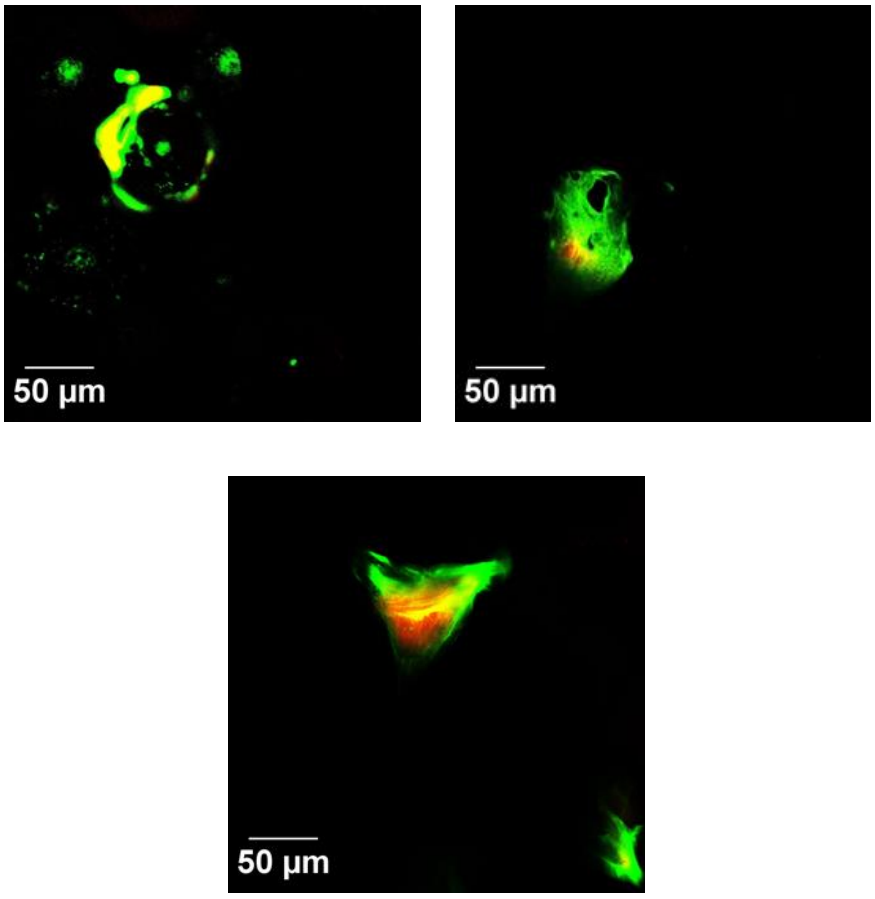

Figure 4-17 Confocal images of hMSCs showing the cellular attachment on beads. Red resemble propidium iodide (nucleus). Green staining is Phalloidin (cells actin)

4.4 Discussion

There were two main aims behind this chapter. The first one was to produce phosphate glasses in a form that is more relevant to the clinical applications where cells can attach to and penetrate and colonise through. The second aim was to comprehensively investigate the zinc and strontium formulations that were exhibiting some aspects of cytocompatibility in the previous chapters.

Glass bead development was successful for all the compositions. This was confirmed through post spheriodisation SEM and light microscopy images. However, glass bead distribution showed that the majority of formed spheres was mostly limited to diameters of 65-106 µm and low cell frequency was found below or above this range. This may be interpreted as the agglomeration of glass powders can prevent small diameter beads to be produced, whereas the short time period of glass powder inside the flame may be the reason for the shortage in produced large diameter glass bead number. All of these findings were compatible with previous studies done by Lakhkar *et al* (Lakhkar et al., 2012).

Many physical, chemical and biological studies were performed in order to assess zinc and strontium phosphate glass beads behaviour. The initial study was the XRD study which was done to confirm the amorphous state of the glass beads and revealed that the produced beads are crystalline free and ready for carrying on the other studies. The degradation study was performed to find out the glass network stability when they are exposed to

fluid. This was done by using SEM imaging for visual examination of bead surface degradation. Although this method had a lot of subjectivity with regard to its image data, it was chosen because of the difficulty and unpredictability of performing quantitative mass loss measurements. Images data provide us with general idea about the glass network stability through evaluating the produced surface changes after exposure to deionised water. After day 1, no clear difference has been found among the glass compositions overall. Though, surface erosion started to appear after a week of immersion. This erosion was more apparent in zinc containing phosphate glass beads than the strontium formulations which were less affected. This was displayed in the form of pores and faint cracks which were more noticeable in ZnO10 phosphate glass beads. Glass beads containing zinc were more affected after two weeks as more deep cracks and pores commenced to appear. The strontium glasses, in turns, started to show few pits with few surface changes on day 14. The trend of glass degradation seemed to be as follows (ZnO10>ZnO5>SrO35>SrO17.5).

These results were compatible with previous findings of dissolution rate trend of both zinc and strontium glass where mass loss at day 14 was as follow ZnO10 =0.41 $mg.cm^{-2}$, ZnO5=0.378 $mg.cm^{-2}$, SrO35=0.2666 $mg.cm^{-2}$and SrO17.5=0.209 $mg.cm^{-2}$. This could be interpreted by relating this with the difference of the ionic bond strength. In the glass network, zinc and strontium combine usually with the oxygen via ionic bonds. However, the variation in these ionic bonds strength may be linked to the strength of the whole glass

system. The dissociation energy of Zn-O bond is (284 Kj. mol^{-1}) which is lower than that of Sr-O bond is (454 Kj. mol^{-1}). Hence, a glass containing zinc seems to be more susceptible to hydrolysis because of its weak bond strength. Furthermore, these results were previously emphasised by the differential thermal analysis findings where the thermal variables (T_g, T_c, T_m) has followed the trend of (ZnO10 < ZnO5 < SrO35 < Sr 17.5).

The pattern of anions and cations release findings was parallel to the dissolution rate pattern where the highest level of released phosphate ions was detected with the glass formulation of the highest degradation rate. This may be interpreted by identifying the bond dissociation energies for both CaO and ZnO which are 383 Kj.mol^{-1} and 284 Kj. mol^{-1} respectively. Consequently, As ZnO ions substitute CaO ions, there are higher numbers of weaker bonds yielding an overall weaker glass network, more degradation and more ions are released. Conversely, ion release data of the strontium containing samples did not coincide with the mass degradation pattern as the more degradable SrO 35 phosphate glass produced fewer ions than that of SrO 17.5. The only exception was the Sr^{2+} ion release which was higher with SrO35 as it had double the amount of strontium than that of SrO17.5. Actually, this may give us a justification to interpret such unexpected results. Although SrO35 had more surface loss and higher degradation rate than SrO17.5, the majority of the released ions were Sr^{2+} which has a molecular weight of 87 more than other ions such as Na^{+}, Ca^{2+} and P^{5-} that have molecular weight of 22, 40 and 30 respectively.

Concerning pH studies, Dulbecco Modified Eagles Medium (DMEM) with pH 8.4± 0.1 was used as an immersion liquid for glass beads in order to copy the cell culture study conditions. Results exhibited an irregular trend where there was an initial increase in pH on the first day. This was followed by a period of stability in pH level which was succeeded by slow decline of pH level. The control and all the compositions showed an initial increase in pH after one day which remained stable until day 4 as a result of gas absorption effects (Brauer, 2015). This rise in pH was higher for the control group in comparison to the glass beads group. On day 7, however, there was a gradual continuous decline in pH until day 14 for all glass beads. The control, however, remained at the same level for the rest of the study period. Surprisingly, ZnO10 showed the lowest pH change followed by SrO35, which was slightly less than the other two groups. It appeared that the pH level was inversely related to the ion release, which was higher with ZnO10. This may be as a result of the increase of phosphate ions release that might form phosphoric acid in the solution and hence increase the culture media acidity.

Regarding the cell studies, there was a generally correlating pattern concerning all the results. CCK cell number findings suggested that the lowest cell number was found in ZnO10 glass beads group. ZnO 5 and SrO17.5 showed cell number quite similar to the control. Furthermore, alkaline phosphatase for hMSCs results acted in a parallel way at day 7 and day 14 as ZnO5 and SrO17.5 exhibited insignificant difference in enzyme levels from control. Finally, Ca assay demonstrated that both ZnO5 and

SrO17.5 resulted in higher rates of mineralisation than other remaining groups of ZnO10 and SrO35. While control group had the lowest mineralisation level.

The explanation of these results studies could be done by understanding the biological effect of the released ions on the cells as shown by other studies (Lakhkar et al., 2013). The most positive promising effects were found to be with ZnO5 and SrO17.5 in comparison to ZnO10 and SrO35 glass beads group that showed poor cytocompatibility. Concerning the calcium and sodium ions, the present experiment measurements revealed that the highest released concentration of these two ions among all glass compositions was about 95 ppm and 106 ppm respectively, which is below the cytotoxic concentration suggested in previous studies (i.e. for Ca^{2+} =400 ppm, Na^{+}= 220 ppm) (Hallab et al., 2002, Maeno et al., 2005). Consequently, the release of Ca^{2+} and Na^{+} ions from these glass systems should not have any harmful impact on cell function.

Although phosphate ions can play an important role in cell proliferation and metabolism, it was difficult to investigate their actual effect due to the presence of high phosphate ion content in the medium.

Regarding the strontium-containing glass beads, it was found that its Sr^{2+} release was about 30 ppm and 25ppm for SrO35 and SrO17.5 respectively. In a previous study, the optimum concentration of $SrCl_2$ to induce calcified matrix deposition was 5 µg/ml, however, data showed that concentration of 10 to 20 µg/ml could also stimulate ALP and matrix deposition. There is a

decline in the positive effect of Sr^{2+}ions as the concentration increase from 10 to 20 µg/ml. Based on ion degradation results, the actual Sr^{2+}ions concentration in the deionised water is 25 ppm. Although we cannot depend on this result in interpreting the ions release in culture media, this can give us an idea about what is happening. If it assumed that ion release was about 25 ppm in culture media which was replaced by half every two days. So, the real concentration of strontium in culture media is probably about 15 ppm (µg/ml) and 12.5 ppm for SrO35 and SrO17.5 respectively based on our assumption. This was within an acceptable range and following the same pattern of cellular activity as discussed previously (Lopa et al., 2013).

Concerning zinc ion release, the current results confirmed previous findings that showed substitution of calcium with zinc at 10 mol% can result in unfavourable and cytotoxic effects. Hence, adding more than 10 mol% ZnO may cause catastrophic effects as it can increase the release of lactate dehydrogenase and induce oxidative stress (Aina et al., 2007, Abou Neel et al., 2008c). According to all of these results it seems that the null hypothesis was rejected in some cellular findings that are related to both ZnO10 and SrO35 glass beads formulation.

In conclusion, the present study revealed that glass beads production was successful. It suggested that ZnO5 and SrO17.5 phosphate glass beads exhibited acceptable results regarding cellular studies which were apparently significant comparing to the ZnO10 and SrO35 glass beads concluding that ZnO5 and SrO17.5 may be more suitable for bone tissue engineering.

Though, more studies are needed to be carried out to further assess the cellular impact of glass compositions. Moreover, surface glass functionalising is required to be performed to enhance the cellular attachment and also provoke the mechanical and chemical characteristics of glass.

Chapter 5 Surface functionalisation of phosphate-based glasses

5.1 Introduction

Bioactive glasses are considered promising biomaterials for craniofacial hard tissue engineering (Gage et al., 2010). Many studies, both *in vivo* and *in vitro* were performed using various forms of bioglasses to test their applicability to repair craniofacial defects. One study used bioglass granules within an *in vivo* environment to repair facial bone defects such as frontal sinus defects and orbital wall reconstruction (Suominen and Kinnunen, 1996). These defects were assessed clinically and radiographically and then compared with autogenous bone graft results. The outcome was very encouraging as there was no evidence of any immunological or inflammatory responses. Another *in vivo* study examined the implantation of bioglass – coated PMMA (poly methyl methacrylate) for skull defect repair and the clinical results were shown to be acceptable without complications and with good evidence of bone adhesion to the implant surface (Peltola et al., 2012). Though, most of these applications need bioceramic glasses to be modified using other techniques in order to produce new biocomposite material that has improved properties (Chen et al., 2008a).

Bearing this in mind, some techniques suggested other materials such as carbon nanotubes (CNTs) and polycaprolactone (PCL) that can be used to improve the mechanical and the biological outcomes of the implanted biomaterial applied (Akasaka et al., 2006). As most synthetic bone

substitutes have osteoconductive properties, tissue engineering facilitated making 3D scaffolds to provide the main structural support and guidance to both osteoblasts and mesenchymal stem cells as well as to ease the transfer of nutrition, oxygen and waste products (Sitharaman et al., 2008). Although the cytotoxicity of CNTs has not been studied thoroughly yet, CNTs demonstrated good osteoconductive properties, cell attachment and proliferation capacity as well as the ability to retain growth factors (Tanaka et al., 2017). In a more comprehensive study, multi-walls CNTs were incorporated in PGLA (Poly-lactic-co-glycolic-acid) biocomposite for bone repair application. This material was studied within an *in vitro* environment and was shown to be beneficial for cell growth provoking and enhancing MSCs differentiation into osteoblasts (Lin et al., 2011). Misra *et al.* (2010) developed bone related biocomposite using a complex of Poly(3-hydroxybutyrate) polymer, bioactive glass particles and multiwall carbon nanotubes (MWCNTs) where CNT concentrations were varied. This biocomposite was cultured within MG63 cells and then studied biologically using both alamar blue and live and dead assays and SEM imaging. The results suggested that this combination of biomaterials has a promoting effect on MG63 cellular metabolic activity. This study also hypothesised that CNT incorporation enhanced cellular attachment through the formation of a rough topographical layer on the biocomposite surface layer, the most favourable outcome was at a CNT concentration of 2 wt. % (Misra et al., 2010).

Polycaprolactone (PCL) is a high molecular weight degradable polymer that has controlled slow degradation rate (Rezwan et al., 2006). PCL was studied thoroughly as a biopolymer for bone regeneration. One of the earlier attempts conducted was to develop a biocomposite material from PCL and fibrin hydrogel. This was studied at 2D and 3D constructs and results showed an enhancement in the cellular osteogenesis ability (Schantz et al., 2003). Other study investigated the addition of polycaprolactone polymer to multiwall carbon nanotubes (MWCNTs) in order to produce a biocomposite scaffold which was seeded later with rat bone-marrow-derived stromal cells (BMSCs). Cellular attachment, proliferation and differentiation were all assessed. The findings suggested that MWCNTs/PCL composite scaffolds have an acceptable capability of bone growth enhancement when the preferred MWCNTs amount was 0.5 wt.% (Pan et al., 2012). In more recent and advanced *in vivo* trial, polycaprolactone 50% and β-TCP 50% were combined to develop special scaffolds implanted in porcine mandible. Following histological and immunofluorescence studies the good clinical potency of such biocomposite scaffolds was seen (Konopnicki et al., 2015).

Despite many studies performed on other biomaterials; bioglass, CNT and PCL, there is no study, to the best of our knowledge, that examined the combination of all these materials together with phosphate-based glass. It is worth mentioning that there were some studies in the literature that involved applying bioglass with either CNT or PCL with the assessed bioglass being a silicate based glass. In the present chapter, a novel study was planned to

investigate the fabrication of two different (zinc and strontium) containing phosphate-based glass compositions that was coated with both PCL/CNT and PCL to investigate the biological impact of coating layer on cellular attachment, proliferation and metabolism. The presented work may have potential implication in the development of 3-D scaffolds for bone tissue engineering.

5.2 Materials and methods

5.2.1 Glass discs preparation

Two different compositions of phosphate glass discs were developed to check the initial ability of surface functionalisation by PCL and CNT, and to evaluate the cellular reaction to the functionalisation by measuring cytocompatibility and metabolic activity. The compositions were ZnO5 %(50 P_2O_5 - 10Na_2O - 5TiO_2 – 30CaO –5ZnO) and SrO17.5% (50 P_2O_5 - 10Na_2O - 5TiO_2 – 17.5CaO –17.5SrO). They were made by using the same procedure and same weight (Table 5.1) described previously in 2.2.3 and 3.2.3.

Table 5-1 Glass composition weight (gram)

Glass composition		***P_2O_5***	***NaH_2PO_4***	***TiO_2***	***$CaCO_3$***	***$SrCO_3$***	***ZnO***
ZnO_5	***$P_{50}Na_{10}Ti_5Ca_{30}Zn_5$***	***56.8***	***24***	***4***	***30***	***0***	***4***
$SrO_{17.5}$	***$P_{50}Na_{10}Ti_5Ca_{17.5}Sr_{17.5}$***	***56.8***	***24***	***4***	***17.5***	***25.8***	***0***

5.2.2 CNT solution preparation

CNT solution preparation enclosed three steps which were: 1- CNT carboxylation, 2- PCL (polycaprolactone) solution preparation and 3- CNT dispersion in PCL solution.

1- CNT Carboxylation: Carbon nanotubes were chemically modified by adding carboxyl group to their structure forming a (COOH) attachment. This was performed by using 0.5g of multi-walled CNT that have the dimensions of 10nm x4.5nm x 3 μm (> 98%, Sigma Aldrich). CNTs were primarily added to a 1 molar solution of H_2SO_4/HNO_3 (Sigma Aldrich) 1:1 aqueous solution and then refluxed at 80^{o}C for 48 hours following the procedure explained by (Ahn et al., 2015). Once the reflux procedure was accomplished, the black solution (CNT+ Acids mixture) was centrifuged by (Mistral 2000R) centrifuger at (1500rpm for 10 minutes) to separate the black CNT precipitated in the bottom of the centrifuge bottle from the light brownish supernatant acid which was then aspirated and dispensed. The remaining CNT sediment was further washed, shaken vigorously in high-purity deionised water (resistivity = 18.2 $M\Omega.cm^{-1}$) gained from a PURELAB UHQ-PS (Elga Labwater, Marlow, UK), centrifuged two times to ensure the removal of any acidic residue on its surface after removal of the deionised water. The CNTs were then dried at 80^{o}C for five hours in a vacuum oven (Townson and Mercer) and milled down by mortar and pestle to be stored in a plastic container ready to be used for future applications. The efficiency of carboxylation was determined through

sonication of both raw CNT and functionalised CNT in 15mm of ethanol and examined at different time points to monitor its sedimentation rate.

2-PCL solution preparation: PCL polymer (Sigma Aldrich) was dissolved in chloroform solvent (> 99%, Sigma Aldrich) at a percentage of 2 wt / volume % following the procedure previously described (Prabhakar et al., 2005). For this, 200mg of PCL were weighed and dissolved in 10 ml of chloroform in glass container for 2 hours with the use of stirrer to enhance the dissolution procedure.

3-CNT dispersion in PCL solution: the previously prepared carboxylated CNT and PCL solution were used in this step. A weight of 500 µg of carboxylated CNT were dissolved in 20 ml of the above PCL solution at the percentage of 25µg/ml. This dispersion step was performed initially by using the stirrer machine for 10 minutes to break down the agglomerated CNT powder and then by introducing the CNT solution glass container into a sonication bath for 1 hour to ensure the full dispersion of CNT in PCL solution. The final produced CNT solution was stored in special glass container for future applications.

5.2.3 Glass discs coating.

Discs from both compositions were cleaned initially with acetone and then left to be dried in two specific labelled glass containers. Two types of coating were performed (figure 5.1):

1-PCL coating: 10 ml of PCL polymer solution was used as an immersion solution for both zinc and strontium glass discs. Immersion procedure was performed for 15 minutes under sonication.

2-CNT-PCL coating: samples of each composition were immersed in 10 ml of the CNT-PCL solution in a sonication bath for 15 minutes to ensure that glass discs were coated with CNTs. Glass discs were removed from the immersion glass containers and left to dry in a desiccator over the night.

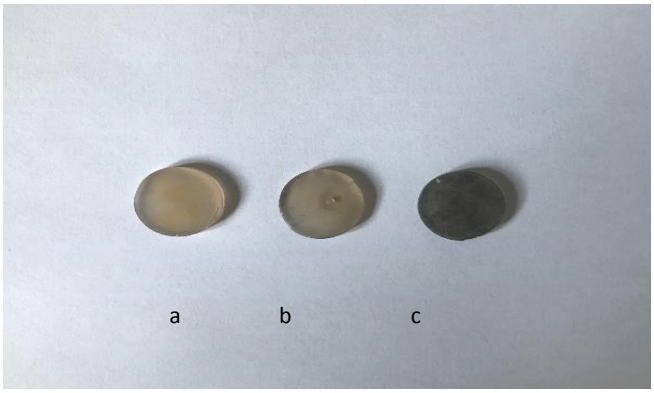

Figure 5-1 ZnO15 glass discs. a- uncoated, b-PCL coated and C- CNT-PCL coated

5.2.4 Characterisation of CNT coated glass discs

The assessment of coating efficiency was performed at both physical and chemical levels. Regarding the physical stability of the coating, one coated glass disc was immersed in deionised water and treated in an ultrasonic bath for 10 minutes. The sample was dried for 24 hours in desiccator and then visualised via SEM. This imaging study was performed for both the ultrasonic treated and the control non-ultrasonic treated glass discs.

Concerning the chemical stability assessment of CNT coating layer, coated discs were soaked in 25ml of deionised water in plastic vials (Sterilin tube) at

a temperature of 37^{o}C at three-time points (7, 14 and 28 days). At each time point, the discs were removed from their plastic containers, dried for 24 hours in desiccator, attached to SEM stubs, gold coated and then assessed under SEM.

5.2.5 Hydrophilicity and hydrophobicity assessment

Water contact angle measurements were performed by using a CAM 200 optical contact angle meter instrument (KSV co, Finland). Special graduated needle (Hamilton co, Nevada, USA) was filled with distilled water to establish the hydrophobicity/hydrophilicity of the prepared and coated glass discs in the normal room temperature environment. Measurements were taken on triplicate samples of zinc glass discs (uncoated glass, PCL coated glass discs and CNT-PCL coated glass discs). The needle was placed in its clamp and was directed above the glass discs surface to ensure water droplet. The contact angle measurement was performed on the water bubble that dispersed on the glass discs surface by using the CAM200 shape analysis software and time lapse camera. This procedure was done by measuring the angle for 10 fast readings (40 ms intervals) and 10 slow readings (1 s interval).

According to (Young's equation)(equation 1), the contact angle (θ) formed on the solid surface is governed by three equilibrium forces: solid–vapor surface tension (γ_{sv}), solid–liquid surface tension (γ_{sl}) and liquid–vapor surface tension (γ_{lv}) *(figure 5.1) (Kwok and Neumann, 1999)*. The angle values that are less than 90°θ indicated surface hydrophobicity while angle values that

are greater than 90°θ are known for surface hydrophilicity (Yuan and Lee, 2013).

$$ylv\ Cos\theta = ysv - ysl \quad \text{.....equation1}$$

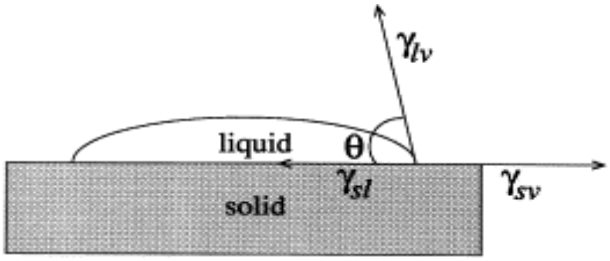

Figure 5-2 Contact angle measurement. Reprinted from Advances in Colloid and Interface Science journal, vol81, issue 3, D.Y.Kwok and A.W.Neumann. Contact angle measurement and contact angle interpretation, page 167, copyright (1999) with permission from Elsevier.

5.2.6 Surface roughness measurement

The surface roughness of the coated and uncoated glass discs was measured by using laser emitted from a Proscan 2000 non-contact profilometer instrument and Proscan software (Scantron Industrial Products, Ltd, Taunton, England). This was carried out in triplicate of each glass discs group. The profilometer scan was done for 2 x 2 mm square area. The scan parameters were as follows: scan rate = 300 Hz, average = 4 and step size = 0.005 mm. Ten representative readings from five different linear points were obtained from each sample and used for the calculation.

Roughness average (Ra) was considered for surface roughness evaluation, this was calculated by measuring the absolute average of the distance extending from fixed mean line to elevations and depressions in the glass surface.

5.2.7 Cell culture studies

5.2.7.1 Cell preparation

Both MG63 cells and hMSCs preparation was described previously in 4.2.6.1.

5.2.7.2 Measurement of metabolic activity of cells

Metabolic activity was performed by measuring the fluorescence reduction of alamar blue for predetermined time points (day 1, 4,7) following the same procedure that is described in 3.2.6.3.

MG63 cells were seeded initially (10000 cells /discs) on triplicate of both zinc and strontium (plain, PCL coated, CNT-PCL coated) glass discs, tissue culture plastics (TCP) were considered as the control samples. DMEM used as a culture media for this study.

5.2.7.3 DNA assessment

Quantification of DNA study was performed by using hMSCs for two different time points (day 7, 14) at initial cellular seeding density of 25000 cells per disc. The determined cells density was prepared in 50µl of culture media to ascertain the even distribution of cells on the glass discs without flowing away from them. Then glass discs were incubated with the seeded cells in incubator at 37^{o}C for 30 minutes to provide enough times for cell attachment on discs. This was followed by adding 1 ml of DMEM and incubation for the two-time points.

At each time point, DNA purification was carried out by using QIAamp® DNA Mini kit (Qiagen). The first step of the purification was cells detachment from the glass discs by using 750 µl of trypsin for 5 minutes at 37^{o}C. then, trypsin was deactivated by adding 750µl of culture media. The resulted culture media solution was aspirated and centrifuged for 5 minutes at 300 x g in 2 ml microcentrifuge tube. Then, the supernatant was removed completely without any disturbance to the hMSCs pellet. At that point, cells pellets were suspended in 200 µl PBS and 20µl of proteinase K and 200 µl of provided buffer solution. The resulted 420 µl solution was vortexed for 15 seconds and incubated for 10 minutes at 56^{o}C. This was succeeded by multiple steps of centrifuging, addition of 200 µl of ethanol, vortexing for 15 seconds and centrifuging again. The produced 620 µl of solution was then aspirated from the normal tubes, introduced in QiAamp spin tubes in a (2ml collection tube) without wetting the rim, centrifuged at 6000 x g for 1 minute. Then, the spin is removed and introduced in new collection tube after discarding the previous collection tube. This was followed by five consequent steps of washing and centrifuging by using different buffer solutions. Finally, elution of 200 µl of DNA was collected and stored at -20^{o}C to be prepared for the next DNA quantification step.

DNA quantification was performed by using Quant-iT™ PicoGreen™ dsDNA Assay Kit (Fischer). The first step was the preparation of 1X of TE buffer solution from the original 20X TE buffer solution which was done by diluting 4 ml of 20 X TE in 76 ml of DNASe-free water (Qiagen). The second step was

preparation of a 200 -fold of Pico Green dsDNA reagent by diluting 200 µl of it in 38 ml of the prepared TE buffer. The resulted diluted solution was prepared in a dark plastic container and used for DNA detection of both the stored study samples and standards solution that were used for calibration.

For DNA quantification, the frozen solutions of DNA samples were initially thawed in room temperature. Then triplicate of 50 µl of each DNA experimental solution was added was added to 950 µl of 1 X TE buffer to end up with 1 ml of experimental DNA solution. Then 1 ml of the 200-fold Pico Green solution was added to each sample and incubated for 5 minutes in light protected well plate at room temperature. The fluorescence reading was then determined by using spectrofluormeter (Infinite M200, Tecan, Männedorf, Switzerland) at wavelength of 520 nm.

Calibration was done by preparing sequence of five low range dilutions of DNA (0, 25, 250, 2500 and 25000 pg/ml). the dilution was done by using the 1 X TE buffer solution. One ml of the prepared Pico Green solution was also added to each standard dilution for five minutes to prepare it for the following fluorescence reading step at wave length of 520nm.

Calibration curve was obtained from the standards readings. The equation of this curve was used to relate the absorbance reading with the DNA concentration in the samples (figure 5.3).

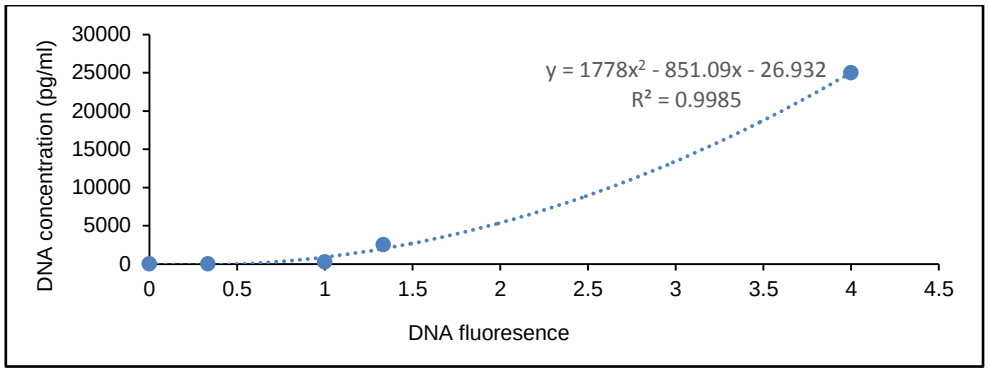

Figure 5-3 Calibration line of DNA assay. Done by preparing different concentrations of DNA and correlate the corresponding fluorescence reading with each of the concentration.

5.2.7.4 Cells imaging by scanning electron microscopy (SEM)

MG63 cells were seeded at density of 10000 cells / disc with use of DMED culture media for the SEM imaging. SEM imaging was performed for day 4 and 7 following the same steps that are described previously in 3.2.6.4.

5.2.7.5 Confocal microscope cells imaging

Confocal imaging was performed for hMSCs that were seeded initially at density of 25000 cell/disc. The imaging was done for two-time points (day 7, day 14) following the same steps that are described previously in 4.2.6.6.

5.2.8 Statistical analysis

Cell studies results were statistically assessed by one-way ANOVA to assess the null hypothesis stated that there is no apparent or significance variation between the control tissue culture plastics (TCP) in one side and the uncoated discs, PCL coated discs and CNT-PCL coated phosphate glass discs in the other side regarding both cellular metabolic and proliferative abilities where $p<0.05$ has been used as a significance degree estimation.

5.3 Results

5.3.1 CNT carboxylation validation.

Figure 5.4 shows the sedimentation rate of both functionalised and non functionalised CNT after two hours. It demonstrated that sedimentation rate was faster for the non-functionalised CNTs in comparison to the slow rate for functionalised CNTs.

Figure 5-4 Carbon nanotube sedimentation after 2 hours A: unfunctionalised B: functionalised

5.3.2 Characterisation of CNT coated glass discs

Figure 5.5 displays the SEM image of CNT coated glass disc layers for the ultrasonic treated and ultrasonic non-ultrasonic treated disc groups. It showed the presence of the coating layer in both groups with no clear visual differences regarding coating efficacy between the two groups.

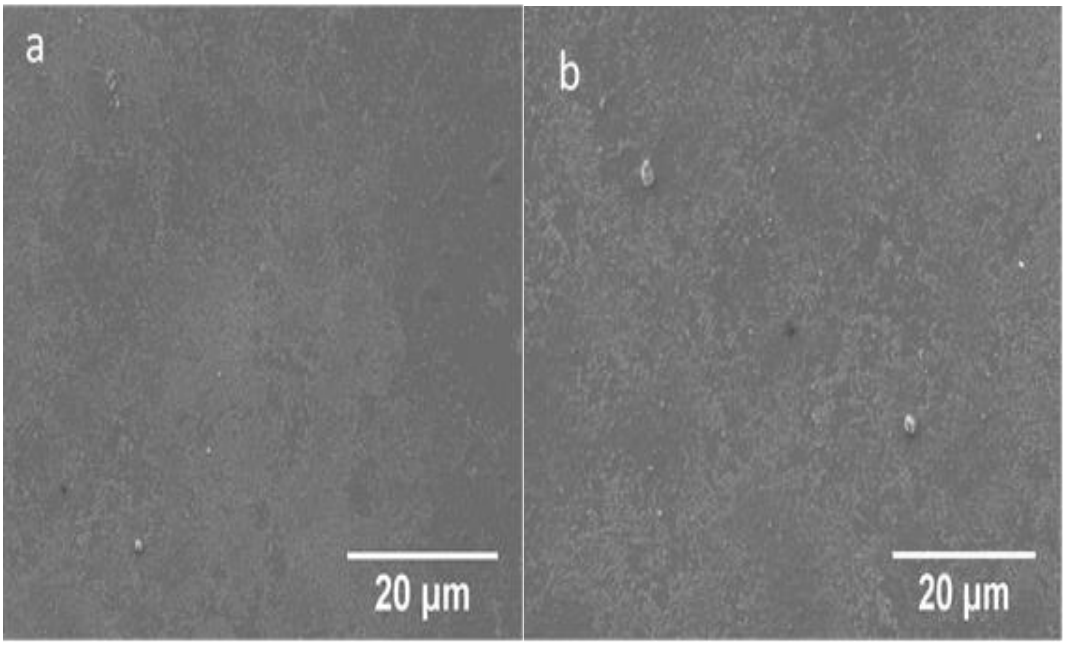

Figure 5-5 SEM images of CNT- PCL coated ZnO5 discs (a) ultrasonic non- treated discs and (b) ultrasonic treated discs, showing the stability of coating layer after the mechanical ultrasonic stimulus.

Figure 5.6 presents SEM images of coated glass discs after immersion in deionised water at three different time points (a) day 7, (b) day 14 and (c) day 28. It showed that the CNT coating layer was unchanged for the all-time points. Though, there was a clear surface and topographical changes in coating layer especially at day 28. These variations were related to cracks size and cracks numbers that may be due to the degradation of PCL

occurred after long time of incubation with deionised water or may be because of sample processing.

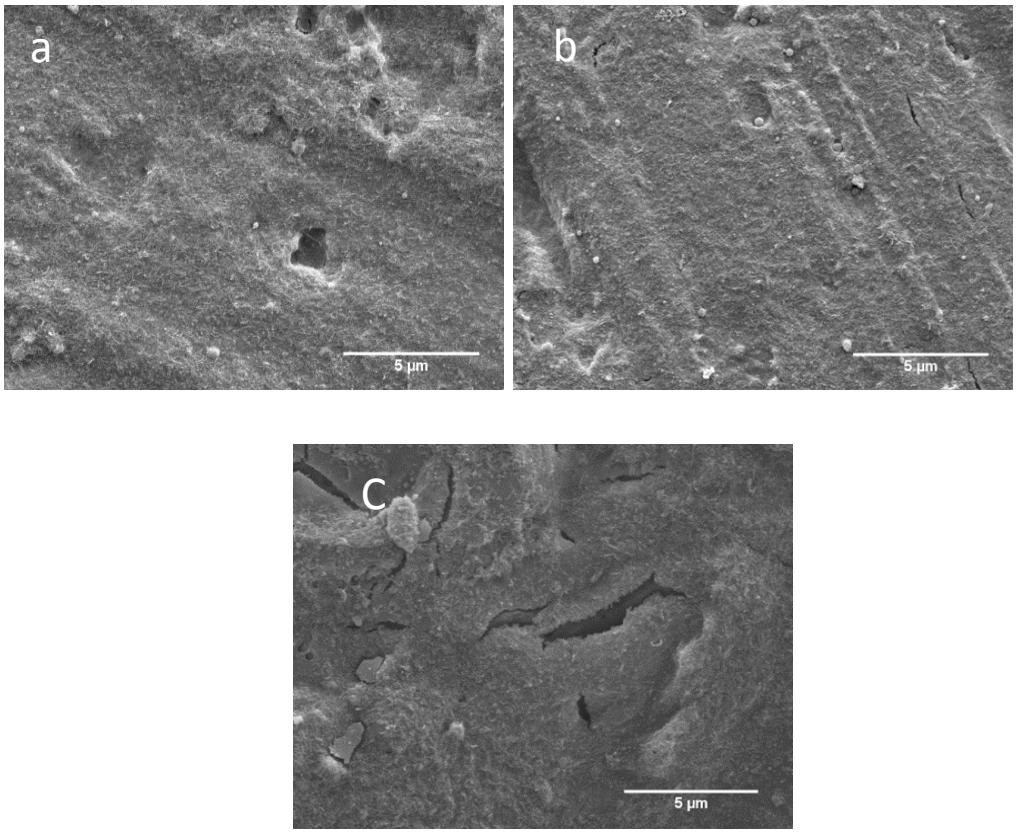

Figure 5-6 SEM images of coated SrO17.5 glass discs after three-time points: (a) day7, (b)day 14 and (c)day28. CNT layer was present along all the whole study, but polymer layer exhibited more cracks within time.

5.3.3 Hydrophilicity and hydrophobicity assessment

Figure 5.7 displays the contact angle (θ) for different coated and non-coated glass discs. Contact angle value was considered as a clear indication for glass surface wettability where 90 ° was used as the demarcation limit between hydrophilicity and hydrophobicity. Results suggested that uncoated glass discs are considered to be slightly hydrophobic as their contact angle were 97.4± 2.7, this was statistically significant with other groups ($p < 0.05$). Other PCL-coated and CNT-PCL coated glass discs groups showed signs of hydrophilicity since their contact angles values were 81.9± 1.4 and 76 ± 3.4 respectively.

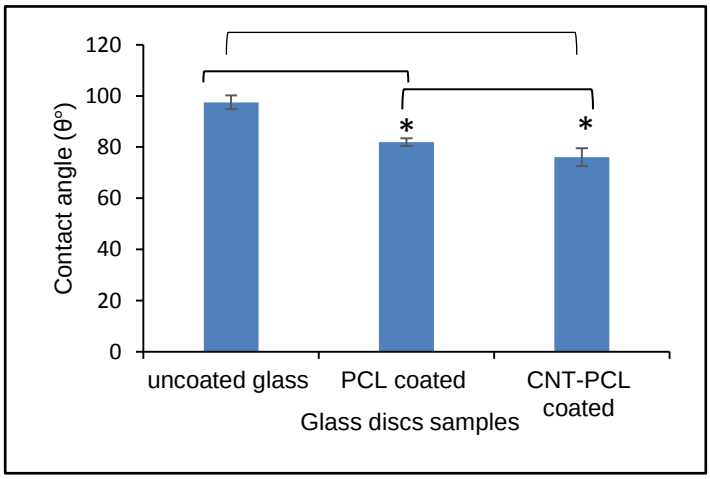

Figure 5-7 Contact angle measurement explaining the difference in hydrophilicity and hydrophobicity of glass surfaces

5.3.4 Surface roughness

Surface roughness results are displayed in figure 5.8. The findings displayed that uncoated glass discs exhibited less roughness at around 1.29±0.28 µm which was significantly lower than the CNT-PCL coated discs at around 1.99±0.36 µm. The PCL coated samples revealed roughness that is in the middle between the other two groups. These data are further clarified in figure 5.9 which shows the laser scan images of roughness.

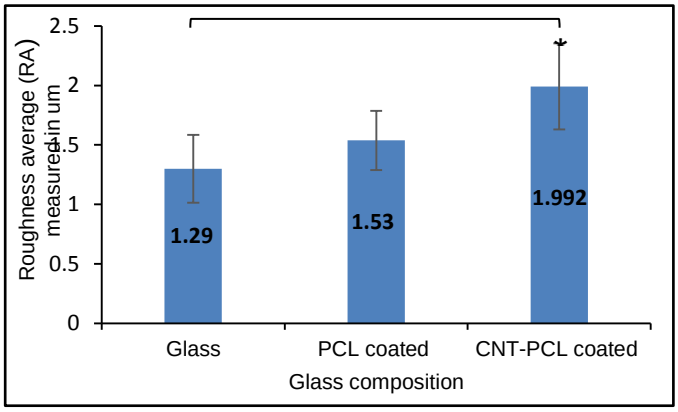

Figure 5-8 Roughness average (RA) for the different glass discs groups showing that CNT-PCL coated glass discs are more rough than other groups

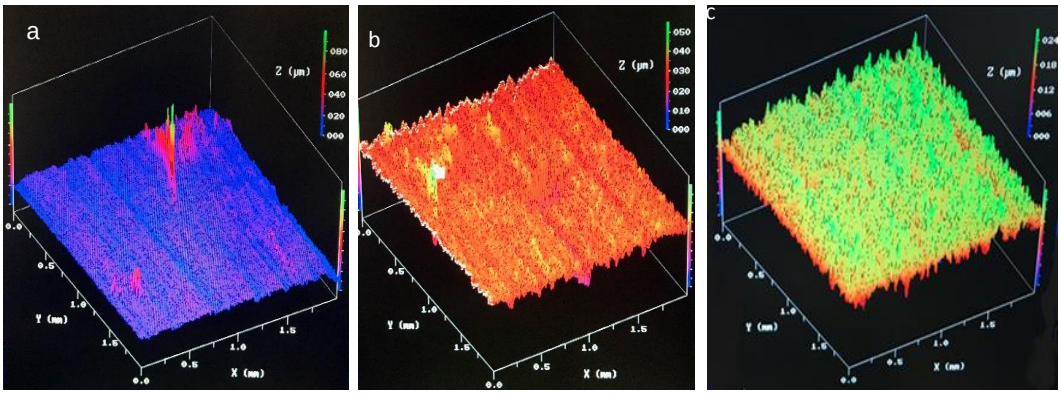

Figure 5-9 Laser scan images for a. uncoated glass discs, b- PCL coated discs and c. CNT-PCL coated discs

5.3.5 Measurement of metabolic activity of cells

Alamar blue study results are displayed in figure 5.10. Generally, all the groups including the control (TCP) revealed acceptable values with time. At day 1, all the samples revealed a similar reduction of around 5% compared to the control. Though, the coated PCL and CNT-PCL were statistically significantly lower from the control ($P \leq 0.05$). At day 4, there was general and prominent increase in the reduction values. This increase in its highest amount for the control (TCP) at about 25% which was also statistically higher than the coated sample which were around 20%. At the last time point at day 7, the trend was similar to the earliest time points where the TCP displayed the highest percentage values at around 53% followed by the uncoated samples at 50% and lastly with the coated samples at around 46%.

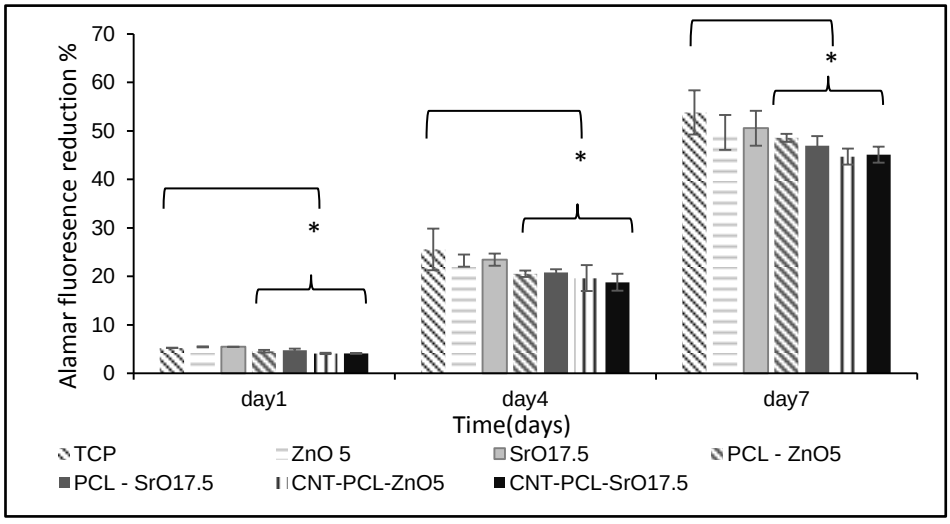

Figure 5-10 Alamar fluorescence reduction percentage for free coated, PCL coated and CNT-PCL coated ZnO5 and SrO17.5 glass discs for three-time points (day 1, 4,7)

5.3.6 DNA assessment

DNA concentration quantification results are demonstrated in figure 5.11. The general trend obtained from the DNA study showed that all groups have a similar cellular DNA content. At day 7, the overall DNA concentration was about 35000 pg/ml apart from the uncoated samples which was statistical different from other groups at around 22000 pg/ml. At day 14, DNA concentration rose in all samples as a result of cellular proliferation. Though, the ultimate upregulation was found in the control (TCP) at 192000 ± 54000 pg/ml followed by CNT-PCL coated samples at 182000 ± 35000 pg/ml and ended in the other four groups displaying DNA concentration ranging from 135000-143000 pg/ml.

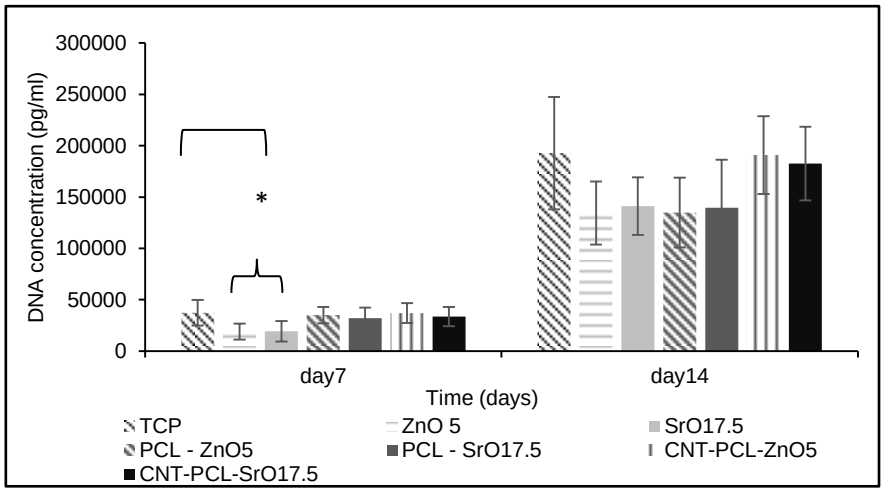

Figure 5-11 DNA concentration measured by pg/ml for the control and all glass disc groups displaying the acceptable detected concentration that was found in all groups after one week and two-week periods

5.3.7 Cells imaging by scanning electron microscopy (SEM)

Figure 5.12 displaying SEM images of seeded MG63 on different non-coated, PCL and CNT-PCL coated ZNO 5 and SrO 17.5 glass discs. At day 4, cells were found to be stably attached to the different produce discs samples. At day 7, cells attachment was maintained with the appearance of more cellular density than day 4 in some parts of glass discs. SEM pictures revealed the ability of cells to use their appendages for attachment despite the presence of some coating layer discontinuity as a function of degradation after culturing in DMEM cell cultures.

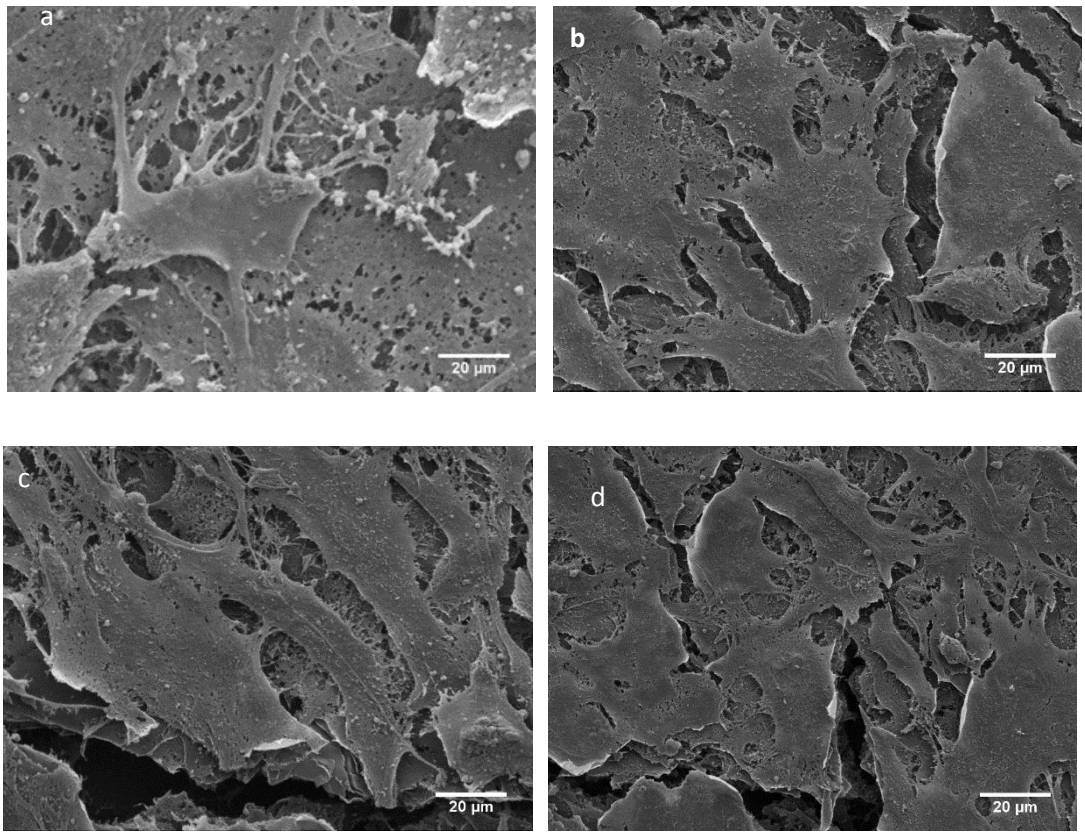

Figure 5-12 SEM images of MG63 cells seeded on CNT-PCL coated glass discs. a-ZnO5 (day4), b- SrO17.5(day4), c-ZnO5 (day7) and d-SrO17.5 (day7)

5.3.8 Confocal microscopy cell imaging

Fluorescence confocal images of hMSCs at day 7 and 14 are displayed in figure 5.13. Generally, cell proliferation seemed to be more abundant in the CNT-PCL coated discs than the PCL coated and uncoated samples. At day 7, cell proliferation on uncoated discs appeared to be less than the other coated samples which was clear through the presence of cell free areas on the discs (figure 5.13 a), this was followed by PCL coated discs (figure 5.13 b), and the CNT-PCL coated discs showing the highest proliferation levels (figure 5.13 c). At day 14, the pattern of cell proliferation was similar to that of day 7 where CNT-PCL coated groups exhibited high levels of cell proliferation and cells looked to have grown in multilayers (figure 5.13 f).

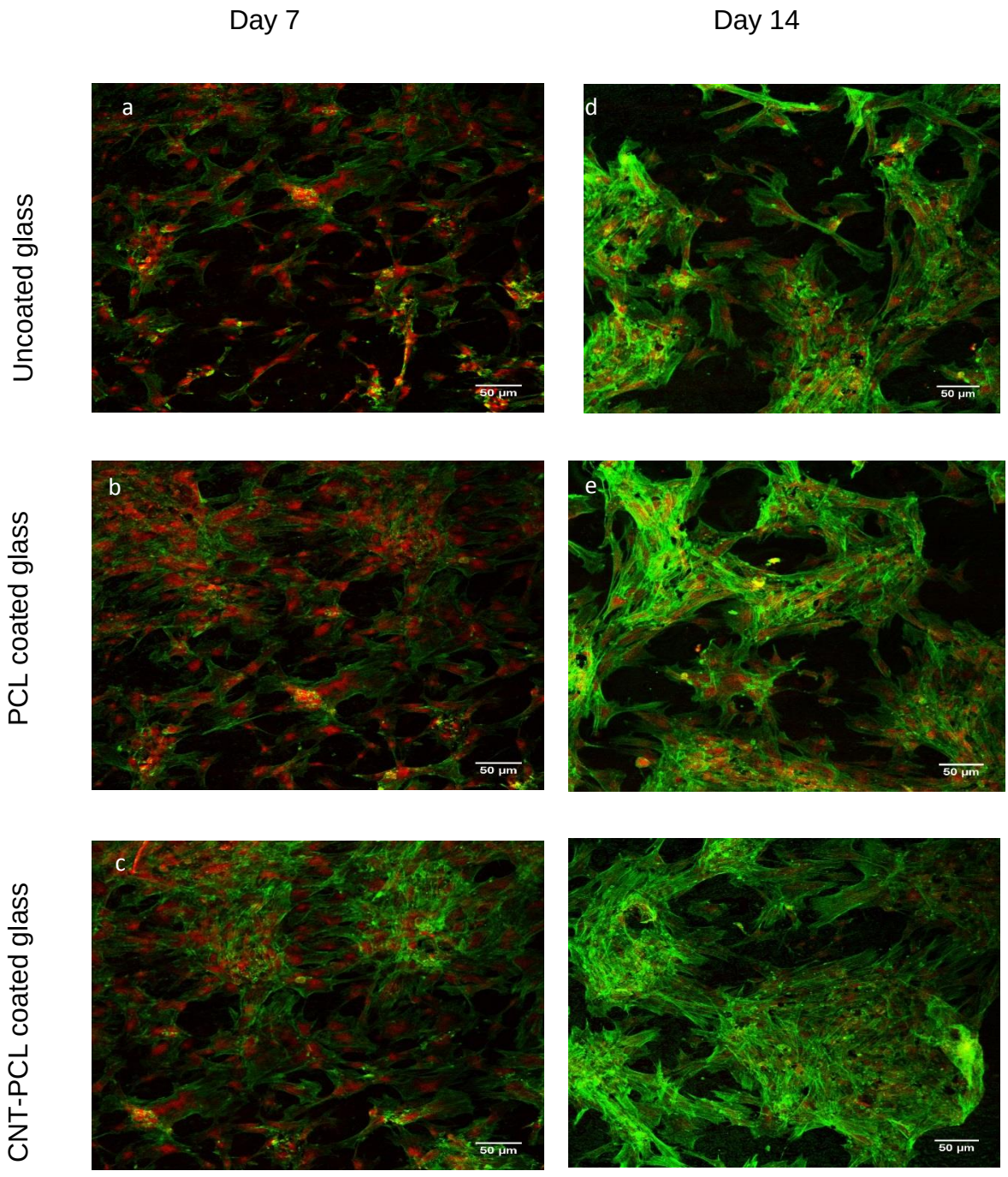

Figure 5-13 Confocal images of hMSCs cells seeded on SrO17.5 glass discs. a-uncoated discs (day7), b- PCL coated discs (day7), c-CNT-PCL coated (day7), d-uncoated discs (day14), e- PCL coated discs (day14) and f-CNT-PCL coated (day14)

5.4 Discussion

This chapter aimed to determine the biological implication of coating the phosphate-based glass. Uncoated zinc and strontium glass discs were investigated in the previous chapter and was shown that the most acceptable findings were found in ZnO5 and SrO17.5 formulations. Many studies have focused on CNTs application for bone regeneration. There are controversial opinions about what the optimum CNT concentration should be; some views hypothesised that this concentration should be around 25µg/ml (Kam and Dai, 2005), A comparison of three different carbon products: multi-walled carbon nanotube (MWCNT), graphene oxide (GO) and nano diamond (ND) was carried out. This study aimed to correlate the carbon type and the cellular uptake and cytotoxicity and revealed that signs of toxicity for MWCNT started to appear at 20µg/ml (Zhang et al., 2012b). Other study suggested it can be increased up to 100µg/ml (Tong et al., 2014) .

One of the recent experiments designed to fabricate CNT with hydroxyapatite (HA) where CNT was added in different concentrations, it suggested that functionalised CNTs are less cytotoxic than the non-functionalised CNTs and that increasing CNT concentration can lead to a decrease in viability of human osteoblast cells and a concentration of 62µg/ ml of functionalised CNTs was found to result in about 2% of cell death (Khalid et al., 2015). Multi-walled CNT's were chosen to be used rather than single walled types because of their high elastic modulus (Mattioli-Belmonte et al., 2012). These

CNTs were oxidatively functionalised by carboxylation through agitating in H_2SO_4/HNO_3 solution since carboxylation may lead to add negative function groups to CNT surface which may promote the hydrophilicity of CNT and also facilitate its dispersion property within solvents (Shin et al., 2011). These functional groups can also help to hasten the growth of HA crystals as they work as calcium chelating sites (Aryal et al., 2006).

In this study, CNT carboxylation was confirmed through examining the CNT dispersion in ethanol. The concentration of 25µg/ml of CNT was used according to recommended findings in previous studies of CNT toxicity while the use of 2% PCL was considered after performing a pilot study including different polymer and CNT mixture concentrations.

Turning to the findings of this study, the first study was performed to thoroughly assess the coating potency after both physical and chemical stimulus treatment. The SEM images of this study suggested that the coating procedure was successful as CNT-PCL coating layer remained stable on glass discs surface data after treatment with ultrasonic bath and immersion in deionised water for 28 days. Therefore, it was a good indication to continue in the application of these CNT-PCL coated glass discs in the following cell culture studies.

Wettability data showed that CNT-PCL coated discs were more hydrophilic than the other groups, this could be explained as CNT are functionalised by carboxyl groups that make surface more hydrophilic (TAKADA et al., 2010).

Surface roughness data showed that roughness has clearly been enhanced by CNT coating, this was also concurrent with other studies that linked CNT coating and enhancement of topographical features (Chen et al., 2008a).

Concerning the cytocompatibility study, alamar blue results aimed to quantify the percentage of fluorescence reduction to serve as an indication of the cellular metabolic activity of which the higher reduction percentage indicates a higher metabolic rate. Although alamar blue findings revealed the presence of statistical differences between all the coated samples and the control samples at the all three-time points, that difference did not neglect their provoking impact on the metabolic activity of MG63 cells as the difference was slightly less than the control and the uncoated glass discs' samples.

Regarding DNA quantification, the assay is considered an indirect way to quantify the number of cells. The findings showed that there was a significant difference on day 7 between the control and the uncoated discs while no difference seen on day 14. Regarding the coated discs, it seemed that CNT-PCL coated glass discs compositions displayed higher DNA concentration which was slightly less than the control discs. According to that, it seemed that glass discs compositions did not have any clear effect on the cellular outcomes comparing to those of surface modification effects. In other words, it appears that coating is the governing factor in controlling the cell metabolism and the cellular proliferation. These results were further confirmed by SEM and fluorescence imaging; CNT-PCL coated glass discs seemed to promote cell proliferation and enhance cell density more than the

other glass discs samples. The explanation of the enhanced cellular response may be due to two factors: 1- the improved surface hydrophilicity by CNT and 2- the improvement in surface roughness which resulted from CNT-PCL coating. This has confirmed the previous results that correlate roughness and hydrophilicity with the enhanced osteogenicity (Boyan et al., 2017) and link the potency of functionalised CNTs to enhance stem cell proliferation and bone marker expression.

In conclusion, coating phosphate glass discs with a CNT-PCL layer was successful and was shown to affect cell growth positively. According to the results of this chapter, a rejection in null hypothesis was determined regarding the metabolic and proliferative cellular activities that are yielded from seeding the same number of cells on differently modified glass discs surfaces. Other studies are needed to be carried out to assess the morphological, mechanical and biological impact of using a CNT-PCL coating layer on phosphate glass 3D scaffolds.

Chapter 6 Development of Zinc and Strontium Phosphate Based Glass Scaffolds

6.1 Introduction

Hard tissue regenerative medicine for craniofacial complex is focused on developing materials that can help clinicians to manage hard tissue loss and provide patients with a functional bone tissue. This is beneficial to patients suffering from trauma, neoplasms and congenital abnormalities on both clinical and psychological aspects (Smith et al., 2015a). Kaur *et al.* (2014) suggested that the ideal material should be biocompatible, does not demonstrate cytotoxicity or immunogenicity, can form a hydroxyapatite layer when in contact with simulated body fluid, has desirable mechanical properties, has a controllable interconnected porosity, and should be cost-effective (Kaur et al., 2014b). Based on this, different materials have been developed including ceramics (e.g. synthetic bioactive glass and hydroxyapatite), polymers (e.g. poly methyl methacrylate and polycaprolactone) or composites (e.g. a combination of any of the above materials and more). The main aim of studying these materials is to achieve a better outcome in terms of physical properties (porosity and mechanical strength), biological responses and clinical outcomes.

Regarding the physical properties, Gerhardt and Boccaccini (2010) stated that scaffolds require to have both micro pores (<50 μm) and high pore sizes

(>300 μm). The first is important for the sake of direct protein and cell adhesion, cell migration and osseointegration whereas the latter is needed for angiogenesis as the small sized pores may cause hypoxia or induce osteochondral differentiation rather than osteogenic differentiation (Gerhardt and Boccaccini, 2010). It was suggested that high porosity percentage (> 90%) in scaffolds structure is necessary and favourable for cellular migration and proliferation growth, however, this can affect the mechanical properties of the scaffold negatively (Hannink and Arts, 2011).

Many studies were performed on scaffold manufacturing aiming to produce bioactive glass ceramic scaffolds or bioactive glasses incorporated biocomposite (Will et al., 2012). One of the earliest studies developed porous bioactive glass scaffold through sintering within hot vacuum conditions. The produced bioglass (silicate based) scaffolds promoted the osteogenic activity of osteoblasts (El-Ghannam et al., 1995). Other studies performed on manufacturing silicate glass bioceramic scaffolds by coating polyurethane polymer by slurry of sintered silicate, and the produced silicate based glass scaffolds were then involved in both *in vitro* study of MG63 cells and *in vivo* study in rabbits. The results suggested the ability of MG63 cells to proliferate within the synthesised scaffold and the formation of new tissue containing collagen and blood vessels in the animal model (Wang et al., 2011). Other attempts were carried out to produce silicate porous glass scaffolds using both the polymer foam replica and the unidirectional freezing techniques. Scaffolds developed via both techniques were mechanically and structurally assessed prior to seeding them with mesenchymal stem cells and implanting

in rats. *In vivo* results revealed a bone like tissue formation in the stem cell seeded scaffolds while the cell free implanted scaffolds did not show any hard tissue deposition (Fu et al., 2010a). Other researchers produced titanium-stabilised porous phosphate glass scaffolds via foaming techniques. The porosity of the produced scaffolds was around 40-50% and the scaffolds did not show any sign of cytotoxicity (Navarro et al., 2004).

One inevitable problem facing most scaffolds is optimisation of cell seeding. Although seeding cells is performed usually by preparing high concentrations, there is a possibility of cells to flow away from scaffolds within the medium (Shimizu et al., 2006). Naturally, cells adhere to their physiological environment with the aid of integrins that attached to integrin bindings site such as Arg-Gly-Asp (RGD) of the extracellular matrix proteins such as collagen, fibronectin and vitronectin through the integrin binding sites such as Arg-Gly-Asp (RGD) (Hynes, 1992). Hence, many attempts were accomplished to use the integrins to manage cell seeding and cell attachment associated problems. Previous studies aimed to visualise the effect of coating titanium implants with collagen, the results revealed the positive effects of collagen coating on promoting initial cellular attachment and enhancing osteogenic activity of titanium implants (Nagai et al., 2002, Rammelt et al., 2004, Costa et al., 2017). Other studies investigated the outcome of coating different calcium phosphate scaffolds with collagen on osteoblasts and stem cells adhesion, metabolic and proliferative activities. The outcomes of collagen coating suggested that the positive impact of collagen coating layers on cell proliferation and metabolism as well as

cellular-scaffold adhesion, as the collagen coating, was hypothesised to enhance surface roughness (Brodie et al., 2005, Zan et al., 2016).

Coating with fibronectin was also assessed in terms of its ability to enhance cellular attachment and growth. One study compared the chondrocyte growth ability between fibronectin coated polymer scaffolds and uncoated scaffolds. The findings revealed that fibronectin coatings encourage cell ingrowth within the porous scaffolds (Bhati et al., 2001). Another correlated study examined PCL scaffold surface modification by plasma, fibronectin and plasma and fibronectin together. This study assessed the topographical effect, the cell attachment, the cell proliferation and the secretion of differentiation markers. The findings suggested that all the surface modification techniques had better results than those of the uncoated scaffolds. Though plasma treated surfaces exhibited more encouraging results than the fibronectin coated groups in term of cell attachment and cell proliferation. However, fibronectin is necessary for osteodifferentiation (Yildirim et al., 2010).

According to the literature, most of the performed studies on glass bioceramic scaffolds are correlated to the silicate based bioglass with no consideration of the cell density optimisation. This chapter is aimed at discussing the production of porous zinc and strontium containing phosphate-based glass scaffolds by sintering a technique and to surface modify these scaffolds by proteins that are known to enhance cell attachment and improve seeding efficiency.

The results of this study may be valuable in terms of producing scaffolds with novel compositions that could be of clinical significance.

6.2 Material and methods

6.2.1 Phosphate glass scaffold preparation

Two different compositions of phosphate glass scaffolds were developed. Glass scaffolds were manufactured by using the following precursors: phosphorus pentoxide (P_2O_5 98%, VWR, Lutterworth, UK), sodium dihydrogen phosphate (NaH_2PO_4, 99%, VWR, Lutterworth, UK), titanium dioxide (TiO_2, 99%, VWR, Lutterworth, UK), calcium carbonate ($CaCO_3$, 98.5%, VWR, Lutterworth, UK), strontium carbonate ($SrCO_3$, 99.9% Sigma-Aldrich, Dorset, UK) and zinc oxide (ZnO, 99.95%, Sigma-Aldrich, Dorset, UK). The two glass formulas were zinc phosphate scaffolds (50 P_2O_5 - 10Na_2O - 5TiO_2 – 30CaO –5ZnO) and strontium phosphate scaffolds (50 P_2O_5 - 10Na_2O - 5TiO_2 – 17.5CaO –17.5SrO). An electronic balance (Sartorius) was used for weighing precursor powders (Table 6.1). The precursors powder was mixed for 1 minute by using Stomacher 400 blender apparatus. This was followed by melting the glass powder in a 200ml volume Pt/10%Rh crucible type 71040 (Johnson Matthey, Royston, UK) at a temperature of 1350^{o}C for four hours using a furnace (Carbolite). The melted glass was quenched directly onto cold stainless surface and left overnight to cool down gradually to room temperature. Following this, the cold quenched glass was ground into small particles using MM 301 Mixer Mill (Retsch

GmbH, Hope, UK) grinder. Glass particles were sieved to select only glass particles with size ranging between 400µm-600µm.

Table 6-1 phosphate glass scaffold composition

Glass composition		P_2O_5	NaH_2PO_4	TiO_2	$CaCO_3$	$SrCO_3$	ZnO
ZnO_5	$P_{50}Na_{10}Ti_5Ca_{30}Zn_5$	56.8	24	4	30	0	4
$SrO_{17.5}$	$P_{50}Na_{10}Ti_5Ca_{17.5}Sr_{17.5}$	56.8	24	4	17.5	25.8	0

A graphite mold with a 5mm diameter rod cavity was loaded with the selected glass particles. Glass sintering was carried out by introducing the glass particle-loaded mold into a furnace for 180 minutes. To identify the optimal sintering temperature, three different temperatures were applied for each glass composition according to the glass transition temperature. For ZnO 5 glass scaffolds, the temperatures were: 470^{o}C, 475^{o}C and 480^{o}C. whereas for SrO17.5 they were 480^{o}C,485^{o}C and 490^{o}C. After the sintering procedure, glass scaffolds were allowed to cool down overnight ending in the manufacturing of 5 mm diameter by 5cm long sintered rod (figure 6.1). The sintered glass rods were cut down to different sizes cylindrical scaffolds using diamond discs burs using a slow speed hand piece (Dremel, USA) to allow testing of both their mechanical and structural properties (figure 6.1 e).

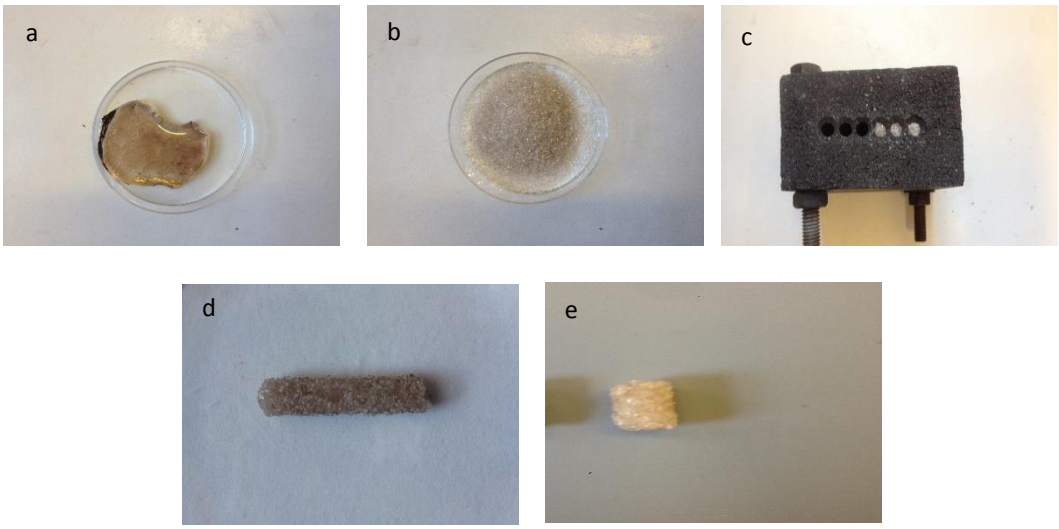

Figure 6-1 Glass scaffold manufacturing steps. a. quenched glass, b. glass powder, c. glass powder loaded into the graphite mold, d. sintered glass rod and e. cylindrical glass scaffold

6.2.2 Glass scaffolds production optimisation

Six different produced glass scaffolds (according to their composition and their sintering temperatures) were structurally and mechanically tested to determine the optimum sintering temperature for scaffold production of each composition.

6.2.2.1 Scaffold porosity estimation

The assessment of the micro-architecture, structure and porosity of the scaffolds was performed using Bruker Skyscan micro CT instrument (Belgium). Six different glass scaffolds were scanned at normal voxel sizes of 4 µm at 70 kV and 100 mA x-ray sources. A thickness of 4 mm of each sample was scanned resulting in multiple image slices. Porosity percentages calculation for each sample was performed using image analysis software (CTvox). The calculation of porosity was performed for all the CT scanned

samples. Moreover, subjective pore size determination was executed on some scaffold slices by using the same software. Other software (NRecon software) was used also to construct a 3D image of each scaffold out of the whole x-ray image slices (figure 6.2).

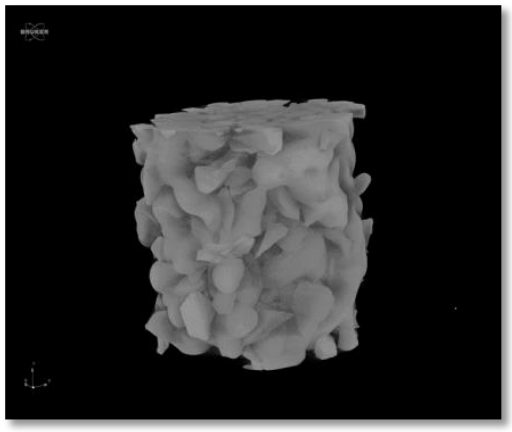

Figure 6-2 3-D image of phosphate -based porous scaffold

6.2.2.2 Diametral compressive strength

Diametral compressive strength was carried out by using a Shimadzu AGS-X (Shimadzu co, Japan) as an alternative method to the conventional compression strength method as glass scaffolds are brittle materials. In this method, ten samples of each prepared glass scaffolds of the dimension 5mm x 10mm were tested at room temperature using an Shmiadzu hydraulic material tester. The speed of testing of the instrument (the hydraulic moving part) was 0.5 mm/min following the previous studies of (Pilliar et al., 2001). All the samples were fixed on special stainless-steel holder positioned horizontally in a position that permits the application of a compressive force on their diameter and not on their long axis (figure 6. 3). Initially, a

compressive force of 5 N was applied until it touched the scaffold passively, then the sample was load until obtaining a fracture. Loading data of the sample fracture were collected using Trapezium x software. The fracture was identified in the software by the appearance of sharp peak considered for tensile stress calculation. Due to the brittleness and porous nature of the scaffolds, it is worth mentioning that this test was challenging to perform and hence bias should be avoided when obtaining the force readings. For this reason, only near –vertical fractures were accepted as results in accordance to the criteria that is previously described (Pilliar et al., 2001). Then, the diametral compressive strength were calculated via the software utilising the equation 1:

$$\sigma x = 2P / \pi DT \quad \text{..... equation 1}$$

Where σx is the compressive strength, P is the load, D is the diameter of glass scaffolds and T is the height of scaffold.

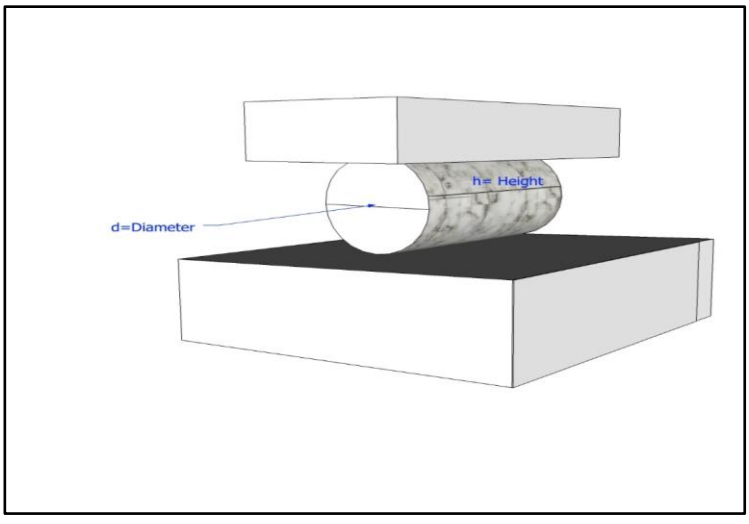

Figure 6-3 Diagram showing the orientation of phosphate glass scaffolds during diametral compressive strength (Drawn by Sketch Up Software)

6.2.3 Cellular studies

6.2.3.1 Cells preparation

Human mesenchymal stem cells (hMSCs) were prepared following the procedure explained in (4.2.6.1).

The culture media used for all cellular studies was DMEM (Thermo Fisher Scientific, USA) supplemented by 50 ml of (FBS) fetal bovine serum (Invitrogen) and 5 ml of penicillin and streptomycin (Sigma Aldrich, Dorset, UK) in 500ml of DMEM.

6.2.3.2 Scaffold Coating

Based on the previous results of sintering temperature optimisation, both zinc (ZnO5) glass scaffolds that were made by sintering temperature 475°C and strontium (SrO17.5) glass scaffolds that were manufactured by sintering temperature 485°C were used for the further cell studies.

Initially these scaffolds were coated by two different proteins known to promote cells attachment to the scaffolds. Coating was either by fibronectin or collagen type 1 as follows:

1-Scaffold coating by fibronectin: Coating with fibronectin was carried out after immersing the scaffolds in (20 µg/ml) fibronectin solution for 1.5 hour under 37°C following the procedure that explained previously (Bhati et al., 2001). The intended fibronectin concentration (20µg/ml) was determined by

diluting 100 µl of 1000µg.ml^{-1} fibronectin (Gibco Thermo Fischer, USA) in 4.9 ml of PBS (Lonza, USA) following the equation M1 X V1= M2 X V2 where:

M1: the main concentration of fibronectin in µg.ml^{-1}.

V1: the volume of the stock fibronectin in ml.

M2: the intended dilution of fibronectin in µg.ml^{-1}.

V2: the final volume of the diluted solution in ml.

2-Scaffold coating by collagen 1: Coating with collagen 1 was carried out by immersing the scaffold in (1 mg.ml^{-1}) collagen solution for 1 hour under 37°C following the procedure explained previously (Linsley et al., 2013). The intended collagen 1 concentration (1 mg.ml^{-1}) was made via the dilution of acetic acid 0.2% solution. A volume of 500 µl of rat tail collagen type 1 stock solution of 2mg/ml (Firstlink.UK) was diluted with the same volume of 0.2% acetic acid following the equation M1 X V1= M2 X V2 where:

M1: the main concentration of collagen 1 µg.ml^{-1}.

V1: the volume of the stock collagen 1 in ml.

M2: the intended dilution of collagen 1 in µg.ml^{-1}.

V2: the final volume of the diluted solution in ml.

6.2.3.3 Cells seeding techniques

Scaffold seeding was performed at six different conditions to optimise the cell culturing procedure ensuring the most efficient cell attachment to the scaffolds.

The various seeding conditions (techniques) varied according to the scaffold coating (uncoated scaffolds, fibronectin coated scaffold and collagen type 1 coated scaffold) in different 48-well plates types (normal well plate and low attachment well plate) culminating in six groups of seeding that are graphically explained in (figure 6.4).

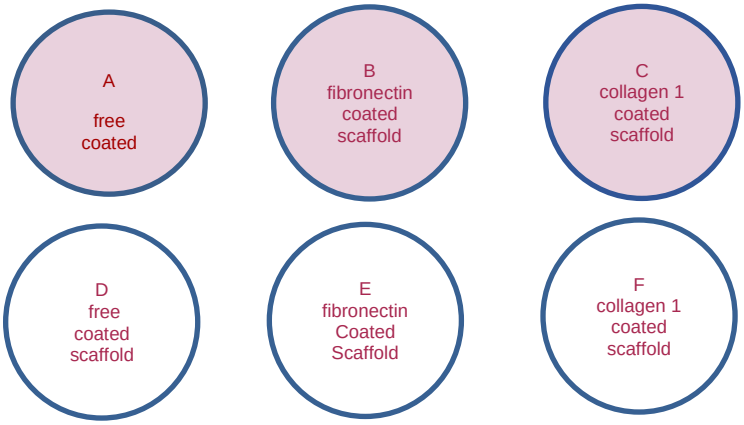

Figure 6-4 Diagram explaining the six different seeding techniques. The upper pink row denotes the low attachment well plates (a. uncoated scaffold, b. fibronectin coated scaffold and c collagen 1 coated scaffold). Whereas the lower row is normal well plates (d. free coated scaffold, e. fibronectin coated scaffold and f collagen 1 coated scaffold).

The intended seeding density (25000 cells / scaffold) was prepared in 30 µl of culture media. Seeding was performed by pipetting out the culture media around all the sides of the scaffold (5 mm x 6mm) sides to ensure an even distribution of hMSCs through the scaffold microstructure. Then, the hMSCs cultured scaffolds were left for 30 minutes in the incubator to provide enough time for cells to attach to the scaffold structure before adding 1 ml of culture media α-MEM (Thermo Fisher, UK) for further investigation.

6.2.3.4 Cells attachment assessment study

Zinc (ZnO5) containing phosphate-based scaffolds prepared at 475 °C were used for seeding optimisation. The aim of this study was to find the best way to permit the cell attachment. The study entailed seeding hMSCs onto zinc based phosphate glasses scaffolds at six different conditions as explained previously.

A triplicate of each of prepared ZnO5 (free coated, fibronectin coated, collagen 1 coated) scaffolds were seeded twice in 1ml α-MEM; first in normal 48- well plates (Corning, USA) and in low attachment 48 -well plates (Corning, USA). The hMSCs seeding density was 25000 cells/scaffold. Cell attachments assessment was performed twice at (1-hour and 2 hours) after seeding.

After one hour, scaffolds were transferred from their initial seeding plate to another new well plate filled with 1ml of α-MEM. Culture media was then aspirated from the first seeding well plate which was then washed with PBS (Lonza, USA). Then around 500 µl of trypsin was added to each well plate for 3 minutes under 37°C to aid in cells detachment. The trypsin was deactivated through adding 500µl of α-MEM culture media. Then the resultant 1 ml of (trypsin+ α-MEM + suspended detached cells) was centrifuged in 1ml plastic tubes under speed of 1000 rpm for 5 minutes.

Following centrifuging, the supernatant culture media was aspirated and hMSCs cells pellets were suspended in 1 ml of culture media. 10 µl of the

suspended cells solution were mixed with 10µl of trypan blue stain (Sigma Aldrich, Dorset, UK). The mixtures were introduced into the hemocytometer and direct cell quantification was performed according to the Strober procedure (Strober, 2001). At the second hour, the same procedure was followed, and the detached cell number was quantified again.

6.2.3.5 Cells metabolism assay

Cells metabolic activity of hMSCs was assessed following their seeding on a triplicate of ZnO5 scaffolds at a density of 20000 cells/ scaffold using the six different seeding conditions explained previously. Metabolic activity assessment was performed using alamar blue assay (Bio-Rad, UK). One milliliter of α-MEM culture media was added to the seeded scaffolds for one hour. After one hour, the scaffolds were transferred to other new plate to avoid any bias in reading the detached cells within the same well plate. Fluorescence reading for fully reduced alamar blue was performed initially following the previous procedure in (3.2.6.3). Fluorescence reduction percentage to the full reduced was quantified at 3 different time points (1, 4 and 7 days) following the same procedure explained in (3.2.6.3)

6.2.3.6 Metabolic activity assay (CCK assay)

Metabolic activity of hMSCs was also assessed on a triplicate of SrO17.5 glass scaffolds sintered at 485 °C. Cells were initially seeded at a density of 20000 cells/ scaffold following the six seeding conditions procedure. One milliliter of α-MEM culture media was added to the seeded scaffolds for one

hour. After one hour, the scaffolds were transferred to other new plate to avoid any bias in reading the detached cells within the same well plate. Absorbance readings were measured at 3 different time points (1, 4 and 7 days) and cell number was quantified indirectly following the procedure described in (4.2.6.2).

6.2.3.7 Confocal Imaging

Human Mesenchymal stem cells (hMSCs) were seeded at a density of 20000 cells/ strontium glass scaffolds. Seeding procedure was performed in six conditions as explained previously and laser confocal images were taken at 3 different time points (1, 4 and 7 days) following the techniques explained previously in (4.2.6.6).

6.2.4 Statistical Analysis

All the data were statistically analysed via one-way ANOVA or Kruskal Wallis according to their data normality. Statistics were performed to test the null hypothesis regarding both scaffolds manufacturing and scaffolds seeding technique.Concerning scaffold manufacturing, the null hypothesis stated that there is no structural and mechanical difference between various sintering temperatures that are used in zinc and strontium scaffolds construction. Whereas for the scaffold seeding technique, the null hypothesis was that there is no statistical variation in seeding efficiency, cellular metabolic activity and cellularproliferation between the different cells seeding techniques. All the statistical analyses considered $p<0.05$ to be the significance degree of estimation.

6.3 Results

6.3.1 Porosity

Figure 6.5 and 6.6 show the relation between percentage of scaffolds porosity and the sintering temperature of strontium (SrO17.5) phosphate-based scaffolds. The highest porosity figure was found in scaffolds sintered at 480°C which was about 47.5±3.6% which was statistically higher than the other sintering temperatures at 40.6 % and 35.5 % for both 485 °C and 490°C sintering temperatures respectively.

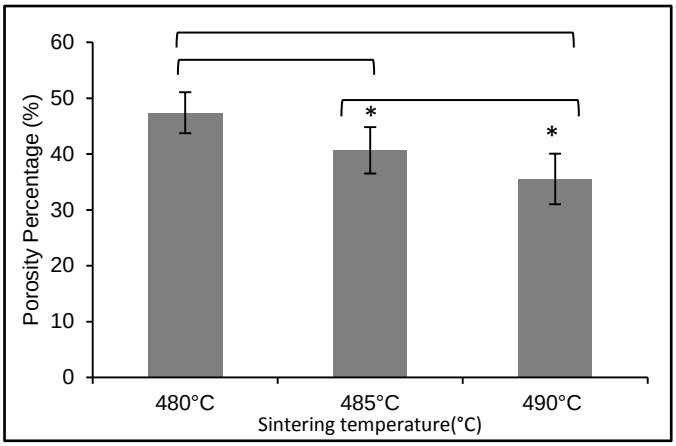

Figure 6-5 Porosity percentage of SrO17.5 scaffolds sintered in different temperatures showing that porosity is indirectly related with the sintering temperature

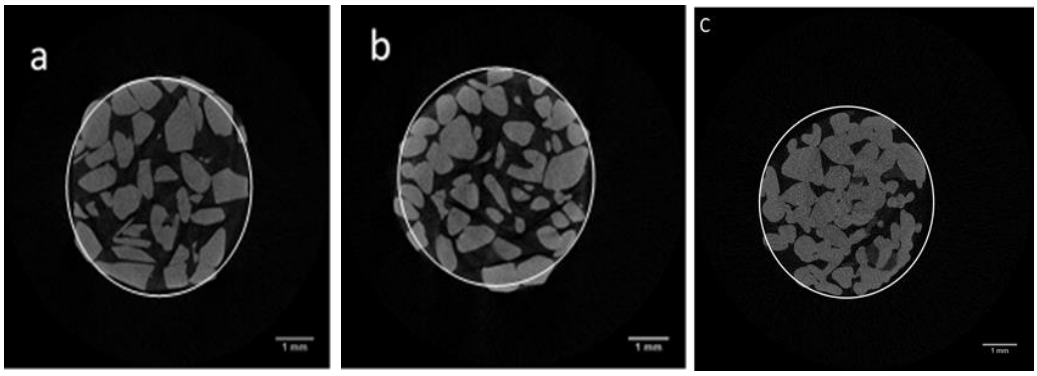

Figure 6-6 CT-cross sections of strontium scaffolds made at different temperatures. a 480°C, b. 485°C and c.490°C displaying the decrease in porosity as sintering temperature rose

The relation between sintering temperature and the porosity of zinc (ZnO5) produced scaffolds is explained in both figures 6.7 and 6.8. The porosity seemed to be inversely correlated with the sintering temperature as it decreased when a high sintering temperature was used for scaffold manufacturing. The highest porosity (58±1.3 %) was found with scaffolds sintered at temperature of 470°C followed by (47.5±2.7%) and (40±3.7%) for both 475°C and 480°C sintering temperatures respectively.

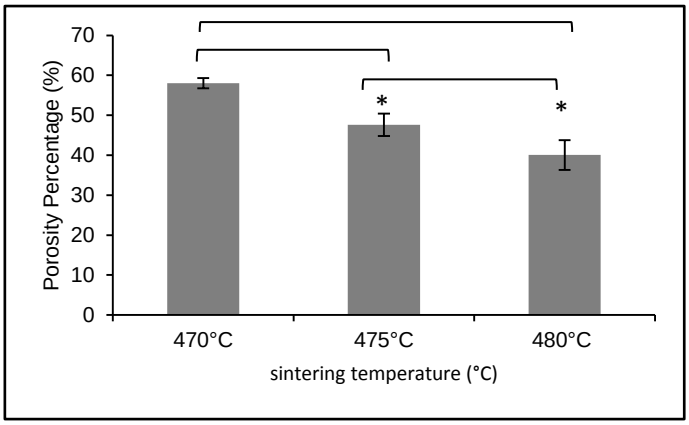

Figure 6-7 Porosity percentage of ZnO5 scaffolds sintered in different temperatures showing that porosity is indirectly related with the sintering temperature

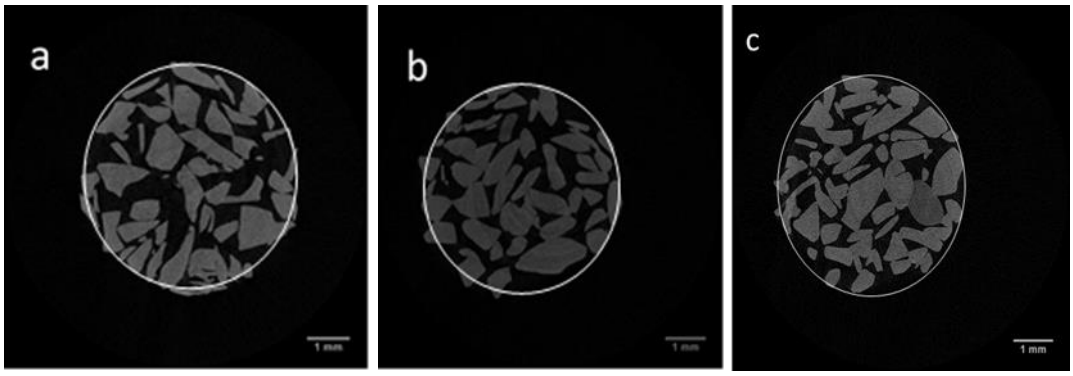

Figure 6-8 CT-cross sections of zinc scaffolds made at different temperatures. a 470°C, b. 475°C and c.480°C displaying the decrease in porosity as sintering temperature rose

6.3.2 Diametral compressive strength

Figures 6.9 and 6.10 present the mechanical property measurement (diametral compressive strength) of the different zinc and strontium scaffolds sintered at different temperatures. Generally, the diametral compressive strength increased with increasing sintering temperature.

Regarding strontium based scaffolds (figure 6.9), the results revealed that the diametral compressive strength of the 490°C sintered scaffolds was around 4.2±0.42 MPa which was statistically different ($P<0.05$) from the other two sintered groups.

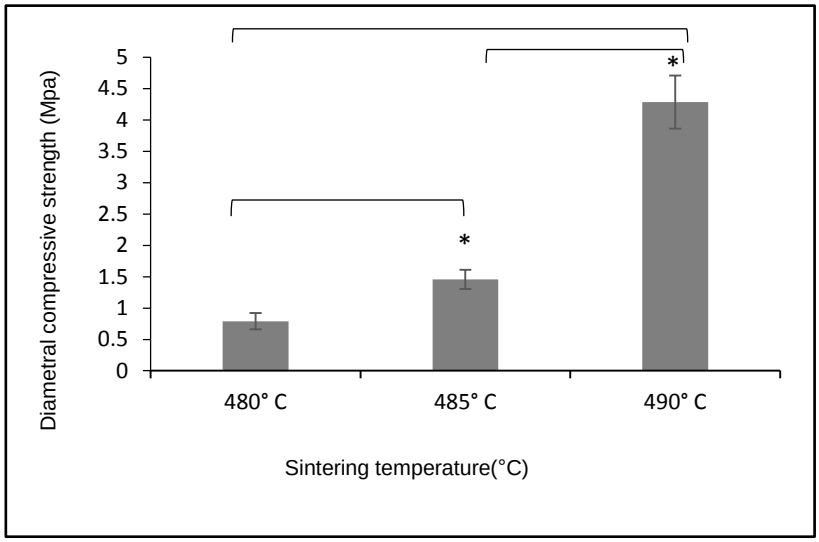

Figure 6-9 Diametral compressive strength for different manufactured strontium glasses

Similarly, zinc scaffolds diametral compression strength (figure 6.10) improved as sintering temperature rose from 470°C to 480°C with a sign of statistical difference (P<0.05). It was 0.36±0.08 MPa for the 470°C group in comparison to 0.6 ± 0.17 MPa and 1.3 ± 0.2 MPa for both the 475°C and the 480°C sintered group respectively.

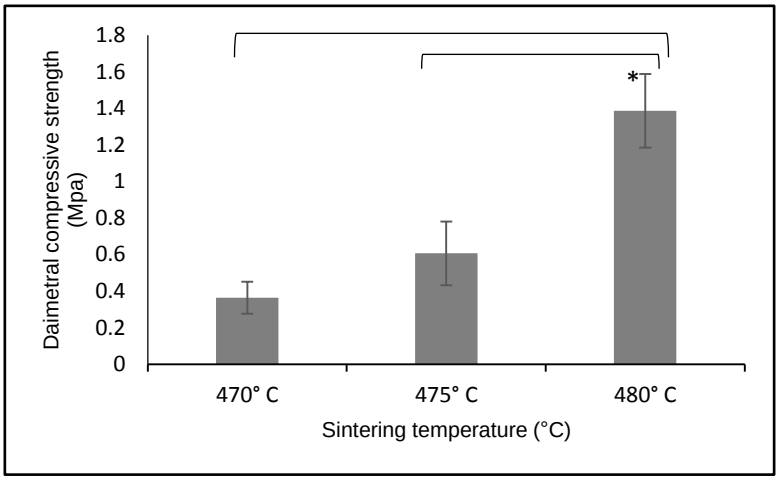

Figure 6-10 Diametral compressive strength for different manufactured zinc glasses

6.3.3 Cell Detachment

Figure 6.11 shows the percentage of detached cells in relation to the initial cell seeding density. Overall, the percentage of the detached cells is higher in the uncoated scaffolds and the majority of cell detachment occurred at one-hour post seeding. At the first hour, the data of uncoated scaffolds groups revealed that about 36±2.6% and 31±4.3 % of the primarily seeded cells were detached in both the normal and the low attachment coated plates respectively with clear statistical significance in comparison with other groups (P<0.05). Regarding the data of the second hour, the uncoated scaffolds exhibited the highest percentage of detached cells which was about 25±1.8%

and this was significantly more than the other groups which displayed cell detachment of around 15%. Another significant point was found suggesting there is no clear effect of the seeding plate on the cells detachment of the same coating material.

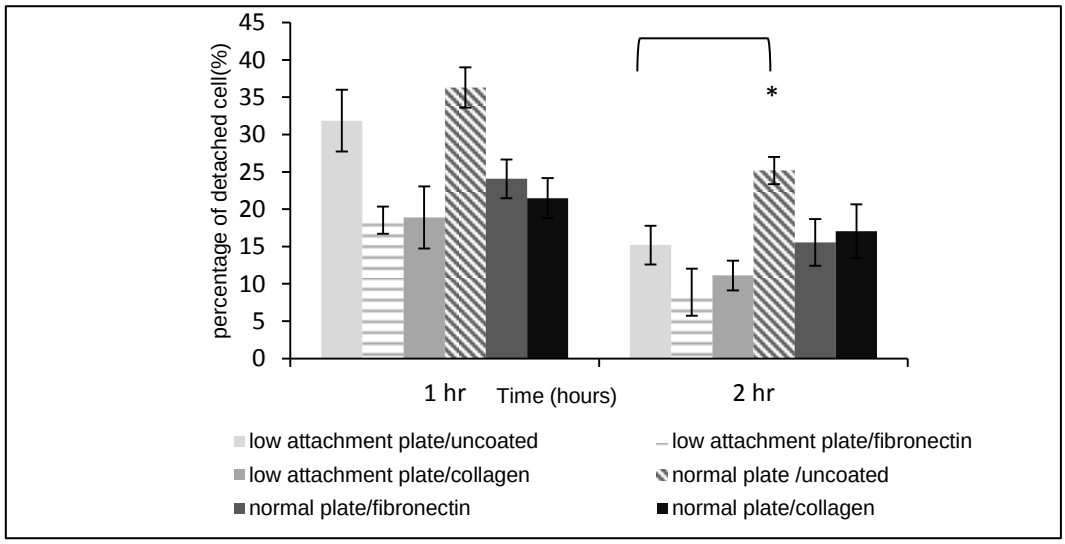

Figure 6-11 The percentage of detached cells from Zn O5 scaffolds(1 and 2 hours post seeding) displaying the most percentage of cells detachment was found in the non-coated scaffold groups

Figure 6.12 displays the images of detached cells on well plates of the six different seeding conditions. The images confirmed the findings of figure 6.11 in which there was more scaffold non-attached cells in the free coating glass scaffolds (figure 6.12 a). Though, both collagen and fibronectin coated scaffolds images suggested that these proteins showed low numbers of detached cells.

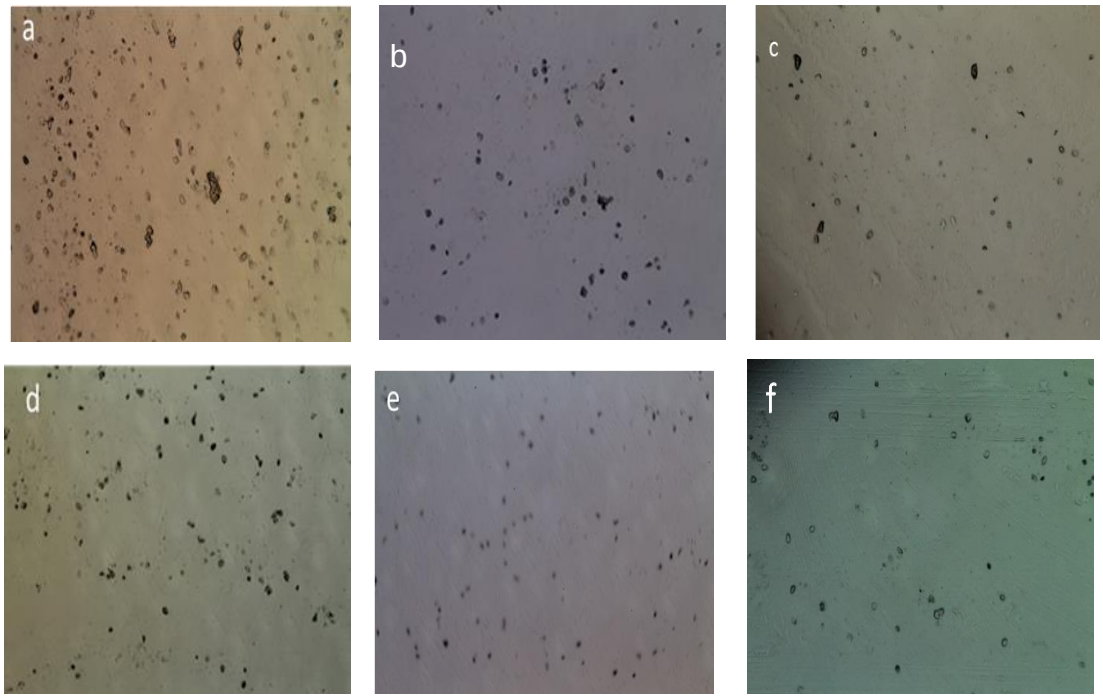

Figure 6-12 Microscope images of the seeding well plates one-hour post seeding. A. normal plate/ uncoated scaffold, b. normal plate/ fibronectin coated scaffold, c. normal plate/ collagen coated, d. low attachment plate/ uncoated scaffold, e. low attachment plate/ fibronectin coated scaffold and f. low attachment plate/ collagen coated

6.3.4 Cell metabolic activity

Figure 6.13 presents the percentage of alamar blue fluorescence reduction (as a percentage of fully reduced alamar blue) of the hMSCs seeded on zinc phosphate glass scaffold using six different seeding conditions at three time-points. The change in fluorescence was considered as an indication of cellular metabolic activity where the low reduction refers to the low metabolic activity. Generally, the lowest reduction was found in the normal uncoated scaffold groups. On day 1, the highest reduction was found in the collagen coated scaffold that was seeded on the low attachment well plates. The amount of reduction was about 13.5%±0.6 which was clearly significant

compared to the other groups (P<0.05). The pattern of data on day 4 and day 7 was similar in which the collagen coated scaffolds exhibited the highest metabolic activity, this was followed by the fibronectin coated samples. Though, there was no statistical variation between the collagen and the fibronectin coated groups (P>0.05). The uncoated scaffolds seeded on normal well plates displayed the lowest metabolic activity on these two days with a reduction of 9±1% and 18±1.5 % on day 4 and 7 respectively. Similar to the detachment study results, there was no clear variation in metabolic activity between the same material coated scaffolds seeded using a different well plate.

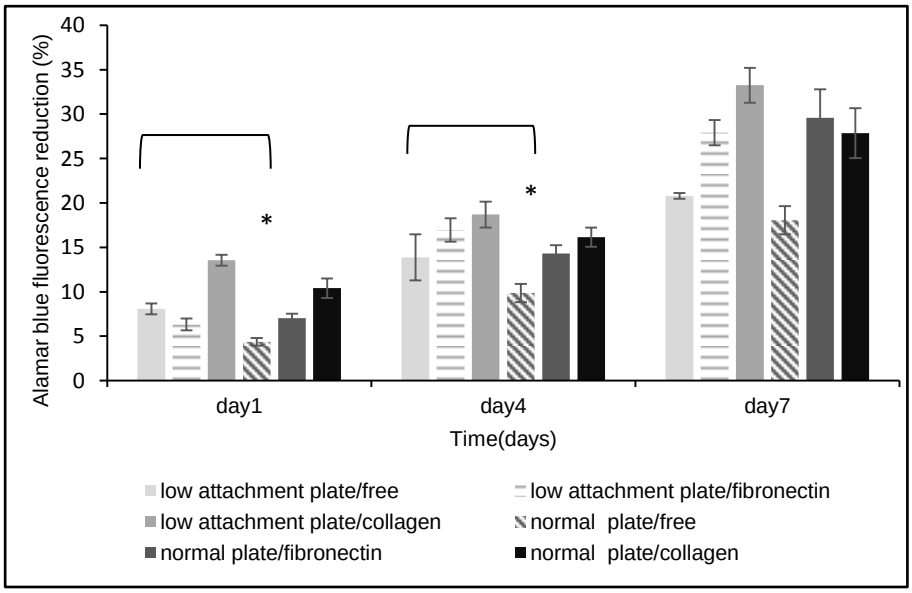

Figure 6-13 Alamar blue fluorescence reduction of the six seeding groups at three-time points (day 1,4,7) displaying that free coating scaffolds groups had the lowest metabolic activity

6.3.5 Metabolic assay (CCK Assay)

Human mesenchymal stem cell proliferation using different conditions at three-time points is presented in figure 6.14. On day 1, the lowest cellular proliferative activity was found in the free coated scaffolds at around 9700±600 cells, this was clearly significant from other groups that showed a better proliferative ability at around 15000-19000 cells. On day 4, all groups showed similar data in which cell numbers were doubled in comparison with the first day. On day 7, there was an increase in the cell number for all the samples. Though, the ultimate cellular growth was more prominent in the low attachment well plate seeded groups which was around 65000 ±2600 cells for the collagen coated scaffolds. The lowest significant proliferation ($P<0.05$) was noticed in the free coated scaffolds at around 34500±3900 cells.

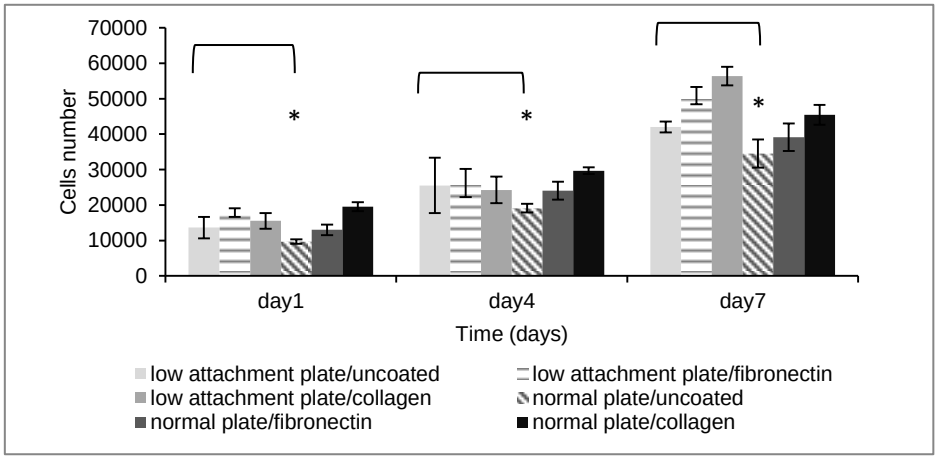

Figure 6-14 Cells number proliferation on different seeding groups at three-time points (day 1,4,7) displaying that free coating scaffolds groups had the lowest proliferative ability

6.3.6 Confocal imaging

Figure 6.15 presents the laser confocal imaging of hMSCs seeded on the strontium glass scaffolds one-week post seeding. The images exhibit samples of the different seeding techniques. Generally, cells seemed to have the ability to attach, adhere and proliferate on scaffolds irrespective of their seeding condition. Some images show the ability of cells to extend around the glass particles and follow the scaffold microstructure (figure 6.15 b and f).

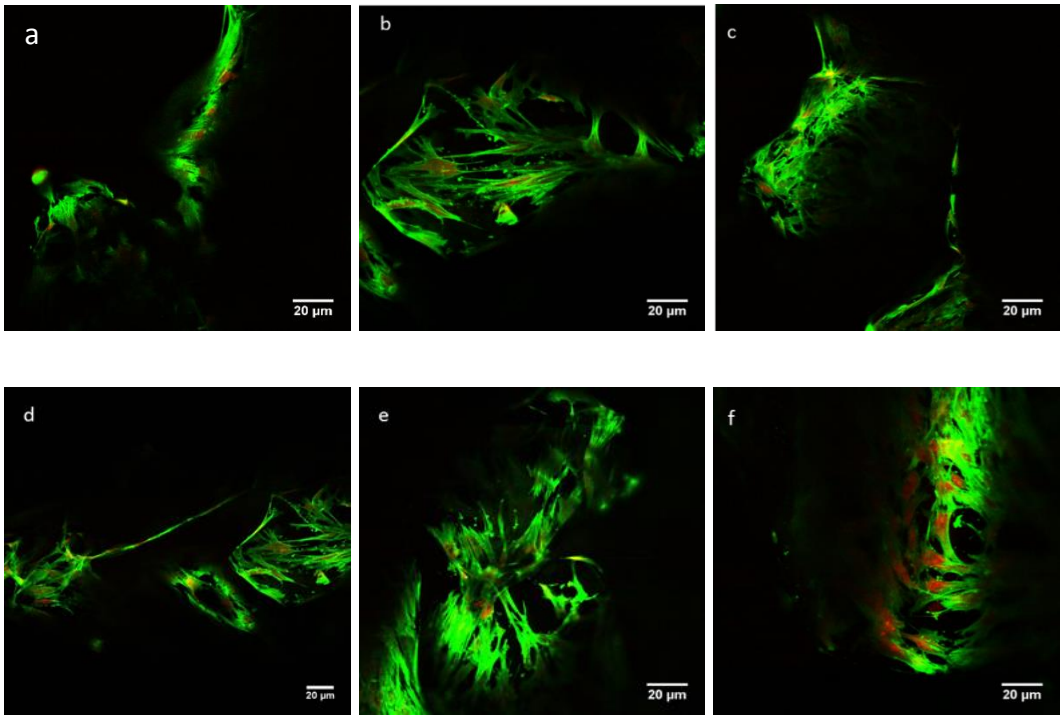

Figure 6-15 Confocal images of hMSCs seeded on strontium glass scaffolds by different seeding conditions. a. normal plate/ uncoated scaffold, b. normal plate/ fibronectin coated scaffold, c. normal plate/ collagen coated scaffold, d. low attachment plate/uncoated scaffold, e. low attachment plate/ fibronectin coated scaffold and f. low attachment plate/ collagen coated scaffold

6.4 Discussion

The main purpose of this chapter was to develop zinc and strontium (ZnO5, SrO17.5) phosphate glass 3D scaffolds based on the findings of the previous chapters. Glass scaffolds were made from phosphate glass powder using sintering technique with no other additives or porosifiers. The main reason for choosing this method rather than other techniques such as sol gel technique or the foam replica technique (Jones et al., 2006, Boccaccini et al., 2007) was to eliminate the effect of the other added ingredients such as polymer and alkoxide that is needed in other techniques. Glass powder size was chosen between (400µm-600 µm) to obtain the intended porosity percentage and the porous size following Kozeny's equation which related the powder size to the porosity and the porous size (Skorokhod et al., 1988). The equation 2 correlating these variables is:

$$Dpo = \frac{2}{3} x \frac{\theta}{1-\theta} x\, Dpa$$ ..... Equation 2

Where D_{po} is the intended pores size, D_{pa} is the particle size and θ is the porosity. Consequently, via applying 60% as the intended porosity percentage and 500 µm as the final intended pores size, the result of particle size is around 500 µm.

The sintering procedure was performed taking into account the differential thermal analysis stated in the previous chapters. The sintering temperature was designed to be the temperature in the window of glass transition

temperature which is the initial temperature when glass starts to soften and changes from solid status to rubbery status. The range of this temperature was about (465°C-480°C) and (475°C-495°C) for both ZnO5 and SrO17.5 glasses respectively. Three different temperatures were considered to optimise the scaffold sintering technique. The produced scaffolds manufactured via different sintering temperatures were studied structurally and mechanically to find out the optimal temperature for the scaffold manufacturing process.

Regarding the porosity results performed via CT image calculation similar to a previous study (Alonso-Sierra et al., 2017), it was revealed that for both zinc and strontium scaffolds the porosity percentage tend to decrease as the sintering temperature increased. It changed for the strontium scaffolds from 47 % at 480°C to around 35.5 % for 490°C and from 58% at 480°C to 40% at 490°C for the zinc scaffolds. The objective pore size quantification followed the same concept of the porosity percentage in which it was around 250-400 µm for the low sintering temperature group. It decreased gradually with increasing the temperature to be around 200- 350µm for the middle sintering parameters and ended at around <150µm for the high temperature- sintered scaffolds. The explanation of this indirect relation between the sintering temperature and the porosity could be related to that rising temperature may influence the glass network and hence might cause a break up in many intermolecular bonds. This may decrease the glass viscosity on its way to changing to liquid. Consequently, the glass status might be changed as the

viscosity may obliterate many pores and spaces among the glass structure via the softened material causing a porosity reduction (Ebbing and Gammon, 2016). According to these results, the glass produced at the highest temperatures (480°C for Zn and 490°C for Sr) yielded a low percentage of porosity and for this reason these temperatures were excluded as their scaffolds may not have the proper structural requirements that permit cellular growth (Jones et al., 2010). On the other hand, the glasses developed at other temperatures produced an acceptable porosity. Although this porosity is not so excessive, it was within the limit (porosity>40%) that was suggested in previous studies to promote osteogenic growth (Yuan et al., 2001, Sepulveda et al., 2002, El-Ghannam, 2004).

The scaffold mechanical property was assessed using the diametral compressive strength measurement technique. This technique is mostly suitable for brittle materials and materials with irregular surface preventing them from optimum loading and positioning by the conventional methods of mechanical characterisation such as compressive and tensile strength testing (Sakaguchi and Powers, 2012). Scaffolds were designed as cylinders with 1:2 diameter height proportion (5 mm in diameter and 10 mm in height or thickness). This was done following the specimen preparation criteria for mechanical tests that was stated previously (Hing et al., 1998). These scaffolds were placed in adjustable two connected metal rods - holder with controlling screws to adjust the distance between the holder components and preventing the scaffolds from moving during the test. Due to the lack of

studies performed on phosphate glass scaffolds, the machine crosshead was set to 0.5 $mm.min^{-1}$ following the procedure suggested for other types of bioceramic material (Pilliar et al., 2001). Both the strontium and the zinc scaffolds findings suggested that using high sintering temperatures may enhance the mechanical properties of the scaffold material. This was compatible with previous findings of which different sintering temperature were used in scaffold manufacturing (Jones et al., 2010). These findings may be explained as being due to an increase in the temperature may lead increased flow and thus and increase in the glass contact points attachment. This might result in improving the mechanical structure of the material. As a result of this study, it seemed that using low sintering temperature produced glass scaffolds with poor mechanical characteristics that cannot withstand the external loads and also may not support the cellular complex for enough time for bone formation.

Depending on the results of the porosity and the diametral tensile strength, the sintering temperatures of 485 °C and 475°C were optimised for both the strontium and the zinc scaffolds production respectively. The scaffolds manufactured at these temperatures were intended to be used in *in vitro* analysis. Though, one of the obstacles in static scaffolds cellular studies is the poor cellular seeding as there is a high chance for cells to detach and flow away from the scaffold framework due to the action of culture media flow (Shimizu et al., 2006). This poor level of seeding can lead to biased findings and poor results. Consequently, proteins such as fibronectin and collagen

type 1 were used to enhance the cell adhesion taking into account previous findings (Hynes, 1992). Also, the low attachment well plates were used as seeding platforms because they have been used previously to ensure efficient stem cells seeding on microcarriers (Nie et al., 2009) .

The detachment study was carried out by seeding the same cells number through different seeding techniques by coating the scaffolds with different materials and using different seeding plates (normal and low attachment 48-well plates) ending in six different seeding groups. The findings of this study suggested that fibronectin and collagen type 1 coated scaffolds play a major controlling factor in seeding optimisation rather than the type of the seeding well plate. This can be interpreted by hypothesising that although the low attachment well plate can prevent the cell immobalisation on the plate surface, it is not necessary that the suspended cells will attach to the scaffold with the possibility of these cells to remain suspended within the culture media. For this reason, the detached cell number between different well plate types in the same scaffold group were slightly similar. However, the statistical variance was clearly present between different scaffolds (whether they were free scaffolds or fibronectin and collagen coated). The findings revealed that the coated scaffolds promoted better cell adhesion and the most positive results were found in the fibronectin coated groups that were non-significantly better than the collagen coated groups. These findings were very compatible with a previous study that examined the intervertebral disc cells attachment to different types of coating proteins. The results showed that

fibronectin notably promoted cell adhesion more than the other coating proteins including collagen (Attia et al., 2011).

The metabolic study using alamar blue was performed to estimate the effect of seeding technique; specifically, the coating, on the physiological metabolic activity of cells. This study was performed on three different days and the general conclusion from the results suggested that there was no clear effect of using different kinds of well plates (normal and low attachment). Though, alamar blue results explained that the scaffold coated with collagen resulted in the most prominent metabolic activity among the fibronectin coated and the free coated scaffolds. These results are very compatible with previous results that examined the effect of coating flask plates with different proteins including collagen and fibronectin and showed a higher alamar blue activity with collagen coated plates than that in fibronectin coated samples (Linsley et al., 2013).

Indirect cellular numbers via the CCK assay revealed that the high rate of proliferation was found with the collagen coated scaffold followed by the fibronectin coated, both of these samples were significantly different from the uncoated scaffolds at all time points ($P<0.05$). Cells were initially seeded at 20000 cells/ scaffold. Though, the cell proliferation data on the first-time point was less than the initial cellular seeding density. This may relate to the seeding procedure being performed according to the detachment study in which scaffolds were transferred into new plates after one hour to eliminate measurement of any metabolic activity due to the detached cells and

ensured that all the results are yielded from the cells seeded on the scaffolds only. Another interesting finding is that both the metabolic and the proliferative studies suggested that there is no clear effect of using different types of well plates in seeding as there is no significant difference in the cellular associated data ($P>0.05$). The only factor affecting the results is the variation in the scaffold coating.

The confocal images confirmed the alamar blue and the CCK assays in which cells seemed to have a denser organisation and multilayer proliferation in collagen and fibronectin coated scaffolds in comparison with the uncoated scaffolds. These results were similar to the cell proliferation studies performed previously on fibronectin and collagen coated titanium and flask plate surfaces in which cell number growth was more enhanced in the presence of these protein coatings than the free uncoated samples (Van Den Dolder et al., 2003, Tsai et al., 2010).

In conclusion, the results revealed that the glass based scaffolds were successfully produced by a sintering technique. Using different temperatures in the sintering procedure affected the mechanical properties of the produced scaffold. Sintering at high temperature may cause a decrease in porosity while sintering at low temperature may affect the glass strength negatively. Hence, using midpoint temperatures as 485 °C and 475°C for the strontium and the zinc glass scaffolds respectively was recommended because the scaffolds manufactured at these temperatures were within acceptable parameters for both structural and mechanical properties. For seeding

techniques, it is suggested to coat the scaffolds with either collagen or fibronectin, however, collagen coated scaffolds displayed slightly better results. Based on the findings of this chapter, null hypothesis was rejected in regard to the different sintering temperatures in which application of various temperatures in producing scaffolds may yield different mechanical and morphological variations between scaffolds. The null hypothesis was also rejected regarding seeding techniques where there was significant difference between cell attachment on collagen and fibronectin scaffolds compared to non- coated scaffolds.

Other studies are needed to improve the mechanical properties of the scaffold by modifying the glass structure or the surface functionalisation to produce biocomposite with enhanced properties. Moreover, it is required to test these scaffolds in a more clinically relevant way to assess the cellular effects of these scaffolds within a dynamic environment.

Chapter 7 Determination the Effect of Cultivating Stem Cells on Scaffolds Under Dynamic and Static Conditions on Osteodifferentiation

7.1 Introduction

One of the main aspirations of bone tissue engineering is to produce a suitable biocompatible biomaterial that is cultivated with bone cells providing a suitable scaffold for them to expand over an extended period of time prior to implanting such scaffold inside the body (Chen and Hu, 2006). Bioreactors are systems used to fulfill the aim of translating cells and tissue based constructs into large-scale biological products that can be cultured for longer times under a controlled environment (Zhao et al., 2016). Birla (2014) stated that each bioreactor could have the following design requirements: bioreactor stimulus, culture variables (pH, oxygen and temperature), sensors for culture variable and stimulus (Birla, 2014). Although there are different types of bioreactors used successfully for bone tissue engineering such as spinner flasks, rotating wall and perfusion bioreactors, the latter type is the more preferred than the others due to its simplicity and better culture perfusion ability (Yeatts and Fisher, 2011).

Many studies were carried out to investigate the effect of cultivating stem cells in perfusion bioreactors. One study seeded the bone marrow stem cells on scaffolds that was made from silicate and tricalcium phosphate (TCP).

These scaffolds were then cultured in a perfusion bioreactor (dynamic conditions) and static conditions separately. The findings showed that the osteodifferentiation ability of stem cells was induced more under dynamic conditions (Bjerre et al., 2008). Similar results were found in another study which aimed to prepare polymer scaffolds to repair small bone tissue defects. These polymer scaffolds were cultivated within mesenchymal stem cells and cultured in both dynamic and static conditions. The osteogenic lineage was found clearly in samples cultured under dynamic conditions (Kleinhans et al., 2015). More recent research aimed to develop an automated type of perfusion bioreactor to control the different culture variables. Two groups of tricalcium phosphate scaffolds were cultured in this bioreactor for 20 days; one group was seeded within bone marrow stem cells whereas the other kept without cells. The results revealed that bone was formed in the cell seeded scaffolds in compare with the free cell scaffolds where no bone formation was noticed (Ding et al., 2016b).

Although there are different kinds of biomaterials used for bone repair in the craniofacial region using metal, ceramics or polymers, there are still drawbacks of using them individually. These drawbacks encouraged researchers to develop new types of biomaterials called biocomposites that are composed of a combination of more than of one of the these materials (Sharif et al., 2016a). These biocomposites are designed to overcome the drawbacks of using bioceramics or polymer individually as they aim to combine the flexibility presenting in polymer with the hardness and

bioactivity of bioceramics resulting in a new material that has better properties than any of the two basic materials separately (Qidwai et al., 2014). Will *et al* (2012) mentioned that there is an advantage of combining polymers with glass ceramics in biocomposite production as the polymer provides the construct with flexibility, plasticity and formability whereas the glass would add stiffness and mechanical strength to the composite (Will et al., 2012).

There are many studies intended to fabricate different types of biocomposites for bone tissue engineering via including different components such as bioactive glasses, polycaprolactone polymer (PCL) and carbon nanotubes (CNT). One study compared the pins made of the PCL polymer with phosphate glass to the stainless-steel pins. These pins were implanted within *in vivo* environment (in rabbits) and the results showed that these hybrid pins were well tolerated with a minimal inflammatory reaction (Lowry et al., 1997). Other related attempts were performed to investigate the mechanical and the structural properties of the phosphate glass fibers with PCL polymer complex. These glass fibers-PCL composite were manufactured via either in situ polymerization or compression molding techniques and their results were promising (Ahmed et al., 2008, Khan et al., 2010).

Other studies modified the PCL polymers to be used for bone tissue repair. Two academic papers examined a potential modification of the PCL-CNT biocomposite by using different concentrations of CNTs to reach acceptable mechanical and biological properties. The results showed that adding CNTs

to the PCL can promote better mechanical properties however this might affect the cellular response negatively (Mattioli-Belmonte et al., 2012, Pan et al., 2012). A different study related to neural tissue engineering was used CNT coated phosphate glass fibers as a candidate material that support neural growth. The findings revealed a great potential for this material to enhance neural growth due to the electrical properties of the CNTs and the morphological features of these glass fibers (Ahn et al., 2015). Despite the huge efforts spent on various bioactive glass biocomposites in the field of bone tissue engineering, there is little published on the phosphate glass biocomposites with most of the work performed previously was on the use of glass fibers or glass powder as a filler material.

This chapter focuses mainly on manufacturing a biocomposite scaffold that is made mainly from zinc (ZnO5) and strontium (SrO17.5) phosphate glasses as core materials. These scaffolds were surface functionalised via CNT-PCL coating layer to enhance the glass characteristics of the scaffolds. The prepared scaffolds were seeded and tested within both dynamic and static conditions to assess the impact of culture media flow on cell activity.

This may provide us with a better understanding of cells response to scaffolds materials as well as to different types of stimulus which can be of clinically relevant value for craniofacial bone defect applications.

7.2 Materials and Methods

7.2.1 Sample preparation

7.2.1.1 Phosphate glass scaffold preparation

Two different compositions of phosphate glass scaffolds were developed based on the previous findings. The compositions were zinc (ZnO_5) containing phosphate glass scaffolds sintered at 475 °C and strontium ($SrO_{17.5}$) phosphate glass scaffolds sintered at 485 °C. Both scaffolds were developed following the procedure mentioned in (6.2.1). Glass scaffolds were prepared in two different sizes cuboidal shapes (5mmx5mm and 5mmx10mm).

The surfaces of some of the prepared glass scaffolds were modified by CNT-PCL coating. Initially CNT–PCL solution was prepared by dissolving the PCL polymer (Sigma Aldrich, Dorset, UK) in chloroform solvent (> 99%, Sigma Aldrich, Dorset, UK) at a percentage of 2 wt/v %. Then, carboxylated CNT (manually prepared as described primarily in 5.2.2) was dispersed in the PCL solution at the percentage of 25µg/ml. The final produced CNT-PCL solution was stored in a glass container for coating scaffolds.

The procedure of coating glass scaffolds (5mmX5mm) was preceded by scaffold cleaning with acetone. Coating was carried out by immersing the scaffolds in 10 ml of CNT-PCL polymer solution within a bath sonication for 15 minutes to ensure that glass scaffolds were coated with CNTs. Glass scaffolds were then removed from the immersion glass containers and left to

dry in the desiccator over 12 hours. Coated scaffolds were stored for further studies.

7.2.1.2 Bio Oss (control) scaffold preparation

Bio-Oss® blocks (1cm width X 1cm height X 2cm length) (Geistlich, Switzerland) were used to prepare the control groups. The block heights were cut firstly into two halves using a diamond bur mounted on a slow speed engine (Dremel, USA) to obtain two half-blocks of (0.5cm X 0.5cm X 2cm). The half block was then cut into various (5mm x 5mm) cylindrical shape BioOss scaffolds using a trephine bur. These cylindrical scaffolds were stored for further biological and non-biological tests. Other Bio Oss scaffolds of the dimension of 5mm x 10mm were prepared for mechanical testing studies.

At the end of this stage, five groups of samples (figure 7.1) were ready for further analyses which are:

1- Uncoated zinc(ZnO5) glass scaffolds named as (ZnO)

2- CNT coated zinc (ZnO5) glass scaffolds named as (ZnO-CNT)

3- Uncoated strontium (SrO17.5) glass scaffolds named as (SrO)

4- CNT coated glass scaffolds named as (SrO-CNT)

5- Bio Oss scaffolds named as (Bio Oss)

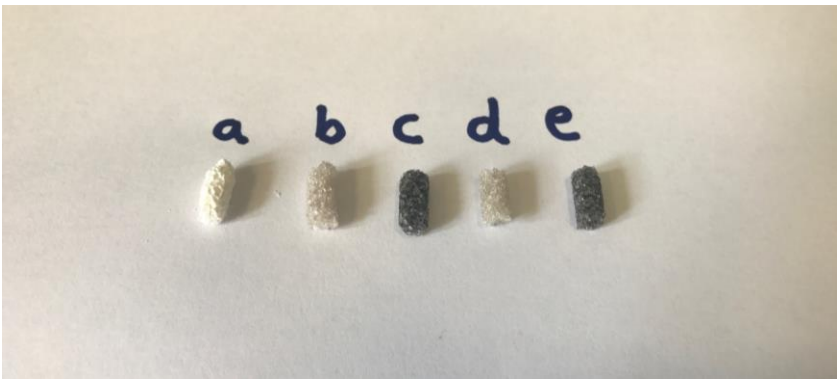

Figure 7-1 Scaffolds samples: a. Bio Oss, b. ZnO, c. ZnO-CNT, d. SrO and e. SrO-CNT

7.2.2 Samples characterisation

7.2.2.1 Scaffold porosity estimation

One sample from each of the five-prepared group was scanned via a micro computed topography (CT) scan (Skyscan Bruker, Belgium). Porosity estimation and pore size quantification was performed for all the sample as described previously in (6.2.2.1).

7.2.2.2 Diametral compressive strength

Ten samples of (5mm x 10mm) from each of the formulated samples were mechanically tested using diametral tensile strength via Shimadzu AGS-X (Shimadzu co, Japan) as explained previously in (6.2.2.2).

7.2.2.3 Scaffold degradation

A degradation study was performed by using a triplicate of 5 mm x 5mm scaffolds from each of the five prepared groups at three-time point (1 month, 2 months and 3 months) within both static and dynamic conditions. Initially

the scaffolds were weighed and stored in plastic vials (Sterilin tube) and then immersed in 25 ml of phosphate buffered saline (PBS)(Lonza.UK).

For the static conditions, triplicate of each scaffold was incubated at 37°C for the whole study period. Whereas, in parallel other triplicates were used within dynamic studies in which scaffolds were shaken continuously at 70 rpm for three months using Mini Orbital shaker SO5 (Stuart Scientific, Staffordshire, UK).

At each time point, scaffolds were removed from their container and left to dry for 6 hours at 50 °C. After dryness, scaffolds were weighed and then introduced again to new sterilin tubes within a fresh 25 ml of PBS.

7.2.3 Perfusion Bioreactor System

A multi-channel perfusion bioreactor was designed, engineered and constructed to study the seeded cells-scaffold complex within dynamic conditions aiming to mimic the fluid flow environment of the human body more closely than a static system.

The perfusion bioreactor was made of plastic resin cylinders (chambers) (2.5 cm x 5cm) which were sterilisable in autoclave and permitting for its contents to be visualised as they are partially transparent. These bioreactor cylinders have two holes, the bottom hole and the top hole within the screw cap. The top screw cap is provided with O ring to secure the bioreactor cap tightly. Each chamber was loaded with three vertically lined up three (6.5 mm diameter 0.4µm pore size) polyester trans-wells inserts (Corning, USA). Each

trans-well in the chamber was loaded with same type of scaffold. Culture medium passed through the chamber at the rate of 1.25 ml/ min from its lower inlet hole, passed through the scaffolds and exited at the tops screw hole. Scaffolds in the trans-wells were surrounded with sterilised glass beads (Polyscience Inc., USA) to increase the culture flow through the scaffolds.

The complete flow system was composed of five chambers, held in metal racks, resembling the five different scaffold groups. Culture media flow passed in and out the system through a group of autoclavable accessories:

1- Heat resistant PharMed BPT tubing (1/4″ outer and 1/8″ inner diameter) (Sigma Aldrich, UK).

2- Connectors

3- Two glass multi-channels flow distributor (Ebers, Spain).

4- PharMed BPT tubes (1/8″ outer and 3/16″ inner diameter) (Sigma Aldrich, UK).

Osteogenic medium; the culture media, was prepared as the previous work (de Girolamo et al., 2007) by using a low glucose Dulbecco's modified eagle medium (DMEM), supplemented with fetal bovine serum, penicillin/streptomycin 1%, dexamethasone (0.1 μM), ascorbic acid 2-phosphate (0.2 mM), and glycerol 2-phosphate (10 mM; the last three reagents were procured from Sigma–Aldrich, UK). This medium was pumped from a 500-ml common reservoir through the system via a peristaltic pump (Watson Marlow, UK). The pressure force of the peristaltic pump drove the

culture media from the common reservoir to the main feeding tube (PharMed BPT tubing 1/4″ outer and 1/8″ inner diameter) that was connected to the first multi-channels flow distributor which was connected to the bioreactor chamber via sterilisable tubes (PharMed BPT tubes 1/8″ outer and 3/16″ inner diameter). The main function of the glass distributor is to dispense the osteogenic media through and out the bioreactors chambers evenly. Then, the medium was pushed out by the peristaltic pressure action. After exiting from the outlet, the culture media passed through the second multi-channels distributor to be delivered back to the common reservoir (Figure 7.2)

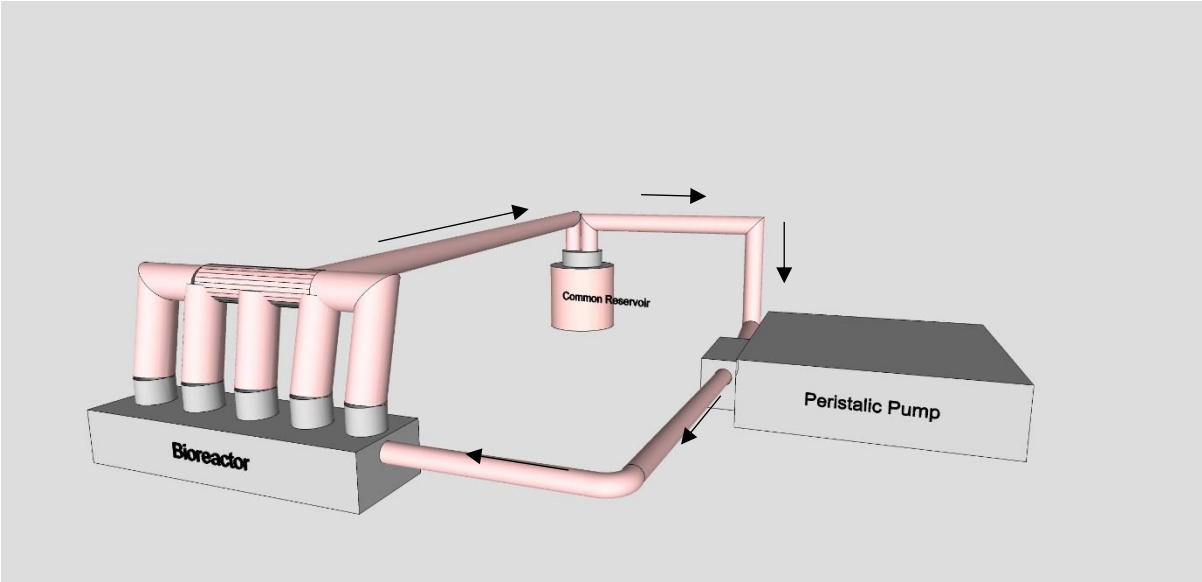

Figure 7-2 Schematic diagram explaining the different parts of the perfusion bioreactor (common reservoir, peristallic pump and the bioreactor chambers) and the culture media flow direction that is notated by the arrows. This diagram was drawn by using Sketchup software

The common reservoir was secured tightly with three holes Duran Cap (Eber, Spain), one hole for the medium outlet, one for the medium inlet and the last one for the gas and the oxygen perfusion through the system via 0.2 um

filter. The culture media was changed on a weekly basis. The whole system was incubated for 28 days at 37°C/ 5% CO_2 as shown in (Figure 7.3).

Figure 7-3 perfusion bioreactor

7.2.4 Cell culture studies

7.2.4.1 Cells preparation

Human mesenchymal stem cells (hMSCs) were prepared following the procedure explained in (4.2.6.1).

7.2.4.2 Cell Seeding

Triplicate of each of the five prepared scaffolds (5 mm x 5 mm) groups were seeded within hMSCs in two separated 24-well plates (Corning, USA). Primarily, the prepared scaffolds were sterilised via immersion in ethanol for 1 minute then under UV light for 20 minutes.

The sterilised uncoated glass scaffolds and Bio Oss scaffolds were coated with 1 $mg.ml^{-1}$ of collagen to improve the cell attachment following the procedure previously stated in (6.2.3.2).

Human mesenchymal stem cells were seeded at different seeding densities depending on the study; 25000 cells/scaffold for the DNA study and 100000 cells/scaffolds for the mineralisation study. The seeded cells were prepared in 30 µl of culture media that was pipetted out around all the scaffold sides to ensure even distribution of the hMSCs through the scaffold microstructure. Then, the hMSCs cultured scaffolds were left for half an hour in the incubator to provide enough time for the cells to attach to the scaffold structure prior to adding 1 ml of osteogenic media for one day. On the next day, the cells of one of the plates were transferred into 6.5 mm trans-well and then to the bioreactor chambers to be assessed within dynamic conditions for 28 days, whereas the seeded scaffolds in the other plate were incubated at 37°C/ 5% CO_2 to be assessed within static conditions, also for 28 days. The osteogenic medium for the static group was changed every three days.

7.2.4.3 DNA Assessment

DNA quantification assay of the hMSCs was carried out within static conditions to primarily assess the cellular proliferative response to the scaffolds materials. This study was performed at two time-points (day 7 and day 14) by using triplicate of seeded scaffolds at an initial density of 25000 cells / scaffold. The culture media used in this study was α-MEM.

At each time point, DNA purification was carried out by using QIAamp® DNA Mini kit (Qiagen). The first step of the purification was to detach the cells by immersing the cylindrical scaffolds in 750 µl of trypsin for 5 minutes at 37^{o}C. Then, the trypsin was deactivated by adding 750µl of culture media. This

solution was then centrifuged and then DNA was purified from the centrifuged samples following the steps described previously in (5.2.7.3). The next step was the DNA quantification performed using Quant-iT™ PicoGreen™ dsDNA Assay Kit (Fischer) following the kit steps as explained in (5.2.7.3).

7.2.4.4 Mineralisation (Ca) Assay

Calcium assay was carried out within both static and dynamic environments. The hMScs were seeded at a density of 100000 cells/discs for 28 days. On day 28, two scaffolds of each group were removed from their container (well-plate or trans-well), washed twice with phosphate buffered saline PBS (Lonza, USA) and then agitated by a shaker for 40 minutes adding 1 ml of HCL to it to aid in the cell lysis. After the lysis step, triplicates of 5 ul of each of the scaffolds lysis liquid was transferred to 96 well-plate and about 200 ul of the prepared Ca working agent was added to each triplicate. Calcium concentration measurement were then determined following the steps described previously in (4.2.6.4).

Another two cell-free samples of each of the compositions were analysed individually to deduce the calcium concentration released from the scaffolds individually and to offset this number from that measured on the samples with cells.

7.2.4.5 Scanning Electron Microscope (SEM) Images

SEM images were taken to each sample on day 28. All scaffolds were removed from culture media then washed with PBS (Lonza, USA). The cells

were then fixed, and the scaffolds were coated prior to finally imaging them following the steps prescribed previously in (4.2.6.6).

7.2.5 Statistical Analysis

All the data apart from the degradation rate were statistically analysed using one-way ANOVA and Kruskal Wallis according to the data normality. Statistical analysis was performed to test the null hypothesis regarding both the scaffolds manufacturing and the cell osteodifferentiation response within different culture conditions; static and dynamic.

Concerning the scaffold manufacturing, the null hypothesis stated that there is no structural and mechanical difference between the various produced prepared scaffolds; the coated and the uncoated ones, and the Bio-Oss scaffolds.

Whereas for the cellular studies, the null hypothesis stated that there is no statistical difference of the osteodifferentiation ability of cells cultured on scaffolds within both static and dynamic conditions.

7.3 Results

7.3.1 Scaffold porosity

Figure 7.4 displays the scaffold porosity percentage of the different prepared scaffolds groups. Data showed that the Bio-Oss scaffold is the most porous 84.6 ± 3.1%. Concerning the remaining groups, the recorded porosity was ranging between 42.8 to 51 % with no statistical difference between them. The only statistical difference was found between the higher porosity Bio-Oss and the other lower porosity scaffolds ($P<0.05$).

Figure 7.5 presents the CT scan images of each of the scaffold groups and clearly confirming the statistical significance between the Bio-Oss and the other scaffold groups.

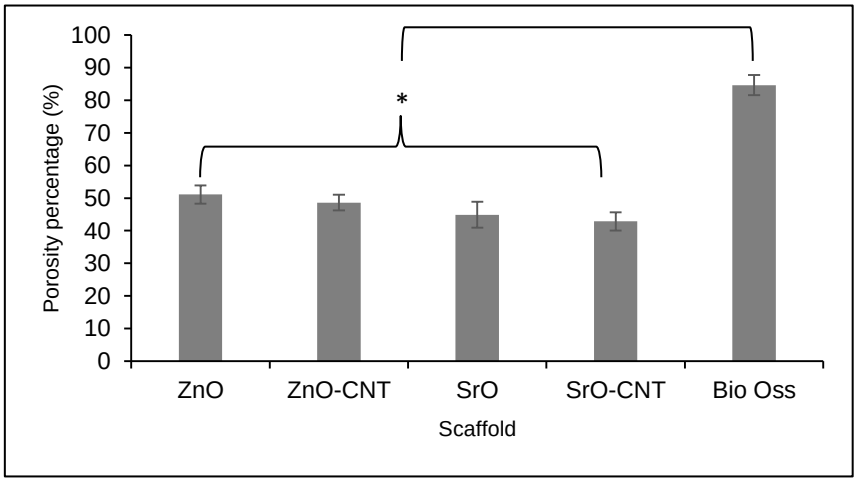

Figure 7-4 porosity percentage of different scaffolds displaying that BioOss is the highest porous material.

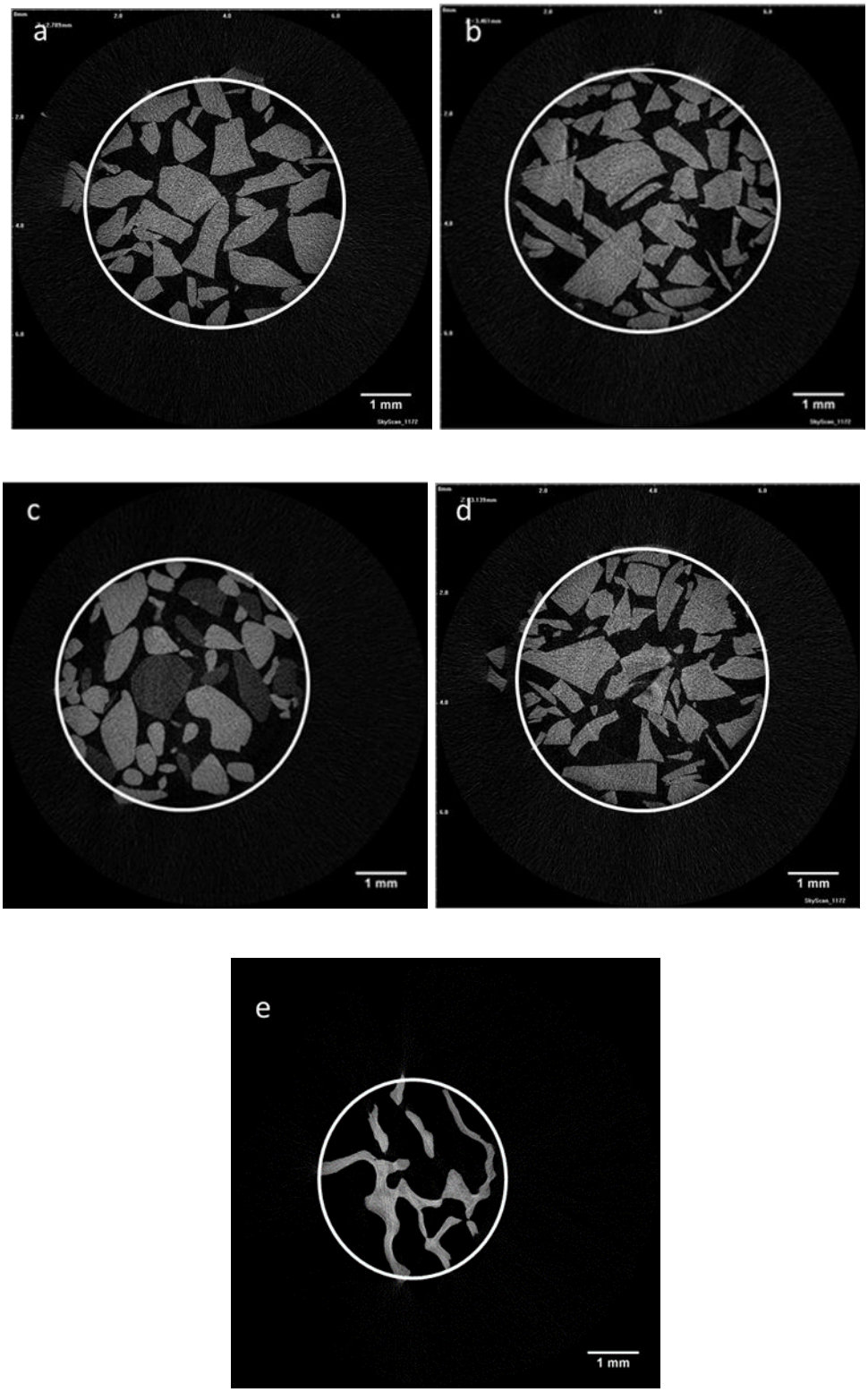

Figure 7-5 CT-cross sections of different scaffolds a. ZnO, b. ZnO-CNT, c. SrO, d. SrO-CNT and e. BioOss

7.3.2 Diametral compressive strength

Diametral compressive strength data of the five tested scaffold groups are displayed in figure 7.6. The findings revealed that the CNT coated SrO scaffolds had the highest diametral compressive strength at 1.6 ± 0.15 MPa followed by the free coating SrO; both were statistically significant from the other groups ($P<0.05$). The Bio-Oss scaffolds were in the third place at about 0.6 ± 0.06 MPa. The coated ZnO and the uncoated ZnO scaffolds were in the fourth and the last place respectively at around 0.3 MPa. Although coating scaffolds with PCL-CNT coating seemed to enhance the scaffold strength, this increase did not seem to be statistically significant ($p>0.05$).

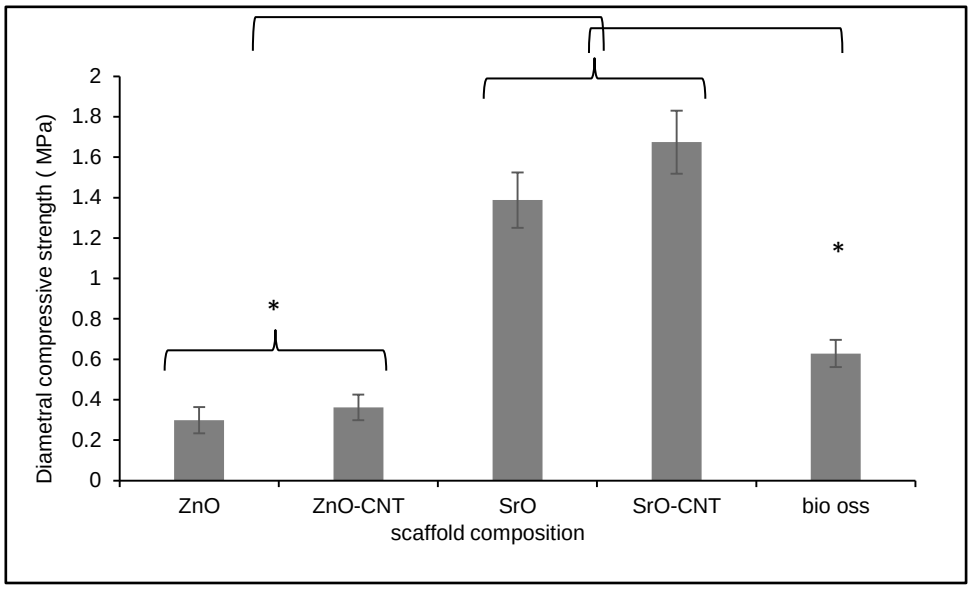

Figure 7-6 Diametral compressive strength for all the tested scaffolds, showing that strontium coated scaffolds had the highest strength among the other prepared scaffolds.

7.3.3 Degradation study (mass loss)

Percentage Mass loss of the scaffolds within dynamic conditions is presented in (Figure 7.7). Generally, the uncoated zinc scaffolds (ZnO) showed the highest rate of mass loss during the whole study period. In the first month, the mass loss of ZnO represented around 8.8±1.8% of the original scaffold weight which was around double the mass loss percentage of the other scaffolds. This pattern continued in the second month where all the scaffold lost around the same lost mass percentage as the first month. In the third month, ZnO scaffolds lost about 22 ± 2.6% of their original weight followed by the strontium scaffold (SrO) which lost around half that of the ZnO; 13±1.5%. The other groups displayed similar mass degradation percentage; 8-11%.

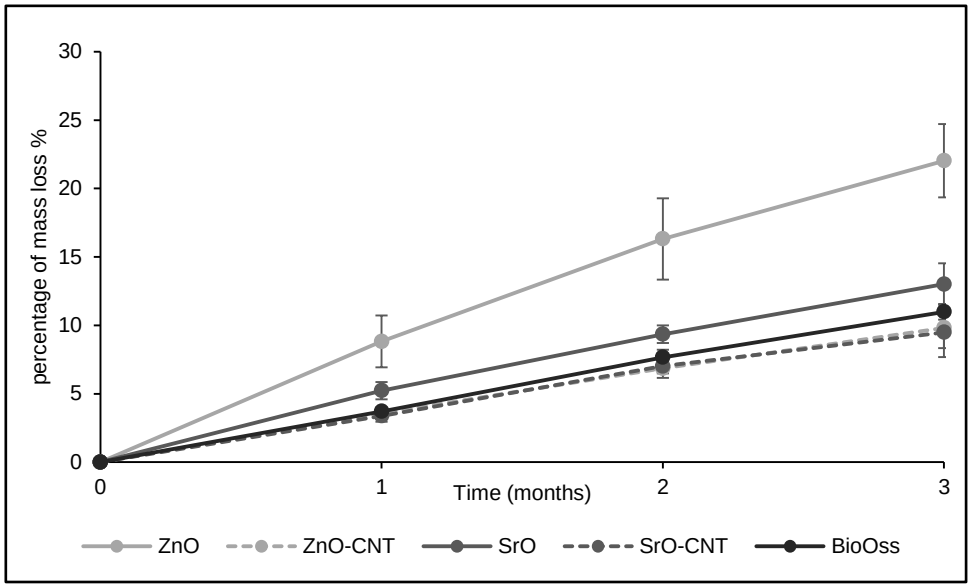

Figure 7-7 Percentage of mass loss under dynamic condition showing that ZnO uncoated scaffolds had the highest degradation percentage in relating to the other groups

Degradation within static conditions had a similar trend to that of the dynamic conditions (Figure 7.8). The zinc uncoated sample exhibited the highest mass loss rate in comparison with the other groups in which they lost about 4±0.6% of their initial mass after 1 month. This increased continuously to reach 11±0.6% at the end of the study. The SrO uncoated scaffolds were in the second place regarding the percentage of their weight loss and was slightly less than that of the ZnO at around 7.2 ±1.4% on the last day. This was followed by the Bio-Oss scaffolds whose loss in percentage mass was around half that of the ZnO over the whole study period. The CNT coated scaffolds were in the last place in which they lost percentage mass of around 1.2% per month.

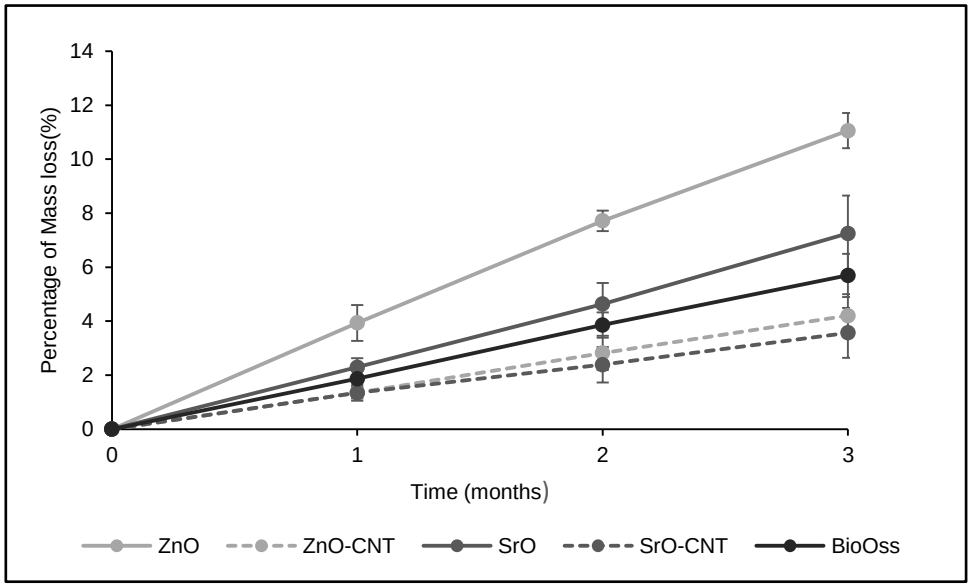

Figure 7-8 Percentage of mass loss under static condition showing that ZnO non-coated scaffolds had the highest degradation percentage in relating to the other groups

Other interesting findings is that all scaffolds lost double the mass within dynamic conditions in compare to the static conditions during the whole experiment.

7.3.4 DNA assessment

DNA concentration quantification results are shown in (Figure 7.9). The general trend obtained from the DNA study explained that all groups did not have statistical variation among them regarding their cellular DNA content. On day 7, both the CNT coated glass scaffolds showed the highest mean of DNA concentration which was around 70000 pg/ml, this was followed by the Bio-Oss and the uncoated scaffolds. A similar trend was found on day 14 where the trend was the CNT coated scaffolds> the Bio Oss> the uncoated scaffolds. On day 14, high DNA contents were detected in the CNT coated scaffolds (around 240000 pg/ml) this followed by the Bio-Oss (around 198000 pg/ml) and finally the coated scaffolds (around 150000 pg/ml).

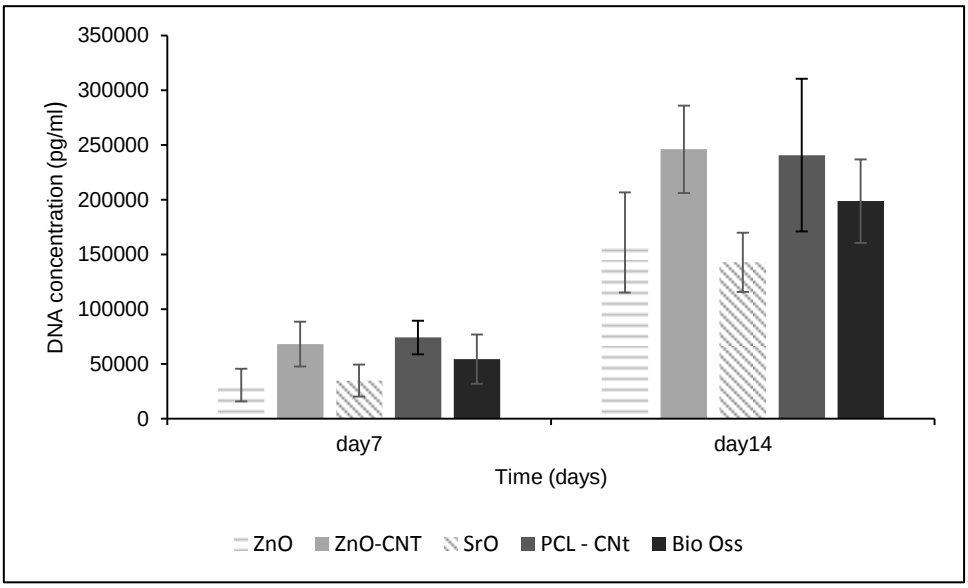

Figure 7-9 DNA concentration measured by pg/ml for the tested scaffolds (CNT-coated glass scaffolds, uncoated glass scaffolds and Bio Oss) after one week and two-week periods.

7.3.5 Mineralisation assay (Ca assay)

Figure 7.10 displays the Ca assay results for the scaffolds cultured within both static and dynamic conditions on day 28. The general summary of the results revealed that the cells seeded within the dynamic conditions (bioreactor) had higher concentration of calcium in comparison to the cells within the static conditions.

Regarding the dynamic conditions group, the cells seeded on the Bio-Oss scaffolds showed the highest Ca concentration which was about 29.7 ±3.1 µg followed by the CNT coated zinc and strontium scaffolds at around 24.7-26.3 µg and finally the uncoated scaffolds exhibited the lowest amounts of calcium at around 18 µg.

The calcium pattern within the static conditions followed the same features similar to the dynamic conditions. The highest calcium concentration was detected in the Bio-Oss groups (19.7 ± 1.8 µg) which was higher than the CNT coated scaffolds at around (16 µg). The uncoated scaffolds revealed the lowest calcium concentration at around (11.7-12.6 µg).

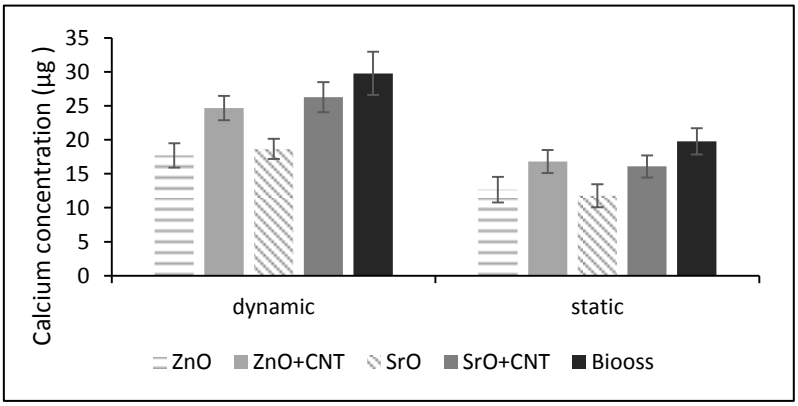

Figure 7-10 Ca concentration under static and dynamic conditions revealing that more calcium was released under dynamic conditions

7.3.6 SEM imaging

Figure 7.11 presents the hMSCs seeded on different scaffolds and cultured within both static and dynamic conditions on day 28. The images were taken at different magnifications. Generally, it appeared that the cells cultured within dynamic conditions exhibited higher levels of proliferation. Figure (Ai) displays the hMSCs and BioOss scaffold complex.

Figure (Bi) shows the cells seeded on the uncoated strontium glass scaffolds cultured under static conditions. The cells were attached to the glass surface by their appendages following the irregularity on the scaffold surface platform. Similarly, the cells looked to be attached to other samples of uncoated glass scaffolds cultured under static conditions (figure Bii), but with lower cell densities than that of dynamic cultured scaffolds. It is worth mentioning that the glass degradation was clearly noted through the presence of cracks and indentations on the glass surface.

The cells cultivated on the PCL-CNT coated strontium glass scaffolds within both static and dynamic conditions (figures Ci and Cii respectively) showed a similar trend in their results to that of the BioOSS and uncoated samples where cells within the dynamic culture had higher density than the static cultured cells. Furthermore, it can be noticed that the presence of the coating polymer layer with CNT on scaffolds confirmed the retention of this layer even within the dynamic flow of the culture media.

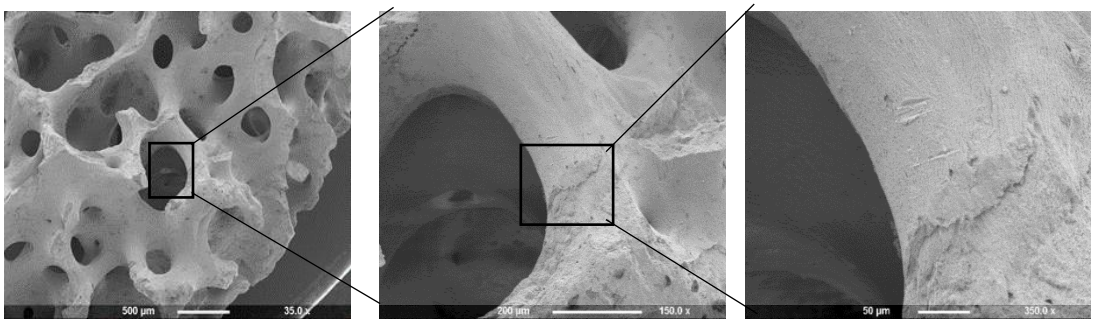
500 µm
35.0 x
200 µm
150.0 x
50 µm
350.0 x

(Ai

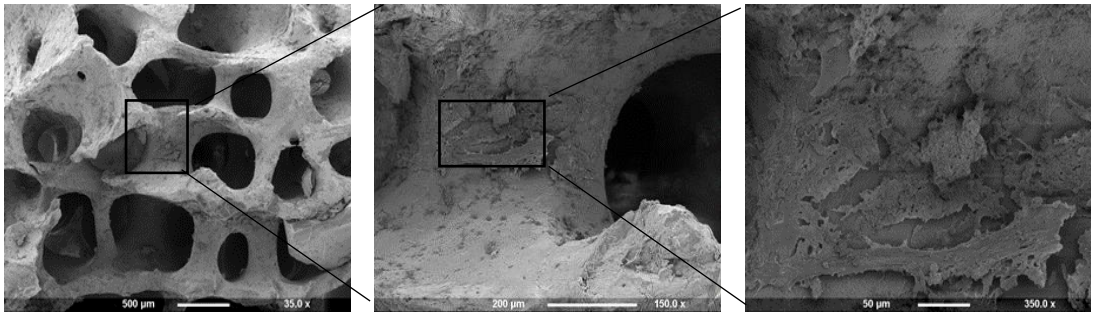
500 µm
35.0 x
200 µm
150.0 x
50 µm
350.0 x

(Aii)

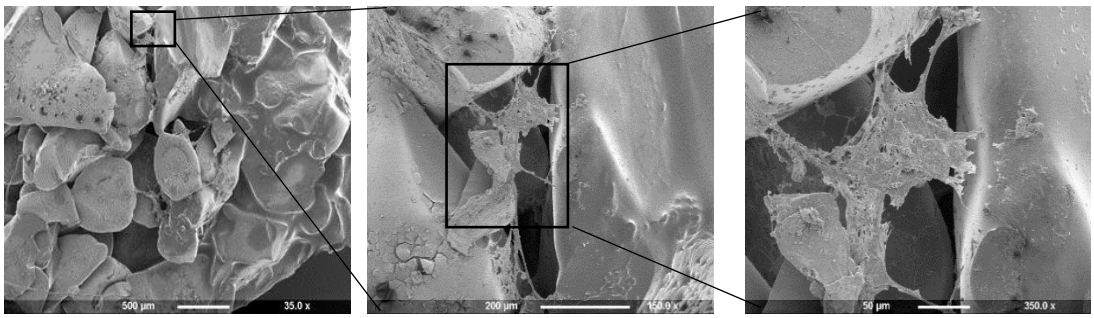
500 µm
35.0 x
200 µm
150.0 x
50 µm
350.0 x

(Bi)

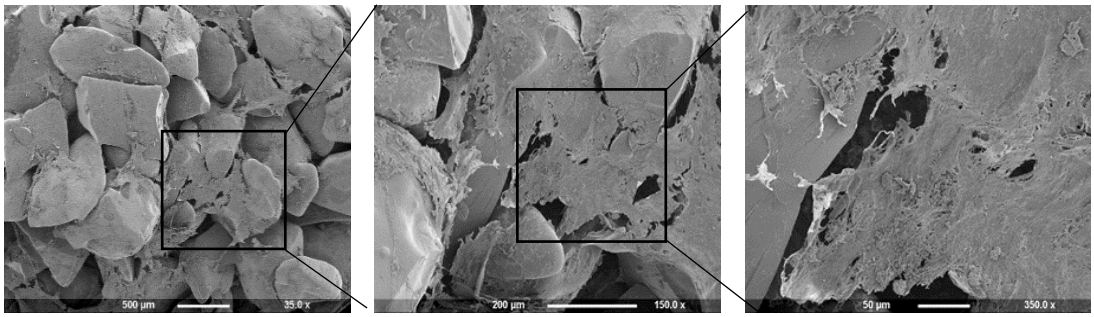

(Bii)

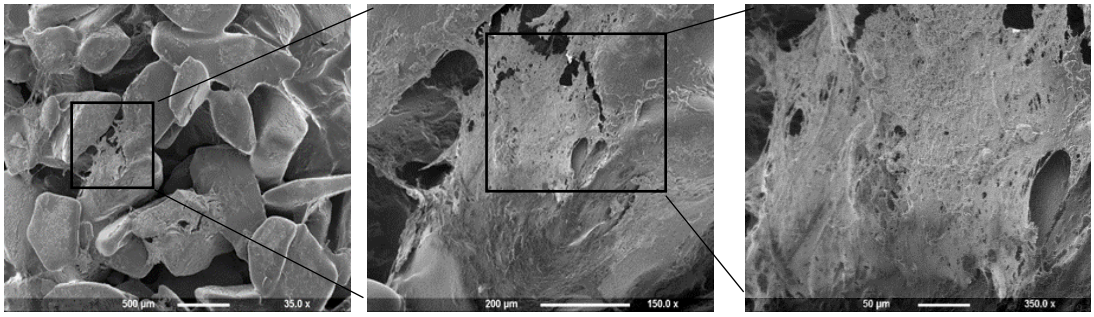

(Ci)

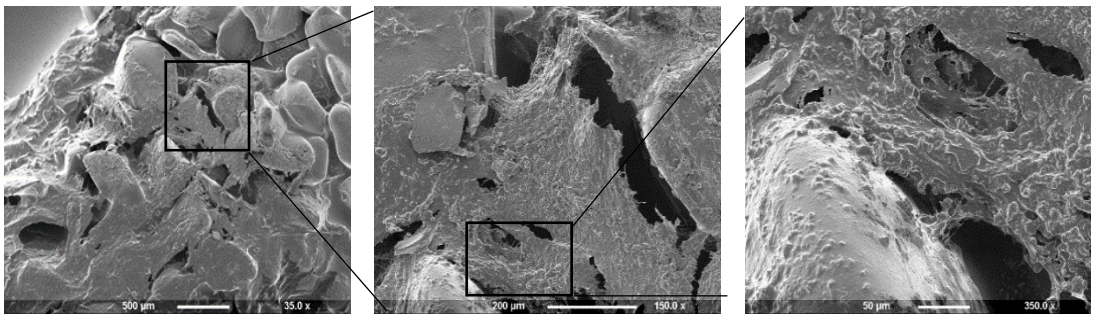

(Cii)

Figure 7-11 SEM showing cells cultured under static and dynamic conditions. (Ai) BioOss scaffolds under static conditions, (Aii) BioOss scaffolds under dynamic conditions, (Bi) uncoated strontium glass scaffolds under static conditions, (Bii) uncoated strontium glass scaffolds under dynamic conditions, (Ci) PCL-CNT coated strontium glass scaffolds under static conditions, (Cii) PCL-CNT strontium coated glass scaffolds under dynamic condition

7.4 Discussion

The main aim of this chapter was to produce glass scaffolds in light of the results of the previous chapters and study them within dynamic conditions to mimic more closely, the normal physiological condition in the human body.

Although the zinc (ZnO5) and the strontium (SrO17.5) glass scaffolds were prepared successfully by sintering technique in the previous chapter, the produced scaffolds did not possess acceptable mechanical properties. Therefore, the preliminary effort was to promote scaffolds' strength by coating them with PCL-CNT layer. PCL (polycaprolactone) polymer was chosen because it can be considered as a good candidate for such application due to both its low degradation rate and potential for long-term implant applications (Ma, 2004). Carbon nanotubes were added also to the polymer coating layer because of their potential to improve the strength of scaffolds used for bone repair applications (Cheng et al., 2013). The Bio-Oss scaffolds were used as control groups due to its clinical applicability and biocompatibility as well as their high success rates (Mordenfeld et al., 2016). The first step following sample manufacturing coating procedure was to assess the morphological and the mechanical characteristics of both the PCL-CNT coated scaffolds and the uncoated scaffolds.

Regarding their porosity, the findings showed that the Bio-Oss samples were superior in their porosity and pores sizes in compare with the other glass scaffold samples. Although coating scaffolds with CNT-PCL decreased the porosity of scaffolds, this decline in porosity did not affect the overall porosity

significantly which remained within the acceptable values required for bone repair applications.

The diametral compressive strength was used to examine all the scaffolds as it is the most suitable test for such brittle materials (Sakaguchi and Powers, 2012). The highest tensile strength was uniformly directed through the central portion of the diametrical plane of the specimens. This yielded in breaking the sample into two similar pieces. The main significant results were related to the coated samples of which their mechanical properties were slightly enhanced for the strontium (1.67 MPa) and for the zinc (0.36 MPa) in compare to the uncoated samples (1.38 MPa for the strontium and about 0.29 for the zinc). This enhancement in the mechanical properties could be correlated to the coating layer of both the PCL and the CNT. The PCL was suggested to promote scaffolds and materials mechanically reducing their brittleness due to its binding effect (Zhang et al., 2014). Whereas adding the CNT incrementally was proven previously to promote the mechanical properties of scaffolds (Gonçalves et al., 2016). The strontium coated scaffolds displayed promising results concerning the scaffold strength as it was slightly higher than the Bio-Oss group (0.7 MPa) and comparably better than the zinc scaffolds. There is a lack of information in the literature about the diametral compression strength of cancellous (trabecular) bone and hence the only information used as a reference was related to the compressive strength of cancellous bone which stated that the cancellous bone compressive strength is between 2-20MPa (Jones et al., 2010, Zheng

et al., 2014). Although the diametral compression strength is not comparable to the compression strength due to the difference in the geometry, the compressive strength was used as a reference to provide an idea about the mechanical property of the scaffold. The degradation results revealed that there was a gradual mass loss during time for all the samples within both the static and the dynamic conditions. Within both conditions, the pattern of mass release was as follows: (ZnO > SrO > BioOss > ZnO-CNT and SrO-CNT). This could be interpreted by relating this to the difference between the ionic bonds strength of each group. In the glass network, the zinc and the strontium combine usually with the oxygen via ionic bonds. However, the variation in these ionic bonds strength can be linked to the strength of the whole glass system. The dissociation energy of the Zn-O bond is (284 Kj. mol^{-1}) which is weaker than that of the Sr-O bond (454 $Kj.mol^{-1}$). Hence, the glass group containing zinc seemed to be more susceptible to hydrolysis because of its weak bond strength. These results were compatible with the findings in the previous chapters which can also be emphasised by the differential thermal analysis where T_g of the glass was 452 °C and 475 °C for both the zinc and the strontium respectively. Though, coating glass discs with CNT-PCL layer changed the whole concept in which the glass degradation was governed by the coating layer and not by the glass composition. This could be due to the effect of the PCL layer which protected the scaffold degradation as the PCL polymers are hydrophobic polymers as well as having high molecular weights (Sung et al., 2004). These results were parallel to other study findings that found that the pure PCL construct's

degradation was much lower than the PCL/ phosphate glass complex, and correlated this increase of degradation rate to the incorporation of the glass within the polymer (Kim et al., 2005b). This could be explained also due to the lower degradation rate of the PCL in compare to the phosphate glass (Onal et al., 2008). The results of the mass loss of the CNT-coated scaffolds were insignificantly different to that of the Bio-Oss.

The mass loss study was performed using both static and dynamic conditions to assess the effects of the dynamic fluid flow on the scaffold degradation. The dynamic motion was applied at orbital movements of 70 rpm following a previous study (Hedberg et al., 2005). The scaffolds mass degradation within the dynamic conditions was much higher than that of the static conditions. This clear variation in mass degradation findings was compatible with previous studies that suggested that the degradation was higher in scaffolds within mechanical and dynamic conditions (Yang et al., 2008b, Kang et al., 2009).

Following the scaffolds characterisation, an initial cell proliferation study was performed to determine the scaffold ability to affect stem cells and as well as assessing the effects of scaffold materials and microstructure on the cellular proliferative activity. The DNA concentration was used as an indirect way for cell proliferation assessment. The results after one and two weeks revealed that the highest DNA concentration was detected in the PCL-CNT coated samples being double that of the uncoated scaffolds. This could be due to the roughness resulting from the PCL -CNT coating layer that might improve

the cell attachment ability. This was in harmony with the previous results that correlate the surface roughness to the enhanced osteogenicity and the cellular proliferation (Boyan et al., 2017). These results supported the previous chapters' findings of the scaffold cytocompatibility.

The next step was to design the bioreactor aiming to assess the cytological osteodifferentiation response of the hMSCs cultivated on the prepared scaffolds for extended time duration as well as comparing these results to those within the static conditions.

Regarding the culture study within the dynamic conditions, a multichannel perfusion bioreactor was designed and installed to gain an advantage of allowing the oxygen and the nutrients to exchange, supplying cells in the deeper parts of the scaffolds and ensuring a more effective medium perfusion into the scaffold using spinner flasks and rotating wall bioreactors (Yeatts and Fisher, 2011). Furthermore, previous comparative study of different bioreactors designed for bone tissue engineering applications showed that the type of bioreactor did not have a clear effect on the osteodifferentiation of the stem cells but has an impact on the cell proliferation in which the perfusion bioreactors displayed a better cell growth than the other two types (Zhang et al., 2010). Moreover, there is a possibility for cells or scaffolds collisions because of the mechanical forces associated with the spinner and the rotating wall bioreactors.

To optimise the culture media flow rate through the bioreactor, calibration was performed prior to the experiment within the same working conditions

(the culture media fluid, the type of tubes, the type of the pump head, the pressure in the reactor). The flow rate was fixed on the rate of 1.25 ml/ minutes in line with the recommendation of previous studies (Bancroft et al., 2002, Zhao et al., 2016).

Scaffold seeding procedures were performed by using a high concentrated culture media to minimise the possibility of cells to escape away from the scaffolds. Furthermore, the uncoated glass scaffolds and the Bio-Oss scaffolds were coated by collagen type 1 prior to seeding to enhance their initial cellular attachment (Linsley et al., 2013).

Following the seeding procedure, scaffolds were transferred into trans-wells. These scaffolds were packed with sterilised glass beads to form a direct perfusion bioreactor by ensuring the tight sealing of the scaffold to the trans-well wall. The direct perfusion bioreactors displayed preferable results regarding the cellular viability and the cytogenic marker expression in comparison with the indirect types. This may be related to the enhanced shear strength inside the scaffold complex associated with the direct type (Rauh et al., 2011). The whole system parameters were controlled by using the incubator at 37°C/ 5 % CO_2.

The mineralisation study results of the different scaffold groups after 4 weeks within both the dynamic and the static conditions revealed that the highest mineralisation activity was seen in the Bio-Oss scaffolds followed by the CNT coated glass scaffolds (ZnO-CNT and SrO-CNT) and finally the coating free glass scaffolds (ZnO and SrO). The high calcium concentration

in the Bio-Oss samples could be related to the positive effect of the Bio-Oss in enhancing the expression of calcium related bone morphogenic proteins such as osteocalcin and Receptor Activator of Nuclear Factor κ B (RANK) (Tapety et al., 2004, Chaves et al., 2012). The CNT-coated scaffolds displayed promising results of Ca concentration in comparison to the Bio-Oss which was higher by 20% than the uncoated samples. This could be due to the high cell proliferation that is correlated with the roughness of the coating layer. This increase in cell number may subsequently lead to the increase of the released calcium. Also it could be related to the effect of the CNT which may enhance the calcium ion concentration that was found previously (Newman et al., 2015).

Other interesting findings that should be mentioned is that the calcium ions concentration within the dynamic conditions was much higher than that within the static conditions. These findings were previously stated in other studies where the mineralisation was enhanced, and the proteins were more highly expressed by mechanically stimulated cells via perfusion bioreactors and not with the normal static normal conditions (Bancroft et al., 2002, Porter et al., 2007, Jagodzinski et al., 2008, Kleinhans et al., 2015).

The SEM images confirmed most of the cellular study results where the cells displayed more proliferative activity within dynamic conditions in comparison to the static conditions. This was significant as it showed the ability of the cells to align in multi overlapped layers in some parts of the scaffold and the

ability to produce a larger cellular layer extending and covering the scaffold pores.

In conclusion, the CNT coated scaffolds were developed successfully and assessed by the cellular studies within both static and dynamic conditions. The findings revealed that the CNT coated scaffolds can show promising results to be used as biomaterial for bone tissue repair when the CNT contents in the coating does not exceed 25ug/ml. The CNT-PCL coating layer improved the scaffold mechanical properties. Moreover, seeding the mesenchymal stem cells in the scaffolds within dynamic conditions can promote mineralisation and osteodifferentiation in comparison to the static conditions. The cellular studies' results of the CNT coated scaffolds did not reveal a significant difference from the Bio-Oss scaffolds. The strontium glass scaffolds are more favourable to be used as scaffolds because they showed better mechanical properties than that of the zinc contained scaffolds enabling them to support the intended bone growth process. According to these results the null hypothesis was rejected in some points related to the scaffold and the Bio-Oss porosity whereas it was accepted concerning the mechanical and the biological properties of the phosphate-based scaffolds constructs. Furthermore, the null hypothesis was rejected also concerning the difference between the culture media conditions in which there was more osteodifferentiation related response in the cells cultivated within dynamic conditions than that in the static conditions.

Further studies are required to be performed to manufacture strontium containing phosphate-based glasses with better mechanical characteristics accompanied with further experiments within dynamic conditions and for a longer time. *In vivo* studies on animals may be needed in the future to study the effect of strontium glass scaffolds implantation on animals' bone growth.

Chapter 8 Conclusions and Future Work Suggestions

8.1 Conclusion

The work carried out in this thesis aimed to use phosphate-based glasses as a biomaterial for craniofacial bone defects repair applications. The work was performed on a hierarchical basis starting from the basic studies performed on glass discs and reaching the manufacturing of phosphate glass scaffolds that were seeded and cultured within dynamic conditions by using custom made multi-channel perfusion bioreactors.

Overall, there are six studies performed aiming to produce phosphate-based glass scaffolds for craniofacial bone tissue repair applications. The first and second studies examined four different compositions of both strontium and zinc phosphate glass discs respectively to obtain a primary idea about the physical, chemical and biological properties of the different glass formulations and to analyse the cellular response of these compositions. The following step (the third study) of this thesis aimed to use the best two compositions of the strontium and the zinc based glass compositions from the preliminary glass discs studies (the first and the second steps) to develop the glass in a more clinically useful form; glass beads.

The next phase (the fourth study) was designed to topographically modify the smooth glass discs surfaces by using the polycaprolactone (PCL)- CNT coating layer. This experiment intended to add roughness to glass discs'

surfaces and examine both the cellular attachment and the metabolic properties. Following this, another study (the fifth study) was performed to produce porous scaffolds depending on the glass compositions obtained from the glass beads study. This study used sintered glass powders of specific size for scaffold manufacturing. This study concluded the optimal scaffold sintering temperatures as well as confirmed the effect of various temperature values on both the mechanical and the morphological properties.

The final study (the sixth study) was to collect and use all the findings of the previous studies to manufacture phosphate glass scaffolds. In other words, it used the best compositions of strontium and zinc glasses obtained from the third study (the glass beads study) and combined them with the PCL – CNT coating layer taking into account the results of the fourth study. The sintering temperature data of the fifth study was adopted to produce these scaffolds. The outcome was producing sintered strontium and zinc glass scaffolds that were coated with PCL-CNT coating layer. Those prepared scaffolds were further analysed mechanically, morphologically and biologically. The next phase of this study was to design and manufacture a custom-made perfusion bioreactor to be used as a source of mechanical stimulus (dynamic conditions) to mimic the normal physiological *in vivo* conditions. This experiment compared the cellular osteodifferentiation activity within both dynamic and static conditions.

The first and second studies were preliminary studies to test both strontium and zinc containing glasses respectively in which different compositions of glass discs were prepared depending on previous studies. Regarding the strontium phosphate glass discs study (the first experiment), four different compositions of glass discs were prepared in which strontium oxides replaced calcium oxides within the glass network at different proportions (SrO0%, SrO1%, SrO17.5%, SrO35%). These formulations were prepared depending on previous studies that investigated specific formulations (Gentleman et al., 2010). The physical, chemical and biological aspects of all the prepared glass discs were assessed to find out the general effect of ion substitution on glass properties. The most significant results showed that an incorporation of strontium oxides ions in favour of calcium oxides ions in glass formulation might upregulate both glass degradation and ion release. These results were confirmed by the differential thermal analysis which emphasised that adding strontium to the glass structure in favour of calcium may have a negative effect on the glass network integrity. The cellular related outcomes showed that adding strontium to the glass network might enhance both the metabolic and the proliferative cellular responses. Though, the most significant effect was found in SrO 17.5 (50 P_2O_5 - 10Na_2O - 5TiO_2 – 17.5CaO –17.5SrO) and ZnO 35 (50 P_2O_5 - 10Na_2O - 5TiO_2 – 0 CaO –35 SrO). Both formulations were considered for further assessment.

Regarding the second study which was focused on zinc phosphate glasses, four different compositions of glass discs were prepared in which zinc oxides

substitute calcium oxides within the glass network at different proportions (ZnO0%, ZnO5%, ZnO10%, ZnO10%). These formulations were prepared depending on previous studies that investigated specific formulations (Salih et al., 2007). Different glass disc formulations were assessed physically, chemically and biologically. The findings showed that adding zinc to the glass formulation instead of calcium may have a negative effect on some of the physical properties. This was confirmed also in differential thermal analysis studies. Furthermore, the incorporation of zinc oxide may enhance glass degradation in aqueous media which will consequently lead to enhanced levels of different ions release into the immersing liquid. One of these ions is the zinc which was found to have unfavourable cellular responses outcomes in case of presenting in a high concentration. These outcomes were clearly identified in the high zinc content formulations ZnO15 (50 P_2O_5 - 10Na_2O - 5TiO_2 - 20CaO -15ZnO) and were compatible with previous related results (Abou Neel et al., 2008c). This study recommended that ZnO5 and ZnO10 showed acceptable results that are needed to be assessed further.

The third study intended to produce phosphate glasses in forms that are more clinically relevant as a step forward towards scaffold manufacturing. Hence, phosphate glass was produced in the form of glass beads rather than glass discs. Glass bead formulations were produced in four different compositions based on the first and the second studies which were SrO 17.5%, SrO 35%, ZnO5% and ZnO10%. The main aim of this study was to examine the cellular response to spherical formed glasses and to determine

the most suitable strontium and zinc phosphate glass composition that might be used in bone tissue engineering applications. Therefore, degradation and ion release studies were performed initially followed by biological related assays. The studies confirmed the previous findings of the first and the second studies that clarified the link between the incorporation of metal ions in the glass and the mass degradation and the ion release rates. The results also highlighted that the zinc-based glass beads had a higher degradation rate than the strontium glass beads. The metabolism and the osteodifferentiation related studies suggested that the glass beads with less degradation resulted in better cellular results. The outcome of the glass bead study offered more information about the most suitable strontium and zinc containing phosphate-based glasses that were considered for the succeeding studies. These formulations were (50 P_2O_5 - 10Na_2O - 5TiO_2 – 17.5CaO –17.5SrO) and (50 P_2O_5 - 10Na_2O - 5TiO_2 – 30CaO –5ZnO).

The fourth study was implemented to determine and examine the biological effects of coating glass discs with specific coating materials (polycaprolactone (PCL)+ carbon nanotube (CNT)) that are known to enhance bone growth (Boyan et al., 2017). The aim of this coating procedure was to modify the smooth surface of glass discs that may help in cell attachment promotion. Initially, the strontium (SrO17.5) and the zinc (ZnO5) glass discs were prepared prior to coating them with PCL and CNT layer. Then the coated glass discs were assessed in terms of roughness and contact angle studies before being analysed for their cellular impacts. The

roughness and the contact angle studies revealed that both the roughness and the hydrophilicity were increased with coating. The cellular results showed that coating provoked cell attachment and did not exhibit any signs of cytotoxicity. The findings were promising concerning the cellular response to the coating layer and displayed a positive role of both PCL and CNT in enhancing the cellular attachment and proliferation.

The fifth study intended to manufacture zinc (ZnO5) and strontium (SrO17.5) glass scaffolds using the glass formulations determined in the glass bead study (the third study). Glass scaffolds were manufactured by sintering technique. To optimise sintering procedure, three different glass temperatures were used for both strontium and zinc glass compositions. The applied different sintering temperatures were assigned based on the glass transition temperature that was determined in the first and the second studies. To find the optimum sintering temperature for strontium and zinc individually, mechanical and morphological assessments for all the produced scaffolds were performed. The results suggested that increasing the sintering temperature is directly correlated with enhancing the scaffold strength and was indirectly correlated with the scaffold porosity; the main morphological scaffold properties. These results were compatible with previously determined findings (Jones et al., 2010).

Following the sintering temperature optimisation, cell seeding optimisation was performed. This was done because the scaffolds are porous constructs and there is a possibility for cells to flow away from the scaffold due to the

culture media flow. For this reason, different techniques were used for seeding optimisation by seeding in different types of well plates and coating the produced sintered scaffolds with different proteins such as fibronectin and collagen which are known for their ability to enhance cell attachment and cell metabolism (Linsley et al., 2013). The outcome of the seeding optimisation showed that both the cell attachment and the metabolic activity was enhanced by coating with collagen and fibronectin. These results support the potential of coating scaffolds specifically with collagen.

The last study (the sixth study) was intended to produce individual strontium and zinc containing phosphate glass scaffolds using all the findings of the previous experiments. The optimal percentages of both strontium and zinc were 17.5 mol% and 5 mol% respectively. These percentages provided the most acceptable cellular responses. The scaffolds were produced by using specific sintering temperatures which were 475°C and 485°C for the zinc and the strontium glasses respectively based on the sintering optimisation study (the fifth study). The produced scaffolds were further coated following the results of the coating study (fourth study). Initially, studies were performed to assess the effect of coating on the mechanical and the morphological properties of the scaffold. These studies aimed to determine if the mechanical strength of scaffolds was promoted and whether the scaffold porosity was significantly affected by the coating procedures. The findings related to the mechanical strength revealed that strength was enhanced after coating. Though, this rise in scaffold strength was not

significantly different from the uncoated scaffolds. This increase was probably correlated to both PCL polymer and CNT components of the coating layer. However, the zinc phosphate scaffolds attained lower strength compared to the strontium based scaffolds. The morphological related findings revealed that coating scaffolds with PCL-CNT layer did not have a clear impact on the glass scaffold porosity. Hence, PCL-CNT coated scaffolds were used for further cellular studies. The first study was performed within static conditions of which the cellular proliferation ability was analysed by the quantification of DNA concentration of the cultivated hMSCs on different scaffolds including the PCL-CNT coated scaffolds with the Bio-Oss scaffolds used as a control group. The results showed that all the samples revealed acceptable results compared to the BioOss samples. Further studies were performed on the same scaffolds by measuring the calcium concentration aiming to obtain an indication of the osteodifferentiation ability after cultivating the seeded scaffolds within both static and dynamic conditions. A perfusion bioreactor was custom made for this study and the calcium concentration was quantified after 4 weeks. The outcomes of this study suggested that cultivating cells in scaffolds within dynamic environment has a positive role on the osteogenic lineage stem cells differentiation.

To conclude, the main aim of this whole study was fulfilled by producing different types of porous phosphate-based glass scaffolds and assessing these scaffolds within conditions mimicking the human body more closely. These scaffolds were containing either zinc or strontium in specific

concentrations. The determined zinc and strontium concentrations were found by performing many basic studies on different zinc and strontium oxide concentrations. The results revealed the success in manufacturing the scaffolds in the intended chemical composition and showed a good biological potential for application in the craniofacial bone repair. Strontium based scaffolds are more favourable in scaffold production because of their better mechanical properties than the zinc based constructs. Strontium containing glass mechanical properties were slightly better than that of the Bio-Oss. This may be of great clinical value and a great potential to be used for craniofacial region bone defects repair as their mechanical properties are suitable for the non-loading cancellous bone characterisations.

8.2 Future work

Major areas should be assessed in future studies as following:

1-Performing further biological related studies of strontium and zinc containing phosphate glass scaffolds especially those related to quantification of the osteodifferentiation enzymes and markers.

2-Determination of the effect of long period (2 or 3 months) scaffold incubation within dynamic conditions via using a perfusion bioreactor or other types of bioreactors such as spinner flask or rotating wall bioreactor.

3-In vivo application of the produced phosphate glass scaffolds. This could be performed by implanting the produced scaffolds specifically to the strontium phosphate glass scaffolds in animals such as rabbits or rats. Performing multiple small size defects in the animal jaw bone can be done prior to implanting the glass scaffolds with the other materials such as BioOss. This can also be used as a comparative study to measure the bone healing ability by using different biomaterials or without using any material.

4-Development of novel bone biocomposites containing zinc or strontium glasses by using different scaffold manufacturing techniques such as the foam replica technique, the thermally phase separation (TIPS) technique or the solvent casting technique. These composites may have better mechanical properties than that of the scaffolds manufactured via the sintering technique used here.

Chapter 9 References

ABOU NEEL E, D. M. P., SABEEL PADINHARA VALAPPILA, ROBERT JOHN NEWPORTB AND, MIZOGUCHI, T., ITO, M., BITAR, M., SALIH, V. & KNOWLES, J. C. 2007. In vitro bioactivity and gene expression by cells cultured on titanium dioxide doped phosphate-based glasses. *Biomaterials,* 28**,** 2967-2977.

ABOU NEEL, E. A., AHMED, I., PRATTEN, J., NAZHAT, S. & KNOWLES, J. 2005. Characterisation of antibacterial copper releasing degradable phosphate glass fibres. *Biomaterials,* 26**,** 2247-2254.

ABOU NEEL, E. A., CHRZANOWSKI, W., PICKUP, D. M., O'DELL, L. A., MORDAN, N. J., NEWPORT, R. J., SMITH, M. E. & KNOWLES, J. C. 2008a. Structure and properties of strontium-doped phosphate-based glasses.

ABOU NEEL, E. A., CHRZANOWSKI, W., PICKUP, D. M., O'DELL, L. A., MORDAN, N. J., NEWPORT, R. J., SMITH, M. E. & KNOWLES, J. C. 2008b. Structure and properties of strontium-doped phosphate-based glasses. *J R Soc Interface,* 6**,** 435-46.

ABOU NEEL, E. A. & KNOWLES, J. C. 2008. Physical and biocompatibility studies of novel titanium dioxide doped phosphate-based glasses for bone tissue engineering applications. *Journal of Materials Science-Materials in Medicine,* 19**,** 377-386.

ABOU NEEL, E. A., O'DELL, L. A., CHRZANOWSKI, W., SMITH, M. E. & KNOWLES, J. C. 2009a. Control of surface free energy in titanium doped phosphate based glasses by co‐doping with zinc. *Journal of Biomedical Materials Research Part B: Applied Biomaterials,* 89**,** 392-407.

ABOU NEEL, E. A., O'DELL, L. A., SMITH, M. E. & KNOWLES, J. C. 2008c. Processing, characterisation, and biocompatibility of zinc modified metaphosphate based glasses for biomedical applications. *J Mater Sci Mater Med,* 19**,** 1669-79.

ABOU NEEL, E. A., PICKUP, D. M., VALAPPIL, S. P., NEWPORT, R. J. & KNOWLES, J. C. 2009b. Bioactive functional materials: a perspective on phosphate-based glasses. *Journal of Materials Chemistry,* 19**,** 690-701.

ABOU NEEL, E. A. A., CHRZANOWSKI, W. & KNOWLES, J. C. 2008d. Effect of increasing titanium dioxide content on bulk and surface

properties of phosphate-based glasses. *Acta biomaterialia,* 4**,** 523-534.

ADAMS, C. S. & SHAPIRO, I. M. 2002. The Fate of the Terminally Differentiated Chondrocyte: Evidence for Microenvironmental Regulation of Chondrocyte Apoptosis. *Critical Reviews in Oral Biology & Medicine,* 13**,** 465-473.

AHMED, I., LEWIS, M. & KNOWLES, J. 2005a. Quantification of anions and cations from ternary phosphate based glasses with fixed 50 and 55 mol% P2O5 using ion chromatography. *Physics and chemistry of glasses,* 46**,** 547-552.

AHMED, I., LEWIS, M., NAZHAT, S. & KNOWLES, J. 2005b. Quantification of anion and cation release from a range of ternary phosphate-based glasses with fixed 45 mol% P2O5. *Journal of biomaterials applications,* 20**,** 65-80.

AHMED, I., LEWIS, M., OLSEN, I. & KNOWLES, J. C. 2004a. Phosphate glasses for tissue engineering: Part 1. Processing and characterisation of a ternary-based P(2)O(5)-CaO-Na(2)O glass system. *Biomaterials,* 25**,** 491-499.

AHMED, I., LEWIS, M., OLSEN, I. & KNOWLES, J. C. 2004b. Phosphate glasses for tissue engineering: Part 2. Processing and characterisation of a ternary-based P(2)O(5)-CaO-Na(2)O glass fibre system. *Biomaterials,* 25**,** 501-507.

AHMED, I., PARSONS, A., PALMER, G., KNOWLES, J., WALKER, G. & RUDD, C. 2008. Weight loss, ion release and initial mechanical properties of a binary calcium phosphate glass fibre/PCL composite. *Acta Biomaterialia,* 4**,** 1307-1314.

AHN, H.-S., HWANG, J.-Y., KIM, M. S., LEE, J.-Y., KIM, J.-W., KIM, H.-S., SHIN, U. S., KNOWLES, J. C., KIM, H.-W. & HYUN, J. K. 2015. Carbon-nanotube-interfaced glass fiber scaffold for regeneration of transected sciatic nerve. *Acta Biomaterialia,* 13**,** 324-334.

AILLON, K. L., XIE, Y., EL-GENDY, N., BERKLAND, C. J. & FORREST, M. L. 2009. Effects of nanomaterial physicochemical properties on in vivo toxicity. *Advanced Drug Delivery Reviews,* 61**,** 457-466.

AINA, V., PERARDI, A., BERGANDI, L., MALAVASI, G., MENABUE, L., MORTERRA, C. & GHIGO, D. 2007. Cytotoxicity of zinc-containing bioactive glasses in contact with human osteoblasts. *Chemico-Biological Interactions,* 167**,** 207-218.

AJAYAN, P. M., WEI, B., ZHU, H., XU, C. & WU, D. 2009. Direct synthesis of long single-walled carbon nanotube strands. Google Patents.

AKAHANE, M., SHIMIZU, T., KIRA, T., ONISHI, T., UCHIHARA, Y., IMAMURA, T. & TANAKA, Y. 2016. Culturing bone marrow cells with

dexamethasone and ascorbic acid improves osteogenic cell sheet structure. *Bone Joint Res,* 5**,** 569-576.

AKASAKA, T., WATARI, F., SATO, Y. & TOHJI, K. 2006. Apatite formation on carbon nanotubes. *Materials Science and Engineering: C,* 26**,** 675-678.

ALONSO-SIERRA, S., VELÁZQUEZ-CASTILLO, R., MILLÁN-MALO, B., NAVA, R., BUCIO, L., MANZANO-RAMÍREZ, A., CID-LUNA, H. & RIVERA-MUÑOZ, E. M. 2017. Interconnected porosity analysis by 3D X-ray microtomography and mechanical behavior of biomimetic organic-inorganic composite materials. *Materials Science and Engineering: C,* 80**,** 45-53.

AMINI, A. R., LAURENCIN, C. T. & NUKAVARAPU, S. P. 2012. Bone tissue engineering: recent advances and challenges. *Crit Rev Biomed Eng,* 40**,** 363-408.

AN, Y. H. & DRAUGHN, R. A. 1999. *Mechanical testing of bone and the bone-implant interface*, CRC press.

ANDERSON, H. C., SIPE, J. B., HESSLE, L., DHAMYAMRAJU, R., ATTI, E., CAMACHO, N. P. & MILLÁN, J. L. 2004. Impaired Calcification Around Matrix Vesicles of Growth Plate and Bone in Alkaline Phosphatase-Deficient Mice. *American Journal of Pathology,* 164**,** 841-847.

ANSELME, K. 2000. Osteoblast adhesion on biomaterials. *Biomaterials,* 21**,** 667-681.

ARYAL, S., BHATTARAI, S. R., KC, R. B., KHIL, M. S., LEE, D.-R. & KIM, H. Y. 2006. Carbon nanotubes assisted biomimetic synthesis of hydroxyapatite from simulated body fluid. *Materials Science and Engineering: A,* 426**,** 202-207.

ATTIA, M., SANTERRE, J. P. & KANDEL, R. A. 2011. The response of annulus fibrosus cell to fibronectin-coated nanofibrous polyurethane-anionic dihydroxyoligomer scaffolds. *Biomaterials,* 32**,** 450-460.

AUBIN, J., LIU, F., MALAVAL, L. & GUPTA, A. 1995. Osteoblast and chondroblast differentiation. *Bone,* 17**,** S77-S83.

AUBIN, J. E. 2001. Regulation of osteoblast formation and function. *Reviews in Endocrine and Metabolic Disorders,* 2**,** 81-94.

AUBIN, J. E. & TRIFFITT, J. T. 2002. *Mesenchymal stem cells and osteoblast differentiation*.

BADR-MOHAMMADI, M. R., HESARAKI, S. & ZAMANIAN, A. 2014. Mechanical properties and in vitro cellular behavior of zinc-containing nano-bioactive glass doped biphasic calcium phosphate bone substitutes. *Journal of Materials Science-Materials in Medicine,* 25**,** 185-197.

BAI, H., WALSH, F., GLUDOVATZ, B., DELATTRE, B., HUANG, C., CHEN, Y., TOMSIA, A. P. & RITCHIE, R. O. 2016. Bioinspired Hydroxyapatite/Poly (methyl methacrylate) Composite with a Nacre‐Mimetic Architecture by a Bidirectional Freezing Method. *Advanced Materials,* 28**,** 50-56.

BALASUBRAMANIAN, K. & BURGHARD, M. 2005. Chemically functionalized carbon nanotubes. *Small,* 1**,** 180-92.

BALUYOT, E. S. & HARTFORD, C. G. 1996. Comparison of polyphosphate analysis by ion chromatography and by modified end-group titration. *Journal of chromatography A,* 739**,** 217-222.

BANCROFT, G. N., SIKAVITSAS, V. I., VAN DEN DOLDER, J., SHEFFIELD, T. L., AMBROSE, C. G., JANSEN, J. A. & MIKOS, A. G. 2002. Fluid flow increases mineralized matrix deposition in 3D perfusion culture of marrow stromal osteoblasts in a dose-dependent manner. *Proceedings of the National Academy of Sciences,* 99**,** 12600-12605.

BASHA, R. Y. & DOBLE, M. 2015. Design of biocomposite materials for bone tissue regeneration. *Materials Science and Engineering: C,* 57**,** 452-463.

BAUER, T. W. & MUSCHLER, G. F. 2000. Bone Graft Materials: An Overview of the Basic Science. *Clinical Orthopaedics and Related Research,* 371**,** 10-27.

BHATI, R. S., MUKHERJEE, D. P., MCCARTHY, K. J., ROGERS, S. H., SMITH, D. F. & SHALABY, S. W. 2001. The growth of chondrocytes into a fibronectin-coated biodegradable scaffold. *J Biomed Mater Res,* 56**,** 74-82.

BIANCO, P., FISHER, L. W., YOUNG, M. F., TERMINE, J. D. & ROBEY, P. G. 1991. Expression of bone sialoprotein (BSP) in developing human tissues. *Calcified tissue international,* 49**,** 421-426.

BIRLA, R. 2014. Bioreactors for Tissue Engineering. *Introduction to Tissue Engineering.* John Wiley & Sons, Inc.

BIRMINGHAM, E., NIEBUR, G. & MCHUGH, P. 2012. Osteogenic differentiation of mesenchymal stem cells is regulated by osteocyte and osteoblast cells in a simplified bone niche.

BJERRE, L., BÜNGER, C. E., KASSEM, M. & MYGIND, T. 2008. Flow perfusion culture of human mesenchymal stem cells on silicate-substituted tricalcium phosphate scaffolds. *Biomaterials,* 29**,** 2616-2627.

BJÖRKENHEIM, R., STRÖMBERG, G., PAJARINEN, J., AINOLA, M., UPPSTU, P., HUPA, L., BÖHLING, T. & LINDFORS, N. 2017. Polymer-coated bioactive glass S53P4 increases VEGF and TNF

expression in an induced membrane model in vivo. *Journal of Materials Science,* 52**,** 9055-9065.

BOCCACCINI, A. R., CHEN, Q., LEFEBVRE, L., GREMILLARD, L. & CHEVALIER, J. 2007. Sintering, crystallisation and biodegradation behaviour of Bioglass®-derived glass–ceramics. *Faraday discussions,* 136**,** 27-44.

BONEWALD, L. F. 1999. Establishment and characterization of an osteocyte-like cell line, MLO-Y4. *Journal of bone and mineral metabolism,* 17**,** 61-65.

BOSCHETTI, F., RAIMONDI, M. T., MIGLIAVACCA, F. & DUBINI, G. 2006. Prediction of the micro-fluid dynamic environment imposed to three-dimensional engineered cell systems in bioreactors. *Journal of biomechanics,* 39**,** 418-425.

BOSE, S., FIELDING, G., TARAFDER, S. & BANDYOPADHYAY, A. 2013. Understanding of dopant-induced osteogenesis and angiogenesis in calcium phosphate ceramics. *Trends Biotechnol,* 31**,** 594-605.

BOSE, S., ROY, M. & BANDYOPADHYAY, A. 2012. Recent advances in bone tissue engineering scaffolds. *Trends Biotechnol,* 30**,** 546-54.

BOSKEY, A. L. & ROBEY, P. G. 2013. The composition of bone. *Primer on the Metabolic Bone Diseases and Disorders of Mineral Metabolism, Eighth Edition***,** 49-58.

BOYAN, B., LOTZ, E. M. & SCHWARTZ, Z. 2017. Roughness and Hydrophilicity as Osteogenic Biomimetic Surface Properties. *Tissue Engineering*.

BOYAN, B. D., HUMMERT, T. W., DEAN, D. D. & SCHWARTZ, Z. 1996. Role of material surfaces in regulating bone and cartilage cell response. *Biomaterials,* 17**,** 137-146.

BOYLE, W. J., SIMONET, W. S. & LACEY, D. L. 2003. Osteoclast differentiation and activation. *Nature,* 423**,** 337-342.

BRAUER, D. S. 2015. Bioactive Glasses-Structure and Properties. *Angewandte Chemie-International Edition,* 54**,** 4160-4181.

BRAUER, D. S., RÜSSEL, C., LI, W. & HABELITZ, S. 2006. Effect of degradation rates of resorbable phosphate invert glasses on in vitro osteoblast proliferation. *Journal of Biomedical Materials Research Part A,* 77**,** 213-219.

BRINKER, C. J., SCHERER, G. W. & ROTH, E. 1985. Sol→ gel→ glass: II. Physical and structural evolution during constant heating rate experiments. *Journal of non-crystalline solids,* 72**,** 345-368.

BRODIE, J. C., GOLDIE, E., CONNEL, G., MERRY, J. & GRANT, M. 2005. Osteoblast interactions with calcium phosphate ceramics modified by

coating with type I collagen. *Journal of Biomedical Materials Research Part A,* 73**,** 409-421.

BRODSKY, B. & PERSIKOV, A. V. 2005. Molecular structure of the collagen triple helix. *Advances in protein chemistry,* 70**,** 301-339.

BROW, R. K. 2000. Review: the structure of simple phosphate glasses. *Journal of Non-Crystalline Solids,* 263–264**,** 1-28.

BROW, R. K., KIRKPATRICK, R. J. & TURNER, G. L. 1990. The short range structure of sodium phosphate glasses I. MAS NMR studies. *Journal of Non-Crystalline Solids,* 116**,** 39-45.

BUCHOLZ, R. W. 2002. Nonallograft Osteoconductive Bone Graft Substitutes. *Clinical Orthopaedics and Related Research,* 395**,** 44-52.

BUNKER, B., ARNOLD, G. & WILDER, J. A. 1984. Phosphate glass dissolution in aqueous solutions. *Journal of Non-Crystalline Solids,* 64**,** 291-316.

BURNIE, J., DOHERTY, R., GILCHRIST, T., DUFF, S., MALCOLM, A. & DRAKE, C. CONTROLLED RELEASE GLASS AS A POTENTIAL BONE-GRAFT SUBSTITUTE. Journal of Bone and Joint Surgery-British Volume, 1983. BRITISH EDITORIAL SOC BONE JOINT SURGERY 22 BUCKINGHAM STREET, LONDON, ENGLAND WC2N 6ET, 364-365.

BURNIE, J., GILCHRIST, T., DUFF, S., DRAKE, C., HARDING, N. & MALCOLM, A. 1981. Controlled release glasses (CRG) for biomedical uses. *Biomaterials,* 2**,** 244-246.

BUTLER, W., RIDALL, A. & MCKEE, M. 1996. Osteopontin. *Principles of bone biology***,** 167-181.

BUTLER, W. T. 1989. The nature and significance of osteopontin. *Connective tissue research,* 23**,** 123-136.

CACAINA, D., YLÄNEN, H., HUPA, M. & SIMON, S. 2006. Study of yttrium containing bioactive glasses behaviour in simulated body fluid. *Journal of Materials Science: Materials in Medicine,* 17**,** 709-716.

CACAINA, D., YLÄNEN, H., SIMON, S. & HUPA, M. 2008. The behaviour of selected yttrium containing bioactive glass microspheres in simulated body environments. *Journal of Materials Science: Materials in Medicine,* 19**,** 1225-1233.

CELIC, S., KATAYAMA, Y., CHILCO, P., MARTIN, T. & FINDLAY, D. 1998. Type I collagen influence on gene expression in UMR106-06 osteoblast-like cells is inhibited by genistein. *Journal of endocrinology,* 158**,** 377-388.

CHAN, O., COATHUP, M., NESBITT, A., HO, C.-Y., HING, K., BUCKLAND, T., CAMPION, C. & BLUNN, G. 2012. The effects of microporosity on

osteoinduction of calcium phosphate bone graft substitute biomaterials. *Acta biomaterialia,* 8**,** 2788-2794.

CHAO LE MENG BAO, E. Y. T., MARK S.K. CHONG, YUCHUN LIU, & K.Y., M. C. A. J. 2013. *Regenerative Medicine and Tissue Engineering*

InTech.

CHAVES, M. D., DE SOUZA NUNES, L. S., DE OLIVEIRA, R. V., HOLGADO, L. A., NARY FILHO, H., MATSUMOTO, M. A. & RIBEIRO, D. A. 2012. Bovine hydroxyapatite (Bio-Oss®) induces osteocalcin, RANK-L and osteoprotegerin expression in sinus lift of rabbits. *Journal of Cranio-Maxillofacial Surgery,* 40**,** e315-e320.

CHEN, G., XU, R., ZHANG, C. & LV, Y. 2017. Responses of MSCs to 3D Scaffold Matrix Mechanical Properties under Oscillatory Perfusion Culture. *ACS applied materials & interfaces,* 9**,** 1207-1218.

CHEN, H.-C. & HU, Y.-C. 2006. Bioreactors for tissue engineering. *Biotechnology Letters,* 28**,** 1415-1423.

CHEN, Q., ROETHER, J. & BOCCACCINI, A. 2008a. Tissue engineering scaffolds from bioactive glass and composite materials. *Topics in tissue engineering,* 4**,** 1-27.

CHEN, Q. Z., EFTHYMIOU, A., SALIH, V. & BOCCACCINI, A. R. 2008b. Bioglass®-derived glass–ceramic scaffolds: Study of cell proliferation and scaffold degradation in vitro. *Journal of Biomedical Materials Research Part A,* 84A**,** 1049-1060.

CHEN, Q. Z., THOMPSON, I. D. & BOCCACCINI, A. R. 2006. 45S5 Bioglass-derived glass-ceramic scaffolds for bone tissue engineering. *Biomaterials,* 27**,** 2414-25.

CHENG, Q., RUTLEDGE, K. & JABBARZADEH, E. 2013. Carbon Nanotube–Poly(lactide-co-glycolide) Composite Scaffolds for Bone Tissue Engineering Applications. *Annals of Biomedical Engineering,* 41**,** 904-916.

CHUENJITKUNTAWORN, B., INRUNG, W., DAMRONGSRI, D., MEKAAPIRUK, K., SUPAPHOL, P. & PAVASANT, P. 2010. Polycaprolactone/hydroxyapatite composite scaffolds: preparation, characterization, and in vitro and in vivo biological responses of human primary bone cells. *Journal of Biomedical Materials Research Part A,* 94**,** 241-251.

CLARKE, B. 2008. Normal bone anatomy and physiology. *Clin J Am Soc Nephrol,* 3 Suppl 3**,** S131-9.

CONTROL, C. F. D. & PREVENTION 2002. Update: allograft-associated bacterial infections--United States, 2002. *MMWR. Morbidity and mortality weekly report,* 51**,** 207.

COOMBES, A. & MEIKLE, M. 1994. Resorbable synthetic polymers s replacements for bone graft. *Clinical materials,* 17**,** 35-67.

COSTA, D. G., FERRAZ, E. P., ABUNA, R. P., DE OLIVEIRA, P. T., MORRA, M., BELOTI, M. M. & ROSA, A. L. 2017. The effect of collagen coating on titanium with nanotopography on in vitro osteogenesis. *Journal of Biomedical Materials Research Part A*.

CUI, D., TIAN, F., OZKAN, C. S., WANG, M. & GAO, H. 2005. Effect of single wall carbon nanotubes on human HEK293 cells. *Toxicol Lett,* 155**,** 73-85.

CURREY, J. D. 2002a. THE SHAPES OF BONES. *In:* CURREY, J. D. (ed.) *Bones.* Princeton University Press.

CURREY, J. D. 2002b. THE STRUCTURE OF BONE TISSUE. *In:* CURREY, J. D. (ed.) *Bones.* Princeton University Press.

CYPHER, T. J. & GROSSMAN, J. P. 1996. Biological principles of bone graft healing. *The Journal of foot and ankle surgery,* 35**,** 413-417.

DAMIEN, C. J. & PARSONS, J. R. 1991. Bone graft and bone graft substitutes: A review of current technology and applications. *Journal of Applied Biomaterials,* 2**,** 187-208.

DE GIROLAMO, L., SARTORI, M. F., ALBISETTI, W. & BRINI, A. T. 2007. Osteogenic differentiation of human adipose-derived stem cells: comparison of two different inductive media. *Journal of Tissue Engineering and Regenerative Medicine,* 1**,** 154-157.

DEMIRKIRAN, H., MOHANDAS, A., DOHI, M., FUENTES, A., NGUYEN, K. & ASWATH, P. 2010. Bioactivity and mineralization of hydroxyapatite with bioglass as sintering aid and bioceramics with Na 3 Ca 6 (PO 4) 5 and Ca 5 (PO 4) 2 SiO 4 in a silicate matrix. *Materials Science and Engineering: C,* 30**,** 263-272.

DIAS, A., LOPES, M., SANTOS, J., AFONSO, A., TSURU, K., OSAKA, A., HAYAKAWA, S., TAKASHIMA, S. & KURABAYASHI, Y. 2006. In vivo performance of biodegradable calcium phosphate glass ceramics using the rabbit model: histological and SEM observation. *Journal of biomaterials applications,* 20**,** 253-266.

DIAS, A., SKAKLE, J., GIBSON, I., LOPES, M. & SANTOS, J. 2005. In situ thermal and structural characterization of bioactive calcium phosphate glass ceramics containing TiO 2 and MgO oxides: High temperature–XRD studies. *Journal of Non-Crystalline Solids,* 351**,** 810-817.

DING, M., HENRIKSEN, S. S., MARTINETTI, R. & OVERGAARD, S. 2016a. 3D perfusion bioreactor ‐ activated porous granules on implant fixation

and early bone formation in sheep. *Journal of Biomedical Materials Research Part B: Applied Biomaterials*.

DING, M., HENRIKSEN, S. S., WENDT, D. & OVERGAARD, S. 2016b. An automated perfusion bioreactor for the streamlined production of engineered osteogenic grafts. *Journal of Biomedical Materials Research Part B: Applied Biomaterials,* 104**,** 532-537.

DONATI, D., ZOLEZZI, C., TOMBA, P. & VIGANO, A. 2007. Bone grafting: historical and conceptual review, starting with an old manuscript by Vittorio Putti. *Acta Orthop,* 78**,** 19-25.

DUCY, P., DESBOIS, C., BOYCE, B., PINERO, G., STORY, B., DUNSTAN, C., SMITH, E., BONADIO, J., GOLDSTEIN, S. & GUNDBERG, C. 1996. Increased bone formation in osteocalcin-deficient mice.

DUPUIS, A.-C. 2005. The catalyst in the CCVD of carbon nanotubes—a review. *Progress in Materials Science,* 50**,** 929-961.

EBBING, D. & GAMMON, S. D. 2016. *General chemistry*, Cengage Learning.

EGGER, D., SPITZ, S., FISCHER, M., HANDSCHUH, S., GLÖSMANN, M., FRIEMERT, B., EGERBACHER, M. & KASPER, C. 2017. Application of a Parallelizable Perfusion Bioreactor for Physiologic 3D Cell Culture. *Cells Tissues Organs,* 203**,** 316-326.

EINHORN, T. A., O'KEEFE, R. J. & BUCKWALTER, J. 2007. *Orthopaedic basic science*, Rosemont,IL.

EL-AMIN, S., LU, H., KHAN, Y., BUREMS, J., MITCHELL, J., TUAN, R. & LAURENCIN, C. 2003. Extracellular matrix production by human osteoblasts cultured on biodegradable polymers applicable for tissue engineering. *Biomaterials,* 24**,** 1213-1221.

EL‐GHANNAM, A., DUCHEYNE, P. & SHAPIRO, I. M. 1995. Bioactive material template for in vitro, synthesis of bone. *Journal of Biomedical Materials Research Part A,* 29**,** 359-370.

EL‐GHANNAM, A. R. 2004. Advanced bioceramic composite for bone tissue engineering: Design principles and structure–bioactivity relationship. *Journal of Biomedical Materials Research Part A,* 69**,** 490-501.

ELBATAL, H., KHALIL, E. & HAMDY, Y. 2009. In vitro behavior of bioactive phosphate glass–ceramics from the system P 2 O 5–Na 2 O–CaO containing titania. *Ceramics International,* 35**,** 1195-1204.

FARHAT, S. & SCOTT, C. D. 2006. Review of the arc process modeling for fullerene and nanotube production. *J Nanosci Nanotechnol,* 6**,** 1189-210.

FARRE-GUASCH, E., WOLFF, J., HELDER, M. N., SCHULTEN, E. A., FOROUZANFAR, T. & KLEIN-NULEND, J. 2015. Application of

Additive Manufacturing in Oral and Maxillofacial Surgery. *J Oral Maxillofac Surg,* 73**,** 2408-18.

FERRAZ, M., MONTEIRO, F. & MANUEL, C. 2004. Hydroxyapatite nanoparticles: a review of preparation methodologies. *Journal of Applied Biomaterials and Biomechanics,* 2**,** 74-80.

FILLINGHAM, Y. & JACOBS, J. 2016. Bone grafts and their substitutes. *Bone Joint J,* 98**,** 6-9.

FLORENCIO-SILVA, R., SASSO, G. R. D. S., SASSO-CERRI, E., SIMÕES, M. J. & CERRI, P. S. 2015. Biology of bone tissue: structure, function, and factors that influence bone cells. *BioMed research international,* 2015.

FOSTER, B., AO, M., WILLOUGHBY, C., SOENJAYA, Y., HOLM, E., LUKASHOVA, L., TRAN, A., WIMER, H., ZERFAS, P. & NOCITI, F. 2015. Mineralization defects in cementum and craniofacial bone from loss of bone sialoprotein. *Bone,* 78**,** 150-164.

FOSTER, K. A., SHIN, S. S., PRABHU, B., FREDRICKSON, A. & SEKULA, R. F. 2016. Calcium Phosphate Cement Cranioplasty Decreases the Rate of Cerebrospinal Fluid Leak and Wound Infection Compared with Titanium Mesh Cranioplasty: Retrospective Study of 672 Patients. *World neurosurgery,* 95**,** 414-418.

FRANKS, K., ABRAHAMS, I. & KNOWLES, J. 2000. Development of soluble glasses for biomedical use Part I: In vitro solubility measurement. *Journal of Materials Science: Materials in Medicine,* 11**,** 609-614.

FU, H., FU, Q., ZHOU, N., HUANG, W., RAHAMAN, M. N., WANG, D. & LIU, X. 2009. In vitro evaluation of borate-based bioactive glass scaffolds prepared by a polymer foam replication method. *Materials Science and Engineering: C,* 29**,** 2275-2281.

FU, Q., RAHAMAN, M. N., BAL, B. S., KUROKI, K. & BROWN, R. F. 2010a. In vivo evaluation of 13-93 bioactive glass scaffolds with trabecular and oriented microstructures in a subcutaneous rat implantation model. *Journal of Biomedical Materials Research Part A,* 95A**,** 235-244.

FU, Q., RAHAMAN, M. N., FU, H. & LIU, X. 2010b. Silicate, borosilicate, and borate bioactive glass scaffolds with controllable degradation rate for bone tissue engineering applications. I. Preparation and in vitro degradation. *Journal of Biomedical Materials Research Part A,* 95A**,** 164-171.

FU, Q., SAIZ, E., RAHAMAN, M. N. & TOMSIA, A. P. 2011. Bioactive glass scaffolds for bone tissue engineering: state of the art and future perspectives. *Materials Science and Engineering: C,* 31**,** 1245-1256.

GAGE, E., LANGEVIN, C.-J., PAPAY, F., EISENMANN-KLEIN, M. & SIEMIONOW, M. Z. 2010. *Biomaterials in Craniofacial Surgery*

Plastic and Reconstructive Surgery.

GAO, H., TAN, T. & WANG, D. 2004. Effect of composition on the release kinetics of phosphate controlled release glasses in aqueous medium. *Journal of controlled release,* 96**,** 21-28.

GARCIA-GARETA, E., COATHUP, M. J. & BLUNN, G. W. 2015. Osteoinduction of bone grafting materials for bone repair and regeneration. *Bone,* 81**,** 112-21.

GENTLEMAN, E., FREDHOLM, Y. C., JELL, G., LOTFIBAKHSHAIESH, N., O'DONNELL, M. D., HILL, R. G. & STEVENS, M. M. 2010. The effects of strontium-substituted bioactive glasses on osteoblasts and osteoclasts in vitro. *Biomaterials,* 31**,** 3949-56.

GEORGIOU, G., MATHIEU, L., PIOLETTI, D. P., BOURBAN, P. E., MÅNSON, J. A., KNOWLES, J. & NAZHAT, S. 2007. Polylactic acid–phosphate glass composite foams as scaffolds for bone tissue engineering. *Journal of Biomedical Materials Research Part B: Applied Biomaterials,* 80**,** 322-331.

GERHARDT, L.-C. & BOCCACCINI, A. R. 2010. Bioactive glass and glass-ceramic scaffolds for bone tissue engineering. *Materials,* 3**,** 3867-3910.

GHADAH S. ALGHAMDI, A. Z. A. 2013. Bonding Formation and Orbitals Nature of Zno Structure. *Middle-East Journal of Scientific Research,* 13**,** 1144-1149.

GIANNOUDIS, P. V., DINOPOULOS, H. & TSIRIDIS, E. 2005. Bone substitutes: an update. *Injury,* 36 Suppl 3**,** S20-7.

GOLDBERG, V. M. 2001. Bone grafts and their substitutes: facts, fiction, and futures. *Orthopedics,* 24**,** 875-876.

GOLUB, E. E. & BOESZE-BATTAGLIA, K. 2007. The role of alkaline phosphatase in mineralization. *Current Opinion in Orthopaedics,* 18**,** 444-448.

GONÇALVES, E. M., OLIVEIRA, F. J., SILVA, R. F., NETO, M. A., FERNANDES, M. H., AMARAL, M., VALLET‐REGÍ, M. & VILA, M. 2016. Three‐dimensional printed PCL‐hydroxyapatite scaffolds filled with CNTs for bone cell growth stimulation. *Journal of Biomedical Materials Research Part B: Applied Biomaterials,* 104**,** 1210-1219.

GOOCH, K. J., KWON, J., BLUNK, T., LANGER, R., FREED, L. & VUNJAK‐NOVAKOVIC, G. 2001. Effects of mixing intensity on tissue‐engineered cartilage. *Biotechnology and bioengineering,* 72**,** 402-407.

GOUGH, J., CHRISTIAN, P., SCOTCHFORD, C. & JONES, I. 2003. Long‐term craniofacial osteoblast culture on a sodium phosphate and a calcium/sodium phosphate glass. *Journal of Biomedical Materials Research Part A,* 66**,** 233-240.

GOUGH, J. E., JONES, J. R. & HENCH, L. L. 2004. Nodule formation and mineralisation of human primary osteoblasts cultured on a porous bioactive glass scaffold. *Biomaterials,* 25**,** 2039-2046.

GRONTHOS, S., STEWART, K., GRAVES, S. E., HAY, S. & SIMMONS, P. J. 1997. Integrin expression and function on human osteoblast‐like cells. *Journal of Bone and Mineral Research,* 12**,** 1189-1197.

GRUNLAN, M. A., ZHANG, D., SCHOENER, C. A. & SAUNDERS, W. B. 2016. Shape memory polymer scaffolds for tissue defects. Google Patents.

GRZESIK, W. J. & ROBEY, P. G. 1994. Bone matrix RGD glycoproteins: immunolocalization and interaction with human primary osteoblastic bone cells in vitro. *Journal of Bone and Mineral Research,* 9**,** 487-496.

GU, Y., YAP, A., CHEANG, P. & KUMAR, R. 2004. Spheroidization of glass powders for glass ionomer cements. *Biomaterials,* 25**,** 4029-4035.

GUYTON, A. C. & HALL, J. E. 2006. *Textbook of medical physiology*.

HAIMI, S., GORIANC, G., MOIMAS, L., LINDROOS, B., HUHTALA, H., RÄTY, S., KUOKKANEN, H., SÁNDOR, G. K., SCHMID, C., MIETTINEN, S. & SUURONEN, R. 2009. Characterization of zinc-releasing three-dimensional bioactive glass scaffolds and their effect on human adipose stem cell proliferation and osteogenic differentiation. *Acta Biomaterialia,* 5**,** 3122-3131.

HALLAB, N. J., VERMES, C., MESSINA, C., ROEBUCK, K. A., GLANT, T. T. & JACOBS, J. J. 2002. Concentration- and composition-dependent effects of metal ions on human MG-63 osteoblasts. *Journal of Biomedical Materials Research,* 60**,** 420-433.

HANNINK, G. & ARTS, J. J. C. 2011. Bioresorbability, porosity and mechanical strength of bone substitutes: What is optimal for bone regeneration? *Injury,* 42**,** S22-S25.

HARMEY, D., HESSLE, L., NARISAWA, S., JOHNSON, K. A., TERKELTAUB, R. & MILLÁN, J. L. 2004. Concerted regulation of inorganic pyrophosphate and osteopontin by akp2, enpp1, and ank: an integrated model of the pathogenesis of mineralization disorders. *The American journal of pathology,* 164**,** 1199-1209.

HARRISON, B. S. & ATALA, A. 2007. Carbon nanotube applications for tissue engineering. *Biomaterials,* 28**,** 344-53.

HARVEY, E. J., HENDERSON, J. E. & VENGALLATORE, S. T. 2010. Nanotechnology and bone healing. *J Orthop Trauma,* 24 Suppl 1**,** S25-30.

HASHIMOTO-UOSHIMA, M., ISHIKAWA, I., KINOSHITA, A., WENG, H. T. & ODA, S. 1995. Clinical and histologic observation of replacement of biphasic calcium phosphate by bone tissue in monkeys. *International Journal of Periodontics & Restorative Dentistry,* 15.

HAUSCHKA, P. V., LIAN, J. B., COLE, D. & GUNDBERG, C. M. 1989. Osteocalcin and matrix Gla protein: vitamin K-dependent proteins in bone. *Physiological reviews,* 69**,** 990-1047.

HAYAKAWA, S., TSURU, K., OHTSUKI, C. & OSAKA, A. 1999. Mechanism of apatite formation on a sodium silicate glass in a simulated body fluid. *Journal of the American Ceramic Society,* 82**,** 2155-2160.

HEDBERG, E. L., SHIH, C. K., LEMOINE, J. J., TIMMER, M. D., K. LIEBSCHNER, M. A., JANSEN, J. A. & MIKOS, A. G. 2005. In vitro degradation of porous poly(propylene fumarate)/poly(dl-lactic-co-glycolic acid) composite scaffolds. *Biomaterials,* 26**,** 3215-3225.

HENCH, L. L. 1998. Bioactive materials: the potential for tissue regeneration. *Journal of Biomedical Materials Research Part A,* 41**,** 511-518.

HENCH, L. L. & POLAK, J. M. 2002. Third-Generation Biomedical Materials. *Science,* 295**,** 1014-1017.

HENCH, L. L. & WEST, J. K. 1990. The sol-gel process. *Chemical Reviews,* 90**,** 33-72.

HING, K., BEST, S., TANNER, K., REVELL, P. & BONFIELD, W. 1998. Histomorphological and biomechanical characterization of calcium phosphates in the osseous environment. *Proceedings of the Institution of Mechanical Engineers, Part H: Journal of Engineering in Medicine,* 212**,** 437-451.

HING, K. A. 2004. Bone repair in the twenty–first century: biology, chemistry or engineering? *Philosophical Transactions of the Royal Society of London A: Mathematical, Physical and Engineering Sciences,* 362**,** 2821-2850.

HING, K. A. 2005. Bioceramic bone graft substitutes: influence of porosity and chemistry. *International journal of applied ceramic technology,* 2**,** 184-199.

HIRANO, S., KANNO, S. & FURUYAMA, A. 2008. Multi-walled carbon nanotubes injure the plasma membrane of macrophages. *Toxicology and Applied Pharmacology,* 232**,** 244-251.

HOLM, E., AUBIN, J. E., HUNTER, G. K., BEIER, F. & GOLDBERG, H. A. 2015. Loss of bone sialoprotein leads to impaired endochondral bone development and mineralization. *Bone,* 71**,** 145-154.

HOPPE, U. 1996. A structural model for phosphate glasses. *Journal of Non-Crystalline Solids,* 195**,** 138-147.

HU, H., NI, Y., MONTANA, V., HADDON, R. C. & PARPURA, V. 2004. Chemically Functionalized Carbon Nanotubes as Substrates for Neuronal Growth. *Nano Lett,* 4**,** 507-511.

HUANG, W. 1992. The Preparation and application of the micro-spheres containing Yttrium-90, J. *Shanghai Inst. of Bldg. Mat,* 4**,** 347.

HUANG, Z., NELSON, E. R., SMITH, R. L. & GOODMAN, S. B. 2007. The sequential expression profiles of growth factors from osteroprogenitors to osteoblasts in vitro. *Tissue engineering,* 13**,** 2311-2320.

HUDGENS, J. J., BROW, R. K., TALLANT, D. R. & MARTIN, S. W. 1998. Raman spectroscopy study of the structure of lithium and sodium ultraphosphate glasses. *Journal of non-crystalline solids,* 223**,** 21-31.

HUGHES, R. C. 2014. *Membrane glycoproteins: a review of structure and function*, Elsevier.

HYNES, R. O. 1992. Integrins: versatility, modulation, and signaling in cell adhesion. *Cell,* 69**,** 11-25.

IIJIMA, S. & ICHIHASHI, T. 1993. Single-shell carbon nanotubes of 1-nm diameter. *Nature,* 363**,** 603-605.

IOZZO, R. V. & SCHAEFER, L. 2015. Proteoglycan form and function: a comprehensive nomenclature of proteoglycans. *Matrix Biology,* 42**,** 11-55.

ITO, A., KAWAMURA, H., OTSUKA, M., IKEUCHI, M., OHGUSHI, H., ISHIKAWA, K., ONUMA, K., KANZAKI, N., SOGO, Y. & ICHINOSE, N. 2002. Zinc-releasing calcium phosphate for stimulating bone formation. *Materials Science and Engineering: C,* 22**,** 21-25.

ITO, A., OJIMA, K., NAITO, H., ICHINOSE, N. & TATEISHI, T. 2000. Preparation, solubility, and cytocompatibility of zinc-releasing calcium phosphate ceramics. *J Biomed Mater Res,* 50**,** 178-83.

JABERI, J., GAMBRELL, K., TIWANA, P., MADDEN, C. & FINN, R. 2013. Long-term clinical outcome analysis of poly-methyl-methacrylate cranioplasty for large skull defects. *Journal of Oral and Maxillofacial Surgery,* 71**,** e81-e88.

JAGODZINSKI, M., BREITBART, A., WEHMEIER, M., HESSE, E., HAASPER, C., KRETTEK, C., ZEICHEN, J. & HANKEMEIER, S. 2008. Influence of perfusion and cyclic compression on proliferation and differentiation of bone marrow stromal cells in 3-dimensional culture. *Journal of biomechanics,* 41**,** 1885-1891.

JING, Z., WU, Y., SU, W., TIAN, M., JIANG, W., CAO, L., ZHAO, L. & ZHAO, Z. 2017. Carbon Nanotube Reinforced Collagen/Hydroxyapatite

Scaffolds Improve Bone Tissue Formation In Vitro and In Vivo. *Ann Biomed Eng*.

JONES, A. C., ARNS, C. H., HUTMACHER, D. W., MILTHORPE, B. K., SHEPPARD, A. P. & KNACKSTEDT, M. A. 2009. The correlation of pore morphology, interconnectivity and physical properties of 3D ceramic scaffolds with bone ingrowth. *Biomaterials,* 30**,** 1440-1451.

JONES, J. R., LEE, P. D. & HENCH, L. L. 2006. Hierarchical porous materials for tissue engineering. *Philosophical Transactions of the Royal Society of London A: Mathematical, Physical and Engineering Sciences,* 364**,** 263-281.

JONES, J. R., LIN, S., YUE, S., LEE, P., HANNA, J. V., SMITH, M. E. & NEWPORT, R. J. 2010. Bioactive glass scaffolds for bone regeneration and their hierarchical characterisation. *Proceedings of the Institution of Mechanical Engineers, Part H: Journal of Engineering in Medicine,* 224**,** 1373-1387.

JOVANOVIC, S. A., SPIEKERMANN, H. & RICHTER, E. J. 1992. Bone regeneration around titanium dental implants in dehisced defect sites: a clinical study. *International Journal of Oral & Maxillofacial Implants,* 7.

KAM, N. W. & DAI, H. 2005. Carbon nanotubes as intracellular protein transporters: generality and biological functionality. *J Am Chem Soc,* 127**,** 6021-6.

KANG, Y., YAO, Y., YIN, G., HUANG, Z., LIAO, X., XU, X. & ZHAO, G. 2009. A study on the in vitro degradation properties of poly (l-lactic acid)/β-tricalcuim phosphate (PLLA/β-TCP) scaffold under dynamic loading. *Medical engineering & physics,* 31**,** 589-594.

KARAGEORGIOU, V. & KAPLAN, D. 2005. Porosity of 3D biomaterial scaffolds and osteogenesis. *Biomaterials,* 26**,** 5474-5491.

KASPERK, C., WERGEDAL, J., STRONG, D., FARLEY, J., WANGERIN, K., GROPP, H., ZIEGLER, R. & BAYLINK, D. J. 1995. Human bone cell phenotypes differ depending on their skeletal site of origin. *The Journal of Clinical Endocrinology & Metabolism,* 80**,** 2511-2517.

KATZ, E. & WILLNER, I. 2004. Biomolecule-functionalized carbon nanotubes: applications in nanobioelectronics. *Chemphyschem,* 5**,** 1084-104.

KAUR, G., PANDEY, O. P., SINGH, K., HOMA, D., SCOTT, B. & PICKRELL, G. 2014a. A review of bioactive glasses: Their structure, properties, fabrication and apatite formation. *J Biomed Mater Res A,* 102**,** 254-74.

KAUR, G., PANDEY, O. P., SINGH, K., HOMA, D., SCOTT, B. & PICKRELL, G. 2014b. A review of bioactive glasses: their structure, properties,

fabrication and apatite formation. *Journal of Biomedical Materials Research Part A,* 102**,** 254-274.

KAUR, G., PICKRELL, G., SRIRANGANATHAN, N., KUMAR, V. & HOMA, D. 2016. Review and the state of the art: Sol-gel and melt quenched bioactive glasses for tissue engineering. *J Biomed Mater Res B Appl Biomater,* 104**,** 1248-75.

KAWASHITA, M. 2005. Ceramic microspheres for biomedical applications. *International Journal of Applied Ceramic Technology,* 2**,** 173-183.

KAWASHITA, M., TODA, S., KIM, H. M., KOKUBO, T. & MASUDA, N. 2003. Preparation of antibacterial silver‐doped silica glass microspheres. *Journal of Biomedical Materials Research Part A,* 66**,** 266-274.

KEENE, D. R., SAKAI, L. Y. & BURGESON, R. E. 1991. Human bone contains type III collagen, type VI collagen, and fibrillin: type III collagen is present on specific fibers that may mediate attachment of tendons, ligaments, and periosteum to calcified bone cortex. *Journal of Histochemistry & Cytochemistry,* 39**,** 59-69.

KHALID, P., HUSSAIN, M. A., REKHA, P. D. & ARUN, A. B. 2015. Carbon nanotube-reinforced hydroxyapatite composite and their interaction with human osteoblast in vitro. *Hum Exp Toxicol,* 34**,** 548-56.

KHAN, R. A., PARSONS, A., JONES, I., WALKER, G. & RUDD, C. 2010. Preparation and characterization of phosphate glass fibers and fabrication of poly (caprolactone) matrix resorbable composites. *Journal of Reinforced Plastics and Composites,* 29**,** 1838-1850.

KHOR, S., TALIB, Z. A., DAUD, W. & SIDEK, H. 2011. Degradation study on ternary zinc magnesium phosphate glasses. *Journal of materials science,* 46**,** 7895.

KIM, H.-W., KNOWLES, J. C. & KIM, H.-E. 2005a. Hydroxyapatite porous scaffold engineered with biological polymer hybrid coating for antibiotic Vancomycin release. *Journal of Materials Science: Materials in Medicine,* 16**,** 189-195.

KIM, H. W., LEE, E. J., JUN, I. K., KIM, H. E. & KNOWLES, J. C. 2005b. Degradation and drug release of phosphate glass/polycaprolactone biological composites for hard‐tissue regeneration. *Journal of Biomedical Materials Research Part B: Applied Biomaterials,* 75**,** 34-41.

KING, R. C., STANSFIELD, W. D. & MULLIGAN, P. K. 2006. A dictionary of genetics.

KIRKPATRICK, R. J. & BROW, R. K. 1995. Nuclear magnetic resonance investigation of the structures of phosphate and phosphate-containing glasses: a review. *Solid State Nucl Magn Reson,* 5**,** 9-21.

KIRSCH, T. 2006. Determinants of pathological mineralization. *Current Opinion in Rheumatology,* 18**,** 174-180.

KISHI, S. & YAMAGUCHI, M. 1994. Inhibitory effect of zinc compounds on osteoclast-like cell formation in mouse marrow cultures. *Biochemical pharmacology,* 48**,** 1225-1230.

KLEINHANS, C., MOHAN, R. R., VACUN, G., SCHWARZ, T., HALLER, B., SUN, Y., KAHLIG, A., KLUGER, P., FINNE‐WISTRAND, A. & WALLES, H. 2015. A perfusion bioreactor system efficiently generates cell‐loaded bone substitute materials for addressing critical size bone defects. *Biotechnology journal,* 10**,** 1727-1738.

KNOWLES, J. C. 2003. Phosphate based glasses for biomedical applications. *Journal of Materials Chemistry,* 13**,** 2395-2401.

KOKUBO, T., KIM, H.-M. & KAWASHITA, M. 2003. Novel bioactive materials with different mechanical properties. *Biomaterials,* 24**,** 2161-2175.

KOKUBO, T. & TAKADAMA, H. 2006. How useful is SBF in predicting in vivo bone bioactivity? *Biomaterials,* 27**,** 2907-2915.

KONOPNICKI, S., SHARAF, B., RESNICK, C., PATENAUDE, A., POGAL-SUSSMAN, T., HWANG, K.-G., ABUKAWA, H. & TROULIS, M. J. 2015. Tissue-engineered bone with 3-dimensionally printed β-tricalcium phosphate and polycaprolactone scaffolds and early implantation: an in vivo pilot study in a porcine mandible model. *Journal of Oral and Maxillofacial Surgery,* 73**,** 1016. e1-1016. e11.

KOROSSIS, S., BOLLAND, F., KEARNEY, J., FISHER, J. & INGHAM, E. 2005. Bioreactors in tissue engineering. *Topics Tissue Eng,* 2**,** 1-23.

KWANG HWAN PARK, B. P., , D. S. Y., , S.-H. K., , D. M. S., , J. W. L., LEE, H. G., , J.-H. S. & , J. H. P., AND JAE MYUN LEE 2013. Zinc inhibits osteoclast differentiation by

suppression of Ca2+-Calcineurin-NFATc1 signaling

pathway. *Cell Communication and Signaling,* 11**,** 74.

KWOK, D. Y. & NEUMANN, A. W. 1999. Contact angle measurement and contact angle interpretation. *Advances in Colloid and Interface Science,* 81**,** 167-249.

LAKHKAR, N., ABOU NEEL, E. A., SALIH, V. & KNOWLES, J. C. 2011. Titanium and strontium-doped phosphate glasses as vehicles for strontium ion delivery to cells. *Journal of biomaterials applications,* 25**,** 877-893.

LAKHKAR, N. J., ABOU NEEL, E. A., SALIH, V. & KNOWLES, J. C. 2009. Strontium oxide doped quaternary glasses: effect on structure, degradation and cytocompatibility. *J Mater Sci Mater Med,* 20**,** 1339-46.

LAKHKAR, N. J., LEE, I.-H., KIM, H.-W., SALIH, V., WALL, I. B. & KNOWLES, J. C. 2013. Bone formation controlled by biologically relevant inorganic ions: Role and controlled delivery from phosphate-based glasses. *Advanced Drug Delivery Reviews,* 65**,** 405-420.

LAKHKAR, N. J., PARK, J.-H., MORDAN, N. J., SALIH, V., WALL, I. B., KIM, H.-W., KING, S. P., HANNA, J. V., MARTIN, R. A., ADDISON, O., MOSSELMANS, J. F. W. & KNOWLES, J. C. 2012. Titanium phosphate glass microspheres for bone tissue engineering. *Acta Biomaterialia,* 8**,** 4181-4190.

LANCASTER, M. V. A. F., R.D. 1996. *Antibiotic and cytotoxic drug susceptibility assays using resazurin and poising agents.* USA patent application 5,501,959.

LARA, W. C., SCHWEITZER, J., LEWIS, R. P., ODUM, B. C., EDLICH, R. F. & GAMPPER, T. J. 1997. Technical considerations in the use of polymethylmethacrylate in cranioplasty. *Journal of long-term effects of medical implants,* 8**,** 43-53.

LAURENCIN, C. T., KUMBAR, S. G. & NUKAVARAPU, S. P. 2009. Nanotechnology and orthopedics: a personal perspective. *Wiley Interdiscip Rev Nanomed Nanobiotechnol,* 1**,** 6-10.

LEE, K., PARK, M., KIM, H., LIM, Y., CHUN, H., KIM, H. & MOON, S. 2006. Ceramic bioactivity: progresses, challenges and perspectives. *Biomedical Materials,* 1**,** R31.

LEGEROS, R. Z. 2008. Calcium Phosphate-Based Osteoinductive Materials. *Chemical Reviews,* 108**,** 4742-4753.

LEWIS, O. 1956. The blood supply of developing long bones with special reference to the metaphyses. *Bone & Joint Journal,* 38**,** 928-933.

LI, Y., RAHAMAN, M. N., FU, Q., BAL, B. S., YAO, A. & DAY, D. E. 2007. Conversion of bioactive borosilicate glass to multilayered hydroxyapatite in dilute phosphate solution. *Journal of the American Ceramic Society,* 90**,** 3804-3810.

LIEBERMAN, J. R. 2009. *AAOS comprehensive orthopaedic review,* Rosemont,IL, American academy of orthopaedic surgeons.

LIN, C., WANG, Y., LAI, Y., YANG, W., JIAO, F., ZHANG, H., YE, S. & ZHANG, Q. 2011. Incorporation of carboxylation multiwalled carbon nanotubes into biodegradable poly (lactic-co-glycolic acid) for bone tissue engineering. *Colloids and Surfaces B: Biointerfaces,* 83**,** 367-375.

LIN, K., CHANG, J., LIU, Z., ZENG, Y. & SHEN, R. 2009. Fabrication and characterization of 45S5 bioglass reinforced macroporous calcium silicate bioceramics. *Journal of the European Ceramic Society,* 29**,** 2937-2943.

LINDFORS, N. C., HYVÖNEN, P., NYYSSÖNEN, M., KIRJAVAINEN, M., KANKARE, J., GULLICHSEN, E. & SALO, J. 2010. Bioactive glass S53P4 as bone graft substitute in treatment of osteomyelitis. *Bone,* 47**,** 212-218.

LINSLEY, C., WU, B. & TAWIL, B. 2013. The effect of fibrinogen, collagen type I, and fibronectin on mesenchymal stem cell growth and differentiation into osteoblasts. *Tissue Engineering Part A,* 19**,** 1416-1423.

LIU, X., GRANT, D. M., PALMER, G., PARSONS, A. J., RUDD, C. D. & AHMED, I. 2015. Magnesium coated phosphate glass fibers for unidirectional reinforcement of polycaprolactone composites. *Journal of Biomedical Materials Research Part B: Applied Biomaterials,* 103**,** 1424-1432.

LIU, X. & MA, P. X. 2004. Polymeric scaffolds for bone tissue engineering.

LIZZI, F., VILLAT, C., ATTIK, N., JACKSON, P., GROSGOGEAT, B. & GOUTAUDIER, C. 2017. Mechanical characteristic and biological behaviour of implanted and restorative bioglasses used in medicine and dentistry: A systematic review. *Dental Materials*.

LOOS, M. 2015. Chapter 3 - Allotropes of Carbon and Carbon Nanotubes. *Carbon Nanotube Reinforced Composites.* Oxford: William Andrew Publishing.

LOPA, S., MERCURI, D., COLOMBINI, A., DE CONTI, G., SEGATTI, F., ZAGRA, L. & MORETTI, M. 2013. Orthopedic bioactive implants: Hydrogel enrichment of macroporous titanium for the delivery of mesenchymal stem cells and strontium. *J Biomed Mater Res A,* 101**,** 3396-403.

LOWRY, K., HAMSON, K., BEAR, L., PENG, Y., CALALUCE, R., EVANS, M., ANGLEN, J. & ALLEN, W. 1997. Polycaprolactone/glass bioabsorbable implant in a rabbit humerus fracture model. *Journal of Biomedical Materials Research Part A,* 36**,** 536-541.

LUCACEL, R. C., MAIER, M. & SIMON, V. 2010. Structural and in vitro characterization of TiO 2-CaO-P 2 O 5 bioglasses. *Journal of Non-Crystalline Solids,* 356**,** 2869-2874.

LUO, F., PAN, L., HONG, G., WANG, T., PEI, X., WANG, J. & WAN, Q. 2017. In Vitro and In Vivo Characterization of Multi-Walled Carbon Nanotubes/Polycaprolactone Composite Scaffolds for Bone Tissue Engineering Applications. *Journal of Biomaterials and Tissue Engineering,* 7**,** 787-797.

LUSVARDI, G., MALAVASI, G., MENABUE, L., MENZIANI, M. C., PEDONE, A., SEGRE, U., AINA, V., PERARDI, A., MORTERRA, C., BOCCAFOSCHI, F., GATTI, S., BOSETTI, M. & CANNAS, M. 2008.

Properties of zinc releasing surfaces for clinical applications. *J Biomater Appl,* 22**,** 505-26.

LYNCH, M. P., STEIN, J. L., STEIN, G. S. & LIAN, J. B. 1995. The influence of type I collagen on the development and maintenance of the osteoblast phenotype in primary and passaged rat calvarial osteoblasts: modification of expression of genes supporting cell growth, adhesion, and extracellular matrix mineralization. *Experimental cell research,* 216**,** 35-45.

MA, P. X. 2004. Scaffolds for tissue fabrication. *Materials Today,* 7**,** 30-40.

MACKIE, E. J., AHMED, Y. A., TATARCZUCH, L., CHEN, K. S. & MIRAMS, M. 2008. Endochondral ossification: how cartilage is converted into bone in the developing skeleton. *Int J Biochem Cell Biol,* 40**,** 46-62.

MAÇON, A. L. B., LEE, S., POOLOGASUNDARAMPILLAI, G., KASUGA, T. & JONES, J. R. 2017. Synthesis and dissolution behaviour of CaO/SrO-containing sol–gel-derived 58S glasses. *Journal of Materials Science,* 52**,** 8858-8870.

MAENO, S., NIKI, Y., MATSUMOTO, H., MORIOKA, H., YATABE, T., FUNAYAMA, A., TOYAMA, Y., TAGUCHI, T. & TANAKA, J. 2005. The effect of calcium ion concentration on osteoblast viability, proliferation and differentiation in monolayer and 3D culture. *Biomaterials,* 26**,** 4847-4855.

MAHER, S., KOLIEB, E., SABIK, N. A., ABD-ELHALIM, D., EL-SERAFI, A. T. & EL-WAZIR, Y. 2015. Comparison of the osteogenic differentiation potential of mesenchymal cells isolated from human bone marrow, umbilical cord blood and placenta derived stem cells. *Beni-Suef University Journal of Basic and Applied Sciences,* 4**,** 80-85.

MALAVAL, L., LIU, F., ROCHE, P. & AUBIN, J. E. 1999. Kinetics of osteoprogenitor proliferation and osteoblast differentiation in vitro. *Journal of cellular biochemistry,* 74**,** 616-627.

MARDAS, N., CHADHA, V. & DONOS, N. 2010. Alveolar ridge preservation with guided bone regeneration and a synthetic bone substitute or a bovine-derived xenograft: a randomized, controlled clinical trial. *Clin Oral Implants Res,* 21**,** 688-98.

MARKS, S. C. & POPOFF, S. N. 1988. Bone cell biology: the regulation of development, structure, and function in the skeleton. *American Journal of Anatomy,* 183**,** 1-44.

MARTINELLI, J. R., SENE, F. F., KAMIKAWACHI, C. N., PARTITI, C. D. M. & CORNEJO, D. R. 2010. Synthesis and characterization of glass–ceramic microspheres for thermotherapy. *Journal of Non-Crystalline Solids,* 356**,** 2683-2688.

MASSERA, J., KOKKARI, A., NARHI, T. & HUPA, L. 2015. The influence of SrO and CaO in silicate and phosphate bioactive glasses on human gingival fibroblasts. *J Mater Sci Mater Med,* 26**,** 196.

MATTIOLI-BELMONTE, M., VOZZI, G., WHULANZA, Y., SEGGIANI, M., FANTAUZZI, V., ORSINI, G. & AHLUWALIA, A. 2012. Tuning polycaprolactone–carbon nanotube composites for bone tissue engineering scaffolds. *Materials Science and Engineering: C,* 32**,** 152-159.

MCDOUGALL, K. E. 2001. *Evaluation of biocompatibility using human craniofacial bone cells.* University of Nottingham.

MCNERNY, E., GONG, B., MORRIS, M. D. & KOHN, D. H. 2015. Bone Fracture Toughness and Strength Correlate With Collagen Cross‐Link Maturity in a Dose‐Controlled Lathyrism Mouse Model. *Journal of Bone and Mineral Research,* 30**,** 455-464.

MEINEL, L., KARAGEORGIOU, V., FAJARDO, R., SNYDER, B., SHINDE-PATIL, V., ZICHNER, L., KAPLAN, D., LANGER, R. & VUNJAK-NOVAKOVIC, G. 2004. Bone Tissue Engineering Using Human Mesenchymal Stem Cells: Effects of Scaffold Material and Medium Flow. *Annals of Biomedical Engineering,* 32**,** 112-122.

MEISENBERG, G. & SIMMONS, W. H. 2016. *Principles of medical biochemistry*, Elsevier Health Sciences.

MENTAVERRI, R., BRAZIER, M., KAMEL, S. & FARDELLONE, P. 2012. Potential anti-catabolic and anabolic properties of strontium ranelate. *Current molecular pharmacology,* 5**,** 189-194.

MIKAEL, P. E. & NUKAVARAPU, S. P. 2011. Functionalized carbon nanotube composite scaffolds for bone tissue engineering: prospects and progress. *Journal of Biomaterials and Tissue Engineering,* 1**,** 76-85.

MILOJKOVIC, N. & HOMSI, S. 2014. Polymethylmethacrylate pulmonary embolism as a complication of percutaneous vertebroplasty in cancer patients. *The Journal of the Arkansas Medical Society,* 111**,** 140-142.

MILORO, M., GHALI, G., LARSEN, P. & WAITE, P. 2004. *Peterson's principles of oral and maxillofacial surgery*, PMPH-USA.

MISRA, S. K., OHASHI, F., VALAPPIL, S. P., KNOWLES, J. C., ROY, I., SILVA, S. R. P., SALIH, V. & BOCCACCINI, A. R. 2010. Characterization of carbon nanotube (MWCNT) containing P (3HB)/bioactive glass composites for tissue engineering applications. *Acta biomaterialia,* 6**,** 735-742.

MITCHELL, B. S. & PEEL, S. 2009. *Histology : Illustrated Colour Text*.

MOHAMAD YUNOS, D., BRETCANU, O. & BOCCACCINI, A. R. 2008. Polymer-bioceramic composites for tissue engineering scaffolds. *Journal of Materials Science,* 43**,** 4433.

MONEM, A. S., ELBATAL, H. A., KHALIL, E. M., AZOOZ, M. A. & HAMDY, Y. M. 2008. In vivo behavior of bioactive phosphate glass-ceramics from the system P2O5–Na2O–CaO containing TiO2. *Journal of Materials Science: Materials in Medicine,* 19**,** 1097-1108.

MORAIS, J. M., PAPADIMITRAKOPOULOS, F. & BURGESS, D. J. 2010. Biomaterials/tissue interactions: possible solutions to overcome foreign body response. *The AAPS journal,* 12**,** 188-196.

MORDENFELD, A., LINDGREN, C. & HALLMAN, M. 2016. Sinus Floor Augmentation Using Straumann® BoneCeramic™ and Bio‐Oss® in a Split Mouth Design and Later Placement of Implants: A 5‐Year Report from a Longitudinal Study. *Clinical implant dentistry and related research,* 18**,** 926-936.

MORISHIMA, A., GRUMBACH, M. M., SIMPSON, E. R., FISHER, C. & QIN, K. 1995. Aromatase deficiency in male and female siblings caused by a novel mutation and the physiological role of estrogens. *Journal of Clinical Endocrinology and Metabolism,* 80**,** 3689-3698.

MULLIGAN, A., WILSON, M. & KNOWLES, J. 2003. The effect of increasing copper content in phosphate-based glasses on biofilms of Streptococcus sanguis. *Biomaterials,* 24**,** 1797-1807.

NAGAI, M., HAYAKAWA, T., FUKATSU, A., YAMAMOTO, M., FUKUMOTO, M., NAGAHAMA, F., MISHIMA, H., YOSHINARI, M., NEMOTO, K. & KATO, T. 2002. In vitro study of collagen coating of titanium implants for initial cell attachment. *Dental materials journal,* 21**,** 250-260.

NAVARRO, M., GINEBRA, M.-P., CLÉMENT, J., SALVADOR, M., GLORIA, A. & PLANELL, J. A. 2003. Physicochemical Degradation of Titania-Stabilized Soluble Phosphate Glasses for Medical Applications. *Journal of the American Ceramic Society,* 86**,** 1345-1352.

NAVARRO, M., MICHIARDI, A., CASTAÑO, O. & PLANELL, J. A. 2008. Biomaterials in orthopaedics. *Journal of the Royal Society Interface,* 5**,** 1137-1158.

NAVARRO, M., VALLE, S. D., MARTíNEZ, S., ZEPPETELLI, S., AMBROSIO, L., PLANELL, J. A. & GINEBRA, M. P. 2004. New macroporous calcium phosphate glass ceramic for guided bone regeneration. *Biomaterials,* 25**,** 4233-4241.

NEVE, A., CORRADO, A. & CANTATORE, F. P. 2013. Osteocalcin: Skeletal and extra‐skeletal effects. *Journal of cellular physiology,* 228**,** 1149-1153.

NEWMAN, P., LU, Z., ROOHANI-ESFAHANI, S., CHURCH, T. L., BIRO, M., DAVIES, B., KING, A., MACKENZIE, K., MINETT, A. & ZREIQAT, H. 2015. Porous and strong three-dimensional carbon nanotube coated ceramic scaffolds for tissue engineering. *Journal of Materials Chemistry B,* 3**,** 8337-8347.

NEWMAN, S. D., LOTFIBAKHSHAIESH, N., O'DONNELL, M., WALBOOMERS, X. F., HORWOOD, N., JANSEN, J. A., AMIS, A. A., COBB, J. P. & STEVENS, M. M. 2014. Enhanced osseous implant fixation with strontium-substituted bioactive glass coating. *Tissue Engineering Part A,* 20**,** 1850-1857.

NG, J., SPILLER, K., BERNHARD, J. & VUNJAK-NOVAKOVIC, G. 2017. Biomimetic approaches for bone tissue engineering. *Tissue Engineering Part B: Reviews*.

NIE, Y., BERGENDAHL, V., HEI, D. J., JONES, J. M. & PALECEK, S. P. 2009. Scalable culture and cryopreservation of human embryonic stem cells on microcarriers. *Biotechnology progress,* 25**,** 20-31.

NYAN, M. 2016. Alpha tricalcium phosphate biomaterials for potential clinical application in bone regeneration. *Myanmar Dental Journal,* 23**,** 4-9.

OBREGÓN, R., RAMÓN-AZCÓN, J. & AHADIAN, S. 2017. Bioreactors in Tissue Engineering. *Tissue Engineering for Artificial Organs.* Wiley-VCH Verlag GmbH & Co. KGaA.

OKLUND, S. A., PROLO, D. J., GUTIERREZ, R. V. & KING, S. E. 1986. Quantitative comparisons of healing in cranial fresh autografts, frozen autografts and processed autografts, and allografts in canine skull defects. *Clinical orthopaedics and related research,* 205**,** 269-291.

OLDBERG, A., FRANZÉN, A. & HEINEGÅRD, D. 1986. Cloning and sequence analysis of rat bone sialoprotein (osteopontin) cDNA reveals an Arg-Gly-Asp cell-binding sequence. *Proceedings of the National Academy of Sciences,* 83**,** 8819-8823.

ONAL, L., COZIEN‐CAZUC, S., JONES, I. A. & RUDD, C. D. 2008. Water absorption properties of phosphate glass fiber‐reinforced poly‐ϵ‐caprolactone composites for craniofacial bone repair. *Journal of applied polymer science,* 107**,** 3750-3755.

ORIMO, H. 2010. The mechanism of mineralization and the role of alkaline phosphatase in health and disease. *Journal of Nippon Medical School,* 77**,** 4-12.

ORTEGA, N., BEHONICK, D. J. & WERB, Z. 2004. Matrix remodeling during endochondral ossification. *Trends in Cell Biology,* 14**,** 86-93.

OWEN, T. A., ARONOW, M., SHALHOUB, V., BARONE, L. M., WILMING, L., TASSINARI, M. S., KENNEDY, M. B., POCKWINSE, S., LIAN, J. B. & STEIN, G. S. 1990. Progressive development of the rat

osteoblast phenotype in vitro: reciprocal relationships in expression of genes associated with osteoblast proliferation and differentiation during formation of the bone extracellular matrix. *Journal of cellular physiology,* 143**,** 420-430.

OWENS, G. J., SINGH, R. K., FOROUTAN, F., ALQAYSI, M., HAN, C.-M., MAHAPATRA, C., KIM, H.-W. & KNOWLES, J. C. 2016. Sol–gel based materials for biomedical applications. *Progress in Materials Science,* 77**,** 1-79.

PACURARI, M., LOWE, K., TCHOUNWOU, P. B. & KAFOURY, R. 2016. A review on the respiratory system toxicity of carbon nanoparticles. *International journal of environmental research and public health,* 13**,** 325.

PAN, L., PEI, X., HE, R., WAN, Q. & WANG, J. 2012. Multiwall carbon nanotubes/polycaprolactone composites for bone tissue engineering application. *Colloids and Surfaces B: Biointerfaces,* 93**,** 226-234.

PARFITT, A. 1994. Osteonal and hemi‐osteonal remodeling: the spatial and temporal framework for signal traffic in adult human bone. *Journal of cellular biochemistry,* 55**,** 273-286.

PARIKH, S. 2002. Bone graft substitutes: past, present, future. *Journal of postgraduate medicine,* 48**,** 142.

PARK, J.-H., PÉREZ, R. A., JIN, G.-Z., CHOI, S.-J., KIM, H.-W. & WALL, I. B. 2013a. Microcarriers designed for cell culture and tissue engineering of bone. *Tissue Engineering Part B: Reviews,* 19**,** 172-190.

PARK, K. H., PARK, B., YOON, D. S., KWON, S.-H., SHIN, D. M., LEE, J. W., LEE, H. G., SHIM, J.-H., PARK, J. H. & LEE, J. M. 2013b. Zinc inhibits osteoclast differentiation by suppression of Ca 2+-Calcineurin-NFATc1 signaling pathway. *Cell Communication and Signaling,* 11**,** 74.

PELTOLA, M. J., VALLITTU, P. K., VUORINEN, V., AHO, A. A. J., PUNTALA, A. & AITASALO, K. M. J. 2012. Novel composite implant in craniofacial bone reconstruction. *European Archives of Oto-Rhino-Laryngology,* 269**,** 623-628.

PEREZ, R. A., EL-FIQI, A., PARK, J. H., KIM, T. H., KIM, J. H. & KIM, H. W. 2014. Therapeutic bioactive microcarriers: Co-delivery of growth factors and stem cells for bone tissue engineering. *Acta Biomaterialia,* 10**,** 520-530.

PHILIPPART, A., BOCCACCINI, A. R., FLECK, C., SCHUBERT, D. W. & ROETHER, J. A. 2015. Toughening and functionalization of bioactive ceramic and glass bone scaffolds by biopolymer coatings and infiltration: a review of the last 5 years. *Expert review of medical devices,* 12**,** 93-111.

PIATTELLI, M., FAVERO, G. A., SCARANO, A., ORSINI, G. & PIATTELLI, A. 1999. Bone reactions to anorganic bovine bone (Bio-Oss) used in sinus augmentation procedures: a histologic long-term report of 20 cases in humans. *International Journal of Oral and Maxillofacial Implants,* 14**,** 835-840.

PIKIS, S., GOLDSTEIN, J. & SPEKTOR, S. 2015. Potential neurotoxic effects of polymethylmethacrylate during cranioplasty. *Journal of Clinical Neuroscience,* 22**,** 139-143.

PILLIAR, R. M., FILIAGGI, M. J., WELLS, J. D., GRYNPAS, M. D. & KANDEL, R. A. 2001. Porous calcium polyphosphate scaffolds for bone substitute applications — in vitro characterization. *Biomaterials,* 22**,** 963-972.

PITTENGER, M. F., MACKAY, A. M., BECK, S. C., JAISWAL, R. K., DOUGLAS, R., MOSCA, J. D., MOORMAN, M. A., SIMONETTI, D. W., CRAIG, S. & MARSHAK, D. R. 1999. Multilineage Potential of Adult Human Mesenchymal Stem Cells. *Science,* 284**,** 143-147.

POH, P. S. P., HUTMACHER, D. W., HOLZAPFEL, B. M., SOLANKI, A. K., STEVENS, M. M. & WOODRUFF, M. A. 2016. In vitro and in vivo bone formation potential of surface calcium phosphate-coated polycaprolactone and polycaprolactone/bioactive glass composite scaffolds. *Acta Biomaterialia,* 30**,** 319-333.

POLAND, C. A., DUFFIN, R., KINLOCH, I., MAYNARD, A., WALLACE, W. A., SEATON, A., STONE, V., BROWN, S., MACNEE, W. & DONALDSON, K. 2008. Carbon nanotubes introduced into the abdominal cavity of mice show asbestos-like pathogenicity in a pilot study. *Nature nanotechnology,* 3**,** 423-428.

POLO-CORRALES, L., LATORRE-ESTEVES, M. & RAMIREZ-VICK, J. E. 2014. Scaffold Design for Bone Regeneration. *Journal of nanoscience and nanotechnology,* 14**,** 15-56.

POORBAYGI, H., AGHAMIRI, S. M. R., SHEIBANI, S., KAMALI-ASL, A. & MOHAGHEGHPOOR, E. 2011. Production of glass microspheres comprising 90 Y and 177 Lu for treating of hepatic tumors with SPECT imaging capabilities. *Applied Radiation and Isotopes,* 69**,** 1407-1414.

PORTER, B., ZAUEL, R., STOCKMAN, H., GULDBERG, R. & FYHRIE, D. 2005. 3-D computational modeling of media flow through scaffolds in a perfusion bioreactor. *Journal of biomechanics,* 38**,** 543-549.

PORTER, B. D., LIN, A. S., PEISTER, A., HUTMACHER, D. & GULDBERG, R. E. 2007. Noninvasive image analysis of 3D construct mineralization in a perfusion bioreactor. *Biomaterials,* 28**,** 2525-2533.

PRABHAKAR, R. L., BROCCHINI, S. & KNOWLES, J. C. 2005. Effect of glass composition on the degradation properties and ion release

characteristics of phosphate glass—polycaprolactone composites. *Biomaterials,* 26**,** 2209-2218.

PRASAD, A., SANKAR, M. R. & KATIYAR, V. 2017. State of Art on Solvent Casting Particulate Leaching Method for Orthopedic ScaffoldsFabrication. *Materials Today: Proceedings,* 4**,** 898-907.

PUETT, C., INSCOE, C., HARTMAN, A., CALLISTE, J., FRANCESCHI, D. K., LU, J., ZHOU, O. & LEE, Y. Z. 2017. An update on carbon nanotube-enabled X-ray sources for biomedical imaging. *Wiley Interdiscip Rev Nanomed Nanobiotechnol*.

QIDWAI, M., SHERAZ, M. A., AHMED, S., ALKHURAIF, A. A. & REHMAN, I. U. 2014. Preparation and characterization of bioactive composites and fibers for dental applications. *Dental Materials,* 30**,** e253-e263.

QUARLES, L. D., YOHAY, D. A., LEVER, L. W., CATON, R. & WENSTRUP, R. J. 1992. Distinct proliferative and differentiated stages of murine MC3T3‐E1 cells in culture: An in vitro model of osteoblast development. *Journal of Bone and Mineral Research,* 7**,** 683-692.

RAMMELT, S., NEUMANN, M., HANISCH, U., REINSTORF, A., POMPE, W., ZWIPP, H. & BIEWENER, A. 2005. Osteocalcin enhances bone remodeling around hydroxyapatite/collagen composites. *Journal of Biomedical Materials Research Part A,* 73**,** 284-294.

RAMMELT, S., SCHULZE, E., BERNHARDT, R., HANISCH, U., SCHARNWEBER, D., WORCH, H., ZWIPP, H. & BIEWENER, A. 2004. Coating of titanium implants with type‐I collagen. *Journal of Orthopaedic Research,* 22**,** 1025-1034.

RATNER, B. 2004. Biomaterials Science (BD Ratner, AS Hoffman, FJ Schoen, JE Lemons ed. Elsevier.

RAUH, J., MILAN, F., GUNTHER, K. P. & STIEHLER, M. 2011. Bioreactor systems for bone tissue engineering. *Tissue Eng Part B Rev,* 17**,** 263-80.

REIS, S., FARIA, D., MARTINELLI, J., PONTUSCHKA, W., DAY, D. & PARTITI, C. 2002. Structural features of lead iron phosphate glasses. *Journal of non-crystalline solids,* 304**,** 188-194.

REZANIA, A., THOMAS, C. H., BRANGER, A. B., WATERS, C. M. & HEALY, K. E. 1997. The detachment strength and morphology of bone cells contacting materials modified with a peptide sequence found within bone sialoprotein. *Journal of Biomedical Materials Research Part A,* 37**,** 9-19.

REZWAN, K., CHEN, Q. Z., BLAKER, J. J. & BOCCACCINI, A. R. 2006. Biodegradable and bioactive porous polymer/inorganic composite scaffolds for bone tissue engineering. *Biomaterials,* 27**,** 3413-3431.

ROBERTS, T. T. & ROSENBAUM, A. J. 2012. Bone grafts, bone substitutes and orthobiologics: the bridge between basic science and clinical advancements in fracture healing. *Organogenesis,* 8**,** 114-24.

ROBEY, P. G. 2002. Bone matrix proteoglycans and glycoproteins. *Principles of bone biology,* 1**,** 225-237.

ROMBERGER, D. J. 1997. Fibronectin. *The international journal of biochemistry & cell biology,* 29**,** 939-943.

ROSSET, E. M. & BRADSHAW, A. D. 2016. SPARC/osteonectin in mineralized tissue. *Matrix Biology,* 52**,** 78-87.

SAKAGUCHI, R. L. & POWERS, J. M. 2012. *Craig's Restorative Dental Materials-E-Book*, Elsevier Health Sciences.

SALASZNYK, R. M., WILLIAMS, W. A., BOSKEY, A., BATORSKY, A. & PLOPPER, G. E. 2004. Adhesion to vitronectin and collagen I promotes osteogenic differentiation of human mesenchymal stem cells. *BioMed Research International,* 2004**,** 24-34.

SALIH, V., FRANKS, K., JAMES, M., HASTINGS, G. W., KNOWLES, J. C. & OLSEN, I. 2000. Development of soluble glasses for biomedical use Part II: The biological response of human osteoblast cell lines to phosphate-based soluble glasses. *Journal of Materials Science: Materials in Medicine,* 11**,** 615-620.

SALIH, V., PATEL, A. & KNOWLES, J. C. 2007. Zinc-containing phosphate-based glasses for tissue engineering. *Biomedical Materials,* 2**,** 11-20.

SANCHEZ-SOTELO, J., MUNUERA, L. & MADERO, R. 2000. Treatment of fractures of the distal radius with a remodellable bone cement. *Bone & Joint Journal,* 82**,** 856-863.

SARTORI, S., SILVESTRI, M., FORNI, F., ICARO CORNAGLIA, A., TESEI, P. & CATTANEO, V. 2003. Ten-year follow-up in a maxillary sinus augmentation using anorganic bovine bone (Bio-Oss). A case report with histomorphometric evaluation. *Clin Oral Implants Res,* 14**,** 369-72.

SAUTIER, J.-M., NEFUSSI, J.-R. & FOREST, N. 1992. Mineralization and bone formation on microcarrier beads with isolated rat calvaria cell population. *Calcified Tissue International,* 50**,** 527-532.

SAYES, C. M., LIANG, F., HUDSON, J. L., MENDEZ, J., GUO, W., BEACH, J. M., MOORE, V. C., DOYLE, C. D., WEST, J. L., BILLUPS, W. E., AUSMAN, K. D. & COLVIN, V. L. 2006. Functionalization density dependence of single-walled carbon nanotubes cytotoxicity in vitro. *Toxicology Letters,* 161**,** 135-142.

SCHANTZ, J.-T., TEOH, S. H., LIM, T. C., ENDRES, M., LAM, C. X. F. & HUTMACHER, D. W. 2003. Repair of calvarial defects with customized tissue-engineered bone grafts I. Evaluation of

osteogenesis in a three-dimensional culture system. *Tissue Engineering,* 9**,** 113-126.

SCHVARTZ, I., SEGER, D. & SHALTIEL, S. 1999. Vitronectin. *The international journal of biochemistry & cell biology,* 31**,** 539-544.

SCOTT, C. D. 2004. Chemical models for simulating single-walled nanotube production in arc vaporization and laser ablation processes. *J Nanosci Nanotechnol,* 4**,** 368-76.

SEELEY, R. 2000. *Anatomy & physiology.*

SENE, F. F., MARTINELLI, J. R. & OKUNO, E. 2008. Synthesis and characterization of phosphate glass microspheres for radiotherapy applications. *Journal of Non-Crystalline Solids,* 354**,** 4887-4893.

SEO, H.-J., CHO, Y.-E., KIM, T., SHIN, H.-I. & KWUN, I.-S. 2010a. Zinc may increase bone formation through stimulating cell proliferation, alkaline phosphatase activity and collagen synthesis in osteoblastic MC3T3-E1 cells. *Nutrition Research and Practice,* 4**,** 356-361.

SEO, H. J., CHO, Y. E., KIM, T., SHIN, H. I. & KWUN, I. S. 2010b. Zinc may increase bone formation through stimulating cell proliferation, alkaline phosphatase activity and collagen synthesis in osteoblastic MC3T3-E1 cells. *Nutr Res Pract,* 4**,** 356-61.

SEPULVEDA, P., JONES, J. R. & HENCH, L. L. 2002. Bioactive sol‐gel foams for tissue repair. *Journal of biomedical materials research,* 59**,** 340-348.

SHAH, R., SINANAN, A. C. M., KNOWLES, J. C., HUNT, N. P. & LEWIS, M. P. 2005. Craniofacial muscle engineering using a 3-dimensional phosphate glass fibre construct. *Biomaterials,* 26**,** 1497-1505.

SHARIF, F., REHMAN, I. U., MUHAMMAD, N. & MACNEIL, S. 2016a. Dental materials for cleft palate repair. *Materials Science and Engineering: C,* 61**,** 1018-1028.

SHARIF, F., UR REHMAN, I., MUHAMMAD, N. & MACNEIL, S. 2016b. Dental materials for cleft palate repair. *Mater Sci Eng C Mater Biol Appl,* 61**,** 1018-28.

SHEIKH, Z., SIMA, C. & GLOGAUER, M. 2015. Bone replacement materials and techniques used for achieving vertical alveolar bone augmentation. *Materials,* 8**,** 2953-2993.

SHELBY, J. 1997. *Introduction to Glass Science and Technology*

SHIMIZU, K., ITO, A. & HONDA, H. 2006. Enhanced cell‐seeding into 3D porous scaffolds by use of magnetite nanoparticles. *Journal of Biomedical Materials Research Part B: Applied Biomaterials,* 77**,** 265-272.

SHIN, U. S., YOON, I.-K., LEE, G.-S., JANG, W.-C., KNOWLES, J. C. & KIM, H.-W. 2011. Carbon nanotubes in nanocomposites and hybrids with hydroxyapatite for bone replacements. *Journal of tissue engineering***,** 674287.

SIKAVITSAS, V. I., BANCROFT, G. N. & MIKOS, A. G. 2002. Formation of three‐dimensional cell/polymer constructs for bone tissue engineering in a spinner flask and a rotating wall vessel bioreactor. *Journal of Biomedical Materials Research Part A,* 62**,** 136-148.

SINHA, N. & YEOW, J. T. 2005. Carbon nanotubes for biomedical applications. *IEEE Trans Nanobioscience,* 4**,** 180-95.

SINLAPABODIN, S., AMORNSUDTHIWAT, P., DAMRONGSAKKUL, S. & KANOKPANONT, S. 2016. An axial distribution of seeding, proliferation, and osteogenic differentiation of MC3T3-E1 cells and rat bone marrow-derived mesenchymal stem cells across a 3D Thai silk fibroin/gelatin/hydroxyapatite scaffold in a perfusion bioreactor. *Materials Science and Engineering: C,* 58**,** 960-970.

SITHARAMAN, B., SHI, X., WALBOOMERS, X. F., LIAO, H., CUIJPERS, V., WILSON, L. J., MIKOS, A. G. & JANSEN, J. A. 2008. In vivo biocompatibility of ultra-short single-walled carbon nanotube/biodegradable polymer nanocomposites for bone tissue engineering. *Bone,* 43**,** 362-370.

SKOROKHOD, V., GET'MAN, O., ZUEV, A. & RAKITIN, S. 1988. Correlation between the particle size, pore size, and porous structure of sintered tungsten. *Powder Metallurgy and Metal Ceramics,* 27**,** 941-947.

SMITH, B. T., SHUM, J., WONG, M., MIKOS, A. G. & YOUNG, S. 2015a. Bone tissue engineering challenges in oral & maxillofacial surgery. *Engineering mineralized and load bearing tissues.* Springer.

SMITH, B. T., SHUM, J., WONG, M., MIKOS, A. G. & YOUNG, S. 2015b. Bone Tissue Engineering Challenges in Oral & Maxillofacial Surgery. *Adv Exp Med Biol,* 881**,** 57-78.

SMITH, L. A., LIU, X., HU, J. & MA, P. X. 2010. The enhancement of human embryonic stem cell osteogenic differentiation with nano-fibrous scaffolding. *Biomaterials,* 31**,** 5526-5535.

SOLGI, S., KHAKBIZ, M., SHAHREZAEE, M., ZAMANIAN, A., TAHRIRI, M., KESHTKARI, S., RAZ, M., KHOSHROO, K., MOGHADAS, S. & RAJABNEJAD, A. 2017. Synthesis, characterization and in vitro biological evaluation of sol-gel derived sr-containing nano bioactive glass. *Silicon,* 9**,** 535-542.

SOMERMAN, M. J., PRINCE, C. W., SAUK, J. J., FOSTER, R. A. & BUTLER, W. T. 1987. Mechanism of fibroblast attachment to bone extracellular matrix: role of a 44 kilodalton bone phosphoprotein. *Journal of Bone and Mineral Research,* 2**,** 259-265.

SON, K. H., HONG, J. H. & LEE, J. W. 2016. Carbon nanotubes as cancer therapeutic carriers and mediators. *Int J Nanomedicine,* 11**,** 5163-5185.

SONG, K., LIU, T., LI, X., CUI, Z., SUN, X. & MA, X. 2007. Three-dimensional expansion: In suspension culture of SD rat's osteoblasts in a rotating wall vessel bioreactor. *Biomedical and Environmental Sciences,* 20**,** 91.

SRIRANGANATHAN, D., CHEN, X., HING, K. A., KANWAL, N. & HILL, R. G. 2017. The effect of the incorporation of fluoride into strontium containing bioactive glasses. *Journal of Non-Crystalline Solids,* 457**,** 25-30.

SRIRANGANATHAN, D., KANWAL, N., HING, K. A. & HILL, R. G. 2016. Strontium substituted bioactive glasses for tissue engineered scaffolds: the importance of octacalcium phosphate. *Journal of Materials Science: Materials in Medicine,* 27**,** 39.

STEFKOVA, K., PROCHAZKOVA, J. & PACHERNIK, J. 2015. Alkaline phosphatase in stem cells. *Stem Cells Int,* 2015**,** 628368.

STEIN, G., LIAN, J., STEIN, J., BRIGGS, R., SHALHOUB, V., WRIGHT, K., PAULI, U. & VAN WIJNEN, A. 1989a. Altered binding of human histone gene transcription factors during the shutdown of proliferation and onset of differentiation in HL-60 cells. *Proceedings of the National Academy of Sciences,* 86**,** 1865-1869.

STEIN, G., LIAN, J., STEIN, J., VAN WIJNEN, A., FRENKEL, B. & MONTECINO, M. 1996. Mechanisms regulating osteoblast proliferation and differentiation. New York: Academic Press Inc.

STEIN, G. S., LIAN, J. B. & OWEN, T. A. 1990. Relationship of cell growth to the regulation of tissue-specific gene expression during osteoblast differentiation. *The FASEB journal,* 4**,** 3111-3123.

STEIN, S. G., LIAN, B. J., GERSTENFELD, G. L., VICTORIA, S., MICHAEL, A., THOMAS, O. & ELIZABETH, M. 1989b. The onset and progression of osteoblast differentiation is functionally related to cellular proliferation. *Connective tissue research,* 20**,** 3-13.

STICH, S., IBOLD, Y., ABBAS, A., ULLAH, M., SITTINGER, M., RINGE, J., SCHULZE‐TANZIL, G., MÜLLER, C., KOHL, B. & JOHN, T. 2014. Continuous cultivation of human hamstring tenocytes on microcarriers in a spinner flask bioreactor system. *Biotechnology progress,* 30**,** 142-151.

STROBER, W. 2001. Trypan blue exclusion test of cell viability. *Current protocols in immunology***,** A3. B. 1-A3. B. 3.

SUCHANEK, W. & YOSHIMURA, M. 1998. Processing and properties of hydroxyapatite-based biomaterials for use as hard tissue replacement implants. *Journal of Materials Research,* 13**,** 94-117.

SUNG, H.-J., MEREDITH, C., JOHNSON, C. & GALIS, Z. S. 2004. The effect of scaffold degradation rate on three-dimensional cell growth and angiogenesis. *Biomaterials,* 25**,** 5735-5742.

SUOMINEN, E. & KINNUNEN, J. 1996. Bioactive glass granules and plates in the reconstruction of defects of the facial bones. *Scandinavian journal of plastic and reconstructive surgery and hand surgery,* 30**,** 281-289.

TAICHMAN, R. S. 2005. Blood and bone: two tissues whose fates are intertwined to create the hematopoietic stem-cell niche. *Blood,* 105**,** 2631-9.

TAKADA, T., SANTIDA, D. & ABE, S. 2010. Suitable conditions for sidewall carboxylation of multi-walled carbon nanotubes. *Nano Biomedicine,* 2**,** 147-152.

TAKADAMA, H., KIM, H.-M., KOKUBO, T. & NAKAMURA, T. 2001. Mechanism of biomineralization of apatite on a sodium silicate glass: TEM− EDX study in vitro. *Chemistry of materials,* 13**,** 1108-1113.

TAMIMI, F., SHEIKH, Z. & BARRALET, J. 2012. Dicalcium phosphate cements: Brushite and monetite. *Acta biomaterialia,* 8**,** 474-487.

TANAKA, M., SATO, Y., ZHANG, M., HANIU, H., OKAMOTO, M., AOKI, K., TAKIZAWA, T., YOSHIDA, K., SOBAJIMA, A., KAMANAKA, T., KATO, H. & SAITO, N. 2017. In Vitro and In Vivo Evaluation of a Three-Dimensional Porous Multi-Walled Carbon Nanotube Scaffold for Bone Regeneration. *Nanomaterials (Basel),* 7.

TAPETY, F. I., AMIZUKA, N., UOSHIMA, K., NOMURA, S. & MAEDA, T. 2004. A histological evaluation of the involvement of Bio‐Oss® in osteoblastic differentiation and matrix synthesis. *Clinical Oral Implants Research,* 15**,** 315-324.

TAYA, M. & KINO-OKA, M. 2011. 2.27 - Bioreactors for Animal Cell Cultures A2 - Moo-Young, Murray. *Comprehensive Biotechnology (Second Edition).* Burlington: Academic Press.

TERRANOVA, L., DRAGUSIN, D. M., MALLET, R., VASILE, E., STANCU, I.-C., BEHETS, C. & CHAPPARD, D. 2017. Repair of calvarial bone defects in mice using electrospun polystyrene scaffolds combined with β-TCP or gold nanoparticles. *Micron,* 93**,** 29-37.

THAKUR, S., GARG, S., KAUR, G. & PANDEY, O. P. 2017. Effect of strontium substitution on the cytocompatibility and 3-D scaffold structure for the xSrO–(10− x) MgO–60SiO2–20CaO–10 P2O5 (2≤ x≤

8) sol–gel glasses. *Journal of Materials Science: Materials in Medicine,* 28**,** 89.

THUAKSUBAN, N., NUNTANARANONT, T. & PRIPATNANONT, P. 2010. A comparison of autogenous bone graft combined with deproteinized bovine bone and autogenous bone graft alone for treatment of alveolar cleft. *International journal of oral and maxillofacial surgery,* 39**,** 1175-1180.

TONG, Q., QINGZHI, W., HONGLIAN, D., XINYU, W., YOUFA, W., SHIPU, L. & JUNLI, L. 2014. A comparative study on the effects of pristine and functionalized single-walled carbon nanotubes on osteoblasts: ultrastructural and biochemical properties. *J Mater Sci Mater Med,* 25**,** 1915-23.

TSAI, K. S., KAO, S. Y., WANG, C. Y., WANG, Y. J., WANG, J. P. & HUNG, S. C. 2010. Type I collagen promotes proliferation and osteogenesis of human mesenchymal stem cells via activation of ERK and Akt pathways. *Journal of biomedical materials research part A,* 94**,** 673-682.

TSURUGA, E., TAKITA, H., ITOH, H., WAKISAKA, Y. & KUBOKI, Y. 1997. Pore size of porous hydroxyapatite as the cell-substratum controls BMP-induced osteogenesis. *The journal of biochemistry,* 121**,** 317-324.

UNTERHOFER, C., WIPPLINGER, C., VERIUS, M., RECHEIS, W., THOMÉ, C. & ORTLER, M. 2017. Reconstruction of large cranial defects with poly-methyl-methacrylate (PMMA) using a rapid prototyping model and a new technique for intraoperative implant modeling. *Neurologia i Neurochirurgia Polska,* 51**,** 214-220.

UO, M., MIZUNO, M., KUBOKI, Y., MAKISHIMA, A. & WATARI, F. 1998. Properties and cytotoxicity of water soluble Na2O–CaO–P2O5 glasses. *Biomaterials,* 19**,** 2277-2284.

VALAPPIL, S. P., READY, D., NEEL, E. A. A., PICKUP, D. M., CHRZANOWSKI, W., O'DELL, L. A., NEWPORT, R. J., SMITH, M. E., WILSON, M. & KNOWLES, J. C. 2008. Antimicrobial gallium‐doped phosphate‐based glasses. *Advanced functional materials,* 18**,** 732-741.

VAN DEN DOLDER, J., BANCROFT, G. N., SIKAVITSAS, V. I., SPAUWEN, P. H., MIKOS, A. G. & JANSEN, J. A. 2003. Effect of fibronectin-and collagen I-coated titanium fiber mesh on proliferation and differentiation of osteogenic cells. *Tissue engineering,* 9**,** 505-515.

VAN GESTEL, N. A., GEURTS, J., HULSEN, D. J., VAN RIETBERGEN, B., HOFMANN, S. & ARTS, J. J. 2015. Clinical Applications of S53P4 Bioactive Glass in Bone Healing and Osteomyelitic Treatment: A Literature Review. *Biomed Res Int,* 2015**,** 684826.

VATER, C., KASTEN, P. & STIEHLER, M. 2011. Culture media for the differentiation of mesenchymal stromal cells. *Acta biomaterialia,* 7**,** 463-477.

VEETIL, J. V. & YE, K. 2009. Tailored carbon nanotubes for tissue engineering applications. *Biotechnology progress,* 25**,** 709-721.

VIGUET-CARRIN, S., GARNERO, P. & DELMAS, P. 2006. The role of collagen in bone strength. *Osteoporosis international,* 17**,** 319-336.

VOGEL, W. & HÖLAND, W. 1987. The development of bioglass ceramics for medical applications. *Angewandte Chemie International Edition,* 26**,** 527-544.

VOLKMER, E., DROSSE, I., OTTO, S., STANGELMAYER, A., STENGELE, M., KALLUKALAM, B. C., MUTSCHLER, W. & SCHIEKER, M. 2008. Hypoxia in static and dynamic 3D culture systems for tissue engineering of bone. *Tissue Engineering Part A,* 14**,** 1331-1340.

WALLACE, S. S., FROUM, S. J., CHO, S.-C., ELIAN, N., MONTEIRO, D., KIM, B. S. & TARNOW, D. P. 2005. Sinus augmentation utilizing anorganic bovine bone (Bio-Oss) with absorbable and nonabsorbable membranes placed over the lateral window: histomorphometric and clinical analyses. *International Journal of Periodontics & Restorative Dentistry,* 25.

WANG, S., FALK, M. M., RASHAD, A., SAAD, M. M., MARQUES, A. C., ALMEIDA, R. M., MAREI, M. K. & JAIN, H. 2011. Evaluation of 3D nano–macro porous bioactive glass scaffold for hard tissue engineering. *Journal of Materials Science: Materials in Medicine,* 22**,** 1195.

WARREN, B. E. 1969. *X-ray Diffraction*, Courier Corporation.

WAZER, J. R. V. 1950. Structure and Properties of the Condensed Phosphates. II. A Theory of the Molecular Structure of Sodium Phosphate Glasses1. *Journal of the American Chemical Society,* 72**,** 644-647.

WHITE, J. E. & DAY, D. E. Rare earth aluminosilicate glasses for in vivo radiation delivery. Key Engineering Materials, 1994. Trans Tech Publ, 181-208.

WIDMAIER, E. P., RAFF, H. & STRANG, K. T. 2006. *Vander's human physiology*, McGraw-Hill New York, NY.

WILL, J., GERHARDT, L.-C. & BOCCACCINI, A. R. 2012. Bioactive Glass-Based Scaffolds for Bone Tissue Engineering. *In:* KASPER, C., WITTE, F. & PÖRTNER, R. (eds.) *Tissue Engineering III: Cell - Surface Interactions for Tissue Culture.* Berlin, Heidelberg: Springer Berlin Heidelberg.

WILSMAN, N. J., FARNUM, C. E., HILLEY, H. D. & CARLSON, C. S. 1981. Ultrastructural evidence of a functional heterogeneity among physeal chondrocytes in growing swine. *American Journal of Veterinary Research,* 42**,** 1547-1553.

WONG, H. M., YEUNG, K. W., LAM, K. O., TAM, V., CHU, P. K., LUK, K. D. & CHEUNG, K. M. 2010. A biodegradable polymer-based coating to control the performance of magnesium alloy orthopaedic implants. *Biomaterials,* 31**,** 2084-2096.

WU, C., FAN, W., GELINSKY, M., XIAO, Y., SIMON, P., SCHULZE, R., DOERT, T., LUO, Y. & CUNIBERTI, G. 2011. Bioactive SrO–SiO 2 glass with well-ordered mesopores: characterization, physiochemistry and biological properties. *Acta biomaterialia,* 7**,** 1797-1806.

WU, C., ZHANG, Y., KE, X., XIE, Y., ZHU, H., CRAWFORD, R. & XIAO, Y. 2010. Bioactive mesopore‐glass microspheres with controllable protein‐delivery properties by biomimetic surface modification. *Journal of Biomedical Materials Research Part A,* 95**,** 476-485.

XIAO, W., ZAEEM, M. A., LI, G., BAL, B. S. & RAHAMAN, M. N. 2017. Tough and strong porous bioactive glass-PLA composites for structural bone repair. *Journal of Materials Science,* 52**,** 9039-9054.

YAMAGUCHI, M. 2010. Role of nutritional zinc in the prevention of osteoporosis. *Mol Cell Biochem,* 338**,** 241-54.

YANG, S.-T., WANG, X., JIA, G., GU, Y., WANG, T., NIE, H., GE, C., WANG, H. & LIU, Y. 2008a. Long-term accumulation and low toxicity of single-walled carbon nanotubes in intravenously exposed mice. *Toxicology Letters,* 181**,** 182-189.

YANG, Y., ZHAO, Y., TANG, G., LI, H., YUAN, X. & FAN, Y. 2008b. In vitro degradation of porous poly (l-lactide-co-glycolide)/β-tricalcium phosphate (PLGA/β-TCP) scaffolds under dynamic and static conditions. *Polymer Degradation and Stability,* 93**,** 1838-1845.

YAO, A., WANG, D., HUANG, W., FU, Q., RAHAMAN, M. N. & DAY, D. E. 2007. In Vitro Bioactive Characteristics of Borate‐Based Glasses with Controllable Degradation Behavior. *Journal of the American Ceramic Society,* 90**,** 303-306.

YEATTS, A. B. & FISHER, J. P. 2011. Bone tissue engineering bioreactors: Dynamic culture and the influence of shear stress. *Bone,* 48**,** 171-181.

YEO, M. G. & KIM, G. H. 2011. Preparation and characterization of 3D composite scaffolds based on rapid-prototyped PCL/β-TCP struts and electrospun PCL coated with collagen and HA for bone regeneration. *Chemistry of materials,* 24**,** 903-913.

YILDIRIM, E. D., BESUNDER, R., PAPPAS, D., ALLEN, F., GÜÇERI, S. & SUN, W. 2010. Accelerated differentiation of osteoblast cells on

polycaprolactone scaffolds driven by a combined effect of protein coating and plasma modification. *Biofabrication,* 2**,** 014109.

YUAN, H., DE BRUIJN, J. D., ZHANG, X., VAN BLITTERSWIJK, C. A. & DE GROOT, K. 2001. Bone induction by porous glass ceramic made from Bioglass®(45S5). *Journal of Biomedical Materials Research Part A,* 58**,** 270-276.

YUAN, Y. & LEE, T. R. 2013. Contact angle and wetting properties. *Surface science techniques.* Springer.

ZACHARIASEN, W. H. 1932. THE ATOMIC ARRANGEMENT IN GLASS. *Journal of the American Chemical Society,* 54**,** 3841-3851.

ZAN, X., SITASUWAN, P., FENG, S. & WANG, Q. 2016. Effect of roughness on in situ biomineralized CaP-collagen coating on the osteogenesis of mesenchymal stem cells. *Langmuir,* 32**,** 1808-1817.

ZELTINGER, J., SHERWOOD, J. K., GRAHAM, D. A., MÜELLER, R. & GRIFFITH, L. G. 2001. Effect of pore size and void fraction on cellular adhesion, proliferation, and matrix deposition. *Tissue engineering,* 7**,** 557-572.

ZHANG, F., WEIDMANN, A., NEBE, J. B. & BURKEL, E. 2012a. Osteoblast cell response to surface-modified carbon nanotubes. *Materials Science and Engineering: C,* 32**,** 1057-1061.

ZHANG, J., ZHAO, S., ZHU, M., ZHU, Y., ZHANG, Y., LIU, Z. & ZHANG, C. 2014. 3D-printed magnetic Fe 3 O 4/MBG/PCL composite scaffolds with multifunctionality of bone regeneration, local anticancer drug delivery and hyperthermia. *Journal of Materials Chemistry B,* 2**,** 7583-7595.

ZHANG, R. & ZHANG, Y. 2017. Horizontally aligned carbon nanotube arrays: growth mechanism, controlled synthesis, characterization, properties and applications. 46**,** 3661-3715.

ZHANG, X., HU, W., LI, J., TAO, L. & WEI, Y. 2012b. A comparative study of cellular uptake and cytotoxicity of multi-walled carbon nanotubes, graphene oxide, and nanodiamond. *Toxicology Research,* 1**,** 62-68.

ZHANG, Z.-Y., TEOH, S. H., TEO, E. Y., KHOON CHONG, M. S., SHIN, C. W., TIEN, F. T., CHOOLANI, M. A. & CHAN, J. K. Y. 2010. A comparison of bioreactors for culture of fetal mesenchymal stem cells for bone tissue engineering. *Biomaterials,* 31**,** 8684-8695.

ZHAO, J., GRIFFIN, M., CAI, J., LI, S., BULTER, P. E. M. & KALASKAR, D. M. 2016. Bioreactors for tissue engineering: An update. *Biochemical Engineering Journal,* 109**,** 268-281.

ZHENG, W., LIU, G., YAN, C., XIAO, Y. & MIAO, X. G. Strong and bioactive tri-calcium phosphate scaffolds with tube-like macropores. Journal of

Biomimetics, Biomaterials and Tissue Engineering, 2014. Trans Tech Publ, 65-75.

ZIMMERMANN, G. & MOGHADDAM, A. 2011. Allograft bone matrix versus synthetic bone graft substitutes. *Injury,* 42 Suppl 2**,** S16-21.